DOCTOR OF PHILOSOPHY

Investigating the performance of continuous helical displacement piles

Jeffrey, John

Award date:
2012

DOCTOR OF PHILOSOPHY

Investigating the performance of continuous helical displacement piles

John Jeffrey

2012

University of Dundee

College of Art, Science & Engineering
School of Engineering, Physics and Mathematics
Department of Civil Engineering

Investigating the performance of Continuous Helical Displacement piles

John Jeffrey

A dissertation submitted for the
degree of Doctor of Philosophy
to the University of Dundee
June 2012

Declaration

This is to certify that, except where specific reference to other investigation is made, the work described in this dissertation is the result of the investigation of the candidate. Neither this dissertation, nor any part of it, has been presented or is currently submitted in candidature for any degree at any other university.

John Jeffrey (candidate) Dundee, 22-June-2012

Dr Michael Brown (supervisor) Dundee, 22-June-2012

Acknowledgements

My first acknowledgement goes to my project supervisor Dr Michael Brown. I am grateful to Michael for his continued support and encouragement throughout the course of the project. He has always been willing to offer assistance in matters of an academic or personal nature.

I am grateful for the support and assistance that I have received from the staff at Roger Bullivant Ltd, in particular Jon Ball, Hugh Sloan and Gavin Hay who have allowed me access to the Roger Bullivant Ltd offices for data collection and have answered my lists of questions and requests. I am grateful to the site teams for allowing me to gain first hand experience of the CHD construction process.

I would like to thank the members of the geotechnical research group at the University of Dundee who have offered assistance and feedback regarding the project over the years. In particular I am grateful to Dr Jonathan Knappett who has always assisted when I have asked questions.

I would like to thank the technical staff within the Department of Civil Engineering the University of Dundee who have manufactured all my equipment and assisted with operations. In particular I would like to thank William Truswell who has always provided support and assistance which has been above and beyond what was expected.

I am grateful for the financial support grants from the EPSRC and from Roger Bullivant Ltd.

I would like to thank my friends who have supported and encouraged me throughout the project. In particular David Michie, Ralph Wardlaw and Fraser Duthie who have provided assistance and motivation when required.

Finally I would like to take the opportunity to thank my family for their continued love and support without which I could not have completed the work.

Abstract

The Continuous Helical Displacement (CHD) pile is an auger displacement pile developed by Roger Bullivant Ltd in the UK. The CHD pile is installed in-situ through the use of a drilling auger, in a similar fashion to European screw piles and as such, it has performance characteristics of both displacement and non-displacement piles Based on field experience, it is known that the load capacity performance of the CHD pile significantly exceeds the current design predictions, particularly when installed in sand

Model CHD piles were created in pluviated test beds at a range of different densities and compared to model displacement and non-displacement piles. The load tests show that the CHD piles have a similar ultimate capacity to displacement piles. Instrumentation of the model piles allowed load distribution throughout the pile length to be determined. The tests allowed design parameters to be established, with it being shown that the CHD has lower bearing capacity factors and higher earth pressure coefficients than current suggestions

The disturbance to the in-situ soil conditions caused by the installation of the CHD piles was measured using a model CPT probe. The CHD pile was found to cause significant changes in soil relative density laterally around the pile shaft while displacement piles show changes predominantly below the pile base. The CHD pile is found to cause a densification of the in situ soil for all relative densities with the greatest increase occurring in loose sand.

The ultimate capacity of the CHD pile is determined from load tests carried out on field CHD piles with the aid of capacity prediction methods for piles which have not been loaded to their ultimate capacity. The results from model testing have been applied to field pile tests to allow the development of design parameters including appropriate pile diameter, bearing capacity factor N_q and the earth pressure coefficient k which are suitable for CHD piles.

Keywords: CHD, pile, auger displacement, model testing, field data, CPT, sand

Contents

List of Figures

List of Tables

Abbreviations and notation

Table i. Abbreviations

Abbreviation	Definition
ADP	Auger Displacement Pile
API	American Petroleum Institute
BGL	Below Ground Level
CFA	Continuous Flight Auger
CHD	Continuous Helical Displacement
CPT	Cone Penetration Test
CRP	Constant rate of penetration
GCG	Geotechnical Consultancy Group
ICE	Institution of Civil Engineers
ICP	Imperial College Pile design method
MG	Made Ground
MLT	Maintained Load Test
PTFE	Polytetrafluoroethylene
RBL	Roger Bullivant Ltd
RHPC	Rapid Hardening Portland Cement
SPERW	Specification for Piling and Embedded Retaining Walls
SPT	Standard Penetration Test
SWL	Safe working load
UWA	University of Western Australia
WIP	Wished In Place pile

Table ii. Notation

Symbol	Description
A_b	Area of pile base
A_{CT1}	Area of concrete at level 1
A_s	Area of pile shaft
B_v	Bridge excitation voltage
C_B	CHD base cone diameter at base
C_T	CHD base cone diameter at top
D	Pile diameter
d_{50}, d_{10}	Particle size characteristics
D_{AVE}	Average pile diameter between strain gauges
D_c	CHD pile core diameter
D_{CPT}	Diameter of CPT probe
D_e	CHD effective design diameter
D_f	CHD pile outer flight diameter
D_r	Relative density of soil
E	Modulus of elasticity of soil
E_A	Modulus of elasticity of aluminium rod
E_B	Soil modulus beneath pile base
E_{CT}	Tangent modulus of concrete
Ep	Elastic modulus of pile material
F	Offset pile head movement

f_s	Sleeve Friction
F_T	CHD flange thickness
G	Shear modulus of soil
G_{avg}	Average shear modulus over the pile length
G_{base}	Shear modulus below the pile base
G_F	Gauge factor
G_L	Shear modulus of soil at a depth equal to pile length
h	Height above the pile base
H	Location depth from soil surface
k	Coefficient of earth pressure
k_c	Bearing capacity factor after Bustamante & Gianeselli design method
K_e	Effective column length factor
k_o	Coefficient of earth pressure at rest
K_T	Torque correlation factor
L	Pile length
L_c	CHD base cone length
M_s	Shaft flexibility factor
M_t	Tangent modulus of the composite pile material
N	SPT blow count
N_a	Number of active arms in a Wheatstone bridge
N_c	Bearing capacity factor for cohesive soils
N_{ICP}	Bearing capacity factor for ICP design method
N_k	Empirical cone factor
N_q	Bearing capacity factor
N_v	Base reduction factor for CPT design suggested by Van Impe
P	Applied load
Pa	Atmospheric pressure
Q_A	Ageing factor
Q_B	Pile base capacity
q_b	End bearing pressure
q_c	CPT cone resistance
Q_c	Compressibility factor
$q_{c3.3D}$	Cone resistance at a distance of 3.3D from the pile
q_{ca}	Average CPT cone resistance around the pile base
Q_{OCR}	Overconsolidation factor
Q_S	Pile shaft capacity
q_s	Shaft unit friction
Q_T	Total pile capacity
R	Pile radius
R_f	Friction ratio
r_m	Maximum limiting radius
r_p	Radial position of CPT probe
S_u	Undrained shear strength of soil
T	Applied torque during CHD installation
V	Output voltage from strain gauge

w	Total pile settlement
w/c	Water-cement ratio
w_s	Shaft settlement
YSR	Yield stress ratio
Z_{CPT}	CPT penetration depth
α	Shaft friction coefficient for CPT design
α_{clay}	Empirical adhesion factor
α_{LCPC}	Shaft friction coefficient for CPT design based on LCPC method
γ_{max}	Maximum unit weight of dry soil
γ_{min}	Minimum unit weight of dry soil
δ	Interface friction angle
Δh	Difference in height between strain gauges
ΔIvy	Log10(clay sensitivity)
ΔL_{AX}	Change in axial load between strain gauges
δp	Elastic shortening of pile
$\Delta\sigma'_{rd}$	Dilatant increase in local radial effective stress due to pile loading
ε	Strain
η	Base enlargement ratio
η_{CPT}	Cone resistance correction factor
η_p	Shaft correction factor for CPT design suggested by Van Impe
ν	Poissons ratio
σ'_r	Radial effective stress acting on pile
$\underline{\sigma'_v}$	Average vertical effective stress
σ'_v	Vertical effective stress
τ_o	Shear stress on pile surface
τ_S	Shear stress along pile shaft
ϕ'	Angle of internal friction
ϕ'_{cv}	Critical state angle of friction
ϕ'_p	Peak angle of friction
ψ	Angle of dilation

1.0 Introduction

1.1 Preface

Piles are used in foundations in order to transfer the load of a superstructure onto a suitable underlying soil stratum. Load is transferred to the ground through shear along the pile shaft and from the bearing pressure of the base. The ratio of capacity generated from either shaft friction and bearing pressure is dependant on the soil conditions and pile type. Traditionally piles can be installed using two approaches. The first drives the pile into the ground through the repeated application of impact load to the pile head until an acceptable installation depth was reached. The second, in the most simplistic form, uses an auger to bore a hole into the ground and replace the soil with concrete.

The use of driven piles can cause significant disturbance in terms of noise and vibration during the installation process, something that can limit the use of the method in particular locations. Utilisation of bored piles, although does not have the noise and vibration issues of driven piles, will produce large volumes of spoil for each installed pile. Due to strict regulations, the disposal of the produced spoil can lead to significant expense to a project.

In an effort to combat the limitations of the existing piling methods, a new pile installation method has emerged which forms a pile in-situ similar to a bored pile but without the formation of spoil. One of these new pile installation methods has been developed in the United Kingdom by piling specialists Roger Bullivant Ltd, known as the Continuous Helical Displacement (CHD) pile. The CHD pile is formed by penetrating an auger bullet into the ground via a high torque drilling rig. At an appropriate depth, concrete is pumped through the retreating auger bullet to leave a concrete pile with a continuous helical rib.

The CHD piles are found to perform well in a variety of different soil conditions. Particularly when installed in sands, the working load capacity of the CHD pile

has significantly exceeded the designed capacity. The exact cause of this improved performance is unknown, although it is assumed it is linked to the conservative design assumptions, in particular the assumption of equivalent diameters, which are currently used for CHD piles.

In order to improve understanding of the behaviour of the CHD pile in sands, a programme of research was commissioned at the University of Dundee. The body of research undertaken included the collection and analysis of data from tests carried out on CHD piles installed on working projects. The load-settlement behaviour of full scale piles was investigated in order to obtain suitable pile capacities which could be compared to designed values. In instances where the ultimate capacity could not be obtained, prediction techniques were utilised.

Along with the field pile data, a series of model tests were also conducted. This consisted of casting CHD piles at a 10^{th} scale of the prototype in prepared test beds in the geotechnical laboratory. Load testing of instrumented model piles coupled with a detailed knowledge of the soil conditions allowed evaluation of the design parameters used for CHD piles.

1.2 Project aims and objectives

The overall aim of this research project is to develop a greater understanding of the effects of CHD pile installation, particularly in sands. With increased knowledge of CHD pile behaviour, the efficiency of the design process can be improved.

To achieve these aims, the following objectives are set out.

1. Collect field CHD test data from Roger Bullivant Ltd's offices and conduct analysis to establish an ultimate pile capacity which can be compared to the design capacity.

2. Develop equipment and procedures to replicate the CHD installation process at model scale in the laboratory.

3. Carry out a series of model pile tests in dry sand in order to determine the load-settlement performance of the CHD pile compared to alternative piling techniques.

4. Conduct investigations into the disturbance the CHD pile has to the in-situ soil conditions and how this affects soil properties.

5. Combine the data gathered from field analysis and model testing to refine the design process

1.3 Structure of thesis

Chapter 2 consists of a review of the available literature on piling methods and techniques. Classification of the CHD pile in relation to alternative piles types is carried out. Attention is given to existing piling methods which are of a similar form to the CHD. Although similarities can be drawn, none are found to be identical to the CHD pile, highlighting the need for further research into the method. Techniques and criteria are investigated which can be used to analyse the collected field data in a consistent manner. Important points are identified regarding model testing which must be considered in order to ensure appropriate data analysis takes place.

The experimental methods adopted are presented in Chapter 3. A brief description of the process involved in field data analysis is given, however the primary focus of the chapter is on model testing. A detailed description of the development of the model testing programme is given along with material characterisation tests carried out on the model sand.

Results and discussion for the field data analysis and series of model tests are contained in Chapters 4 and 5. The field data analysis in Chapter 4 highlights how the initial comparisons between measured pile capacity and design capacity were difficult to achieve due to the limited settlements displayed by the piles

under the test loads. Attempts to determine the ultimate pile capacity and load distribution throughout the CHD piles are also presented. Chapter 5 presents the results from a number of model pile tests. Utilisation of model cone penetration tests (CPT) allows the investigation of the soil disturbance due to CHD installation.

Application of the model test findings to the field data analysis is presented in Chapter 6. Knowledge regarding soil property changes along with load-distribution findings from the model tests is applied to CHD field data in an effort to allow design refinement to take place.

Chapter 7 summaries the primary conclusions from the research and provides suggestions for design procedures for CHD piles. Areas of further research regarding CHD piles are suggested in Chapter 8.

2.0 Literature Review

2.1 Introduction

The continuous helical displacement (CHD) pile has been developed by the UK piling specialist Roger Bullivant Ltd. This literature review aims to investigate existing piling techniques in order to compare them with the CHD pile. An investigation of the CHD pile including the installation and formation process is carried out along with a review of existing research carried out on the CHD pile.

As was mentioned in Chapter 1, the aim of this research is to improve the understanding of CHD piles in an effort to refine the design procedures currently used. General pile design techniques which are currently used for different pile types are reviewed in order to obtain appropriate procedures which can be applied to the design of CHD piles. Specific design procedures also used for the design of piles similar to the CHD piles are also reviewed to determine the compatibility of use for CHD design.

Pile design refinement of the CHD requires the interpretation of load tests carried out in the field. Suitable procedures for the interpretation of the load test data are investigated since it is known that the definition of ultimate pile capacity can vary. It has also been found that not all pile load tests fully mobilise the ultimate capacity of the pile and as such it must be interpolated from the available data. A number of techniques are investigated which allow this to happen.

It is intended that model pile testing will be used during the research and therefore an investigation into existing research which has been conducted on cast in situ model piles. Techniques and equipment used in previous research are investigated in an effort to determine the suitability for use in the creation of model CHD piles.

2.2 Pile foundation classification

Traditionally, pile foundations can be classified in either two ways, driven or bored, Tomlinson and Woodward (2008) based on the installation method used. Driven piles generally consist of pre-formed elements (e.g. Timber, pre-cast concrete or steel elements) which are penetrated into the ground. Bored piles are formed in-situ by first removing the soil through either boring or drilling and then replacing it with concrete.

Developments in piling technology has seen a new generation of pile type which are formed using an auger tool which displaces the soil laterally creating a void that is then filled with concrete. These pile types have installation characteristics of both traditional driven and bored piles

The development of this auger based piling technique has resulted in the generic terms 'driven' and 'bored' becoming obsolete. It is now common practice to use the definitions displacement or non-displacement, Baxter *et al* (2006), Fleming *et al* (2009), which stems from the soil movement characteristics around the installed pile. Piles constructed using auger tools tend to have characteristics of both the more traditional displacement and non-displacement piles. As will be discussed later in the chapter, a variety of different terminology exists to describe these piles. Throughout this research, piles installed using an auger tool, such as the CHD, will be referred to as auger displacement piles.

2.2.1 Non-Displacement Piles

A non-displacement pile is one in which a pile is formed whilst soil extraction takes place as represented in Figure 2-1. Examples of non-displacement piles are bored cast-in-situ and continuous flight auger CFA piles. The formation of a typical bored cast-in-situ pile requires the formation of a borehole which is then filled with concrete. Depending on the in-situ ground conditions the borehole is supported through the use of steel casing or through stabilisation slurry such as bentonite, before concrete is poured. The formation of the CFA pile is slightly

different in that concrete is pumped into the borehole at the same time as soil removal. This removes the need to install casing or for the use of slurry. This installation process is similar to that found in auger displacement piles.

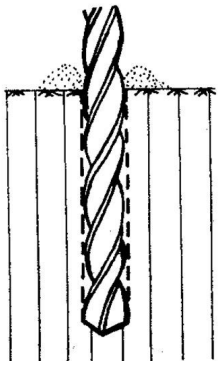

Figure 2-1. A schematic representation of non-displacement pile behaviour in the ground (Van Impe, 1988)

The concept of the CFA pile was initially developed in the 1950s, Van Impe (2004) but its widespread use did not fully occur until the 1980's, Fleming (1995). Since then, advancements in technology have allowed greater utilisation of this piling method. The CFA pile is constructed by using a drilling auger with cutting flights which extend up the central core, Figure 2-2a.

(a) **(b)**

Figure 2-2. A continuous flight auger drilling rig showing the auger stem and drilling flights (a) and the production of spoil during formation of the CFA pile (b)

The auger is drilled down into the soil to the required pile depth. Once at the required depth, the rotation is stopped and the auger is pulled vertically out of the

ground, removing the soil which is trapped in between the flights. As the auger is removed concrete is pumped down through the central core of the auger and flows out through the bottom where it replaces the void created by the excavated soil. Once the pile has been fully formed and the auger removed from the ground, reinforcement can then be installed into the fresh concrete pile.

During the installation process the soil within the auger will begin to move up the flights towards the surface (Figure 2-2b). The soil encased within the flights is known as the soil ribbon as shown by in Figure 2-3.

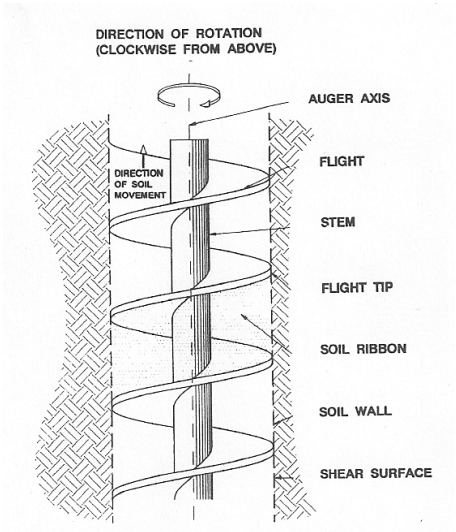

Figure 2-3. Soil behaviour around a CFA pile drilling operation (Thorburn et al., 1993)

CFA piles have the advantage that they are quick to install and compared to driven piles, the installation process is significantly quieter. However, the process does have some disadvantages compared to displacement piles. One of the biggest is the volume of spoil which is produced during construction. The quantity of spoil produced causes spoil disposal issues which can be difficult and expensive to remove. If the piles are installed in contaminated land, the contaminants are brought to the surface where, as well as being expensive to remove, they pose environmental and health risks.

Although the installation process of CFA piles appears straight forward, it requires skilled operation in order to avoid potential problems, Van Weele (1988). It is necessary to achieve a balance between the rotational speed of the auger and the advancement rate. If the CFA auger rotation is too great for the penetration

rate, the soil wall around the auger begins to loosen. This loosening occurs due to the lack of soil being fed from the base of the auger, which allows the soil wall to collapse into the soil ribbon, Fleming (1995), Thorburn *et al* (1993), Troughton *et al* (2012). This infiltration of the soil wall to the soil ribbon reduces the horizontal pressure of the in-situ soil which can cause excessive ground settlements and soil structure instability, Hird *et al* (2008).

2.2.2 Displacement Piles

Displacement piles are generally classed as those which are either driven or jacked into the ground, Tomlinson and Woodward (2008). The driving action during installation does not remove the in-situ soil but causes compaction primarily around the base of the pile, Randolph and Gourvenec (2011).

Displacement piles can be pre-formed from a range of materials, the most common being concrete and steel. Precast concrete piles are usually made in a square cross section while steel piles can be either circular tubing or in the form of I and H sections. Installation of precast concrete piles can be seen in Figure 2-4.

Figure 2-4. Example of installation of driven precast concrete piles (Roger Bullivant Ltd)

Driving of the pile sections can be carried out through repeated application of impact load to the pile head or it can take place by applying a constant load. Driving of the piles will continue until the design installation depth has been

achieved or where no further penetration occurs with repeated load application. If the pile reaches the point where no further penetration occurs, it is known as the refusal point. Pile refusal can occur where an obstruction occurs within the soil strata such as a relatively large boulder or possibly underlying layers of rock.

Using pre-cast displacement piles can be advantageous due to the fact that the quality of the pile material is known before installation. Both the quality of pile material along with the exact pile dimensions are both known before installation takes place which aids in the design process. Unlike non-displacement piles, no spoil is produced due to the installation of displacement piles which requires disposal.

There is however disadvantages to using a displacement pile which have been discussed by Fleming *et al* (2009) and Troughton and Hislam (2012). The primary being that damage to the pile, particularly to the head, can take place during installation which will reduce the soundness of the pile. Other factors include the high levels of vibration and noise which is caused during the installation process, which can restrict their use particularly within urban sites White *et al* (2010). Installation of groups of displacement piles have also been found to cause significant ground heave in the vicinity of the installation site, Fleming *et al* (2009). This soil heaving can cause issues with neighbouring structures and in some cases cause structural damage.

2.3 Auger displacement piles

Auger displacement piles have behavioural characteristics of both displacement and non-displacement piles in terms of how the soil reacts to the installation process. Auger displacement piles cause lateral soil displacement as represented in Figure 2-5.

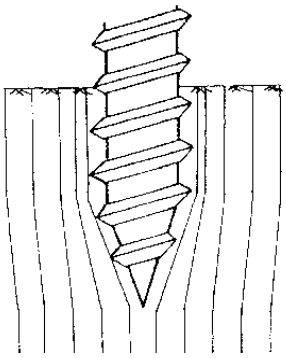

Figure 2-5. A schematic representation of soil displacement around an auger displacement pile (Van Impe, 1988)

Auger displacement piles are constructed in-situ through the use of an auger head attached to a hollow delivery shaft which is drilled into the ground using a high torque rig (Figure 2-6). The auger is advanced through the soil until a suitable founding depth is reached upon which extraction takes place. During extraction of the auger, concrete is pumped down through a hollow central core forming a pile in the process. Once cast, reinforcement can be installed into the pile if required. The auger head is usually sealed with a temporary disposable tip which stops the ingress of soil into the delivery shaft during the installation process. This disposable tip is blown out of the auger head once the concrete pumping begins.

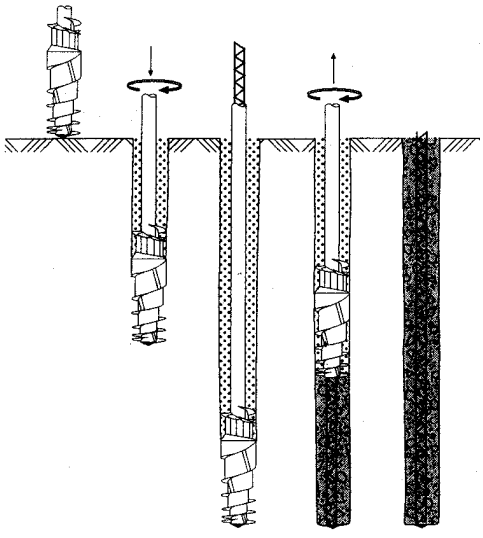

Figure 2-6. Typical installation procedure for auger displacement piles (Bottiau et al 1998)

Auger displacement piles display benefits of both displacement and non-displacement piles. Unlike traditional non-displacement piles, auger displacement

piles do not produce spoil since soil displacement takes place in a similar fashion to the installation of displacement piles. This lack of spoil production makes the piling method an ideal choice on sites with limited space or contaminated land, Wade *et al* (2012), Roger Bullivant Ltd (2007). Compared to the installation of displacement piles, there is virtually no vibration or noise from the installation of auger displacement piles, Van Impe (2004), making them ideally suited for use in congested urban environments. Auger displacement piles have operational benefits due to the speed and ease with which they can be installed. It has also been found that auger displacement piles produce greater load capacities compared to a similar sized non-displacement pile, Bell (2010), Busch *et al* (2010).

Although auger displacement piles have some significant advantages over traditional piling techniques, they do have some limitations. The quality of the constructed pile is known to be dependant on the installation process. A high dependency on multiple factors such as rotation speed, vertical speed and concrete supply rate can all affect the pile installation, Van Impe (2004). This shortcoming is being rectified through the use of fully instrumented piling rigs which will automatically monitor and adjust the relevant installation parameters in order to maintain a quality pile. The installation technique does not allow the assessment of the quality of the installed pile such as measuring the installation energy, therefore a dynamic assessment of the pile is not possible, Bell (2010). To overcome this, a detailed site investigation is required in order to determine a detailed ground investigation report.

Depending on the country where the piles are installed, auger displacement piles can be referred to in a number of different ways. Around mainland Europe they are commonly referred to as screw piles, while in the USA the term drilled displacement pile is used, Nesmith (2002), Basu and Prezzi (2009). In the UK, no specific name is given to the technique and is referred to by utilising both the European and US descriptions, Baxter et al (2006). The Institution of Civil Engineers SPERW (2007) piling guidelines defines them as piles constructed using displacement augers. Some typical example names used throughout the UK

piling industry are 'bored displacement piles', 'screw cast-in-place displacement piles' or the 'Atlas Piling System', Fleming *et al* (2009).

2.3.1 Screw Piles in Mainland Europe

As the use of auger displacement piles, or screw piles as they are more commonly referred to, has developed, many European geotechnical specialist contractors have introduced their own variations. There are five primary screw pile systems used within the European piling market, namely the Atlas, Omega, De Waal, Olivier and the Fundex pile. Each system has been developed by a specific company and although they are all based on a similar principle, there are subtle differences between each.

All the screw pile techniques consist of an auger head which is attached to a hollow delivery shaft. The auger head varies for each of the different screw pile systems as shown in Figure 2-7.

The Atlas pile was originally developed by the Atlas Piling Company which later became the part of the Franki Group, De Cock and Lhoest (1993). The system consists of a main displacement head with a sacrificial tip as shown in Figure 2-7a. The Olivier pile system, installed by the Olivier Co, Holeyman and Charue (2003), consists of a single screw displacement auger head with a small sacrificial tip as shown in Figure 2-7b. The Fundex piling system operates by using a displacement auger head which is completely sacrificial and is left in-situ during the formation of the pile Figure 2-7c.

Both the Omega and De Waal systems have a different auger head than is found on the previous examples. The Omega drilling auger (Figure 2-7d) consists of a varying diameter central core with screw flanges which have varying pitch height, Bottiau *et al* (1998). The auger head has been designed in such a ways as to optimize the effectiveness of soil transportation during the installation stage. A similar design is also witnessed for the De Waal auger head Figure 2-7e.

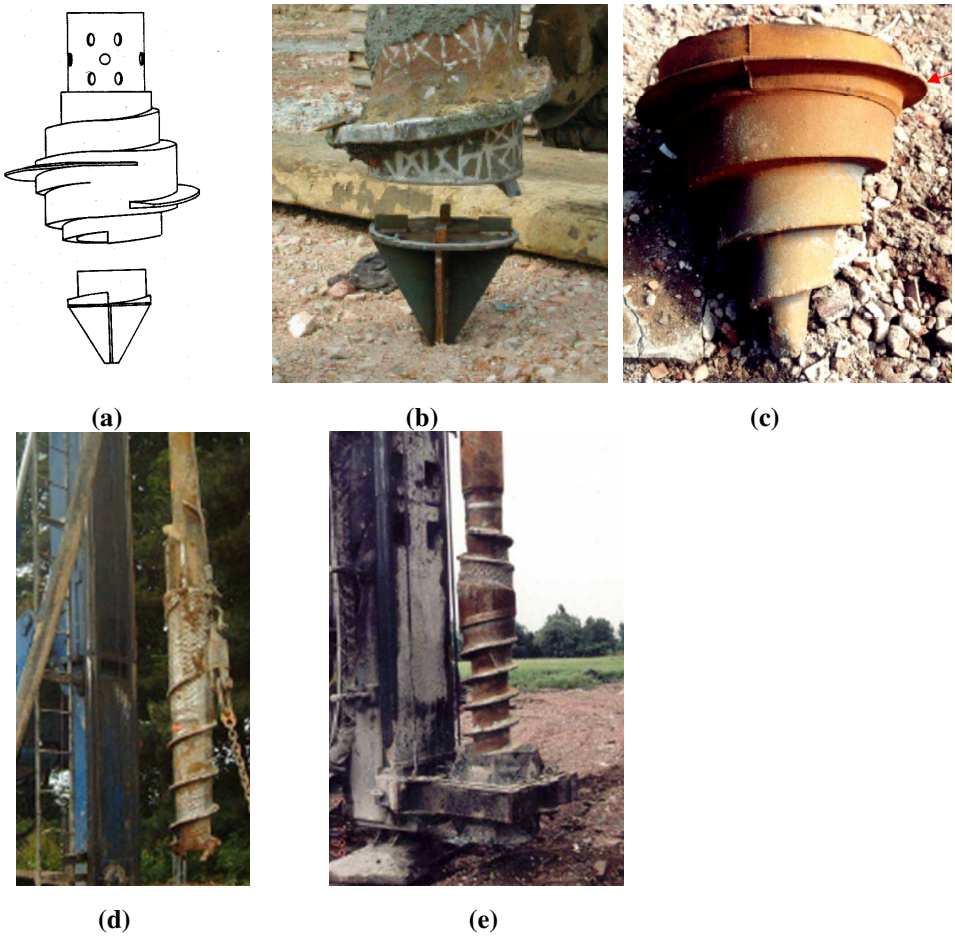

Figure 2-7. Screw pile auger heads for (a) Atlas pile (Hollingsworth & Imbo-Burg, 1992), (b) Olivier pile (Holeyman and Charue, 2003), (c) Fundex pile (Van Impe 2004), (d) Omega pile (Holeyman and Charue, 2003) and (e) De Waal pile (Huybrechts and Whenham, 2003)

Each of the screw piles systems are installed by rotating the auger head in a clockwise direction. Each installation rig applies both high torque and vertical thrust. In the case of the Atlas piling system, vertical thrust is delivered by two hydraulic rams at the lower part of the drilling rig just above the surface of the ground. The rams can be used in an alternative fashion in order to provide a constant vertical force or can be used in tandem to provide short intervals of thrust for instances where soil penetration is difficult, Van Impe (2004).

Variations exist on the extraction process for different screw piling systems. For the Atlas and Olivier system, the auger head is rotated in an anti-clockwise direction during the extraction and formation of the pile. The Omega and De Waal systems are rotated in the same direction used during installation, i.e. clockwise. The Fundex pile has a completely different extraction process. Once ready for

extraction and formation, the sacrificial auger head (Figure 2-7c) detaches while the delivery shaft is rotated in alternating rotations of 180° clockwise and anti-clockwise whilst risen vertically, Holeyman and Charue (2003).

Although similar installation procedures are followed for the different screw pile systems, the completed piles have subtle differences in the characteristics. The Atlas and Olivier piling systems create piles with helical flights surrounding a central core Figure 2-8. The piles completed using Omega, De Waal and Fundex pile systems have comparatively smooth side piles, similar in nature to traditional cast-in-situ non-displacement piles.

Figure 2-8. Excavated Atlas pile displaying the continuous helical flights along the shaft

Full scale tests were conducted using each of the screw pile systems in Belgium between 1998-2002, Huybrechts and Whenham (2003) in order to determine a greater understanding of each system. Holeyman and Charue (2003) reports the load testing results from test piles on the site. Each pile was of similar diameter and installation depth. It was found that a greater capacity was developed from the Atlas and Olivier piles compared to the Omega, De Waal and Fundex piles, suggesting that the helical flight develop greater capacity. It was also found that the Atlas piles developed around 12% greater capacity than the Olivier piles. It was also determined that the bearing capacity of the screw piles was comparable to the capacities determined from driven displacement piles, Van Impe (2004).

Although the European screw piles operate on a similar principle of construction, it is clear that depending on the drilling auger and installation procedures, the final pile constructed differs. The Atlas and Olivier piles have distinctive screw flanges throughout their length while the Omega, De Waal and Fundex piles have relatively smooth edges, similar to those found on traditional non-displacement piles. This difference in the constructed shape of the pile also affects the bearing capacity of the pile, Van Impe (2004).

2.3.2 Auger displacement piles in the UK

Auger displacement piles in the UK have been used since 1990 when the Atlas pile was introduced, Hollingsworth and Imbro-Burg (1992) but their use has been increasing over recent years, Baxter (2006). This increase can be attributed to the number of benefits associated with the piling technique that have already been discussed.

Similar to the European experience, a number of UK geotechnical foundation specialists have introduced auger displacement piles, all of which are based upon the European systems. Each individual company has carried out modifications or alterations to each system and market them under specific commercial names.

Cementation Skanska offer a variation of the Atlas pile known as the screw displacement pile and also an auger displacement piling system similar to the Omega pile (Figure 2-9). The screw displacement pile forms a central core with large helical flanges along the pile length while the auger displacement system produces a relatively straight sided pile.

(a) (b)

Figure 2-9. Auger displacement piles offered by Cementation Skanska (a) screw displacement pile (b) auger displacement pile (Cementation Skanska)

Bachy Soletanche UK offer a piling system known as the Rotary Displacement Pile or the 'Screwsol' pile. The screwsol drilling auger, Figure 2-10, is a similar in nature to the Olivier or De Waal piling augers. The auger forms a central core with helical ribs along the pile length.

Figure 2-10. Screwsol drilling auger (Bachy Soletanche)

In the developing market of auger displacement piles in the UK, these piling systems mentioned are not an exhaustive list but simply highlight a few of the more commonly used systems at present.

2.4 The Continuous Helical Displacement Pile (CHD)

The Continuous Helical Displacement (CHD) pile is a form of auger displacement pile which has been developed by Roger Bullivant Ltd (RBL) and has been in common use since the later 1990's. The CHD consists of a hollow auger head and helical flange which extends up the head for 1.2 full revolutions (Figure 2-11). The auger head has a maximum diameter at the central core which then tapers at both ends. The upper section of the auger head attaches to the delivery shaft while the lower tapered end forms the discharge tip. Concrete is pumped down through the hollow delivery shaft and flows out at the discharge tip which is sealed with a temporary sacrificial bung to stop the soil plugging the discharge tip during penetration.

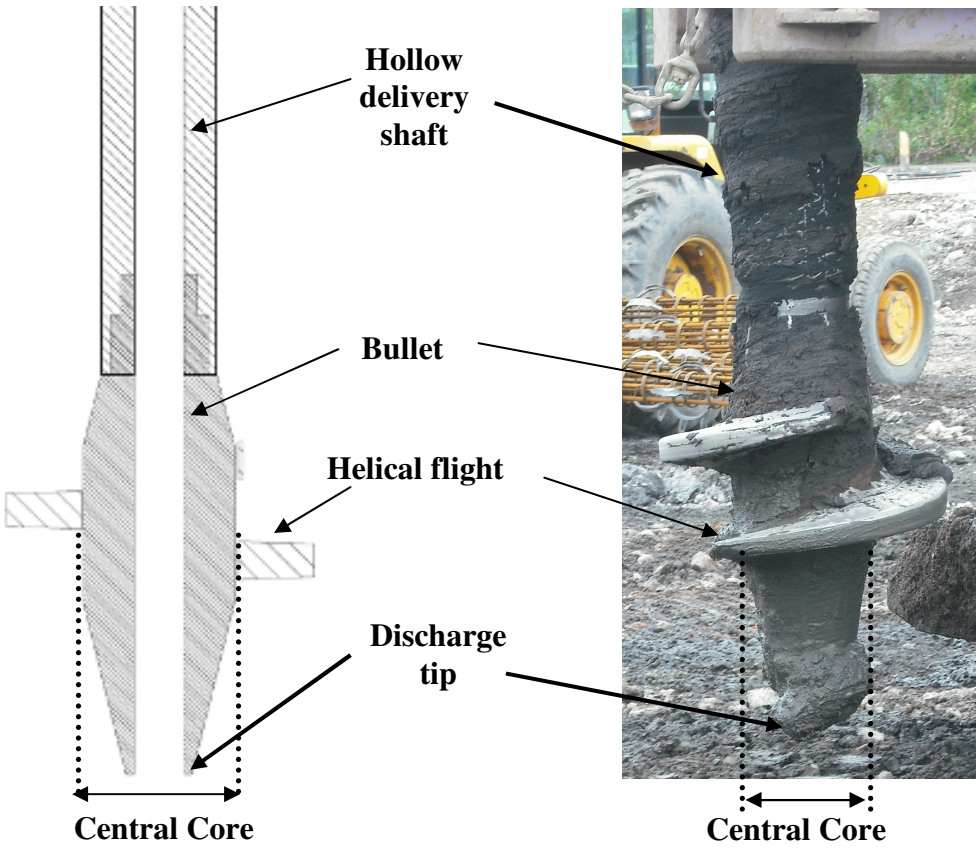

Figure 2-11. CHD bullet and delivery shaft cross section view

The auger is more commonly referred to as the CHD bullet and is shown in Figure 2-12. At the delivery tip of the bullet are two small cutting teeth. These teeth aid the insertion of the bullet during the installation stage but do not contribute to the

pile construction. The CHD bullet's closest comparison in terms of physical structure is to the Atlas pile however there are subtle differences such as the bullet length, flight pitch and the cutting teeth.

Figure 2-12. The CHD bullet

The bullet is attached to a drilling rig which provides both vertical force and a high torque, Figure 2-13. The drilling rig is constructed on a set of caterpillar tracks with a specially modified superstructure (Figure 2-13a). The rig contains all the necessary motor and compressors to provide the required vertical force and high torque. Concrete is supplied into the drilling rig using a concrete pumping truck. With the sacrificial plug in place, the bullet is rotated in a clockwise direction while an instantaneous vertical force is applied (Figure 2-13b). During the penetration of the bullet, the maximum rotation and vertical force the drilling rig is capable of producing is used. The penetration rate will vary depending on the in-situ ground conditions but typical advance rates can be 3.5m/min.

(a) (b)

Figure 2-13. The complete CHD drilling rig with concrete supply feed (a) and close up of the CHD bullet in the drilling rig prior to penetration (b)

Once the necessary pile depth is reached the bullet is stopped and retracted to create a gap in the soil to allow the removal of the sacrificial tip. This is achieved by rotating the bullet in an anti-clockwise direction whilst applying a vertical upwards force. The bullet is only moved enough distance to release the soil around the discharge tip. Once ready for extraction, concrete is pumped at pressure through the hollow shaft and bullet where it blows out the sacrificial tip and starts to form the pile. Depending on the ground conditions encountered, the pumping pressure typically ranges from 0.5-1.25 MPa (5-12.5bar). As the concrete is pumped the bullet is rotated in an anti-clockwise direction whilst a vertical upward force is applied. As the bullet is extracted, the concrete fills the void in the soil to form the helical pile. Once the pile has been formed, reinforcement can be installed if required.

The pile integrity and ultimate performance is dependent on both the extraction rate and the rate at which the concrete is supplied. Early CHD piles were highly dependant on the operators experience however, the installation and extraction process are now carried out with the aid of an onboard computer.

The rotation speed and vertical thrust of the drilling rig are adjusted depending on the resistive torque produced by the soil and also the flow of the concrete. To ensure a uniform pile, the onboard computer will increase or decrease the bullets rate of extraction if there are fluctuations in concrete delivery rate. The optimum extraction rate for a CHD pile is currently 5 revolutions per metre which ensures the helical flights have a pitch of 200mm. The speed with which a CHD pile can be formed will depend on the in-situ ground conditions but a typical CHD can be formed at a rate of 1.5m/min, meaning for a 10m long pile, a CHD will take around 12 minutes to construct.

A completed CHD pile has a central core with helical flights continuing the entire length as shown in Figure 2-14. There are two CHD piles sizes which are currently used, the 300/600 and the 400/700 style. The style sizes correspond to the core and flight diameter of the bullet in millimetres. The most commonly used bullet size is the 300/600 which has a central core diameter of 300mm and a flight diameter of 600mm. In terms of the completed pile that is cast, the Atlas piling system is found to be of a similar nature to the CHD pile. Although numerous alternative auger displacement piles are available, the Atlas pile is the only method which has similarities with the CHD in terms of the bullet design, installation procedure and completed pile.

(a) **(b)**

Figure 2-14. Well formed CHD piles (a) partial excavated (b) exhumed pile (Roger Bullivant Ltd) showing the helical flights surrounding the central core

2.4.1 Existing Research on CHD piles

In 1998, research was conducted by the Geotechnical Consulting Group (GCG) on the CHD pile to improve the understanding of the method. This work analysed a collection of pile tests with the aim of establishing an appropriate design procedure suitable for CHD piles. Although the research investigated a large collection of CHD test piles, most were terminated before an ultimate pile capacity could be determined. The back analysis of the pile data was used simply as an indication of the pile performance and could not fully reflect the true pile behaviour.

An issue highlighted from the GCG research was the appropriate selection of CHD diameter for use in pile design. Because of the varying cross section of the CHD piles, a number of different diameters can be found along the pile length as highlighted in Figure 2-15. At the time of the research, it was estimated that taking the central core diameter, D_c, would result in conservative design capacities. However with limited knowledge of this new piling method at the time, taking the flange diameter, D_f, was felt to potentially over predict the pile capacity.

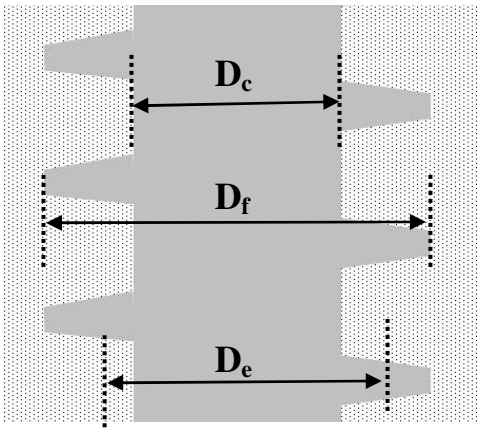

Figure 2-15. CHD pile cross section showing different diameters

The GCG report tried to determine the design or 'effective' diameter (D_e) for a CHD pile by referring to work carried out on other auger displacement piles of a similar nature to the CHD, typically the Atlas pile. It highlights two methods which try to determine the effective diameter of an auger displacement pile.

The first method is that proposed by Van Impe (1988). After research carried out on the Atlas screw pile, he suggested that the effective diameter is dependent on the flange thickness. The flange thickness is controlled by the vertical pull out force of the drilling rig during construction, Van Impe *et al* (1988). An increased pulling force will produce thicker flanges and consequently the distance between each flange in the vertical plane will increase. This increased distance allows soil remoulding and compaction to take place around the flanges, as shown as the shaded region between points A and B in Figure 2-16. The soil within this region was removed from excavated field piles during the research and was found to have greater shear strength than the surrounding soil, Van Impe *et al* (1988). Due to this increased shear strength it is suggested that the effective diameter can be taken as the outer flange diameter. However, this theory is only valid for thick flanges, Van Impe *et al* (1988). For small flanges, the same shear strength increase is not present and therefore it is suggested that the effective diameter be taken as the core diameter plus an additional 10%, $1.1D_c$. The actual definition of thick or thin flanges is not provided by Van Impe *et al* (1988).

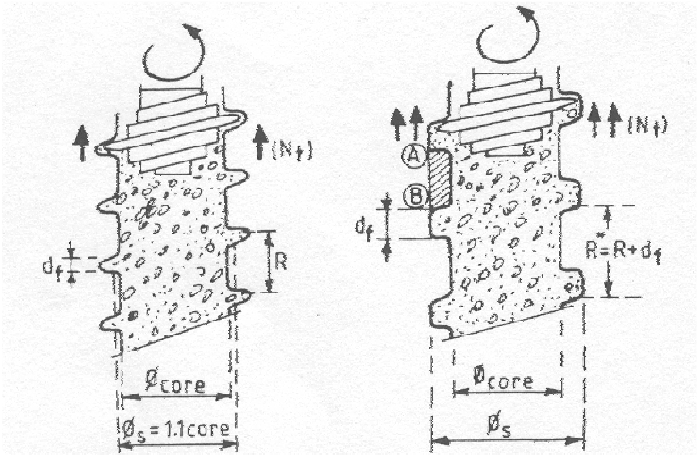

(a) **(b)**

Figure 2-16. Atlas pile flange characterisation (a) thin flanges (b) thick flanges (Van Impe, 1988)

The second proposal for effective diameter is that suggested by Bustamante and Gianeselli (1993). Again, research conducted on Atlas test piles in a variety of soil conditions concluded that the effective diameter should be taken as $0.9D_f$. This was determined through observations on Atlas piles after extraction and confirmed by back analysis from test load data.

As an alternative to adhering to either the Van Impe or Bustamante & Gianeselli methods, it was suggested for CHD piles that the effective diameter be taken as the average of the core and external flange diameters by the Geotechnical Consulting Group (1998). For a standard RBL 300/600 CHD pile this places the effective diameter at 450mm. This design diameter was adopted across the RBL network of offices until around 2002 when the Scottish office changed to a full 600mm design diameter since the piles appeared to be over designed.

Research on the CHD pile was conducted by Frangoulides (1999) in order to investigate the performance of model CHD piles installed in clay soil. Analysis of the model tests concluded that the soil shear surface did not develop until the edges of the flights and it was therefore suggested that the full flight diameter be used in the design. However, this research was carried on an early bullet design which has subsequently been changed. The original 'long nose' bullet design, as used in the Frangoulides (1999) model tests, had almost twice the distance between the discharge tip and the flanges than the current 'short nose' bullet, as shown in Figure 2-17. Although it is assumed this change has created improved flow of concrete to create a more sound pile, no investigation has been carried out on this new design.

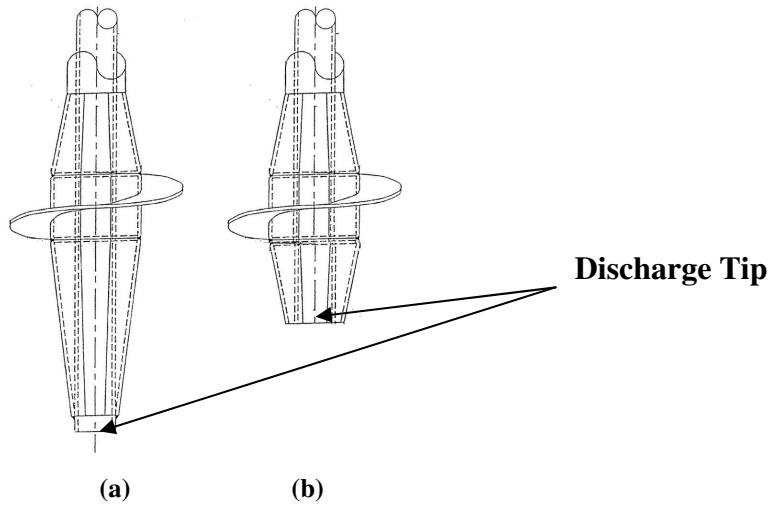

Figure 2-17. Differences in CHD bullet design (a) original long nose and (b) current shorter version (cutting teeth at the discharge tip are not shown for clarity)

2.5 Design of pile capacity

Regardless of the installation method, it is important that an appropriate pile design can establish the ultimate capacity of the pile. A pile must be designed in such a way as to ensure the applied load is transferred to the in-situ soil without causing either geotechnical failure of the soil structure or structural failure of the pile itself. This is achieved by using the in-situ soil properties in well established design methods to predict the maximum load which can be safely applied to the pile. In order to enable an analysis of the CHD pile test data, an understanding of current procedures used in general pile design must be established.

Pile capacity can be assumed to develop in three ways based on Tomlinson and Woodward (2008), as shown in Figure 2-18. Firstly, capacity can be attributed from the shear resistance developed between the pile-soil interfaces. These piles are known as skin friction piles and are generally found in fine-grained soils. The second form of pile are called end bearing piles. These types of piles are generally found in course-grained soils or in soil where there is a firm stratum, such as rock, at the pile tip. The third assumption is where the pile gains capacity from both shaft and base. In general all piles will have some contribution to capacity from both shaft friction and base resistance albeit in varying ratios.

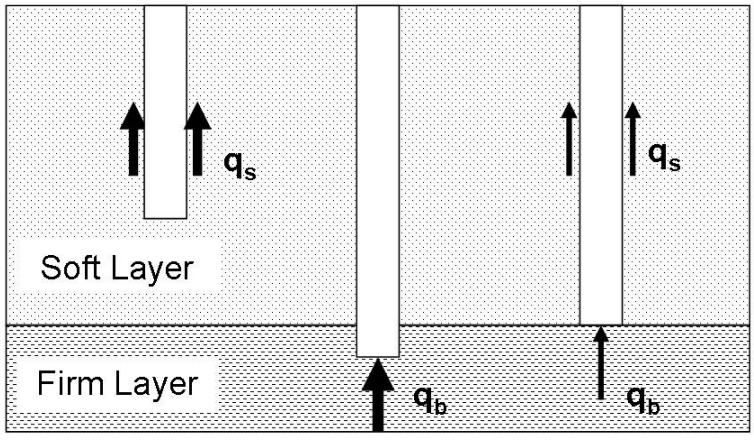

Figure 2-18. Types of pile bearing piles (a) skin friction piles (b) end bearing piles and (c) combination of skin and base resistance

The ultimate pile capacity of a pile is determined using the general formula in equation 2-1 as described by Tomlinson (1994), Fleming *et al* (2009) and Bell and Robinson (2012).

$$Q_T = Q_S + Q_B = q_s A_s + q_b A_b \quad \textbf{2-1}$$

Where: Q_S = Total Shaft Capacity
Q_B = Total Base Capacity
q_s = Unit shaft resistance
A_s= Area of shaft
q_b= Unit base resistance
A_b= Area of pile base

The specific site investigation method used at a project location will usually dictate the design process used for the piles. Some different design procedures used in pile design are summarised below.

2.5.1 Effective stress design approach for piles

An effective stress approach is historically used to design piles installed in course grained soils while a total stress approach is used for fine grained soils, Bell and Robinson (2012). The effective stress design approach utilises soil properties determined through site investigations techniques such as borehole logs or standard penetration tests. The shaft friction is calculated using equation 2-2.

$$q_s = k\bar{\sigma}_v^{'} \tan\delta \quad \textbf{2-2}$$

Where: k = coefficient of earth pressure
$\bar{\sigma}_v^{'}$ = average vertical effective stress around pile shaft (kPa)
δ = Interface angle of friction between pile and soil

The interface angle of friction can be determined using a number of techniques. It can be established through direct shear box tests as discussed by Subba Rao *et al* (1998). It can also be related to the surface roughness of the material of the pile as detailed by Kishida and Uesugi (1987), however this is difficult for cast-in-situ piles where the surface roughness is unknown. Alternatively, Fleming *et al* (2009) suggests the interface friction angle can be conservatively estimated as equal to the critical state angle of friction of the in-situ soil. Relationships between the pile material and the in-situ friction angle of between 0.8 and 1.0 have been suggested by Kulhawy (1984) and discussed by Tomlinson and Woodward (2008).

The earth pressure coefficient is dependent on the coefficient of earth pressure at rest K_0, the pile installation method and the soil density. The selection of the K_0 value can be determined through the use of equation 2-3 after Kulhawy (1984), where ϕ_p' is the peak angle of shearing resistance of the in-situ soil. The effect of the soil stress history on the K_0 is considered by Mayne and Kulhawy (1982a) using equation 2-4. The earth pressure coefficient k is assumed to vary with pile installation technique and often expressed as a function of K_0 (Table 2-1).

$$K_o = 1 - \sin\phi' \qquad \textbf{2-3}$$

$$K_0 = (1 - \sin\phi')OCR^{\sin\phi'} \qquad \textbf{2-4}$$

*OCR = Overconsolidation ratio

Table 2-1. Relationship between k and K_0 for different pile types after (Kulhawy 1984)

Pile Installation Method	k/K_0
Displacement – Large displacement	1-2
Displacement – Small displacement	0.75-1.25
Non-Displacement	0.7-1

Fleming et al (2009) suggests general k values which could be adopted based on the installation method. A k value of 0.7 could be used for 'conventional' bored piles, 0.6 – 0.9 for continuous flight auger piles while 1.2 and greater can be applied to cast-in-situ driven piles. These values do not account for variations in soil conditions however. Bell (2010) and Jeffrey (2010) suggest that the selection

of an appropriate k value for auger displacement pile are in excess of those currently suggested for current displacement and non-displacement piles.

The end bearing pressure from equation 2-1 is defined in equation 2-5.

$$q_b = N_q \sigma_v^{'} \qquad \textbf{2-5}$$

Where: N_q = Bearing capacity factor

$\sigma_v^{'}$ = Effective vertical stress at pile base (kPa)

The bearing capacity factor can be determined using the soil friction angle ϕ' at the pile base through relationships proposed by Berezantzev *et al* (1961) or Brinch Hansen (1961) shown in Figure 2-19. It was found that the bearing capacity factor varies with the ratio of pile depth/ pile diameter as discussed by Meyerhof (1976). Bearing capacity factors suggested by Berezantzev are widely accepted for use in driven pile design, Tomlinson and Woodward (2008), Fleming et al (2009) and Bell and Robinson (2012).

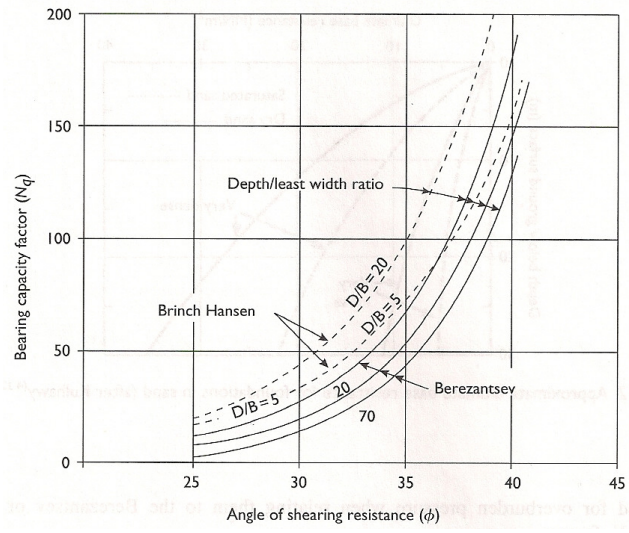

Figure 2-19. Bearing capacity factors based on Berezantzev (1961) and Brinch Hansen (1961) from (Tomlinson and Woodward, 2008)

2.5.2 Total stress design approach for piles

As was mentioned previously, a total stress design approach is typically followed for piles installed in fine grained soils, Bell and Robinson (2012). Piles installed

in fine grained soils tend to have a greater proportion of capacity development from the shaft than is typically found in piles installed in sands, Fleming *et al* (2009). The unit shaft resistance is given in equation 2-6.

$$q_s = \alpha s_u \qquad \textbf{2-6}$$

Where: α = empirical adhesion factor

s_u = undrained shear strength of the soil

For the purpose of design of piles in fine grained soils, the undrained properties are used. Suggested adhesion factors can range from 1.0 to 0.25 depending on the undrained shear strength of the in-situ soil. Some typical values for piles installed in a uniform soil deposit are presented in Figure 2-20.

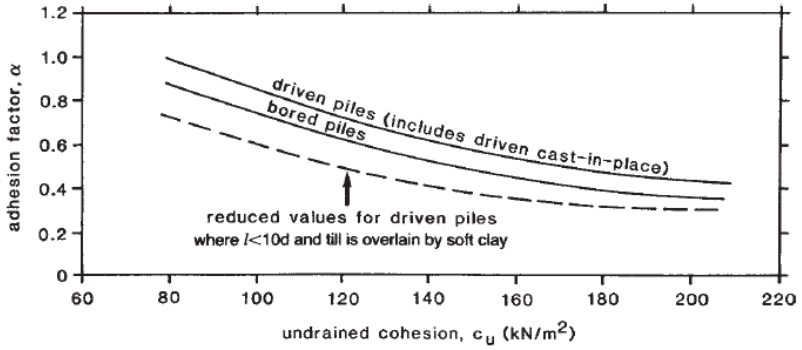

Figure 2-20. Suggested adhesion factors for piles installed in uniform soil deposit after (Weltman and Healy, 1978) (reported by (Fleming et al., 2009)

The American Petroleum Institute (API) defines the adhesion factor in terms of the vertical effective stress at the mid shaft of the pile. Typical ranges given for driven pipe piles are suggested by using equation 2-7 from API (2005).

$$\alpha = 0.5\left(\frac{s_u}{\sigma_v^1}\right)^{-0.5} \quad \text{for} \quad \frac{s_u}{\sigma_v'} \le 1$$

$$\alpha = 0.5\left(\frac{s_u}{\sigma_v^1}\right)^{-0.25} \quad \text{for} \frac{s_u}{\sigma_v'} > 1 \qquad \textbf{2-7}$$

The end bearing pressure is given in terms of bearing capacity factor, N_c, and the undrained shear strength, s_u, of the soil as shown using equation 2-8.

$$q_b = N_c s_u \qquad \textbf{2-8}$$

The bearing capacity factor is taken as 9 after research carried out by Skempton (1951) assuming that the pile has been penetrated to a depth greater than 5 times the pile diameter.

2.5.3 Design using cone penetration test cone resistance

The use of the cone penetration test (CPT) as part of the geotechnical site investigation allows in-situ soil properties to be obtained. The penetration of a CPT probe resembles the bearing response of a pile, Gavin and Lehane (2007) and as such, a number of relationships between CPT cone resistance and pile capacity have been established. Many organisations, primarily in the offshore industry, have adopted their own interpolations of linking pile shaft and base resistance to the CPT cone resistance for use in the design of pile capacity

A widely used method to determine the end bearing pressure for a pile foundation based on cone resistance is know as the Dutch method, Brouwer (2007), Meigh (1987) and Lunne et al (1997). The Dutch method establishes an average cone resistance over a distance of 4D below and 8D above the pile base. This average cone resistance is then used directly as the end bearing pressure in equation 2-1.

The Dutch method determines the unit shaft resistance by taking a percentage of the CPT cone resistance. For course grained soils, the unit shaft resistance q_s is taken as 1.0% of q_c with a maximum value of 150kPa. For fine grained soils, the unit shaft resistance for the pile is taken as 3.5% of the CPT cone resistance q_c up to a maximum of 120 kPa, Brouwer (2007).

A more in depth design procedure than the Dutch method has been developed, known as the Imperial College pile design method (ICP), as discussed by Jardine

et al (2005). It was previously known in the offshore industry as the Marine Technology Directorate (MTD) method, however, the MTD no longer exist, so the method adopted the name of the Imperial College. The design methods primarily relate the CPT cone resistance to the design of driven steel piles used in the offshore industry.

The unit base resistance for closed ended piles is related to the average cone resistance at 1.5D above and below the pile base using equation 2-9.

$$q_b = N_{ICP} q_c \qquad \textbf{2-9}$$

For piles installed in cohesive soils, the N_{ICP} factor is equal to 0.8 for undrained loading conditions or 1.3 for drained loading conditions. For piles installed in course grained soils, the N_{ICP} factor is defined using the pile diameter D to CPT diameter ratio using equation 2-10.

$$N_{ICP} = 1 - 0.5 \log\left(\frac{D}{D_{CPT}}\right) \qquad \textbf{2-10}$$

The unit shaft resistance of the pile is determined through the use of equation 2-11.

$$q_s = \sigma_r^{'} \tan\delta \qquad \textbf{2-11}$$

Where $\sigma_r^{'}$ = Radial effective stress acting on the pile.

For course grained soils, the radial effective stress is defined using equation 2-12

$$\sigma'_r = \left(0.29 q_c \left(\frac{\sigma_v^{'}}{P_a}\right)^{0.13} \left(\frac{h}{R}\right)^{-0.38}\right) + \Delta\sigma_{rd}^{'} \qquad \textbf{2-12}$$

Where $\Delta\sigma_{rd}^{'}$ is the dilatant increase in local radial effective stress during loading of the pile, the cone resistance q_c, is integrated across the installed pile length. The

P_a is the atmospheric pressure, h is the height above the pile base and R is the pile radius. For fine grained soils, the radial effective stress from equation 1-11, is defined using equation 2-13.

$$\sigma'_r = \left(\left(2.2 + 0.016YSR - 0.87\Delta I_{vy}\right) YSR^{0.42} \left(\frac{h}{R}\right)^{-0.2} \right) \sigma'_{v0} \qquad \textbf{2-13}$$

YSR = yield stress ratio

ΔIvy = log10(clay sensitivity)

Similar to the ICP method, a widely utilised CPT pile design method is the UWA-05 method as explained by Lehane *et al* (2005). The UWA-05 method defines the end bearing pressure on a close ended pile in fine grained soils as $0.6q_{ca}$. The average cone resistance around the base, q_{ca} is determined through the use of the Dutch averaging method. The shaft resistance is determined using equation 2-11. The radial effective stress for the UWA-05 is defined using equation 2-14.

$$\sigma'_r = 0.03 q_c \left(A_{rs}\right)^{0.3} \left[\max\left(\frac{h}{D}, 2\right) \right]^{-0.5} \qquad \textbf{2-14}$$

The A_{rs} value takes into consideration the potential for soil filling when pipe piles are installed and is dependant on the pile diameter. It is equal to 1 for solid piles.

Both the ICP and UWA-05 pile design methods are firmly based on the design of driven off shore piles, and as such, the applicability to either onshore displacement or non-displacement piles may need to be verified.

2.5.4 Procedures used in Auger displacement pile design

The research carried out on screw piles has provided tailored design procedures for auger displacement piles. One procedure presented by Van Impe (1988) establishes the pile capacity by using the data from CPT cone resistance. In the Van Impe method, the unit shaft resistance is established using equation 2-15.

$$q_s = \eta_p q_c \quad \textbf{2-15}$$

The correction factor η_p values are suggested for varying soil conditions in Table 2-2. The correction factors established are based on research conducted predominantly on Atlas screw piles.

Table 2-2. Suggested CPT cone resistance correction factors for shaft friction screw pile design from Van Impe (1988)

Soil Type	Range of q_c Values (MPa)	Shaft correction factor η_p
Silty Clay	3-5	0.03
Loose Sand	3-5	0.03
Stiff Clay	> 2	0.013
Medium compact sand	≤ 15	0.01
Compact sand	> 15	0.005

The unit base resistance is determined through the use of equation 2-16.

$$q_b = N_V q_c \quad \textbf{2-16}$$

The reduction factor N_v takes into account the pile installation method and suggested values are shown in Table 2-3.

Table 2-3. Base correction factors for CPT cone resistance for the Van Impe method (Van Impe 1988)

Pile Type	Base reduction factor N_v
Driven displacement	1.15
Auger displacement	1.0
Non-displacement	0.8

Bustamante and Gianeselli (1982) propose a procedure for pile design which accounts for different installation techniques along with variation in soil type. The unit base resistance is determined using equation 1-17.

$$q_b = k_c q_{ca} \quad \textbf{2-17}$$

Where k_c = bearing capacity factor

q_{ca} = average cone resistance around pile base

Suggested bearing capacity factors k_c are presented by Bustamante and Gianeselli (1982) in Table 2-4. Group classification depends on the pile installation method. Group I consists of traditional non-displacement piles while displacement and auger displacement piles are considered group II. These are seen to be much lower than those suggested in Table 2-3 by Van Impe (1988).

Table 2-4. Bearing capacity factors, k_c from Bustamante and Gianeselli (1982)

Soil Type	Bearing capacity factor k_c	
	Group I	Group II
Soft clay	0.4	0.5
Moderately compact clay	0.35	0.45
Stiff clay	0.45	0.55
Loose sand	0.4	0.5
Moderately compact sand	0.4	0.5
Compact sand	0.3	0.4

The average cone resistance q_{ca}, is determined using a similar technique to the Dutch method, using Figure 2-21. The average CPT cone resistance $q_{ca}^{'}$ is determined over a distance equal to 1.5D, where D is the pile diameter, above and below the pile base. Limitations on cone resistance are put in place which corresponds to a range equal to $0.7\,q_{ca}^{'}$ and $1.3\,q_{ca}^{'}$. By excluding any cone resistance q_c values which fall out with this range, the average cone resistance is determined.

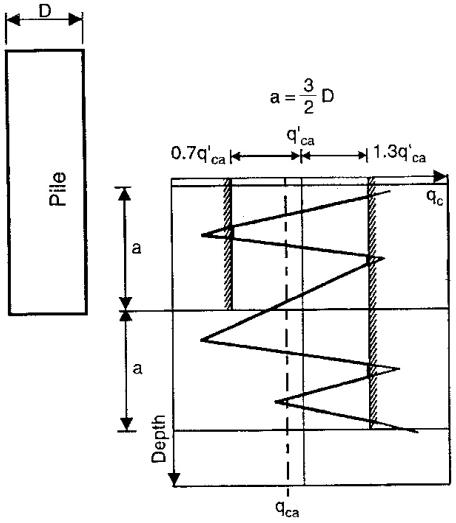

Figure 2-21. Determination of the equivalent average cone resistance using the Bustamante and Gianeselli (1982) method

The shaft friction based on the Bustamante and Gianeselli (1982) method is determined by dividing the measured CPT cone resistance by a friction coefficient α using equation 1-18. The selection of friction coefficients are based on pile installation methods in different soil types as presented in Table 2-5. In the classification of the piles, non-displacement and auger bored piles fall into group IA, while concrete displacement piles are group IIA according to Bustamante and Gianesilli (1982). They are found to correspond with values suggested by Van Impe.

$$q_s = \frac{q_c}{\alpha} \qquad \textbf{2-18}$$

Table 2-5.Shaft friction coefficient α for varying pile types from Bustamante and Gianeselli (1982)

Soil Type	Friction coefficient α	
	Group IA	Group IIA
Soft clay	30	90
Moderately compact clay	40	40
Stiff clay	60	60
Loose sand	60	60
Moderately compact sand	100	100
Compact sand	150	150

In Bustamante and Gianeselli (1998), further design coefficients are provided specifically for auger displacement piles. The revised and specific bearing capacity factor k_c for auger displacement piles are between 0.5-0.75 in sands and 0.55-0.65 in clay (Table 2-6), slightly higher than those previously suggested in Table 2-4 but still lower than those suggested by Van Impe (1988) in Table 2-3. The unit shaft resistance is determined through the use of design curves shown in Figure 2-22, the curve selection is determined through the use of Table 2-7, Bustamante and Gianeselli (1993).

Table 2-6. Bearing capacity factors for different soil types specifically suited for auger displacement piles after Bustamante & Gianeselli (1998)

Soil Type	Bearing capacity factor k_c
Clay	0.55-0.65
Sands	0.5-0.75

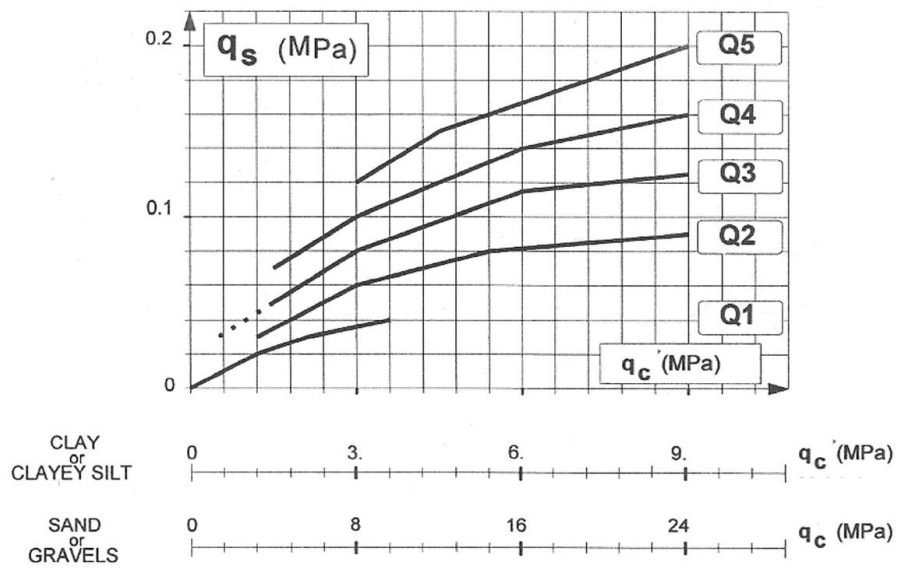

Figure 2-22. Design curves for skin friction q_s for use with screw piles to be used with Table 2-7, Bustamante and Gianeselli (1993)

Table 2-7. Design curve selection for different soil conditions, Bustamante and Gianeselli (1993)

Soil Type	q_s Curve	For use with q_c (MPa)
Clay or clayey silt	Q1	<1.0
	Q3	>1.5
	Q4	≥3.0
Sand or Gravel	Q1	<1.0
	Q4	>3.5
	Q5	>8.0

2.5.5 Roger Bullivant Ltd CHD Pile Design

The design procedure for CHD piles was investigated during the research carried out by the Geotechnical Consulting Group (GCG) in 1998. The initial design procedure was based on procedures and parameters set out for standard non-displacement piles (sections 2.5.1 and 2.5.2). Possible design procedures for auger displacement piles were investigated, with the Van Impe (1988) and the Bustamante & Gianesilli (1982) methods being suggested as potential options.

The Van Impe method was disregarded as an option due to the fact that it relied on CPT, a site investigation method which is not as commonly used in the UK at the time compared to mainland Europe. The Bustamante & Gianesilli (1982) method was investigated due to the fact that the method offered correlations with SPT blow counts. It was found that the Bustamante & Gianeselli (1982) method with SPT correlations were unreliable for accurately predicting the capacity and was found to over-estimate. For this reason it was recommended not to adopt the correlations of the pile design method. Similar for the reasons regarding the lack of CPT use, the Bustamante & Gianeselli (1982) method was not suggested as the primary design procedure for CHD piles.

The GCG report suggested that RBL design the CHD piles using a design approach similar to that used for CFA piles, using assumed parameters for CHD piles. The CFA design method follows the effective stress design process

described in section 2.5.1 and 2.5.2. It was suggested that the effective diameter used in the design process should be taken as the mid point between the central core and the outer flange, known as the effective pile diameter. In sands, the earth pressure coefficient *k* in equation 2-2 was suggested to fall within the range of 1.0 – 2.0 but is currently taken as 1.2, similar to what is suggested for displacement piles. The end bearing coefficient, N_q is based on those suggested by Berezantzev *et al* (1961). In fine grained soils the empirical factor α in equation 2-6 is suggested to be taken as 1.0 as this produced a conservative design, Geotechnical Consulting Group (1998). The end bearing factor N_c in equation 2-8 is kept as equal to 9.

Where CPT data is available for a project site, the CHD piles follow a modified design procedure which utilises the cone resistance. The unit base resistance for both fine grained or course grained soils is assumed to equal the cone resistance value obtained directly from the CPT, Geotechnical Consulting Group (1998).

The unit shaft resistance in sands is determined by dividing the measured cone resistance by a correction factor, α_{LCPC}. The correction factors were initially based on those suggested by Bustamante and Gianeselli (1982), however they are typically taken as 150-300 for CHD piles. For fine grained soils, the CPT cone resistance is used to calculate an estimated soil shear strength value using equation 2-19 after Lunne *et al* (1997).

$$S_U = \frac{q_c - \sigma_v'}{N_K} \qquad \textbf{2-19}$$

Where the term N_k can vary from 11 to 20 depending on the soil type but is generally assumed to equal 15 when CHD piles are used. The calculated shear strength value is then used in equation 2-6 in a similar manner used in the total stress approach.

Table 2-8. Summary of parameters used in CHD pile design following the Roger Bullivant Ltd method

Effective Stress	Unit Resistance	Design Parameter
Sand	Shaft	k = 1.2
	Base	N_q = Berezantzev (1961)
Cohesive Soil	Shaft	α = 1.0
	Base	N_c = 9
CPT Design		
Sand	Shaft	α_{LCPC} = 150-300
	Base	Measured CPT q_c
Cohesive Soil	$S_U = \frac{q_c - \sigma_v'}{N_K}$	N_K = 15
	Shaft	α = 1.0
	Base	N_c = 9

2.6 Interpretation of pile load tests

The procedures discussed for pile design in section 2.5 allow an estimate pile capacity to be determined. In order to assess the accuracy of these design procedures it is usual to conduct load tests which determine the ultimate pile capacity. Pile testing is typically undertaken using the guidelines set out by the Institute of Civil Engineer (2007), *Specification for Piles and Embedded Retaining Walls,* SPERW. Numerous pile testing methods are available, as discussed by Brown (2012), however CHD piles which are investigated during the course of this research are tested using the Maintained Load Test (MLT).

The following section discusses the interpretation of pile load test results in order to obtain an appropriate pile capacity.

2.6.1 Determination of ultimate pile capacity from load tests

The determination of the ultimate capacity from a pile test can be difficult to define due with various criteria available, Brown (2012). The ultimate pile capacity can be defined by Weltman (1980) and SPERW (2007) as the maximum

load that can be applied to a pile that will induce an increase in pile settlement without any further increase in load, shown as the ultimate capacity in Figure 2-23. The ICE SPERW (2007) guidelines suggest that this is the only definition for ultimate pile capacity which should be used. The application of this method can however be difficult on piles installed in course grained soils where the pile test load-settlement curve continually increases and the criteria limitations are never achieved, Ellis and Williams (1972), Brown (2012).

Alternative definitions of pile capacity stem from settlement limits based on the pile dimensions. The most common definition relates to ultimate pile capacity to the load which causes a settlement of 10% the diameter of the pile, Weltman (1980), Fleming (1992), Bustamante and Gianeselli (1998) and Tomlinson and Woodward (2008). It has been also been suggested by Van Impe *et al* (1988) that pile capacity can occur at a settlement equal to 30% of the pile diameter for non-displacement piles.

A commonly used criteria used in North America is the Davisson offset limit method as discussed by Fellenius (2001b). The offset limit was developed by Davisson (1973)) to suggest a capacity based upon the elastic shortening of the pile, Fellenius (2006). The offset limit load is defined as the intersection point of the load-settlement line of the test pile with the line created using equation 2-20.

$$w_o = \delta_p + (4 + 8D) \qquad \textbf{2-20}$$

Where w_o = Offset pile head movement

δ_p = Elastic shortening of the pile calculated using equation 2-21

$$\delta_p = \frac{PL}{AE} \qquad \textbf{2-21}$$

Where P = Applied load

L = Pile length

A = Cross sectional area of pile

E = Elastic modulus of the pile material

The Davisson offset limit does not give the ultimate capacity of a pile, it gives a limiting value of where it is expected that the soil will displace without the effects of the pile stiffness, Fellenius (2006). The benefit of the method is that the offset line can be determined before the load test has started and can therefore be used as an acceptance criterion during the load test, Canadian Geotechnical Society (2006). The disadvantage is that it is highly reliant on the Young's modulus of the pile material which, particularly in a bored pile, can be difficult to determine accurately. The method is therefore intended for driven piles and when applied to bored piles, becomes highly conservative, Canadian Geotechnical Society (2006).

General limitations to ultimate capacity based on pile settlement can also be applied. The load which gives as a maximum settlement value of 10mm at working load and 15mm at 150% working load (when the factor of safety is 2.5) can be classified as the capacity limits, Tomlinson (1994). For bored piles, the limit has also been found as the load which causes a settlement of 5% of the pile diameter, O'Neill and Reese (1999).

There are of course a wide variety of serviceability limits which can be imposed on a pile depending on the structure which the pile will support. The sensitivity of the overlying superstructure will dictate these limits and therefore can be project specific.

Throughout the analysis of both working CHD projects and model CHD piles (discussed later) the pile load-settlement behaviour is frequently referred to. In order to avoid confusion, various sections of the load-settlement curves will be defined as shown in Figure 2-23. The aim of these definitions is to provide clarity as to the pile behaviour during loading.

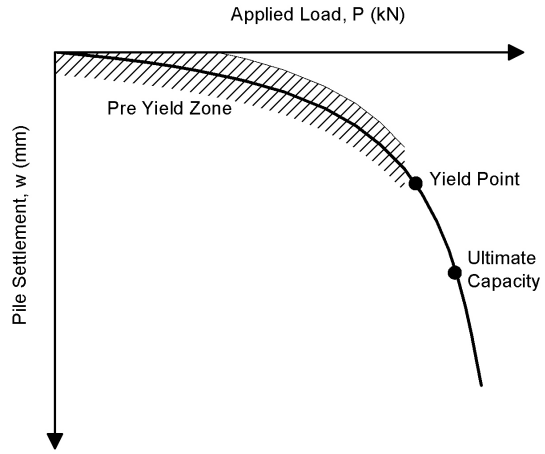

Figure 2-23. Typical pile load-settlement behaviour definitions used throughout this research

Unfortunately in the field, testing of piles does not always mean that the ultimate capacity is reached. It is common practice for test loads to be taken only as much as 150% of the designed working load of the pile in order to verify the design, Weltman (1980). There are a number of reasons why the piles are not taken to the ultimate capacity. One reason being that once the pile has reached an adequate load as dictated in the design standards, contractors are hesitant to continue to load the pile to the point where geotechnical or structural failure is seen to occur due to the negative connotations this has with clients. Additionally, once it has been proved that the pile performs within the safety limits, there is no requirement to continue to load the pile. Although these make operational sense for the contractor, it does not aid research into the piling method.

Due to this fact, not all pile load tests will be taken far enough to determine the ultimate capacity. This has been found during the research conducted on CHD piles by the Geotechnical Consulting Group (1998). To account for this a number of methods have been developed which try to estimate the ultimate capacity of piles which have not been taken to this value during the load test. Some of the more recognised methods will be reviewed.

2.6.2 Predicting ultimate capacity from limited load test data

The inverse slope method, commonly known as the Chin criterion, was originally proposed by Chin (1970) in order to estimate the ultimate capacity of a pile from load-settlement curve which does not reach ultimate capacity, Chin (1972). The method plots settlement/load against the settlement as shown in Figure 2-24. After some initial fluctuation, the data forms a linear slope. The ultimate pile capacity is given as the inverse of the slope of the line, C_1 in Figure 2-24. The load-settlement curve for the pile test can be estimated using equation 2-22.

$$Q_T = \frac{w}{(C_1 w) + C_2} \qquad \textbf{2-22}$$

Where C1 = Slope of linear line in Chin plot

C2 = Intersection of the linear line in Chin plot

w = Pile settlement

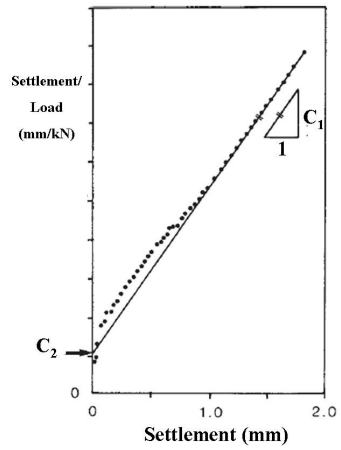

Figure 2-24. Chin analysis example plot (after Chin 1970)

The initial research carried out by Chin (1970) focused on the development of the ultimate capacity prediction method. In 1972 Chin carried out evaluation of the method by comparing the predictions to actual piles taken to their ultimate capacity. It was found that the prediction method, in most cases, had a tendency to over-predict the capacity by as much as 20%, Chin (1972).

Tests were carried out on a mixture of driven and bored piles and installed in sand, silt or mixed alluvium soil type. The driven piles consisted of both steel and concrete while the bored piles were Vibro cast-in-situ concrete (VCC). The research showed that there was an over-prediction of the ultimate capacity. The typical over-prediction for each pile type is shown in Table 2-9.

Table 2-9. Inverse slope analysis over-prediction values determined by (Chin, 1972)

Pile Type	Prediction/Observed Capacity
Driven Steel	1.08
Driven Concrete	1.08
VCC	1.12
Average	1.09

Although the Chin method does not require a pile test to continue until ultimate there is a minimum level which must be achieved in order to obtain a prediction. Usually the test load will have to exceed the load limit calculated using the Davisson offset limit. It is expected that the Chin method will generate bearing capacity values in the order of 20% to 40% of the Davisson value, Fellenius (2006).

Further to the Chin method procedure, Fleming (1992) describes a settlement prediction method which utilises a hyperbolic function to curve fit the load test data from a pile test. The method estimates the pile settlement through the analysis of the base and shaft resistance, whilst also taking into consideration the elastic shortening of the pile material. The Fleming hyperbolic method is reviewed by Knappett and Craig (2012), and the settlement of the rigid pile is represented by equation 2-23.

$$aw_p^2 + bw_p + c = 0 \qquad \textbf{2-23}$$

Where $a = \eta(Q - \alpha) - \beta$

$b = Q(\delta + \lambda\eta) - \alpha\delta - \beta\lambda$

$c = \lambda\delta Q$

$$\alpha = Q_S$$

$$\beta = DQ_B E_B$$

$$\delta = 0.6Q_B$$

$$\lambda = M_S D$$

$$\eta = DE_B$$

D = Pile diameter

E_B = Soil modulus beneath pile base

M_S = Shaft flexibility factor

w_p = Settlement of pile

In order to use the Fleming hyperbolic settlement prediction method, a number of key pieces of information must be known such as the individual shaft-base capacities, the soil modulus beneath the pile E_B and the shaft flexibility factor M_S. Suggested values for E_B and M_S are available in the literature such as those from Azizi (2000).

The elastic shortening of the pile material w_e is accounted for separately using equation 2-24**.**

$$w_e = \frac{4Q_T\left[L_0 + K_e\left(L - L_o\right)\right]}{\pi D^2 E_p} \qquad \text{for } Q_T \le Q_S$$

$$w_e = \frac{4\left[Q_T L - Q_s\left(1 - K_e\right)\left(L - L_o\right)\right]}{\pi D^2 E_p} \quad \text{for } Q_T \ge Q_S \qquad \textbf{2-24}$$

Where: L_o = Length of pile where negligible shaft resistance occurs

L = Total pile length

K_e = Effective column length factor ≈ 0.4, Knappett and Craig (2012)

E_p = Elastic modulus of pile material

By combining the elastic settlement determined from equation 2-24 with the pile settlement from equation 2-23, a load-settlement curve can be established for the pile, the procedure for which is described in detail in Fleming (1992).

The application of the Fleming Hyperbolic method to a typical pile test requires a number of soil parameters to be determined or estimated. An appropriate selection of shaft and base capacities must also be known in order to obtain accurate settlement predictions. As found by Gavin *et al* (2009), the accurate determination of shaft capacity of a pile is of high importance during pile design. This may not pose a problem where historical results allow appropriate estimations to be made, however where a new piling system is used or when new soil conditions are encountered, the application of the hyperbolic method requires a range of assumptions to be made.

A similar prediction analysis to the Chin inverse slope method is the Decourt (1999) extrapolation. In the Decourt method the test data is plotted as load/settlement against load. This plot again creates a tendency for the data to form a linear line such as that shown in Figure 2-25. The ultimate bearing capacity can be found using equation 2-25.

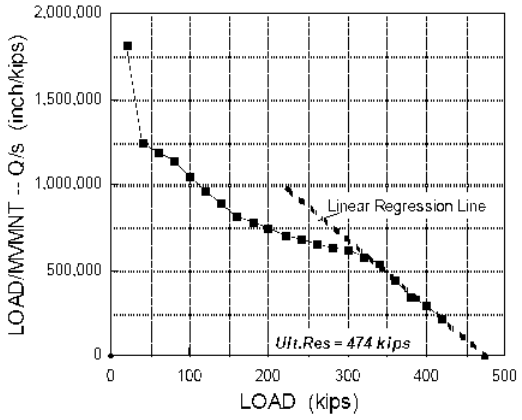

Figure 2-25. Decourt extrapolation method example plot (Fellenius, (2006))

$$Q_T = \frac{C_2}{C_1} \qquad \textbf{2-25}$$

Where C_1 = Slope of the straight line

C_2 = y-intercept of the straight line

The method has been found to give reasonable prediction results without the over prediction which can occur from the Chin analysis (Abdelrahman (2002)). The method also has the advantage of allowing an operator the chance to estimate the pile capacity during the load test as soon as the straight line plot becomes apparent, Fellenius (2001b)

2.7 Modelling of piles

Part of the investigation of this current research involves creating scale model piles. As discussed by Wood (2004), modelling of geotechnical processes has the benefit of allowing the replication of soil conditions in a controlled environment. Compared to full scale, modelling allows multiple repeat tests to be conducted with relative ease.

Physical modelling of CHD piles has previously been conducted by Frangoulides (1999), replicating the entire installation process of the CHD piles. The model setup, shown in Figure 2-26, consisted of model auger and hollow delivery shaft that was attached to a variable speed model which provided the required rotational torque. Vertical auger movement was provided manually via a pulley system. A model grout mixture was prepared to replicate the concrete which consisted of Rapid Hardening Portland Cement (RHPC), fine sand, Ground Granulated Blastfurnace Slag (GGBS) and water. The grout was delivered to the auger via the use of a peristaltic pump, ensuring a continuous supply of grout during pile formation.

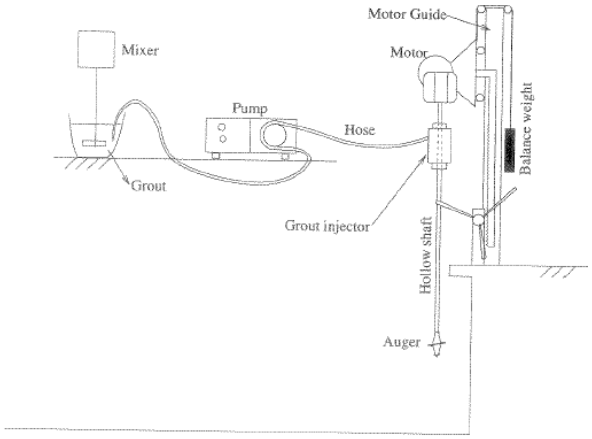

Figure 2-26. Model CHD pile setup after Frangoulides (1999)

The piles were installed in a range of clay samples which had been prepared in a container which was around 6.5 times greater in diameter than the model CHD bullet ($6.5D_f$), and $11.5D_f$ in length.

Although the model setup provided a reasonable representation of the CHD construction process, the manually operated vertical movement introduces a degree of uncertainty to the system. As has been found in reality, the formation and quality of the CHD piles (along with auger piles in general) is dependant upon many things, one being the relationship between bullet rotation and vertical movement. Being able to manually control the vertical movement at a consistent rate for all tests would be difficult and could provide a source of errors.

This variability in manual operation has been eliminated by use of stepper motor control by Hird *et al* (2008, 2011) during the modelling of CFA and auger displacement piles in clay. Similar control techniques were also implemented during the installation of model helical piles by Hird and Stanier (2010) where the vertical installation rate and rotational movement were critically related.

Emmett (2007) describes the installation of model CFA piles in clay using a specially manufactured drilling rig (Figure 2-27). The rig is attached to a hydraulic ram system which provides the vertical movement. All other components required for the pile construction are held within the rig itself.

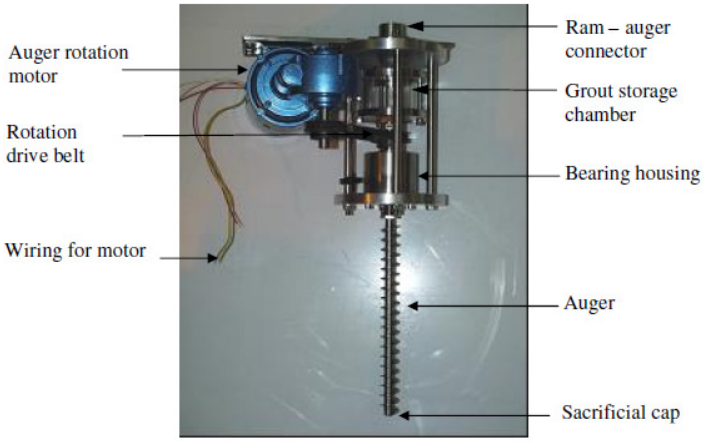

Figure 2-27. Model CFA drilling rig used by Emmett (2007)

The grout storage chamber allowed a predetermined volume of model grout to be mixed and held, ready to be used in the construction of the pile. The grout was left to flow into the void left by the auger under the self weight. In the formation of a CFA pile the delivery system is acceptable however, for the formation of a CHD pile, it is unlikely that enough pressure will be provided by the grout self weight in model scale to create the formation of the flights.

Although modelling provides a number of benefits over full scale testing, there are a number of issues which must be carefully considered in order to allow the application of results derived from model testing to full scale applications which have been highlighted from the investigation of existing research. Issues such as the behaviour of the soil at model scale compared to full scale behaviour due to the typical low effective stresses involved in model tests are important to consider (Wood (2004)). It is also important to consider any influences that may occur due to the experimental setup. In all the model research investigated, take into consideration the size of the container used to store the model soil in order to limit any potential influence the container has on the behaviour of the soil.

Further to the physical modelling of model piles, finite element modelling (FEM) has also been conducted on auger displacement piles. Basu and Prezzi (2009) conducted a finite element analysis on the installation of an auger displacement pile similar to an Omega pile. Through the use of FEM, an indication of the increase in radial horizontal stress due to pile installation is determined.

2.8 Important findings from literature review

It has been found that there are a number of different descriptions for piles depending on the installation technique. The continuous helical displacement pile is part of a new generation of piling systems which has installation and performance characteristics of more traditional piling systems. A number of issues have been found, as follows;

1. The CHD pile system has installation characteristics of both displacement and non-displacement piles

2. A number of auger displacement piles are available in Europe where they are known as screw piles. The CHD pile is most similar to the Atlas pile, both in terms of the construction process and the completed pile.

3. The CHD pile however, is not identical to the Atlas pile and therefore research carried out on Atlas piles may not be directly applicable to CHD

4. Procedures for pile design are widely available however many parameters are dependant on the installation procedure of the pile such as the end bearing capacity factor N_q or coefficient of earth pressure k.

5. The selection of an appropriate diameter for the CHD pile design procedure currently causes some debate due to the varying nature of the pile cross section. Current guidance suggests a diameter equal to $0.75D_f$, however research from similar Atlas piles suggests the use of $1D_f$ can be used.

6. The evaluation and refinement of the CHD design procedure requires the analysis of suitable load-settlement data from pile tests. A number of interpretation procedures have been reviewed in order to determine the ultimate pile capacity from a load test.

7. Previous research on the CHD piles suggests that not all load tests have been carried out to the point where ultimate pile capacity has been determined. As such, the investigation and review of techniques aimed at extrapolating available load-settlement results to determine an ultimate capacity has taken place. The Chin and Decourt prediction methods have been determined as suitable procedures however, the Chin method is know to have a tendency to over estimate the capacity.

8. From the evaluation of field tests it has been determined that auger displacement pile formation and quality is dependant on a good relationship between vertical penetration rate, rotational speed and concrete supply.

9. For future model tests, previous research carried out on similar pile systems have developed methods for controlling the critical parameters in the formation of the piles which include a motor for rotational control, a vertical actuating system and also a method of delivering model grout in a consistent fashion.

3.0 Methodology

3.1 Introduction

The research carried out in this project was conducted using two methods of investigation. The first will be to research and analyse project data collected from Roger Bullivant offices where CHD piles have been installed in the field. By collecting information regarding the site investigation data and the pile load test results the intention will be to evaluate the performance of the CHD piles and evaluate the effectiveness of the design techniques.

The analysis of field project data was complimented with model testing carried out in the University of Dundee geotechnical laboratory. Physical modelling allowed a greater degree of control than is available in the full scale piles. The focus of the model testing was to determine the effect the pile installation has on the soil structure and how this affects the pile performance, particularly in varying soil densities.

This chapter details the way in which the research has been conducted, for the model piles in particular. Development of the modelling equipment is detailed along with information regarding the preparation of the model tests.

3.2 Field Data Analysis

The aim of the field data analysis was to determine how the CHD piles perform in the field by investigating the load-settlement data. Data from field pile data was obtained through data mining sessions carried out at Roger Bullivant Ltd regional offices. Along with the load-settlement data for each CHD pile, the ground investigation report for the project site and the designed pile capacity was also obtained.

The ground investigation for the majority of the projects consists of standard penetration tests (SPT), with only a small number that utilises cone penetration tests (CPT). The site investigation reports give information on the soil parameters which can then be used in the pile design. Although the main focus of the research project is on piles installed in sands, the collection of data did not preclude piles which had been installed in other materials.

Utilising the load-settlement data for the field piles, it was hoped that the ultimate capacity could be compared to the capacity estimated from the design procedures described in Chapter 2, in order to establish the accuracy of the design prediction. However, upon examination of the load-settlement data from field tests, it was found that applied loads were not large enough to observe or define ultimate capacity. The ultimate capacity was therefore estimated using prediction methods discussed in Chapter 2.

3.3 Model Testing

The model CHD piles are tenth scale replicas of field piles, constructed using a specially manufactured model bullet, and installed at 1-G stress level. In order to provide a comparison to the CHD piles, two additional installation techniques were also modelled which were designed to represent displacement and non-displacement piles. The displacement piles will be modelled using precast piles which are pushed into the sand under a constant penetration rate (Pushed) while the non-displacement piles will be wished-in-place (WIP) during the sand bed preparation.

The piles are installed and tested by utilising an Instron 1196 testing machine located in the University of Dundee geotechnical laboratory. The Instron is capable of applying accurate rates of vertical movement whilst recording the applied load.

Model testing was carried out in two series, this resulted in the formation of piles with different characteristics as summarised in Table 3-1. The first series consisted of piles that were not instrumented while the second series had

instrumentation inserted in the piles. The piles in series 1 have an embedment depth of 280mm whilst series 2 piles were increased to 400mm. This increase in length was accommodated through improved space utilisation in the CHD installation rig which allowed greater depths to be reached during the casting process, as will be discussed further at a stage. The increase in the length allows piles with a larger length/diameter L/D ratio which are more typical to field piles to be constructed.

In the series 1 pile tests, the pushed and WIP piles were designed to have two different diameters, one that matches the inner core of the CHD and another that matches the outer flange of the CHD. These piles were intended to allow investigation of the effective diameter of the CHD pile.

Table 3-1. Summary of model pile configurations formed for the different test series

	Diameter (mm)	Length (mm)
Series 1 Piles		
CHD	60	280
Pushed	60	280
Pushed	30	280
WIP	60	280
WIP	30	280
Series 2 Piles		
CHD	60	400
Pushed	60	400
WIP	60	400

CHD diameter refers to the outer flight diameter D_f

3.3.1 Model CHD drilling equipment

In order to create realistic model CHD piles, the full scale process of installation was replicated in model scale. This requires the installation of an auger bullet into the sand bed followed by the casting of the CHD pile in a model form of concrete (referred to as grout) during extraction of the auger. At all stages of the installation and extraction of the auger bullet, both the vertical and rotational

speeds must be accurately controlled since both are crucial to the formation of the CHD pile

Vertical movement is achieved using the Instron machine (Figure 3-1) which has pre-determined speed settings. In the field, the rotational speed of the auger is dependant on the vertical penetration speed. In the model scenario, the vertical speed is fixed at 500mm per minute via the Instron. The vertical movement of the Instron was recorded using a Micro-Epsilon WDS-2000-P96-SR-U draw-wire displacement sensor. Both the draw-wire and Instron load readings were recorded via a Flyde data acquisition unit as will be discussed in detail later in this chapter.

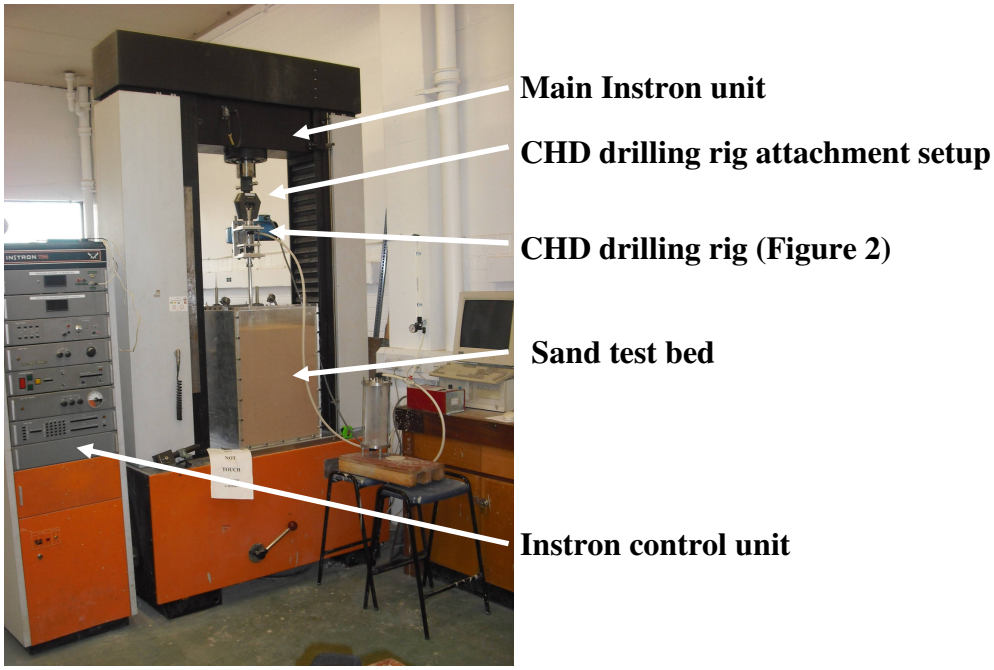

Figure 3-1. Instron machine showing setup for installation of model CHD pile

In order to create controllable rotational movement, the bullet is rotated via a motor driven belt drive (Figure 3-2). The motor selected is a Parvalux SD12C with a LIW gear head. A permanent magnet and double worm gear head gives a maximum output speed of 3000rpm and an output torque of 28Nm, ensuring adequate ability to install the model piles. The motor is controlled by a 750w DC motor reversing speed controller from RS components. This enables the rotational speed to be adjusted to match the vertical advance rate set by the Instron. It also

allows the reversing of the rotational direction to accommodate the installation and extraction of the bullet.

The motor is secured on an aluminium frame which secures the main shaft in position, Figure 3-2. The drive motor must be offset from the main shaft in order to allow access for the grout. The main shaft is secured in the drilling rig using thrust bearings which resist the vertical forces encountered during the installation and extraction of the bullet whilst also allowing rotational movement.

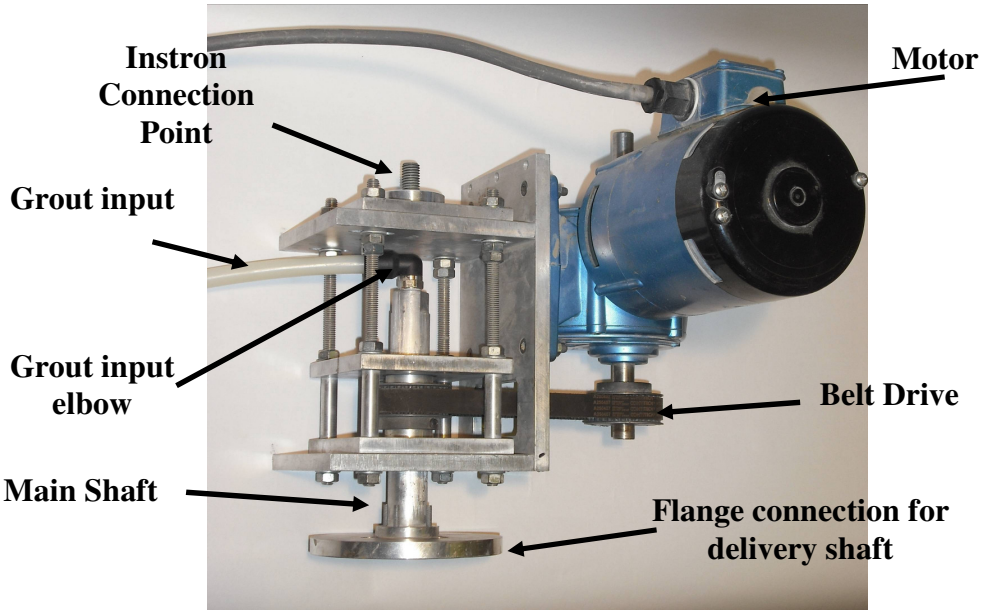

Figure 3-2. Model CHD drilling rig

The main shaft is hollow to allow the flow of grout to the bullet. At the top of the main shaft a rotating push fit elbow connector is located into a threaded housing. The elbow connector has a thread size of R1/4 and accepts a 12mm outer diameter hose. The connector allows the delivery shaft to rotate whilst keeping the hose in a fixed position during model concrete delivery.

The main shaft connects to the delivery shaft via a flange connection and is sealed with an o-ring. Attached at the end of the delivery shaft is the model CHD bullet, Figure 3-3. The bullet is a 10^{th} scale model of the bullets used in the field, the dimensions of which are shown in Figure 3-4. In the series 1 tests the CHD bullet and delivery shaft had a combined length of 300mm which allows an average pile

installation depth of 280mm. The series 2 tests had an increased combined length to allow the formation of 400mm long piles.

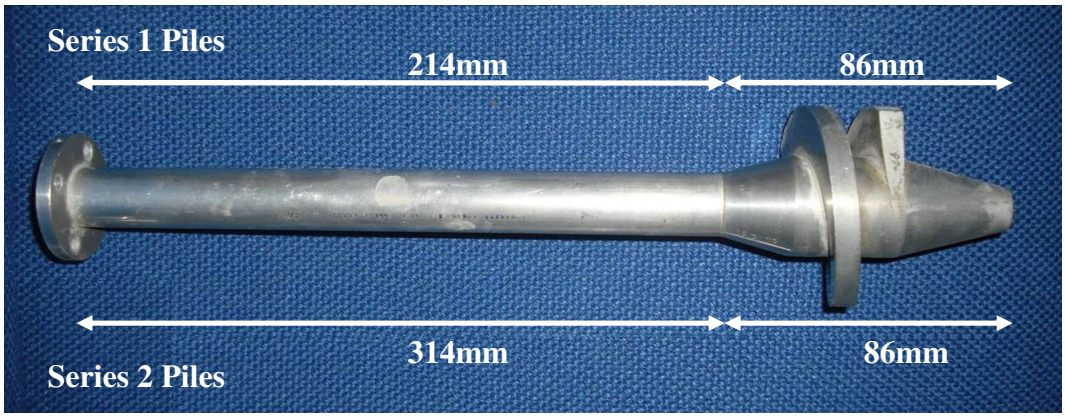

Figure 3-3. Model CHD bullet and delivery shaft for series 1 and 2 piles

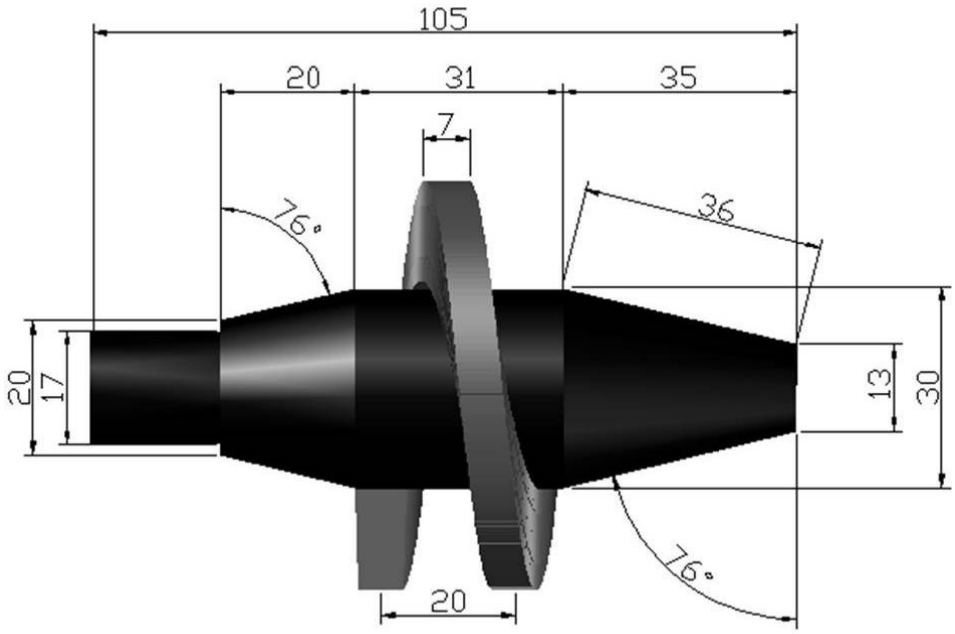

Figure 3-4. 10th scale model CHD bullet dimensions

The model bullet is machined down from a solid stainless steel block to the correct shape and dimensions shown in Figure 3-4. The bullet is attached to the delivery shaft using polyepoxide adhesive. The delivery shaft has an external diameter of 20mm and an internal diameter of 10mm which matches the internal diameter drilled through the bullet. Unlike the bullets used in the field, the model bullet does not have cutting teeth at the discharge end. In the field, the bullet feet are used to assist in material breakup during advancement through the soil strata

and do not influence the formation of the CHD pile and are therefore not required in model scale. Additionally, teeth on such a scale as the model bullet would be fragile and would most likely break off easily during pile construction.

The model bullet for series 1 and 2 model tests used a 10^{th} scale bullet which gave length/diameter (L/D) ratios of 4.7 and 6.7 respectively. A bullet on a scale of 1:33 was manufactured which produced CHD piles with an outer flange diameter of 18mm and a central core of 9mm. The smaller scale bullet allowed CHD piles with an L/D ratio of 16 to be constructed, with represents a suitable ratio for a relatively long field pile. Preliminary investigations were carried out on the small scale bullet (McNeilly (2010)). It was found that the 1:33 scale bullet posed significant problems during the CHD installation procedure. The CHD piles produced using the 1:33 scale bullet did not have the typical pronounced helical flange of the CHD piles. In most piles produced, the inner core diameter was only around 10% smaller than the outer flange diameter, not the typical 50%. The formation of the piles was also found to vary, sometimes significantly, between different tests. Due to the difficulties and inconsistencies experienced in the formation of the 1:33 scale piles, it was decided to focus purely on the 10^{th} scale models.

The concrete grout used in the pile construction had to be delivered through the bullet at a consistent and controllable rate. In the field this is achieved using a concrete pump. A similar system will be utilised in the model scale. The grout is fed into the delivery shaft through the rotating elbow connecter via a 12mm diameter polyurethane tube (Figure 3-2). The tube connects to a storage chamber, filled with grout.

The grout delivery chamber, Figure 3-5, consists of an acrylic chamber, 5mm thick, 63mm diameter and 300mm high, sandwiched between two aluminium end plates 15mm thick. The plates are recessed to accommodate the acrylic tube and an o-ring seal. The tube and plates are tensioned together using 10mm threaded rod with wing nut fittings at the end.

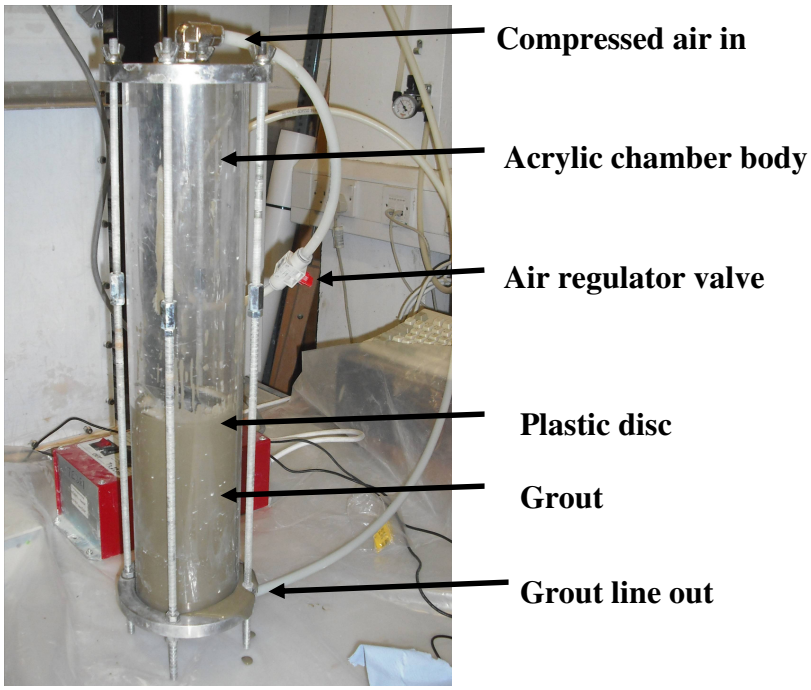

Figure 3-5. Grout storage and delivery chamber

Each of the end plates has an elbow push fit connector, 12mm in diameter, in the centre. Compressed air is fed in through the top inlet via an air regulator valve. The grout stored in the chamber is then forced out via the bottom outlet which feeds the CHD drilling unit.

It was initially anticipated that the chamber could be filled with grout via an access hole on the top plate whilst the chamber was fully assembled. However, after trialling this system it was found that a steady flow was not produced as anticipated. The pressurised air caused a void to form in the grout mixture above the lower plate outlet, similar to a vortex column above a draining body of water. Once the void had occurred, no further grout is pumped through the pipe. To overcome this problem a plastic disc with similar diameter to the chamber diameter was placed on the surface of the grout. The disc then acted as a plunger, forcing the grout out of the chamber in a continuous and consistent flow. Due to the requirement for the insertion of the plastic disc, the grout storage chamber is partially assembled, the grout is then poured in and the top end plate attached before being tightened into position.

3.3.2 Preparation of sand test bed

The model piles are installed in dry sand samples. The sand used throughout the testing process was HST95, a fine quartz based silica sand sourced from Bent Farm in Congleton, Cheshire. A summary of the HST 95 sand properties determined from Lauder (2010) is shown in Table 3-2. Shear box test results carried out on the HST sand are discussed later in this chapter.

Table 3-2. Physical properties HST 95 sand used in model tests

Soil Property	HST 95
d_{10} (mm)	0.1
d_{30} (mm)	0.12
d_{60} (mm)	0.14
C_U	1.4
C_z	1.0
G_s	2.63
γ_{max} (kg/m^3)	1760
γ_{min} (kg/m^3)	1461
e_{max}	0.769
e_{min}	0.467
Shape	Rounded

The sand bed is created by carrying out air pluviation. The sand is passed through a mesh from a storage hopper before is falls into the testing box as shown in Figure 3-6. The density of the sand sample is controlled by the rate at which the sand falls into the box through the use of different mesh sizes as discussed by Ueno (2000). The fall height is monitored continually through the pluviation process in order to maintain a minimum of 0.8m above the sand surface.

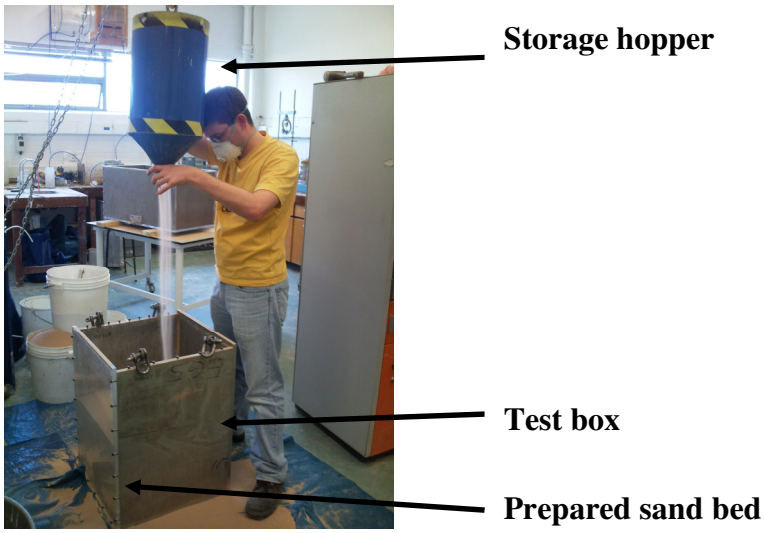

Figure 3-6. Sand sample preparation by means of pluviation

By varying the mesh size, varying densities of sand can be achieved. A mesh size of 2mm will give a medium dense sample, while a mesh size reduction to 1mm will give a dense sample. Preparation of the samples using mesh pluviation was carefully carried out over a number of hours, typically 4-5 hours for a medium dense sample and 7-8 hours for a dense sample.

In order to obtain loose sand beds, the sand is poured into the test box using a tube delivery system, Figure 3-7, as described by Schawmb (2009). The open end of the tube is continually held at a set height of around 40mm above the sand surface. This ensures a consistently even loose sample is produced. The final surface of the test bed is levelled prior to testing using a plastic scraper set to the suitable height.

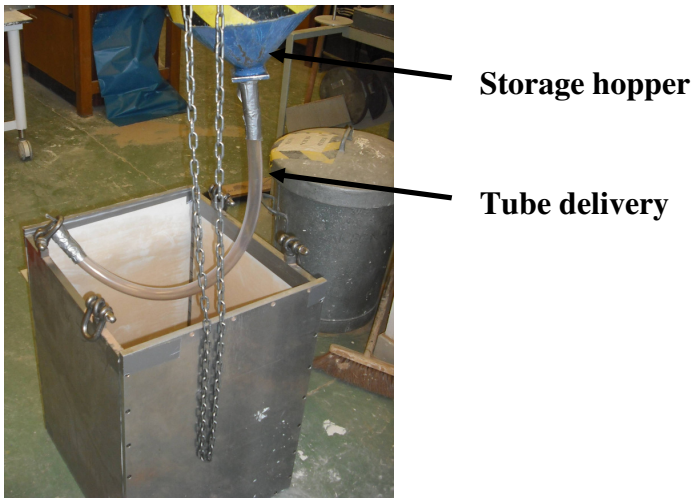

Figure 3-7. Sand sample preparation by means of tube delivery system

The density of the in-situ sand sample is verified through the use of density pots which are placed throughout the test bed and pluviated over. The pots are carefully located to ensure they will not be disturbed by the drilling auger. After the pile has been installed and a load test has been carried out, the sand is carefully excavated to allow the removal of the pots. Once removed from the sand bed, the pots are levelled off and weighed. With the volume and weight of the empty pots known, the density, γ of the sand in each pot during can be established. For comparison between different test beds it is easier to present the sample densities in terms of relative density using the sand properties in Table 3-2 and equation 3-1.

$$D_r = \frac{\gamma_{max}(\gamma - \gamma_{min})}{\gamma(\gamma_{max} - \gamma_{min})} \qquad \textbf{3-1}$$

3.3.3 Boundary Effects on model tests

During the installation of piles at full scale, the stresses induced will be dissipated throughout the surrounding in-situ soil which will continue to infinity. During model testing however, the soil test bed does not continue to infinity and will have a limiting size based on the geometry of the test box used. The limiting box geometry can potentially influence the behaviour of the test soil. The influence of the test box on the behaviour of the sand is known as boundary effects.

Ideally, the test bed of sand should be large enough so that the box sides do not interfere in any way with the installed piles however this can mean test boxes which can be up to 40 times the diameter of the installed pile (Phillips and Valsangkar (1987), Klotz and Taylor (2001)). In model testing, limitations on test box sizes are often dictated through the available equipment and handling abilities. It was found by Phillips and Valsangkar (1987), that the influence of boundary effects was dependant on the material that the test box was constructed from. Rigid materials would allow a reduction in the minimum size required to eliminate boundary effects compared to flexible materials.

Research carried out on centrifuge pile modelling suggests that if the ratio of test box diameter to the pile diameter is greater than 40 then the effects of the side boundary become negligible. However, it has also been found that the ratio of test box diameter to pile diameter can be as low as 5 which allows a much smaller test box to be used for the test (Phillips and Valsangkar (1987)). This value corresponds to that found by White and Bolton (2004) during investigations of horizontal soil movements around displacement piles.

Similarly, if the ratio of the distance between the pile tip and test box base is greater than 12 then boundary effects can again be neglected, Klotz and Taylor (2001). However this ratio can be reduced to greater than 10 for base effects to be negligible based on research carried out by Phillips and Valsangkar (1987).

Since the test box will be used within the Instron machine, there are limitations to its allowable size. The strong box is restricted to an internal dimension of 500x500x670mm. The 10^{th} scale model piles have a maximum outer diameter of 60mm and for series 2 piles, are installed to a maximum depth of 400mm.

This gives a box to pile diameter ratio of 8, greater than the minimum value of 5 suggested by Phillips and Valsangkar (1987). The ratio of base clearance to pile diameter is found to be a maximum of 3.3 when the piles are first installed. This reduces to 2.3 if the pile settlement reaches $1D_f$. The 3.3 value is lower than the value of 10 suggested in previous work. However work carried out by Emmett (2007) suggests that the limit of influence on the soil below the pile base can be as low as one pile diameter away from the pile base. The possibility of base influences to the performance of the installed pile will be considered when carrying out data analysis. These limitations are primarily for use in dense samples, when loose sand is used the effects of boundary conditions in a similar sized chamber are negligible, Phillips and Valsangkar (1987).

In order to reduce any side boundary effects as much as possible, the walls of the strong box were covered with 1mm thick Polytetrafluoroethylene (PTFE) sheets, Figure 3-8. The PTFE has a friction coefficient of around 0.04, compared to around 0.61 for the aluminium box (Young and Freedman (2000)). Due to the low

friction of the PTFE sheets, there will be a reduction in the friction resistance experienced between the sand-PTFE interface compared to the aluminium box sides.

Figure 3-8. Strong box internal PTFE

3.3.4 Effective stress issues

The piles constructed at model scale are subjected to significantly lower effective stresses than those installed at full scale. This low effective stress could present problems when making comparisons between model tests and full scale tests since the effective stresses experienced at full scale will be orders of magnitude larger.

As discussed by Bolton (1986), the confining pressure of a soil will affect the angle of shearing. An increase in the confining, or overburden pressure will produce a reduction in the dilation angle. The dilation angle experienced in the model testing will therefore be much greater than from what would be found in the field. The dilatancy of the soil is also found to increase with reduction in the overburden pressure. Therefore, particularly in dense model samples, the dilation angle will be much greater than the values measured in the field.

As discussed by Wood (2004), it is important to use appropriate soil properties when carrying out scale model testing. The use of soil properties typical to the field will be unsuitable for model testing and as such, properties like peak angle of friction must be derived under similar effective stresses to those experienced in

the model. Results of shear box testing carried out under these conditions are discussed in section 3.4.

The effect of low effective stress on the assessment of the piles, particularly on the shaft friction capacity experienced, can be investigated using cavity expansion theory, Wood (2004), Randolph (2003). The effect of dilation on the radial stress is found to be a function of the soil shear modulus shear modulus and the dilation normalised by pile diameter, Lehane *et al* (2005). From the investigation of the model test piles, it was found that the change in radial stress due to dilation was around 0.25 times lower than the change in radial stress due to the installation of the pile.

3.3.5 Model grout mixture details

Prototype piles are constructed from concrete mixtures which have enough workability to allow it to be pumped whilst maintaining suitable compressive strengths. It would be impossible to scale down the full scale concrete mix exactly for the model piles, therefore a model grout mix was used. Various design mixes were trialled to find an optimum mix which had suitable workability to allow it to be pumped through the model system, whilst also providing sufficient strength to allow load testing to take place in a suitable timeframe. After carrying out trials of different mixes it was determined that the use of aggregate in the concrete was unsuitable due to the tendency for blockages to occur. Even with the use of fine aggregate (sand) in the concrete, the mixture would become easily blocked within the delivery system which caused an inconsistent flow and segregation of the concrete mix.

The design mix was reduced to a pure cement-water grout. The inclusion of alternative cementation binders such as ground granulated blast furnace slag, (GGBS) or pulverised fuel ash (PFA) was found to have no significant benefit on mixtures of such small quantities. The cement binder used for the mix is rapid hardening Portland cement, RHPC. The use of RHPC reduced the time required

for the concrete to reach a suitable strength for load testing to take place, typically within 24 hours for all CHD piles.

After trialling with different water-cement ratios (W/C), it was found that a W/C of 0.5 was suitable for use. For a typical test, 2.1kg (762kg/m^3) of RHPC and 1.16kg (419kg/m^3) of water is used. In order to further reduce the risk of blockages occurring within the pumping system, the cement powder was sieved through a 600μm mesh which eliminated course clumps and produced a fine powder. As part of quality assurance of the grout, it was mixed by hand. This hands on approached allowed the pulverisation of any cement clusters which formed before being pumped through the system.

The concrete strength was determined through standard cube tests carried out as per BS EN 12390-1:2000 (2000). This involved casting 100x100mm cubes and then testing them at standard time intervals after casting takes place, namely 24 hours, 7 days and 28 days. The cubes are loaded to destruction using a standard cube crushing machine at the University of Dundee. It was found that the grout strength was 90MPa after 24 hours, increasing to 262MPa after 7 days and then finally reached 272MPa after 28 days, Figure 3-9.

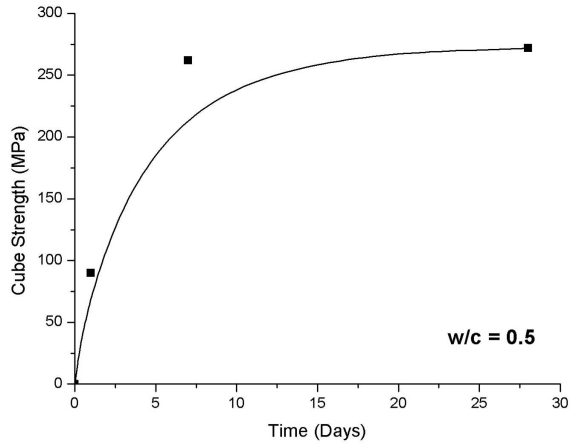

Figure 3-9. Cube strength variation with time for model grout with a water –cement ratio of 0.5

The grout is of sufficient strength to perform load tests within 24 hours of casting the piles. Due to the small scale, the loads applied are unlikely to cause significant

elastic shortening of the pile, meaning that settlements measured during the load test will be purely from soil-pile failure and not from grout deformation.

3.3.6 Construction and development of the model CHD piles

Initially, the model piles were constructed in large plastic containers of sand while the process is perfected. For the purpose of the initial trials, loose sand is modelled by simply pouring the sand into the container while dense sand is modelled by placing the container of loose sand on a vibrating plate for a short time.

The vertical penetration and extraction speed was set at 500mm per minute via the Instron. The rotational speed had to be carefully adjusted to create the correct pitch of the CHD flights. The rotational speed was found to be 22rpm, similar to the rotation speed of prototype CHD drilling rigs. The combination of a pullout rate of 500mm/min and rotational speed of 22rpm, produced a flange pitch of around 20mm, the scale size of a prototype CHD pile.

Before the bullet is drilled into the sand, a small plastic plug is placed in the end which represents the sacrificial tip on the prototypes. This plug is blown out once the grout is pumped.

Initial trials with different concrete mixes that contained fine aggregate required a high air pressure of around 150-200 kN/m^2 (1.5 – 2 bar) in order to pump the concrete through the pipes. Even with the high pressures, the concrete mix regularly became blocked, leading to the use of a pure cement grout. Once the pure cement grout mix was used, the pressures used previously were found to be unnecessarily high, causing considerable deformations (bulging) to the constructed pile. The air pressure was subsequently reduced to around 0.5bar.

The effects of the adjustments of the rotational speed and pumping pressures are shown in Figure 3-10. The pile in Figure 3-10a was the first trial carried out and its lack of formation is a result of a blockage of concrete within the delivery system. This led to the development of the pure cement grout, used in the

formation of all subsequent piles. In Figure 3-10b, the deformed pile is a result of too high a pumping pressure and a sub optimum speed of rotation, while Figure 3-10c shows a pile which has an above optimum speed of rotation and low pumping pressure. Both rotation speed and grout mixture have been resolved for the pile in Figure 3-10d, however pumping pressure is too low. For the pile in Figure 3-10e, rotational speed, grout design and pumping pressure have been resolved to produce a reasonably accurate model CHD pile.

(a) **(b)** **(c)** **(d)** **(e)**

Figure 3-10. Model CHD pile evolution through the adjustment of rotational speed and grout mixture

The effects of adjusting the pumping pressure are shown in Figure 3-11. The first two piles, (a) and (b) are both constructed in dense sand while the third pile (c) was in loose sand. Piles (a) and (b) have been installed with different pumping pressures, pile (a) at 0.5bar and (b) at 0.55bar. The effect of pressure difference on the pile geometry is evident by comparing these two piles. A 10% increase in the pumping pressure changes the physical appearance of the pile considerably. The helical flights are less defined and the pile becomes similar to a straight shafted pile. Due to the lack of overburden pressure towards the surface of the pile, the high pressure has also increased the pile diameter. When installed in loose sand, the flights can be seen to be less defined. The central core diameter becomes similar to the flight diameter, particularly towards the ground surface.

The only parameter which changes between the piles in (a) and (c) is the soil density. Pile (c) has been constructed in loose sand, the effects of which can be seen towards the head. The definition of the helical flights begins to deteriorate, presumably due to the lack of over-burden pressure at the soil surface which provides resistance against the pressure of the grout. This can be overcome by reducing the grouting pressure slightly as the bullet reaches the surface of the soil, something which is performed during real pile construction.

(a) **(b)** **(c)**

Figure 3-11. Effects of soil density and pumping pressure on model CHD piles (a) Dense sand, installation pressure = 0.5bar (b) Dense sand, installation pressure = 0.55bar and (c) Loose sand, installation pressure = 0.5bar

In preparation for the load tests, a cap must be placed on the model piles which will create an even surface to distribute the applied load, the sequence of which is shown in Figure 3-12. The pile cap is created during construction of the pile by placing a plastic pipe of 50mm diameter into the fresh grout at surface level. The pipe is coated with a de-bonding agent to allow easy removal once the grout has cured. The resultant is a level pile head on which loading can take place.

(a) **(b)** **(c)**

Figure 3-12. Construction of the CHD pile cap (a) extraction of the auger bullet (b) placing of mould into freshly cast grout (c) removal of mould from cured grout to create level surface

The piles are left to cure for a minimum of 24 hours before load testing takes place, with load testing typically conducted no longer than 25 hours after the pile has been installed. The pile is loaded via the Instron applying a constant rate of penetration (CRP). The penetration rate is set at 2mm per minute which is within the limits set out in BSI8004:(1986). It has been noted that BS8004:1986 has now been superseded by BS EN 1997-1:2004 (Brown (2012)). In order to protect the pile cap from excess point loads, a loading plate is placed on the pile surface. This plate distributes the applied load evenly and stops structural failure of the pile cap, Figure 3-13. The load is applied to the pile via a ball applicator to ensure it remains axial throughout the test so as not to induce moments.

Figure 3-13. Model pile loading plate and load applicator

3.3.7 Development of Pushed and WIP Piles

The model CHD piles will be compared to alternative piling techniques in order to try to quantify the performance of the CHD. Field alternatives to CHD piles typically consist of displacement piles such as pre cast driven piles or non-displacement piles such as continuous flight auger (CFA) bored piles. For the purposes of modelling, field installation processes of these piles are not be replicated identically, however the interaction between the soil and pile will be simulated as closely as possible. The driven piles will be modelled as pushed in place piles, where a pre-cast concrete pile is pushed into the test bed at a constant rate of penetration. The non-displacement piles will be replicated by installing a wished-in-place pile. The pile will be held in position in the test box during pluviation and the sand will be pluviated around it, replicating the minimal soil structure disturbance experienced in a well formed cast in-situ pile.

The piles will be constructed from the same grout as used in the CHD pile. Plastic piping is used as moulds to create circular cross section piles. The pipe has an inner diameter equal to 60mm, matching the full flight diameter of the CHD piles. In order to assist removal of the mould once the grout is cured, the pipe is cut into two halves. It is held together using cable ties while the pouring takes place. The internal surface of the mould is given a light coating of de-bonding agent in order to ensure the pile surface is smooth once removed. The model driven piles are left with a smooth grout surface, ensuring a concrete-sand failure interface as would be the case in field pre-cast piles. For the simulated bored piles, a layer of the test sand is glued onto the surface of the pile using a thin coating of polyvinyl acetate (PVA) adhesive. This replicates the rough sand-sand failure interface that would be experienced within a typical bored pile.

For the construction of the Wished-in-place (WIP) pile, the sand bed is initially pluviated as per the CHD test bed until the intended pile base depth has been reached. Once the pluviated surface has reached the pile base depth, the WIP pile is placed on the sand surface and held in position within the test box using an arm and clamp which is secured to the box side, Figure 3-14. Once secured, pluviation

of the sand continues around the pile until the required embedment depth of the pile is achieved, which for series 1 piles equals 300mm and 400mm for series 2 piles.

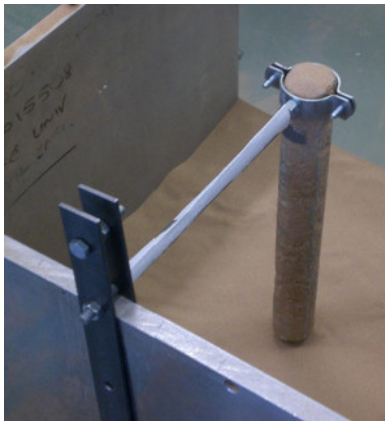

Figure 3-14. Wished-in-place pile held in position ready for pluviation

The pushed pile is installed in a prepared test bed of sand using the Instron machine, shown in Figure 3-15. The pre-cast pile is placed in the centre of the box and secured plumb via a specially machined housing. The housing allows the pile to fit tightly over the head of the pile and is secured in the Instron clamping jaws. The pile is pushed into the test bed at a rate of 20mm/min until an embedment depth matches that of the model CHD piles. As the pile advances the plumb is checked using spirit levels to ensure it is perfectly vertical. Both the pushed pile and WIP piles are load tested by employing the same loading plate procedure as used in the CHD piles.

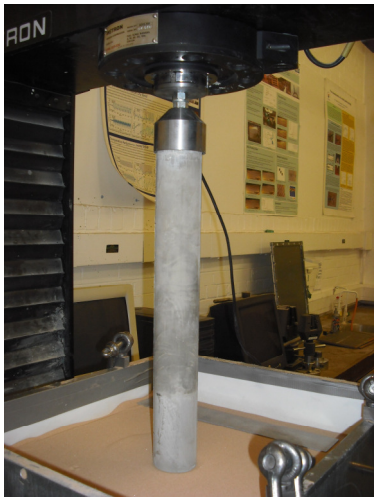

Figure 3-15. Pushed pile installation setup

3.3.8 Instrumentation of Model Piles

The series 1 model piles provided basic load test performance information and pile installation effects on the soil. In order to establish improved design procedures for the CHD pile, a second series of model pile tests were carried out which contain instrumentation to record the load exerted on the pile base and load distribution during the load test. Along with instrumentation, the piles are also increased in length to give a more typical pile length/diameter L/D ratio of 6.6. The increase in length is achieved by making alterations to the manner in which the drilling rig is held in position within the Instron. Unlike the original drilling rig used in the series 1 tests which was held in the Instron via the gripping jaws, the altered drilling rig for the series 2 tests attaches directly into the Instron via a specially manufactured threaded connector. The connector uses the attachment point used for the jaw unit and fits directly onto the drilling rig. The removal of the jaws creates extra head room within the Instron which equates to increased pile installation depth.

Data acquisition of the signals from all the transducers in the pile instrumentation was carried out using a Flyde modular instruments FE-MM8 8 channel data acquisition unit (DAQ). The DAQ was connected to a PC control system via a USB connector. The DAQ contains 4 FE-366-TA signal conditioning cards which provide the ability to power and monitor up to 8 different transducers at the same time. This system is also used in the acquisition of readings from the Instron and draw-wire displacement transducer.

Each signal conditioning card allowed the selection of the excitation voltage for the transducer which is 10V for all transducers used in this study. For each transducer, the signal amplification could be individually set within a range of x1 to x5000. The signal amplifications for the transducers in the project typically ranged from x1 to x1000.

The transducer signals were recorded using the data acquisition software MADAQ. The MADAQ programme is a LabView based software which allows

the simultaneous signal acquisition from up to 8 individual transducers. The MADAQ software has a sampling rate of up to 50,000 samples a second however during the course of this research the sampling rate was set at 5000 samples per second with 5 samples a second being saved in an output file. The recorded test data is stored in a text file format which can then be opened and saved in Microsoft Excel ready for processing

All transducers used throughout the experiments have been issued with manufacturers calibration certificates. In addition to these certificates they were also calibrated within the experimental setup.

Instrumentation of the both the pre-cast piles consisted of installing a load cell at the pile base. The restricted dimensions available to install the loadcell, along with the range of anticipated loads, controlled the selection of a suitable loadcell. A Novatech Measurements Ltd F317 high performance fatigue rated cylindrical load-cell is used, Figure 3-16. The load cell measures both compression and tension up to a maximum of 25kN. The load is transferred to the load cell via M24 x 2 x 30 threaded connection points at both ends. The load-cell had also been specially adapted to allow insertion into the model pile by installing the cable perpendicular to the loadcell axis.

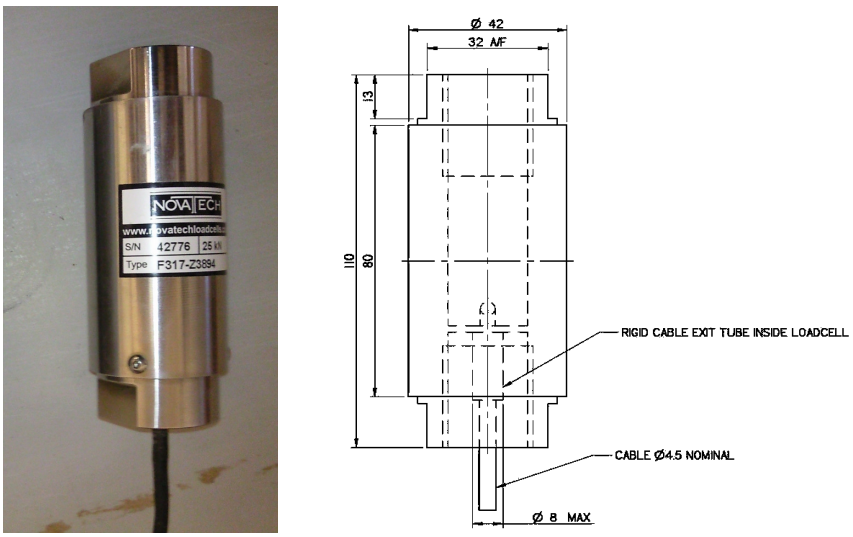

(a) **(b)**

Figure 3-16. Pre-cast pile base loadcell (a) awaiting installation in the pile and (b) cross-section dimensions in mm (Novatech Measurements Ltd)

The load cell must be attached to the base of the pre-cast piles in order to record the base load. This is achieved by placing the loadcell into a housing which has been formed as part of the pile during the casting process. The housing, Figure 3-17, consists of a 1.5mm thick steel tube with an outer diameter of 57mm. The diameter of 57mm allows a 1.5mm layer of grout to cover the unit, taking the final diameter to 60mm. At one end of the tube, a top cap is attached using high strength araldite adhesive. The cap has a thread which matches the thread of the load cell. The loadcell cable is fed up through the pre-drilled hole down the centre of the cap. There is a clearance of 6mm around the load cell in the housing. The housing unit has a total length of 115mm which fully encases the load cell. On the exposed end of the load cell, another cap is placed. This also has a matching thread which allows it to be secured into the load cell. Recessed in the cap is an o-ring which will stop the ingress of sand when the pile is installed. The bottom cap forms the base of the pile.

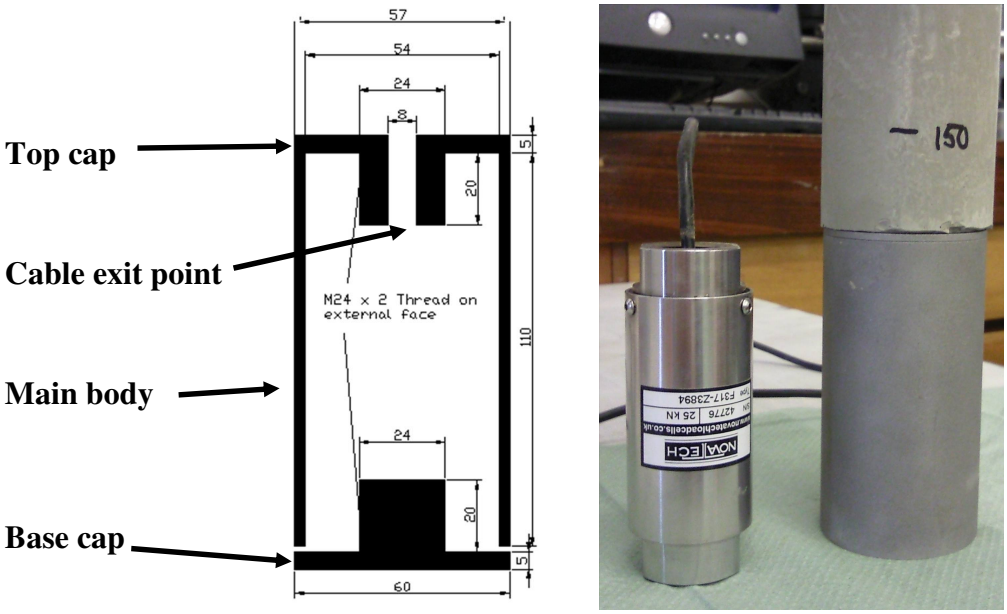

Figure 3-17. Load cell housing unit cross section (a) and in-situ at the base of the pushed pile along with the loadcell (b)

The housing unit is sand blasted to give a rough texture to the steel surface before it is cast in the pile to improve the bonding with the grout. The housing unit is placed in the pile mould and forms part of the pre-cast piles when the grout is poured in. A plastic pipe, equal to the 8mm drilled hole in the top cap of the

housing unit, is inserted and held rigid through the length of the pile mould. The plastic resists bonding with the grout, allowing it to be removed once curing has taken place. This leaves a full length hole through which the load cell cable can be fed. Using another small section of pipe, a recess is made on the pile surface where the cable can be fed without risk of damage from the loading plate during the installation or load testing of the pile.

The grout bonds to the outer surface of the housing unit, leaving a thin layer of grout over the surface of the steel. This allows a continuous grout-sand interface through the entire length of the pile. The thickness of the grout over the housing is only a few millimetres making it susceptible to impact damage however, the shearing resistance remains unaffected. As with previous piles, the surface of the pushed pile remains a smooth grout surface while the wished-in-place piles have a layer of sand glued on.

The CHD piles are cast in situ and it will therefore be difficult to install instrumentation to record the variation of loading through the pile length. Typically in full scale pile tests, load distribution is recorded by inserting sister bars which have strain gauge sensors attached. The strain variation throughout the length of the pile can be used to determine the axial load distribution and therefore the shaft friction as discussed by Brown (2004) and Fellenius (2001a).

The model CHD piles do not have reinforcement and as such strain gauges will have to be attached to an external rod which is then inserted into the pile. Aluminium was chosen as the preferred material for the rod since it has a relatively low stiffness with a Young's modulus of around 70MPa compared to alternative metals such as steel which has a Young's modulus of around 200MPa. The lower stiffness of the aluminium will have a greater sensitivity to deflections within the pile during loading. Aluminium rods of diameter 10mm and length 400mm were used for the application of the strain gauges. The strain gauges themselves were Vishay Micro-Measurement general application gauges (L2A-13-125LW-120), as shown in Figure 3-18. The rod diameter was selected to be as small as possible so as to limit the influence on pile stiffness however it had to be large enough to attach the strain gauges.

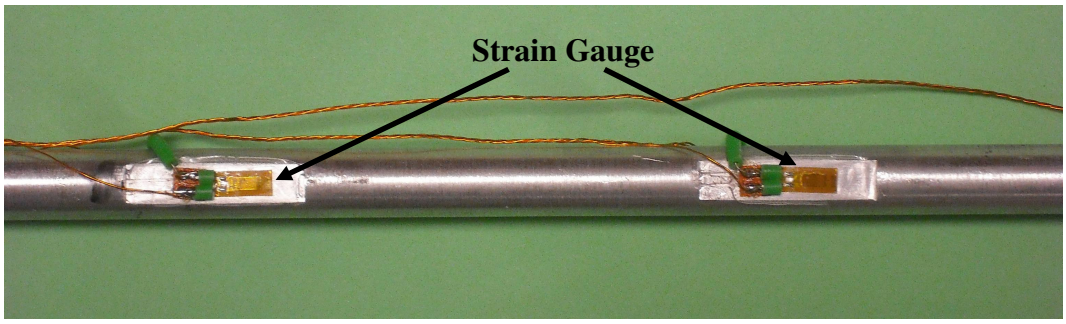

Figure 3-18. Strain gauge attached to the 10mm diameter aluminium rod

The aluminium rod was roughened around the strain gauge location using fine abrasive paper in order to ensure a good bond was achieved. The gauges were attached to the rod using M Bond 200 adhesive (Figure 3-18). The gauges were attached diametrically opposite each other at predetermined levels along the aluminium rod as shown in Figure 3-19 in order to cancel any possible effects of rod buckling which may occur. The gauges were wired in a wheat-stone bridge arrangement with a half bridge configuration, with the balancing resistor in the data acquisition unit.

Once the strain gauges have been bonded to the aluminium rod, they are covered with M-Coat J polysulfide protective coating. A debonding agent is applied over the gauges to stop the M-Coat J from bonding directly onto the gauge itself. The gauges are finally sealed with a heat shrink sleeve which ensures that the gauges are fully protected and insulated from the harsh grout environment.

It is important that shearing forces are not applied directly to the strain gauges and are applied only in the aluminium rod. Between the gauge locations, the aluminium rod is shot-blasted to give a rough surface for the grout to adhere to once it has been installed in the pile. The outer surface of the heat shrink sleeve around the gauge protection is given a light coating of debonding agent to ensure that the grout does not adhere and apply load directly to the gauge.

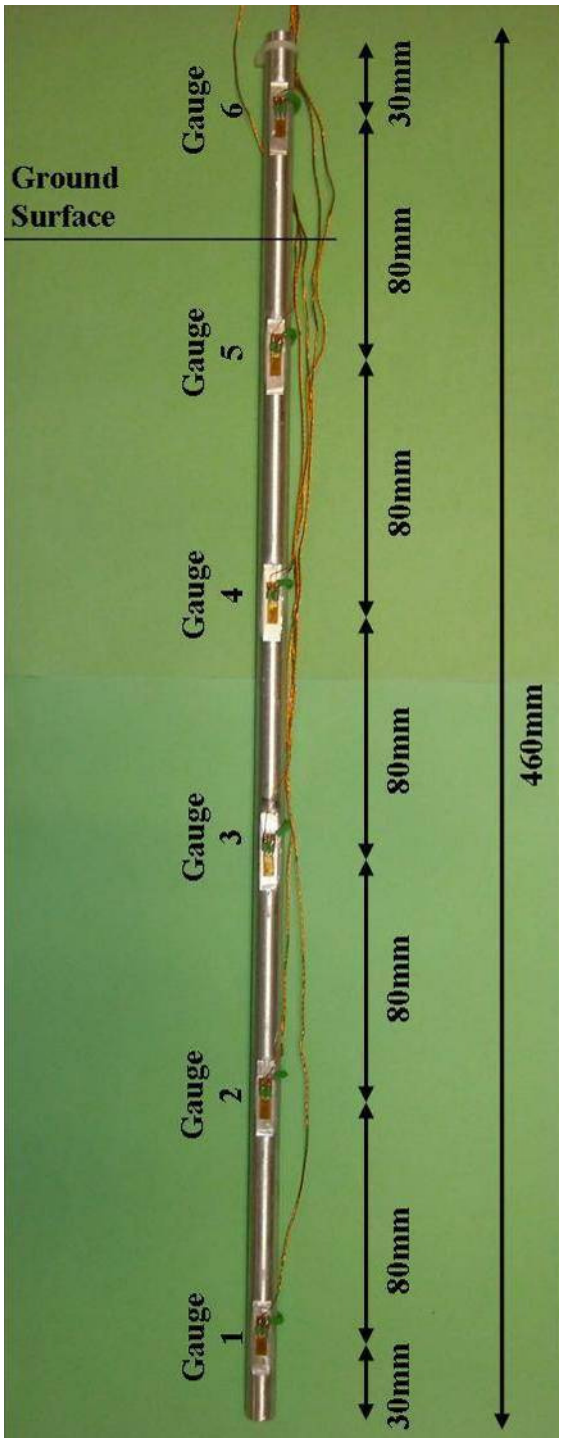

Figure 3-19. Strain gauge location along aluminium rod showing location of soil surface with respect to gauge locations (only one gauge of the pair is shown, partner gauge at each location is diametrically opposite on the other side of rod)

The strain gauged rods are installed into the freshly cast CHD pile through the use of the Instron. A housing unit secures the strain gauge rod in the Instron whilst it is slowly pressed into the pile, Figure 3-20.

(a) (b)

Figure 3-20. Strain gauged rod installation in a freshly cast CHD pile (a) full instrumented rod (b) close up view showing rod housing unit used during penetration

Further to the strain gauges installed, the series 2 CHD piles will have additional instrumentation in the form of torque measurement which will measure the torque required to advance and withdraw the auger bullet. The torque transducer is installed between the main shaft and the delivery shaft of the CHD drilling rig.

The torque transducer, a Novatech Ltd F311-Z3862, is rated to 25kNm which was considered adequate for the model tests. The torque transducer, Figure 3-21a, has a central bore to allow an inline insertion with the main shaft and delivery shaft of the drilling rig, Figure 3-21b. The transducer has threaded attachment points to allow it to be securely attached to the flange connections on the drilling rig shafts.

Having the torque transducer installed inline with the main shaft ensures the most accurate measurement of the torque experienced by the bullet.

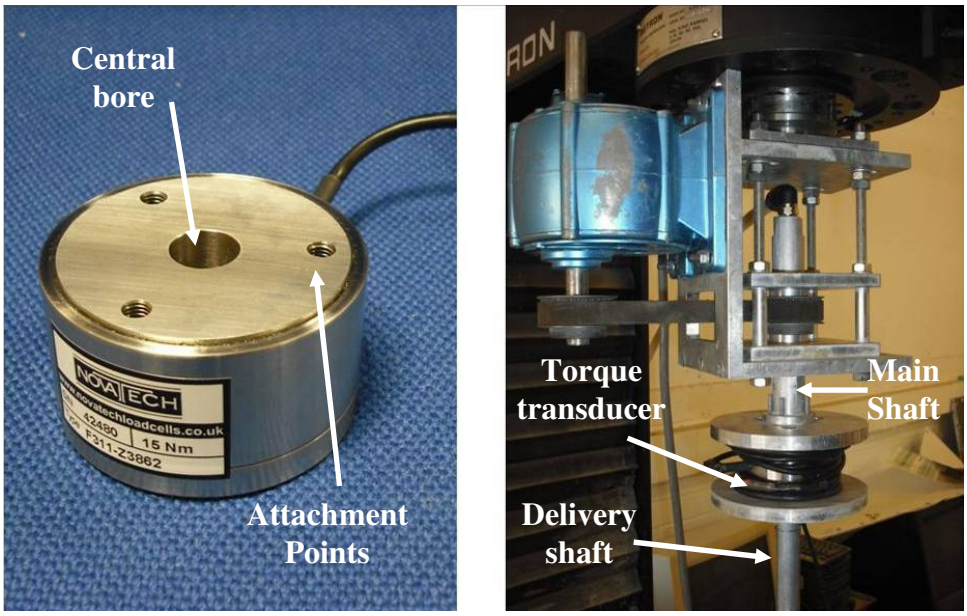

(a) (b)

Figure 3-21. Torque transducer (a) pre installation and (b) installed in the CHD drilling rig

3.3.9 Investigation of sand movement around CHD pile during load test

An attempt to track the sand particle movement around a CHD pile during loading was also conducted. The aim was to track the movement of the sand around a simulated CHD pile using particle image velocimetry (PIV) developed by White (2002). An aluminium post installation analogue CHD pile was manufactured and cut in half to allow it to be placed flat against a clear acrylic plate which forms part of a purpose built strong box, Figure 3-22a. Sand is pluviated over the half pile, perpendicular to the pile longitudinal axis to ensure sand penetrates the flange gaps by turning the box on its side, Figure 3-22b. Once pluviation of the sample has taken place, the strong box is tightly sealed and carefully rotated through 90°. Load to the half pile is applied via the Instron, Figure 3-22c. Lines of dyed sand have been poured along the acrylic plate in order to allow a visual aid to highlight movement of the sand particles when the pile is loaded.

(a) (b) (c)

Figure 3-22. Construction of CHD half pile test (a) locating the half pile in the strong box against the acrylic face (b) pluviation over the half pile (c) strong placed in the Instron ready to apply load to pile

However, despite repeated attempts, clear images of the soil movement around the pile during loading could not be obtained which would allow PIV to take place. When loading took place, the CHD half pile did not remain flush with the acrylic plate allowing the ingress of sand particles between the pile-acrylic interfaces. This soil movement around the pile was therefore not attributed solely to the movement of the CHD pile in the vertical plane. The problems encountered during this experiment could have been solved but this would have taken time to achieve. The setup allowed a visual observation of the sand movement during the loading of the CHD pile however the acquisition of quality images for use in PIV has been left for a potential future research work.

3.3.10 Cone Penetration Test

Significant research has been carried out on screw pile performance in relation to in situ cone resistance. In order to investigate the suitability of the available prediction methods for the application to CHD piles, a model CPT was developed.

It was also determined that due to the small scale of the models, measurement of the shaft friction independently within the model CPT would require an unacceptably long time to develop. Additionally, it is the tip cone resistance that

is primarily used in pile design techniques and also in the determination of soil properties. The average shaft friction would therefore be determined by looking at the difference in measurements between the globally applied load and the local cone tip load.

The model CPT is an accurately scaled model of prototype CPT cones made from stainless steel. The model CPT consists of a 600mm long, 16mm diameter tube with a loadcell and cone at the base. The cone has an apex angle of 60° and a base diameter of 16mm, giving a surface area of 377mm^2. The cone is screwed to the loadcell that sits in specially machined housing unit which is attached to an extension tube using high strength epoxy adhesive, as shown in Figure 3-23. The penetration of the CPT probe is controlled using the Instron at a rate of 500mm/min, with a specifically manufactured attachment tool used to secure the CPT probe. The loadcell was energised using a 10V supply using the Flyde unit and logged in a similar manner as was previously used for instrumentation components.

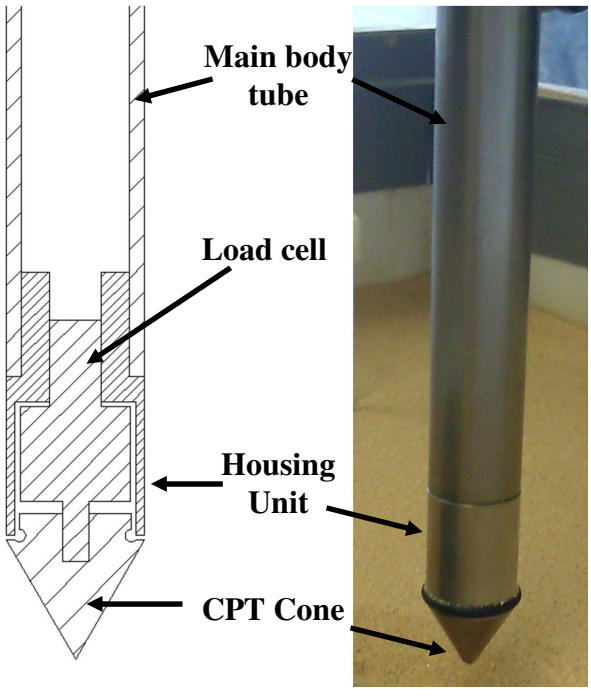

Figure 3-23. Model CPT cone details (a) Cross sectional view (b) constructed view

The loadcell used to measure the cone tip load is a Novatech Measurements Ltd F259 miniature diaphragm loadcell (Figure 3-24). The selection of the loadcell

was restricted to the strict dimension requirements imposed by the model CPT. Because of the size limitations in the model CPT, the maximum load capacity of the loadcell was 1kN. Although suitable for the majority of the tests performed, this maximum load rating restricted the penetration depth of the CPT in very dense sand beds where the cone resistance often reached the operating limit of the loadcell. During the penetration of the CPT into the sand bed, the loadcell output reading was closely monitored and when reached the operating limit, the CPT was stopped. The loadcell had been specially modified to allow the power and data cable to exit axially through the threaded attachment and up through the CPT unit. This cable runs through the centre of the unit and brought out at an access point at the top of the extension tube.

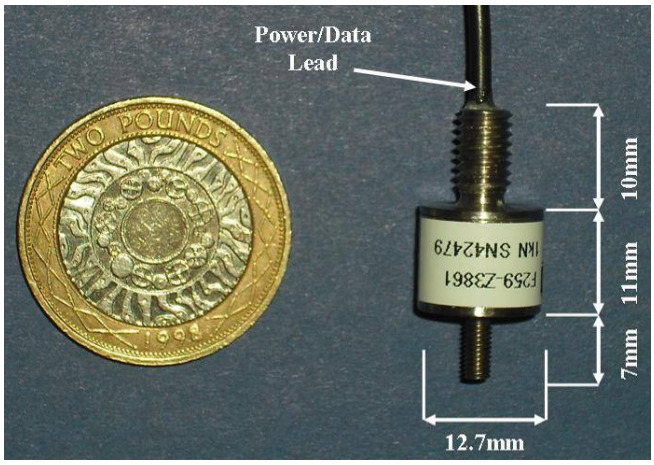

Figure 3-24. CPT cone loadcell dimensions

A prototype CPT cone is sealed using an oil seal to stop ingress of soil which would stop the loadcell compressing and measuring the cone tip load. The model CPT cone was initially sealed from the housing unit by a miniature o-ring, visible in black above the CPT cone in Figure 3-23b. However, the o-ring began to stretch and deform during repeated testing. During penetration of the cone, the distorted o-ring became constantly dislodged from the recess, causing errors in the recorded results. As a result, the o-ring was removed and the cone-housing interface was sealed with silicone sealant. The silicone was flexible enough so that it did not influence the cone resistance and it also produced a semi-permanent seal

The tip loadcell was pre-calibrated before being installed into the CPT unit. The output voltage was recorded using the Flyde data acquisition unit in a similar way to those used already. Since the cone surface area was known, the recorded tip load in kilo-Newtons could be converted into a stress reading as is typical in CPT recordings.

In order to establish a CPT design procedure for the CHD, cone resistance q_c, values have to be determined for an undisturbed sample of sand. Ideally, a CPT would be carried out in each test bed before a pile was installed however, due to the limited size of the model strong box, conducting a CPT would influence the soil structure which in turn could influence the behaviour of the installed pile. Instead, a number of CPTs will be carried out in specifically prepared sand samples in order to create a database of undisturbed or 'virgin' cone resistances, as shown in Figure 3-25.

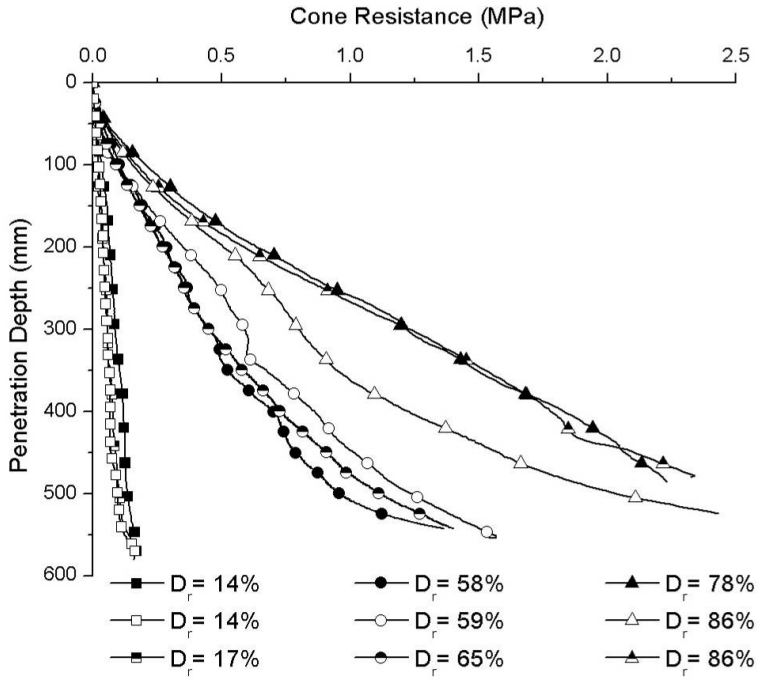

Figure 3-25. CPT cone resistances in undisturbed test beds prepared at different relative densities

In addition to the undisturbed cone resistances, the model CPT can also be used to assess the radial influence that the model piles installation has on the in-situ sand bed by measuring the cone resistance after the installation of the pile and

comparing it to the undisturbed cone resistance. The CPT probe is penetrated at set locations around the pile centre which equate to a distance of 1D, 1.5D, 2D and 3.3D where D is the pile diameter, as shown in Figure 3-26. The area of the box which had buried density pots was sectioned off so as to avoid any possibility of the CPT coming in contact with a pot.

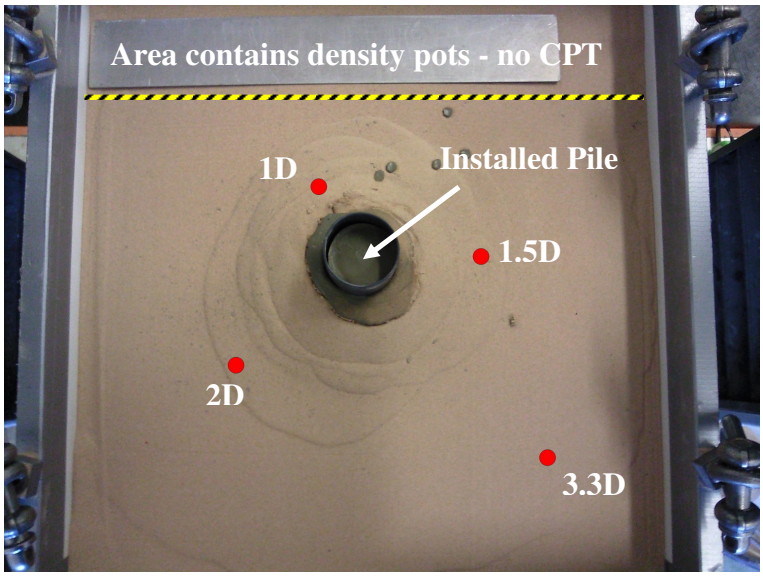

Figure 3-26. Radial CPT probe locations around an installed pile in terms of pile diameter

3.4 Direct Shear box testing of sand used in model tests

In order to determine the shear strength characteristics of the sand used in the model tests, direct shear box tests were conducted in accordance with BS 1377-7:1990 (1990). The sand used throughout the model tests was a HST 95, a quartz based silica sand from Bent Farm in Congleton, Cheshire.

The shear box tests were carried out at the University of Dundee in standard small shear box apparatus. The shear box itself was 60x60mm in plan with a total height of 50mm. Sand samples were prepared by pluviating directly into the shear box. The mass of sand in the sample was measured in order to obtain the relative density.

Since the model piles are installed in a test bed at 1G stress level, the effective stresses experienced will be considerably smaller than those experienced in the

field. To reflect this, the shear box tests will be carried out at low effective stresses which will typically be less than 10kPa.

Shear box testing will be carried out to determine the sand shearing characteristics, however interface shear tests will also be conducted in order to determine the friction angles for sand-concrete and sand-rough concrete interfaces, similar to those found in the pre-cast model piles.

During the shear box tests, both the shear stress and normal stresses on the sand sample are deduced which are then used in the determination of the angle of internal friction of the sample through the application of the Mohr-Coulomb failure criteria in equation 3-2.

$$\tau_f = c' + \sigma' \tan \phi' \qquad \textbf{3-2}$$

Where τ_f = shear stress on the failure plane (kPa)

σ' = normal stress on the failure plane (kPa)

ϕ' = Angle of internal friction

C' = Cohesion (equal to zero for dry sand)

3.4.1 Sand-Sand shear box test results

The peak and critical state shear stresses plotted against the low normal effective stress are shown in Figure 3-27. The low effective stresses shown in these tests are typical to those experienced in the model pile tests. It can be seen that the linear relationship between the normal effective stress and shear stress at low effective stresses does not go through zero. This can be seen more prominently when shear box data from higher effective stresses are plotted with a wider range of effective stresses such as those shown in Figure 3-28. It shows that at low effective stresses, there is a greater dilation of the soil. The critical state shear stress displays a more typical linear relationship.

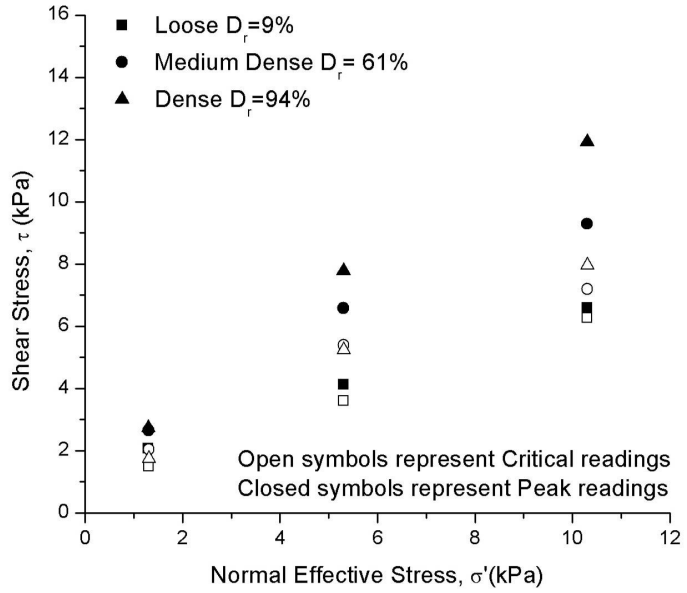

Figure 3-27. Shear box tests for sand-sand shearing for HST 95 sand at effective stress levels similar to model test values

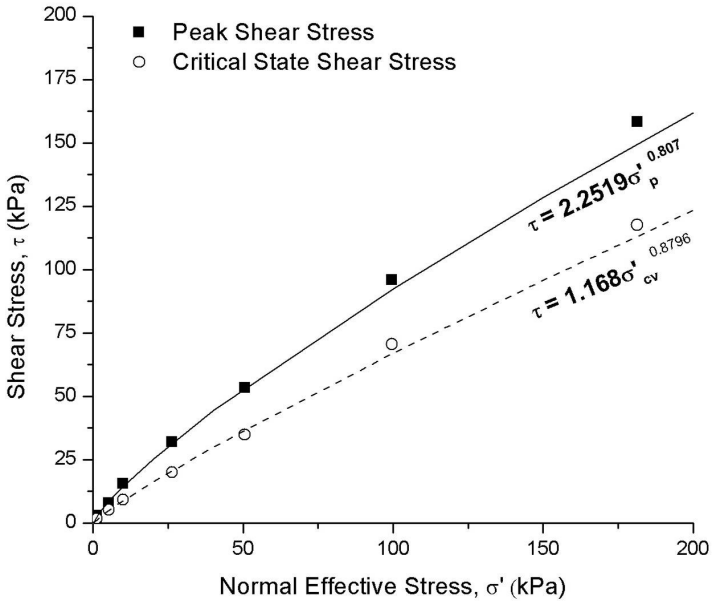

Figure 3-28. Shear box results for HST 95 sand at a D_r = 94%

The shear stress is shown to vary with the normal stress applied. The shear stress is plotted against the shear displacement in Figure 3-29 for dense sand at low effective stress. It highlights the increase in the ultimate shear stress as the normal effectives stress increases. This also occurred in loose and medium dense samples.

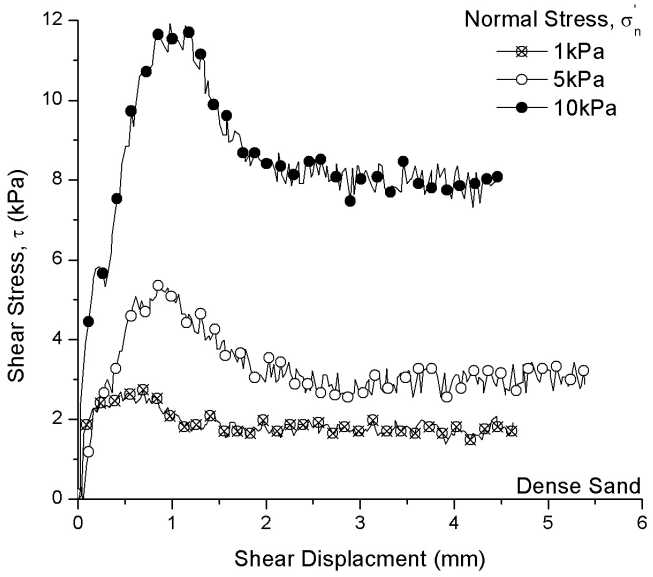

Figure 3-29. Shear stress against shear displacement for dense HST 95 sand at low effective stress

The influence of dilation on the model pile tests will be critical during the back-figuring of design parameters with significantly larger peak friction angles for the models than found in the field. Bolton (1986) shows that a reduction in normal effective stress causes an increase in the dilation angle. This is witnessed in the shear box tests as shown in Figure 3-30 for dense sand. The increase in the dilation angle at low effective stresses will cause a reduction in the horizontal effective stresses experienced in the soil, something which could affect the shaft resistance of the model piles.

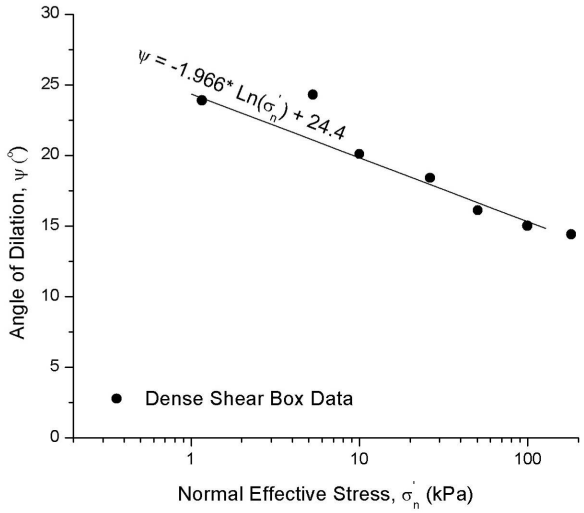

Figure 3-30. Dilation angle changes with normal effective stress from shear box tests in HST 95 sand at D_r = 93%

Using the data in Figure 3-28 in equation 3-2, the angle of internal friction of the HST 95 sand in a dense state can be calculated, as shown in Figure 3-31. It can be seen that both the peak and critical friction angles for the sand at low effective stresses are much greater than those experienced at high effective stresses which would be experienced in the field. The increase in the critical state friction angle with reducing effective stress has also been shown by Lauder (2010).

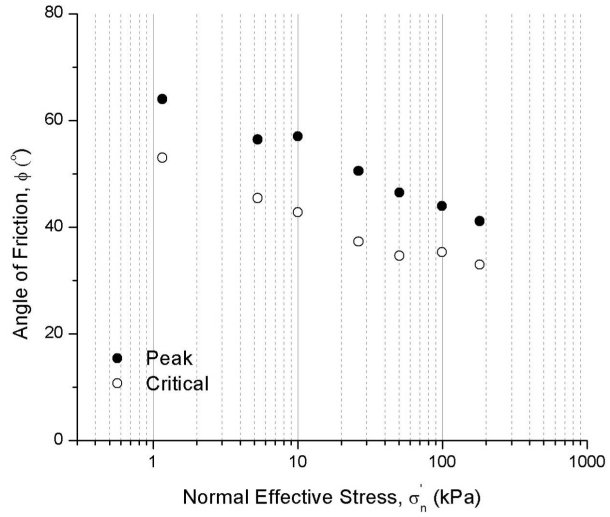

Figure 3-31. Friction angle variation with normal effective stress in HST 95 sand at D_r = 93%

The friction angles for the HST 95 sand at different sand states are summarised in Table 3-3 and Figure 3-32. The friction angles are seen to increase with the increase in relative density. The critical friction angles are seen to increase with relative density at low effective stress. As the relative density increase, the critical friction angle tends towards a value of 39°. The increase in the critical state friction angle with low effective stress as shown in Figure 3-31 is found to be more prominent as the relative density increases.

Table 3-3. Peak and critical state angles of friction for HST 95 sand at low effective stress

Soil State					
Loose – Dr = 9%		**Medium Dense – Dr = 62%**		**Dense – Dr = 93%**	
ϕ_{peak} (°)	ϕ_{crit} (°)	ϕ_{peak} (°)	ϕ_{crit} (°)	ϕ_{peak} (°)	ϕ_{crit} (°)
34	32	44	38	51	39

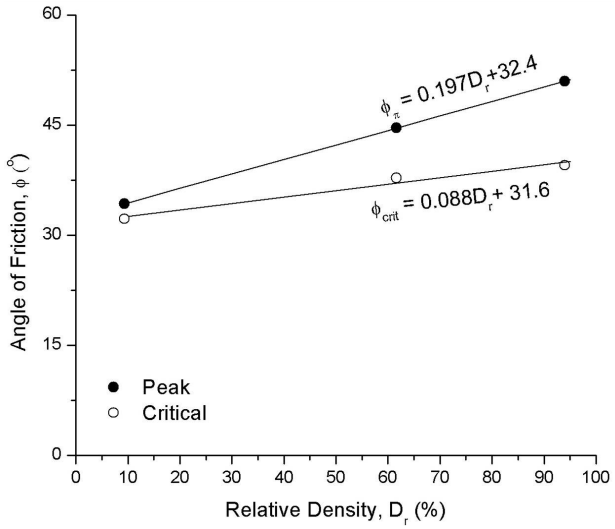

Figure 3-32. Variation in peak and critical frictions angles at low effective stress with relative density based on Table 3 data for HST 95 sand – sand friction

3.4.2 Sand-Concrete interface shear box test results

The model piles will induce soil shearing which is not sand-sand but will occur along the interface of the pile surface. To account for this, shear box testing has taken place on both smooth concrete and rough concrete. The smooth concrete will simulate the surface of the pushed piles while rough concrete will simulate the sand-concrete interface found in the WIP piles. The shear box tests were conducted by placing a pre-cast block of the model grout, one smooth and one roughened, in the lower half of the shear box.

The interface friction angles δ for smooth and rough concrete facings in dense sands are shown in Figure 3-33. As would be expected, the interface friction angle for the smooth concrete, δ_{peak} = 37.2°, is lower than that for the rough concrete, δ_{peak} = 48.4°.

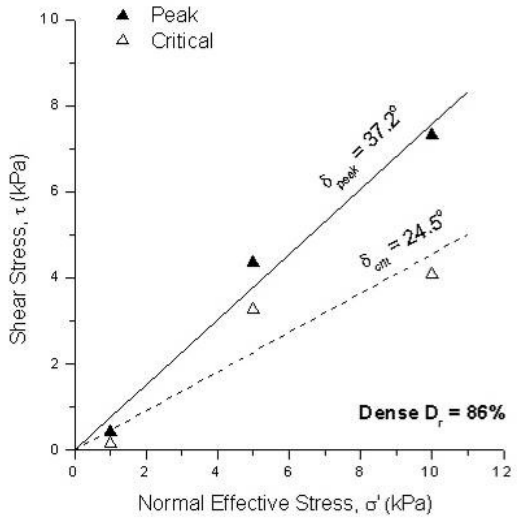

(a)

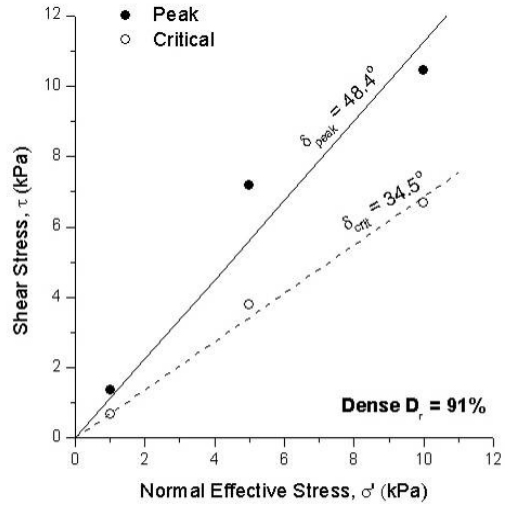

(b)

Figure 3-33. Interface shear box results for dense HST 95 sand at low effective stress for (a) sand-smooth concrete and (b) sand - rough concrete

Similar to the evaluation of the sand-sand shear box results, the interface friction angle shear box tests are evaluated at the low effective stress range similar to that experienced in the model tests. The interface friction angles for the sand-smooth concrete shown in Table 3-4, are typically 72% of the sand-sand friction angle while the sand-rough concrete is typically 86%. Compared to the values suggested by Tomlinson and Woodward (2008) of 80-100% for smooth concrete and 100% for rough concrete, the results obtained from shear box give a slightly lower estimate. The variation of interface friction angle with relative density which is utilised in the analysis in future model tests are presented in Figure 3-34.

Table 3-4. Peak and critical interface friction angles based on shear box tests

Interface Type	Sand State					
	Loose		Medium Dense		Dense	
	δ_{peak} (°)	δ_{crit} (°)	δ_{peak} (°)	δ_{crit} (°)	δ_{peak} (°)	δ_{crit} (°)
Sand-Smooth Concrete	27.1	23.7	30.8	24.1	37.2	24.5
Sand – Rough Concrete	29.7	25.7	40.5	28.6	48.4	34.5

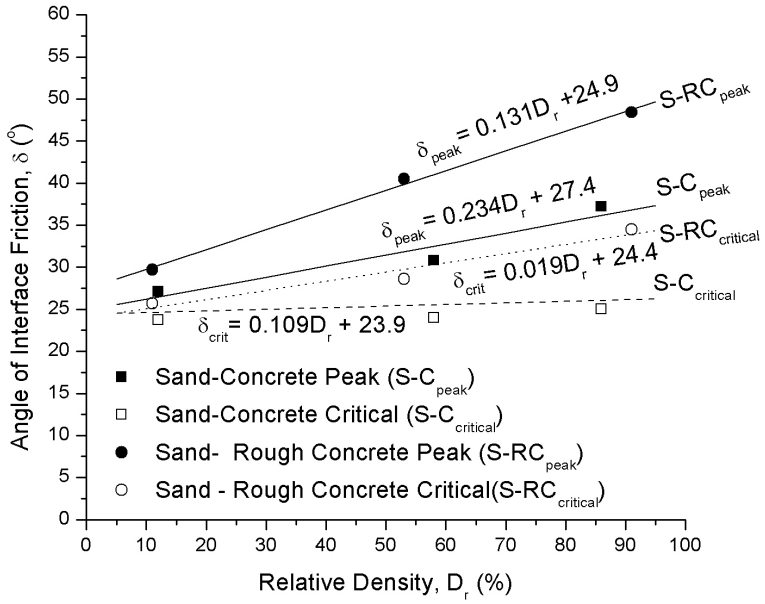

Figure 3-34. Interface friction angle variation with relative density for sand-concrete and sand-rough concrete interfaces

3.5 Summary

The techniques used in the collection of data for the body of research have been discussed in detail throughout this chapter. The collection and analysing of the field data will be discussed in section 4.0 while the model testing will be in section 5.0. A summary of the model pile tests carried out for the research is given in Table 3-5.

Through the use of shear box testing, it has been found that the selection of the sand angle of friction will depend on both the density of the in-situ sand and also the effective stress. It is therefore important that the low effective stresses

encountered in the model testing are taken into consideration during the analysis of the results.

Table 3-5. Summary of model testing to be undertaken including the outputs from instrumentation measurements

Pile Type	Diameter (mm)	Length (mm)	Measurements taken
Series 1 Piles			
CHD	60	280	Total load
Pushed	30, 60	280	Total load
WIP	30, 60	280	Total load
Series 2 Piles			
CHD	60	400	Total load, torque, strain gauges, radial CPT
Pushed	60	400	Total load, base load, radial CPT
WIP	60	400	Total load, base load, radial CPT

4.0 Field Data Analysis

4.1 Introduction

The first stage in the investigation of the CHD pile was to analyse field test data from full scale pile tests. Field data was obtained from the Roger Bullivant offices for projects where CHD piles had been installed between the years of 2004 and 2011. The data collected covered projects from across the United Kingdom and therefore a wide variety of soil conditions were incorporated in the data set.

This chapter contains the data analysis of the collected field CHD pile tests. The selection of CHD diameter on the pile design capacity is investigated using the load-settlement behaviour obtained from the pile tests in order to determine an appropriate value.

The investigation of the load-settlement response of the CHD test piles highlights the difficulty in determining the ultimate capacity of the CHD pile. The development of ultimate pile capacity behaviour during a load test is found to rarely occur. Because of this issue, prediction methods were implemented in order to determine the ultimate pile capacity using the available test data.

Utilising the available data, a number of techniques have been used to estimate the base and shaft capacity contributions to the overall pile capacity. This includes the use of pile settlement analysis and also a computer software analysis. The accuracy and suitability of the determined base and shaft capacities are discussed.

4.2 Collection of CHD project data

In total, geotechnical data for 76 load tested CHD piles were collected from 58 different projects. The site investigation data provides information on the geotechnical soil data for each pile and was used as a basis to filter the large amounts of data into a workable database. Of the 76 test piles, 27 were installed predominantly in sands, 28 were in fine grained (referred to as clay) soils and 21

of the piles were in mixed soil layers. The main focus of the research project is on the behaviour of the CHD pile installed in sand, however, a selection of piles installed in clay soils conditions have also been investigated. In order to ease the analysis process, piles installed in layered mixed soils will be excluded from the investigation.

Some basic information regarding the pile performance for the selected piles which were installed in sandy soils are summarised in Table 4-1, whilst Table 4-2 lists those installed in clay soils. The piles in clay soils were selected because of the apparent display of ultimate capacity in pile E31-1 and also due to the fact that project E28 used cone penetration testing (CPT) during the site investigation, as will be discussed later. As discussed in Chapter 2, the ultimate design capacity of the CHD pile is determined using the RBL design process which predominantly assumes a design diameter equal to $0.75D_f$, however a diameter equal to $1D_f$ has also been used on a number of occasions. The safe working load, (SWL) is the load which the pile will be subjected to from the intended superstructure during its working life. The SWL is determined from the design capacity load by application of a factor of safety, which is typically assumed by RBL to be 2.5 for the CHD piles investigated.

The pile ID prefixes S and E refer to the RBL region from which the data was originally collected, S for those in the Scottish region and E for those in the English region. The predominant in-situ soil type is determined by splitting the pile into three equal zones corresponding to exactly one third of the pile length. The zones are classified as head, mid-shaft and toe. In most instances the ground around the surface of the pile, the head zone, is formed of made ground, which usually consists of granular, man made materials and is assumed to contribute very little to the total capacity of the pile.

Table 4-1. Field data for CHD piles installed in sands

Project ID	General Ground conditions*			Pile Length BGL (m)	SWL (kN)	RBL Design Capacity (kN)	
	Head	Mid-shaft	Toe			$0.75D_f$	$1D_f$
E21	MD Sand	MD Sand	MD Sand	11.6	645	1553	2211
E16	MD Silty Sand	MD Silty Sand	D Silty Sand	10	600	1920	2969
E1-2	MG	D Sand	D Sand	7.3	290	1824	3139
E27-1	MG	D Gravel	VD Sand	6	650	1364	2278
E27-2	MG	D Gravel	VD Sand	6.16	665	1364	2278
E27-3	MG	D Gravel	VD Sand	4.9	570	777	1286
E27-4	MG	D Gravel	VD Sand	5.25	610	740	1199
E27-5	MG	D Gravel	VD Sand	4.73	658	814	1372
E27-6	MG	D Gravel	VD Sand	4.44	655	814	1372
E27-7	MG	D Gravel	VD Sand	6.03	650	1364	2278
E27-8	MG	D Gravel	VD Sand	7.6	710	2139	3559
S26	MG	L Sand	MD Sand	19	900	2049	3015
S25	MG	MD Sand	MD Sand	14	625	2605	3939
S4-1	MG	L Sand	MD Sand	12	650	1506	2556
S4-2	MG	L Sand	MD Sand	12	650	1506	2556
S6	MG	MD Sand	MD Sand	5.4	690	727	1203
S14	MD Sand	MD Sand	MD Sand	11.6	750	1641	2683
S21	Silt/Clay	MD Sand	MD Sand	7	450	877	1403
S19-1	MD Sand	MD Sand	MD Sand	15	1000	1612	2379
S19-2	MD Sand	MD Sand	MD Sand	17	1000	1922	2807
S12-1	MG	Sand-Silt	Sand-Silt	10.3	385	982	1883
S12-2	MG	Sand-Silt	Sand-Silt	16	385	1497	2279
S12-3	MG	Sand-Silt	Sand-Silt	12	385	1201	1569
S27-1	MG	MD Sand	VL Sand	19	300	616	888
S27-2	MG	MD Sand	VL Sand	19	300	616	888
S27-3	MG	MD Sand	VL Sand	19	300	616	888
S27-4	MD	MD Sand	VL Sand	19	300	616	888

*Ground Condition Classification Codes

MG = Made Ground VL = Very Loose L = Loose

MD = Medium Dense D = Dense VD = Very Dense

Table 4-2. Field data for CHD piles installed in clay soils

Project ID	Ground Conditions			Pile Length BGL (m)	SWL (kN)	RBL Design Capacity (kN)	
	Head	Mid-Shaft	Toe			$0.75D_f$	$1D_f$
E28-1	Loose Silt	Soft Clay	V. Stiff Clay	11	500	1038	1510
E28-2	Loose Silt	Soft Clay	V. Stiff Clay	15	750	2050	2939
E28-3	Loose Silt	Soft Clay	V. Stiff Clay	15	750	2050	2939
E31-1	Stiff Clay	Soft-Firm Clay	Soft-Firm Clay	19	875	1093	1491

For each of the selected piles, the load-settlement data was collected and plotted to show comparative behaviour between different projects, as is shown in Figure 4-1a-d. The data for CHD piles installed in sands has been split using density classification, with those installed in loose sand shown in Figure 4-1a, medium dense sand in Figure 4-1b, and dense sand in Figure 4-1c. It can be seen that the total pile settlement experienced in the load test is very low, typically between $0.01D_f$ and $0.02D_f$, with settlements never reaching $0.1D_f$, the general failure criterion of 10% of the pile diameter. The load tests do not appear to show yield behaviour as defined in Figure 2-23, with the exception of pile E31 which will be discussed at a later point.

All CHD piles considered in the database are loaded using a maintained load test, MLT. Load is applied to the pile as a percentage of the SWL in incremental stages as defined by Weltman (1980) and the ICE SPERW (2007). In the majority of cases, the load test is taken to a predetermined magnitude which equals 150% of the SWL. The magnitude of load applied fulfils the requirements for safety and performance criteria however that does not always mean that the ultimate capacity of the pile is determined. In some instances, CHD piles have been loaded to greater magnitudes than 150% of the SWL, with some having reached as high as 500% SWL, however these are rare.

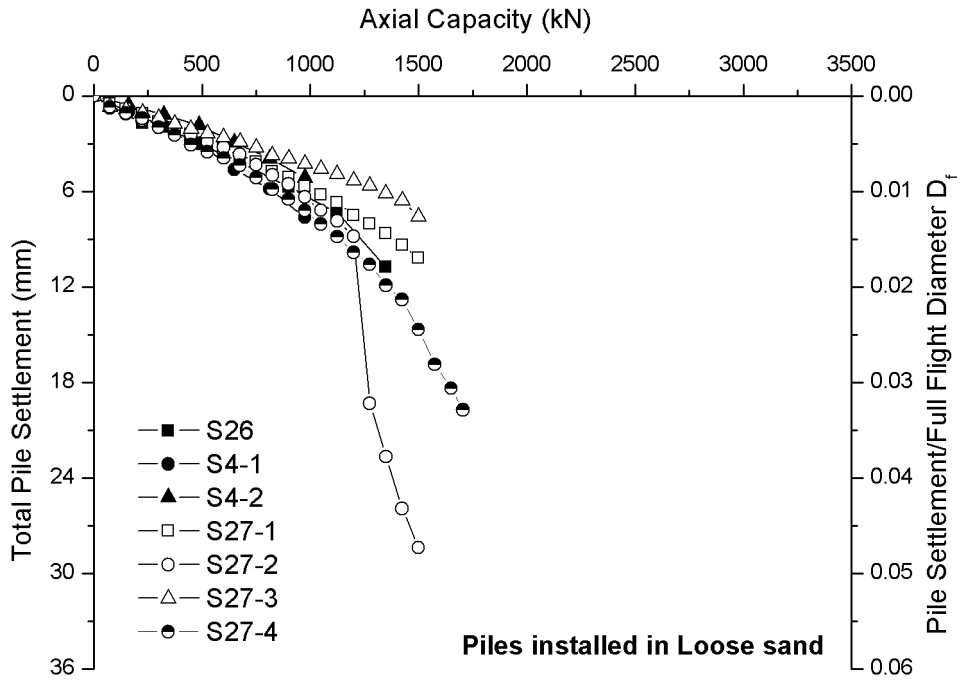
Axial Capacity (kN)
0
500
1000
1500
2000
2500
3000
3500
Total Pile Settlement (mm)
0
6
12
18
24
30
36
Pile Settlement/Full Flight Diameter D_f
0.00
0.01
0.02
0.03
0.04
0.05
0.06
S26
S4-1
S4-2
S27-1
S27-2
S27-3
S27-4
Piles installed in Loose sand

(a)

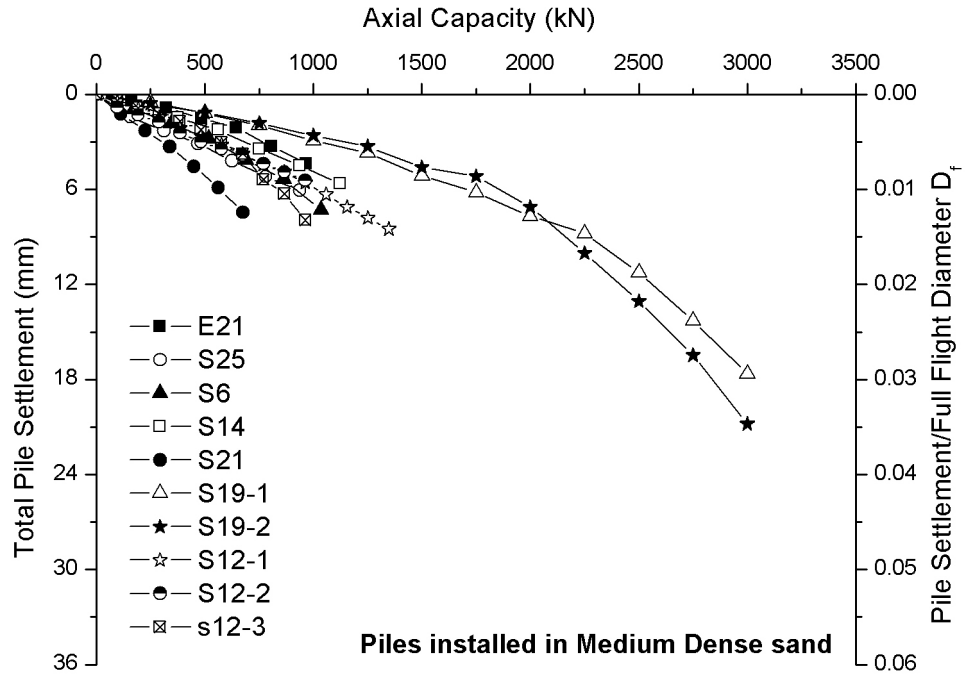
Axial Capacity (kN)
0
500
1000
1500
2000
2500
3000
3500
Total Pile Settlement (mm)
0
6
12
18
24
30
36
Pile Settlement/Full Flight Diameter D_f
0.00
0.01
0.02
0.03
0.04
0.05
0.06
E21
S25
S6
S14
S21
S19-1
S19-2
S12-1
S12-2
s12-3
Piles installed in Medium Dense sand

(b)

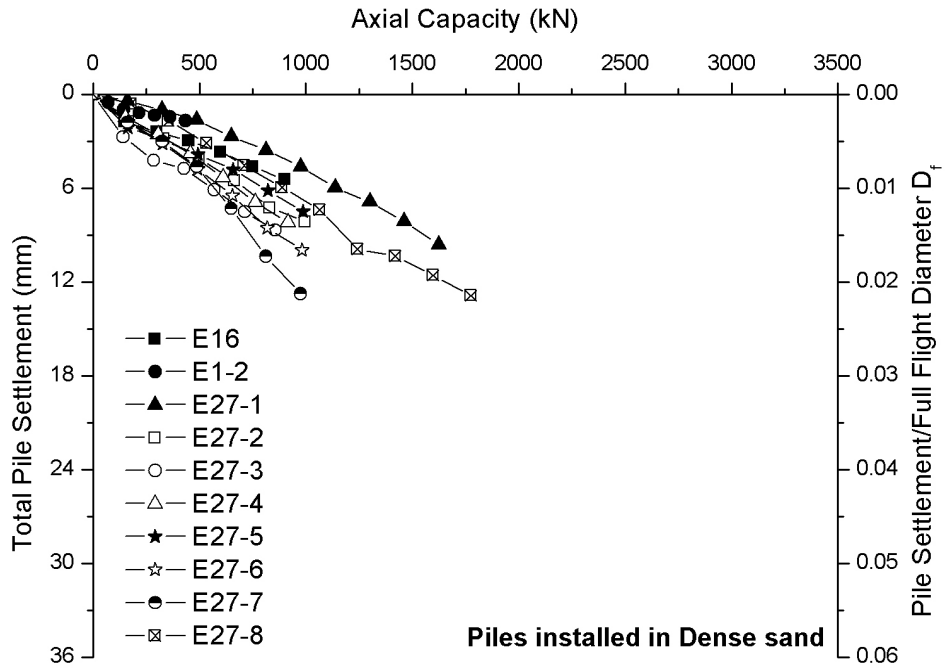

(c)

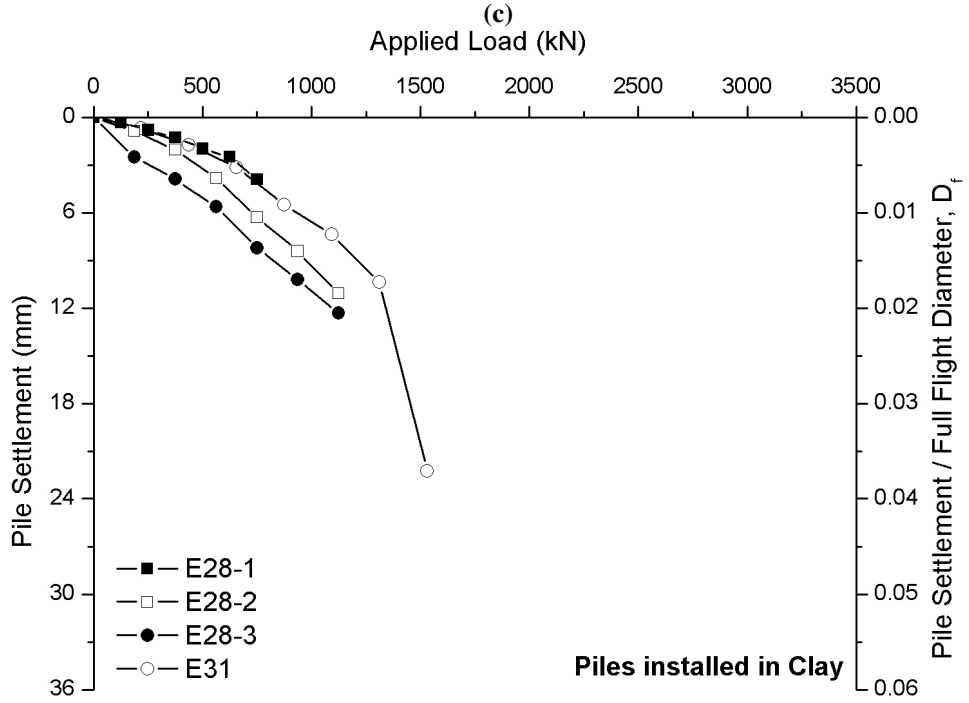

(d)

Figure 4-1. Load-settlement plots for selected CHD test piles installed in (a) loose sand, (b) medium dense sand, (c) Dense sand and (d) those installed in clay soils

Looking at the load settlement data for piles installed in sands, variations can be seen on the curves depending on the density of the soil the piles have been installed in. As shown in Figure 4-2, depending on the in-situ sand density, the relative stiffness of the CHD piles varies. Looking at a specific settlement of 6mm ($0.01D_f$), it can be seen that pile-settlement behaviour is very similar for all field

piles. It is noted however that piles installed in loose sand display greater stiffness than those installed in dense sands. It would be expected that for piles installed in dense sand would have a stiffer response than those installed in lower densities however this does not appear to be the case. This suggests that the CHD installation process gives substantial improvement when installed in loose sand.

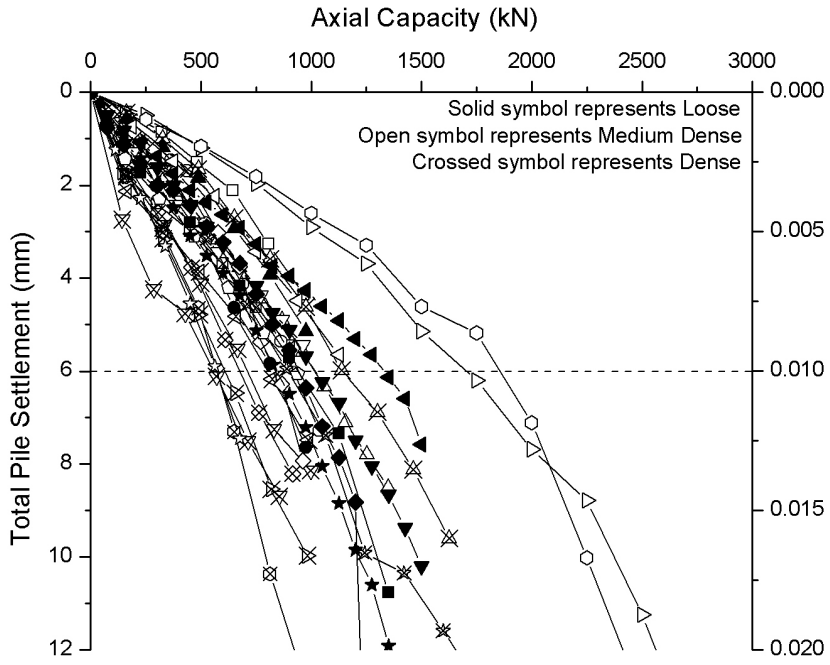

Figure 4-2. Comparison of CHD load settlement data for piles installed in different sand densities

4.3 Investigation of suitable CHD design diameter using field data

The load-settlement data for the selected CHD projects show that the piles have not reached a sufficient load to allow the determination of the ultimate capacity using the traditional definitions discussed in Chapter 2, such as a settlement of 0.1D or when there is no further increase in load carrying capability without significant settlement. The maximum load applied during the MLT is limited to a percentage of the SWL and does not correspond to the ultimate capacity of the pile. Based on the load-settlement plots in Figure 4-1, it can be seen that none of the pile tests in the database display typical characteristics of ultimate pile capacity. It can therefore be assumed that the maximum load applied during the load test does not correspond to the ultimate pile capacity.

With this assumption in mind, the pile capacity calculated using the Roger Bullivant design procedures detailed in Chapter 2 can be compared to the maximum load applied during the MLT to assess the accuracy of the design calculations when different pile diameters are used (Figure 4-3). From Figure 4-3 it can be seen that the loads applied during the tests are seldom equal in magnitude to the designed capacity. It should be assumed that, unless otherwise stated, the term design capacity refers to the unfactored capacity of the pile determined using design methods discussed in Chapter 2.

When the piles are designed using a diameter equal to $0.75D_f$ (450mm), it can be seen (Figure 4-3a), that the applied test load exceeds the design capacity for almost half the test piles. From the load-settlement behaviour plotted in Figure 4-1, the piles which have been loaded beyond their designed capacity in Figure 4-3a, do not display typical capacity failure behaviour, suggesting that the design is conservative.

If the design diameter is increased to match the outer flight diameter of the pile, $1D_f$ (600mm), Figure 4-3b, only a few test piles appear to be loaded to their design capacity, those being from project S19, S27 and E31. The load-settlement

behaviour for the piles (Figure 4-1) shows that for pile E31-1, post yield behaviour appears to have been attained. Piles from projects S19 and S27 have greater settlement than the other piles in the database, however being able to define at what yield stage the piles has reached in relation to Figure 2-23, is difficult. It is therefore not easy to determine if the load applied during the MLT corresponds to the ultimate pile capacity or not. If it is assumed that the MLT load for piles S19 and S27 does correspond to the ultimate pile capacity, it can be seen that the design capacity determined from the use of the full flight diameter gives conservative values.

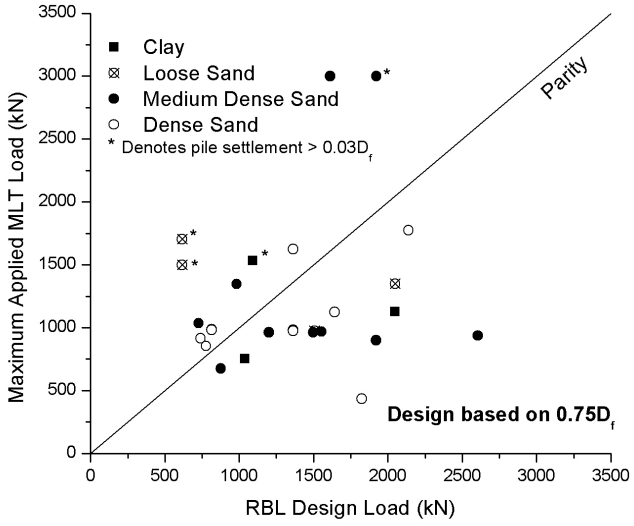

(a)

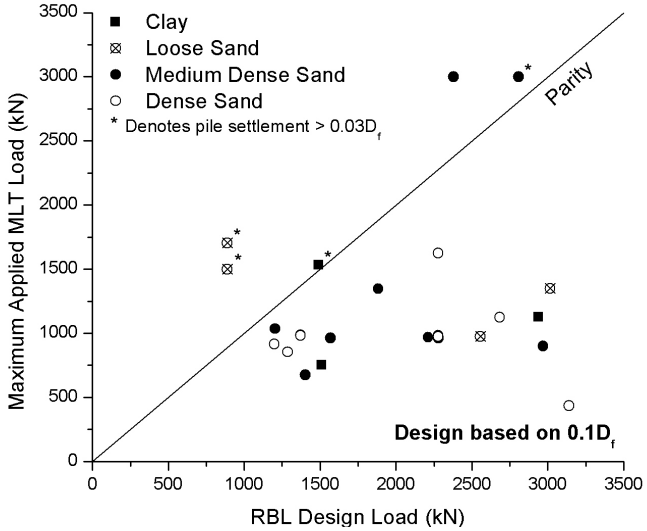

(b)

Figure 4-3. Designed load using RBL method assuming diameter equal to (a) $0.75D_f$ and (b) $1D_f$ compared to the maximum applied load during the MLT

Without proving the ultimate capacity of each pile, the selection of appropriate design diameter is difficult. However, the evidence available from the load tests suggests that the use of the full flight diameter in the design of the piles produces a design capacity load which is conservative in nature. In order to fully refine the design parameters however, the ultimate capacity for each test pile must be established. Ideally, the ultimate capacity would be measured from the MLT, however as has been shown, in the case of the CHD test piles this is not possible and therefore a prediction must take place.

4.4 Determination of ultimate pile capacity

It can be seen from the available load-settlement data from the CHD database that the determination of an ultimate capacity using definitions from Weltman (1980) or the ICE SPERW (2007) guidelines, relating the pile diameter to pile settlement or where settlement occurs with no increase in further applied load is not possible. This is a similar situation found by the Geotechnical Consulting Group (1998) as was discussed in section 2.4.1 for CHD piles. In order to conduct refinement of the design process of the CHD piles, the ultimate capacity must be predicted. If determination of the ultimate capacity directly from the load-settlement plots is not possible, it must be estimated through the use of prediction methods such as those suggested in section 2.6.2.

4.4.1 Extrapolation of load test data

Both the Chin and Decourt methods have been used to predict ultimate capacities for the majority of the CHD piles. The predicted capacities are highly dependant on the shape of the load-settlement curve from the pile tests and therefore, in order to predict an accurate ultimate capacity, the test pile must be subjected to a sufficient magnitude of load which produces an appropriate settlement. This can generally be regarded as the load determined from the Davisson 1973 offset capacity, as discussed by Fellenius (2001b).

Each prediction plot for a test pile was carefully analysed in order to assess the suitability of the data for use in a capacity prediction and in most instances it was clear when the data was suitable or not. Typical examples of Chin analysis plots in Figure 4-4 show project data which both allows the determination of a capacity prediction and also data which does not. It can be seen that for the piles in project S19, the data tends to a straight line indicating that the load applied during the MLT was sufficient to enable a Chin prediction. In project S25, the pile does not yet tend to straight line, indicating that the applied load in the MLT is not sufficient.

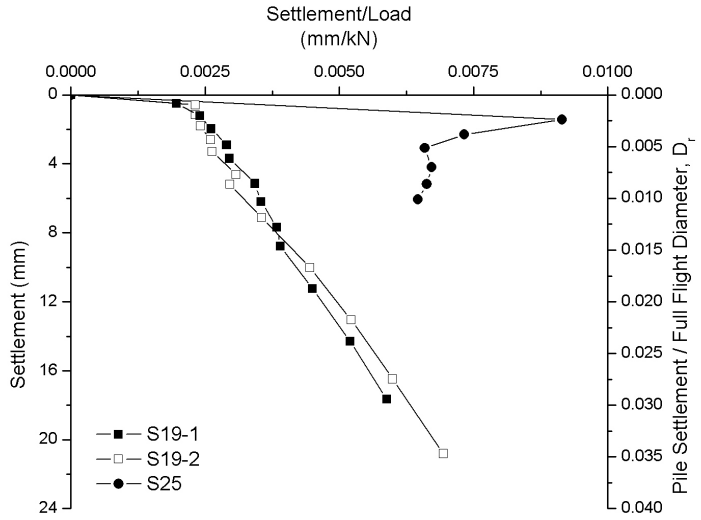

Figure 4-4. Chin analysis plots showing example CHD project that shows data which tends to a straight line (project S19) and where the Chin plot has not reached a steady state (project S25)

Similar to the Chin capacity predictions, the DeCourt method can fail to give predictions for all test piles due to an insufficient magnitude of load applied on the test piles. Typical plots for the Decourt analysis are shown in Figure 4-5. Project S19 represents piles which appear to have been loaded sufficiently to allow the formation of a straight line which can be extrapolated to intersect with the abscissa. Project S25 represents typical piles which have not been loaded to a sufficient level to show the formation of the straight line which therefore fails to intersect with the abscissa.

Only piles in the database which allow easy determination of ultimate capacity such as those displayed by S19-1 and S19-2 in Figure 4-4 and Figure 4-5 were analysed further. The suitability of the prediction methods in determining an ultimate capacity did not appear to do depend on pile settlement. In some cases, convergence of the data points occurred after a settlement of less than 0.01D however in most cases settlements exceeding 0.01D provided improved predictions.

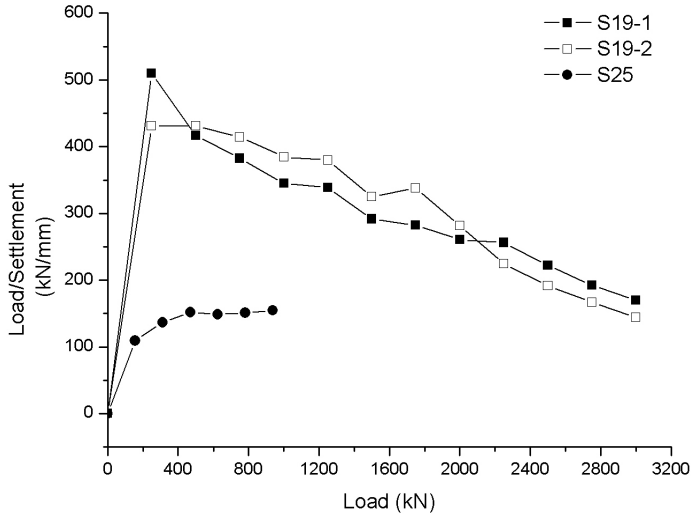

Figure 4-5. Decourt analysis example plots showing CHD project S19 which tends to a straight line and project S25 which represents projects which have not been loaded enough to display a straight line

Since the predicted values are dependant on the suitable formation of curves from the test data, the accuracy of the obtained predictions was investigated. Since the piles in project S19 have the largest settlement, they were utilised in determining the prediction accuracy depending on available data. Both the Chin and Decourt analysis methods were repeated on the S19 datasets but assuming smaller subsets of data. It was found that, as would be expected, the accuracy of the prediction value improves with an increase in the settlement of the piles. If only a small data set was used in the analysis, it was found that the predicted capacities could be 20% under-estimated and up to 30% over estimated depending on the load-settlement data. This range dropped to around 10%-20% if the pile settlement reached 6mm ($0.01D_f$). It is therefore important when using the prediction methods that an adequate pile settlement has been achieved in the load test.

The analysed CHD pile data which allowed the determination of an ultimate capacity using the different methods is shown in Table 4-3. As has been mentioned, capacities for a number of test piles were unable to be determined using the prediction methods. Fellenius (2001b) describes how the Davisson criteria load is suggested as a minimum to which the pile should achieve in order for the prediction methods such as Chin or Decourt, to be considered accurate. However, not reaching the Davisson criteria load during the load tests does not render the prediction methods unusable, they must simply be used with caution. From the analysis, it can be seen that the Davisson criteria load is rarely achieved during a CHD load test, suggesting that the ultimate pile capacity is significantly greater than the maximum loads imposed during the MLT.

Table 4-3. Ultimate pile capacity predictions for CHD piles compared to RBL design capacities and the maximum applied test load

Pile ID	RBL Design Capacity (kN)		Max MLT Load (kN)	Davisson Criteria Load (kN)	Predicted Ultimate Capacity		
	$0.75D_f$	$1D_f$			Chin (kN)	DeCourt (kN)	Average (kN)
E21	1553	2211	968	-	1974	1891	1893
E27-1	1364	2278	1625	1600	3870	2722	3219
E27-4	740	1199	915	-	4837	-	4837
E27-7	1364	2278	975	750	2221	2198	2165
E27-8	2139	3559	1775	1200	4502	3247	3784
S26	2049	3015	1350	-	3733	3152	3368
S4-1	1506	2556	975	-	3080	2934	2945
S4-2	1506	2123	975	-	2426	2321	2325
S6	727	1203	1035	-	2831	3241	2979
S14	1641	2683	1125	-	3746	3286	3441
S21	877	1403	675	-	3347	3135	3174
S19-1	1612	2379	3000	2500	4637	4511	4482
S19-2	1922	2807	3000	2350	4130	4113	4039
S12-1	1201	1569	963	-	1530	1463	1466
S12-3	982	1883	1347	-	5283	5292	5182
S27-1	616	888	1500	1550	5822	5039	5314
S27-2	616	888	1500	1200	2856	2755	2748
S27-3	616	888	1500	-	3639	2845	3169
S27-4	616	888	1705	1250	3036	3162	3038
E28-1	1038	1510	750	-	1353	1362	1330
E28-2	2050	2939	1125	1050	1982	1819	1861
E31-1	1093	1491	1531	1300	1967	1918	1903

It is seen in Figure 4-6 that the capacities predicted for the CHD piles using the two separate methods give similar results. The Decourt capacities for a number of piles can be seen to give as much as 4% lower estimations of the ultimate capacity compared to the Chin predictions.

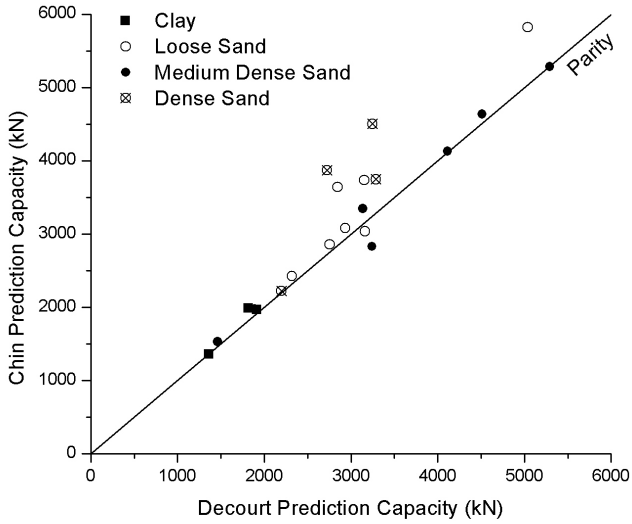

Figure 4-6. Comparison of Chin and Decourt analysis capacity predictions for CHD piles

Using equation 2-22, an ideal curve for both the Chin and Decourt predictions can be plotted and compared to the original load-settlement data. From Figure 4-1 it can be seen that pile S19-1, S19-2 and E31 have some of the largest settlements in the test pile database. This increased settlement indicates that these piles are more likely to display the ultimate capacity of the CHD pile compared to the others in the database. The predicted capacities for these projects are shown in Figure 4-6 along with the recorded load-settlement from the maintained load test.

The average curves are determined from the MLT data using techniques described by Weltman (1980). Each loading increment is held on the pile for designated time spans as dictated by SPERW (2007). Once the load has been held on the pile for the required minimum time, the load-settlement readings of the pile are recorded to give the average values.

It can be seen that the Decourt prediction provides a closer prediction of the measured load-settlement data than the Chin prediction, which tends to over-predict. The over estimation in pile capacity using the Chin analysis is known, as was discussed in section 2.6, however the degree of over-estimation has not previously been quantified for CHD piles. Assuming that the Decourt capacity more accurately represents the true pile behaviour, the Chin analysis can be seen to over-predict the CHD capacity by a factor of 1.04. This compares to an over-prediction of 1.08 for driven piles, as determined by Chin (1972).

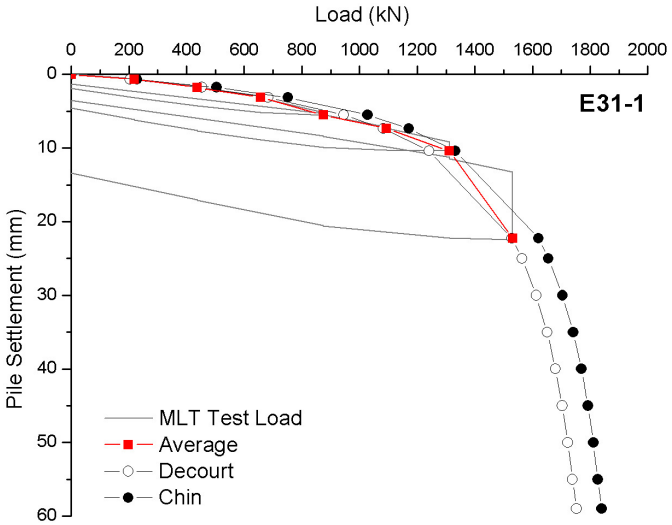

(a)

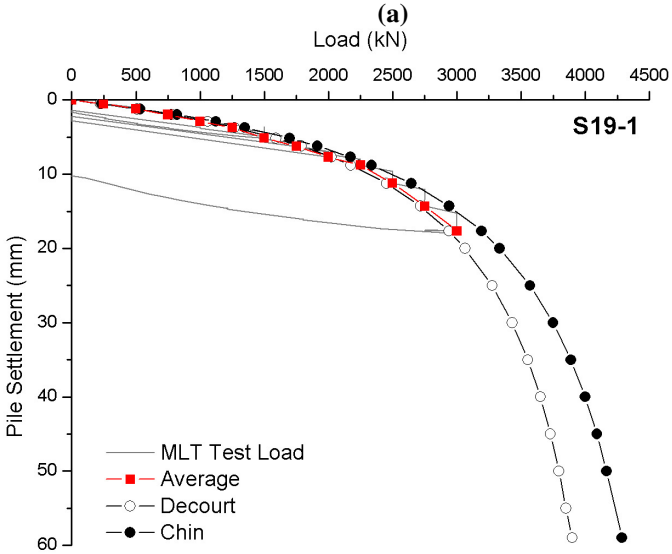

(b)

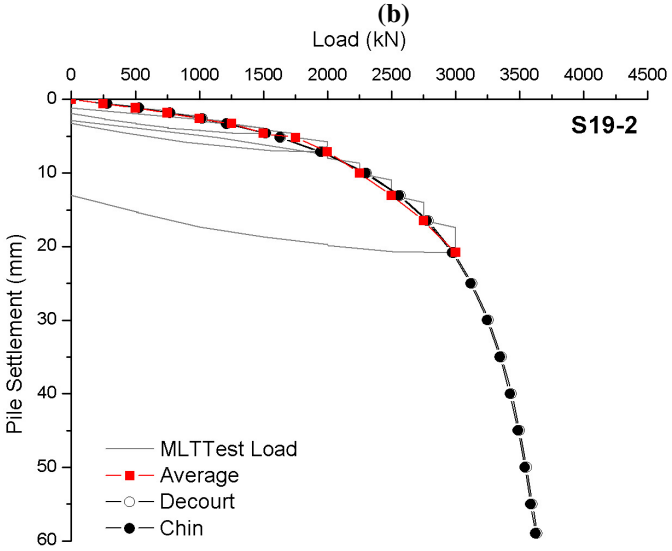

(c)

Figure 4-7 Predicted capacities compared to maintained load test data for piles with large settlements

Based on this information, a correction factor of 0.96 should be applied to the Chin capacity determined for CHD piles. The correction factor of 0.96 determined for Chin predictions for CHD piles can be applied to the capacity predictions using the Chin method in Table 4-3. The pile capacity can be determined using either the corrected Chin prediction or the Decourt prediction. Since both methods are an estimated prediction, for the analysis of the test data, an average of the corrected Chin and the original Decourt values have been used to determine a predicted ultimate capacity for the CHD pile data (Table 4-3).

The predicted capacity is compared to the designed pile capacity determined using the current RBL design procedures in Figure 4-8, assuming a design diameter of D_f. For the majority of the piles, the design capacity is still conservative compared to the predicted capacity. Although this can be seen to occur in most soil conditions, the under prediction is more prominent in loose to medium dense sands. Piles installed in clay appear to have a relatively close approximation of design capacity to the predicted values. Since the full flight diameter has been assumed in the design of the piles, it would appear that there is need for improvement in the existing design techniques for piles installed in sand.

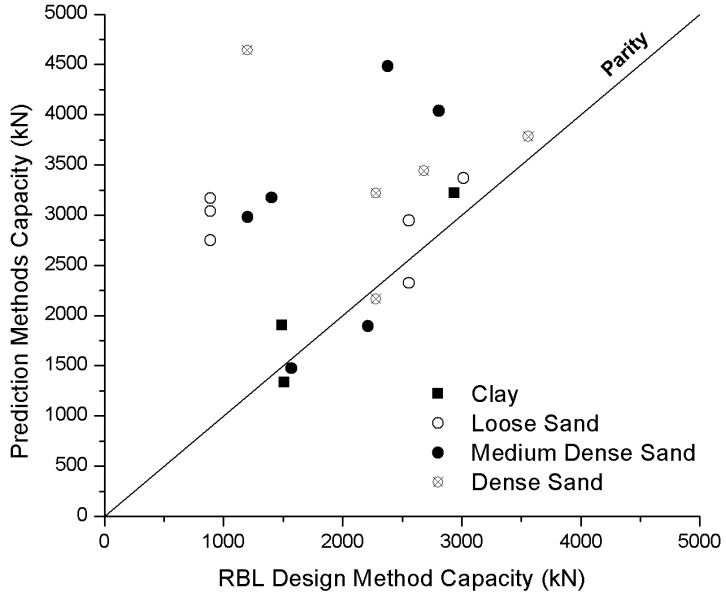

Figure 4-8. Pile bearing capacity determined from the RBL design method assuming full flight diameter compared to those determined using prediction techniques

4.4.2 Pile capacity determined from CPT design method

As has been mentioned previously, the use of cone penetration test (CPT) as a site investigation method was utilised on a select number of projects in the database. The projects which have CPT cone resistance data are E16, E28, S4, S14 and S27 with four projects installed in sand and one in clay soils. A number of methods which utilise the CPT cone resistance to directly determine the ultimate capacity of a pile exist, as has been discussed in section 2.5.3. Current RBL procedures use the CPT cone resistance primarily as a site investigation tool in order to determine soil properties as is highlighted in section 2.5.5. Reviewing the current CPT based pile design procedures in section 2.5.3, it was established that Bustamante and Gianeselli (1993) suggest design methods to determine the ultimate pile capacity using cone resistance which are specific for auger displacement piles. Due to the specific nature of the Bustamante and Gianeselli (1993) design procedure to auger displacement piles, it is appropriate to use the technique to determine an ultimate capacity for the CHD piles.

At each of the 5 CHD project locations, multiple CPT probes were carried out, producing a number of different cone resistance profiles across the project site. Because the location of the CPT probe in relation to the location of the CHD test piles could not be determined, a typical soil profile for each project site was established from all the cone resistance profiles. At each project location, the cone resistance profiles carried out across the site were found to be fairly uniform with minimal variation recorded.

For each 1m soil layer, the cone resistances from each CPT probe is collated to determine the average values shown in Figure 4-9 along with the skin friction and friction ratio. Soil categorisation based on cone resistance can be achieved using numerous calibration charts as discussed by Lunne *et al* (1997). The calibration chart presented by Brouwer (2007) has been used in this analysis to determine the soil categorisation for the CHD piles as shown in Figure 4-10. Project E28 is shown to consist predominantly of firm clay while E16, S4 and S14 consist of medium dense sands with layers of loose or dense sand at the head and base. Piles

from project S27 can be seen to be installed predominantly in loose to very loose sands.

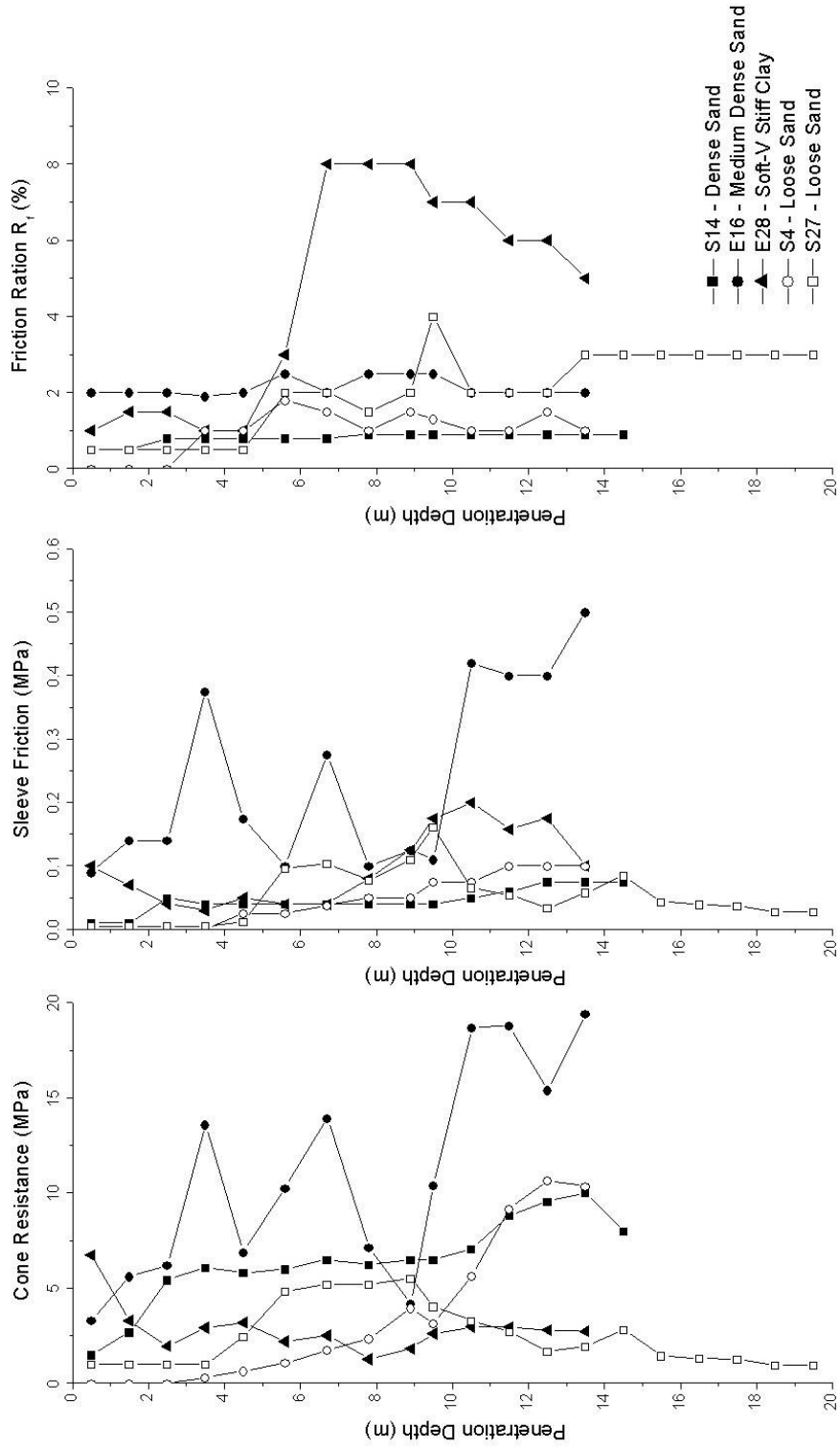

Figure 4-9 CPT cone resistance, sleeve friction and friction ratio site investigation data for CHD projects

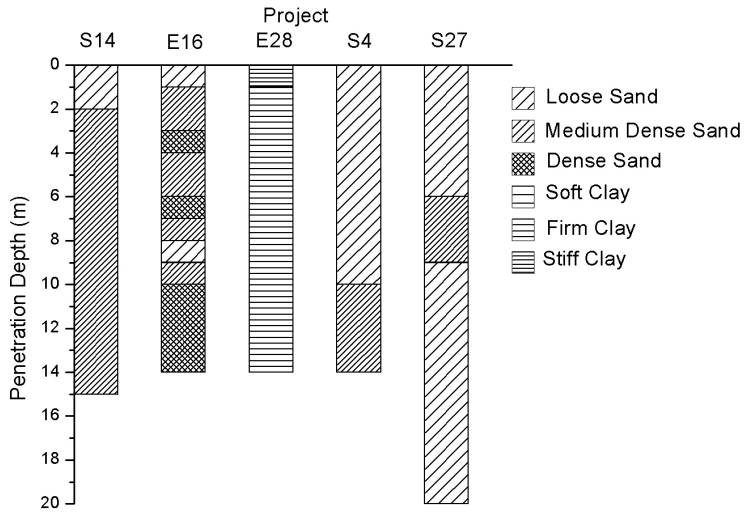

Figure 4-10. Soil strata profile for CHD projects based on measured CPT cone resistances

The pile capacity design procedure based on Bustamante and Gianeselli (1993) have been discussed in section 2.5.4. The base pressure is determined through the use of equation 2-17 where the bearing capacity factor k_c values are summarised in Table 4-4 for different soil types.

$$q_b = k_c q_{ca} \qquad \textbf{2-17}$$

Table 4-4. Typical soil classification based on cone resistance and bearing capacity design parameters for auger displacement piles based on Bustamante & Gianeselli (1993)

Soil Type	q_c (MPa)	Bearing Capacity Factor k_c
Silt/Loose Sand	<5	0.75
Moderately compact sand	5 to 12	0.63
Compact Sand	>12	0.5
Soft Clay/Mud	<1	0.65
Firm Clay	1 to 5	0.65
Compact to Stiff Clay	>5	0.55

The unit shaft friction, q_s is determined from the design curves suggested by Bustamante and Gianesilli (1993), as shown in Figure 2-22 in Chapter 2. The pile capacity is determined assuming the pile diameter is equal to the full flight diameter.

The design capacity determined using the Bustamante & Gianeselli (1993) method is shown in Table 4-5 compared to the original RBL design capacity and the predicted ultimate pile capacities determined in section 4.4.1. For the pile in project E16, the capacity prediction methods were not able to determine an ultimate capacity from the available load-settlement data and therefore comparisons are not possible.

Table 4-5. Design capacities using Bustamante & Gianeselli (1993) method compared to predicted capacity and RBL design capacity

Pile Project	Predicted Ultimate Capacity (kN)	RBL Design Capacity (kN)	Bustamante & Gianeselli (1993) CPT Design
S14	3441	2683	3215
E16	-	2211	4471
E28-1	1330	1510	1574
E28-2	1860	2939	2130
S4-1	2945	2556	2746
S4-2	2325	2123	2387
S27-1	5314	888	1565
S27-2	2748	888	1565
S27-3	3169	888	1565
S27-4	3038	888	1565

As can be seen in Figure 4-11, the correlation between the CPT design capacities and the predicted ultimate capacities for piles installed in dense and clay is typically within a range of ±20%, which can be considered allowable range by the Geotechnical Consulting Group (1998). The piles installed in clay soil, project E28, show a slight over prediction using the CPT design based method compared to those in sands. There is however a significant difference between the predicted ultimate capacity and the CPT design capacity for piles installed in loose sand in project S27, with the CPT design capacity typically half the predicted value.

For piles installed in loose sand, namely those in project S27, the predicted pile capacity suggests much larger values than those determined from the CPT based design process. The under-prediction of the CPT method for loose sands suggests that the design parameters used to relate the measured in-situ CPT cone

resistances from the original site investigation are not appropriate in the case of CHD piles based on the pile capacities predicted in this case.

The use of the Bustamante and Gianeselli (1993) design parameters for CHD piles installed in other soil types excluding loose sand, do not cause as big a variation between the design and predicted pile capacity. In order to obtain a CPT based design capacity which is similar to those determined from the prediction methods for project S27, the average cone resistance must be increased. The piles installed at project location S27 were installed in very loose sand, suggesting that the installation process of the CHD pile causes significant densification of the sand which causes an increase in the pile capacity. The design parameters must therefore be modified to take this densification into account.

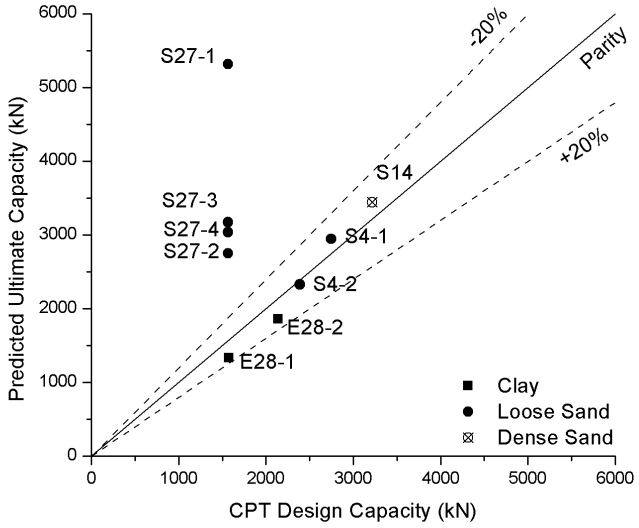

Figure 4-11. CPT design capacities based on Bustamante & Gianeselli (1993) method compared to predicted ultimate bearing capacities for CHD piles

The CPT design procedures allow the contributions from the shaft friction and base resistance to the overall pile capacity to be estimated, Figure 4-12. It can be seen that there is a clear difference in base-shaft ratio between piles installed in sands (S14, E16, S4 and S27) and clay (E28). The base contribution for piles installed in clay is found to account for around 27% of the total capacity. In medium dense and dense sands it typically accounts for 55%, however in loose sands (E27) the base resistance contribution drops to 14%. This gives an indication that the CHD piles develop most capacity from shaft friction. However,

these are only estimates based on design calculations. The true development of pile capacity from shaft friction and base resistance must be determined through the use of instrumentation.

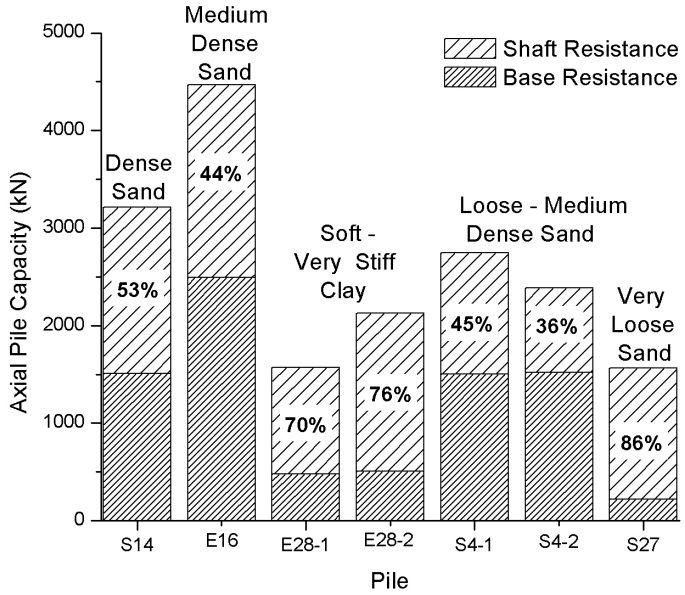

Figure 4-12. Shaft-Base axial capacity based on CPT design procedure

4.5 Settlement prediction analysis

It has been shown in Figure 4-1 that for almost all the CHD piles in the database, the load-settlement plot provides limited information on the ultimate pile capacity. A preliminary basic investigation has determined an estimated pile capacity however this does not allow a particularly detailed analysis to take place in terms of refining the pile design. A number of more detailed methods can be implemented in order to gain an understanding of the CHD pile capacity using settlement. These methods allow the estimation of shaft and base contributions to the overall pile capacity, something which is required in order to establish appropriate design parameters in equation 2-1. The application of these settlement prediction methods to the CHD data are investigated in this section.

4.5.1 Hyperbolic settlement prediction method

The hyperbolic pile prediction method was proposed by Fleming (1992) in order to predict the settlement of a pile during a maintained load test. As described in Chapter 2, the method uses a hyperbolic function to represent the behaviour of the pile, allowing settlement and corresponding load to be estimated, similar to the Chin and Decourt methods used previously. The hyperbolic method was applied to the CHD pile tests in order to extrapolate a load-settlement curve from the available test data and give an estimate of both the shaft and base component contributions to the overall capacity. The hyperbolic curve is represented by equation 2-23, reproduced here from section 2.6.2.

$$aW_S^2 + bW_S + c = 0 \qquad \textbf{2-23}$$

Where $a = \eta(Q - \alpha) - \beta$

$b = Q(\delta + \lambda\eta) - \alpha\delta - \beta\lambda$

$c = \lambda\delta Q$

$\alpha = Q_S$

$\beta = DQ_B E_B$

$\delta = 0.6Q_B$

$\lambda = M_S D$

$\eta = DE_B$

D = Pile diameter

E_B = Soil modulus beneath pile base

M_S = Shaft flexibility factor

w_p = Settlement of pile

Where, E_b is the soil modulus beneath the pile base and M_s is the shaft flexibility factor as discussed in Chapter 2. Based on Fleming (1992), the shaft flexibility factor M_s is typical between 0.004-0.005 for clays, while values of 0.001-0.0015 can be used for piles installed in sand. Based on a database of pile load tests, it was found the analysis was relatively insensitive to the value of *Ms*, and as such a

value of 0.0015 can generally be assumed for most piles, Fleming (1992) and Knappett and Craig (2012).

The soil modulus beneath the pile base, E_b, was found by Fleming to be related to the soil properties and could also be influenced by the installation method. As such, it is likely to be affected by the CHD installation. Ideally, the base modulus is determined directly from the pile test data using $Q_B/4$ (Azizi (2000)). In order to calculate the base modulus a substantial amount of base resistance has to be mobilised. In the case of the CHD piles from the study database this is difficult to ascertain with any accuracy due to the low pile settlements witnessed during load tests. As a conservative estimate, the values suggested by Azizi (2000) for bored and driven piles, shown in Table 4-6, can be adopted.

Table 4-6. Range of soil modulus E_B values for bored and driven piles (Azizi 2000)

Soil Type	E_B (kN/m^2)
Sand	
Very Loose	<15000
Loose	15000 - 30000
Medium Dense	30000 – 100000
Dense	100000 – 200000
Very Dense	>200000
Clay	
Very Soft	<3000
Soft	3000 – 6000
Firm	6000 – 15000
Stiff	15000 – 25000
Very Stiff	25000 – 40000
Hard	>40000

The hyperbolic settlement prediction method also takes into account the effects of elastic shortening of the pile material to the overall settlement using equation 2.24.

$$S_e = \frac{4Q_T\left[L_o + K_e\left(L - L_o\right)\right]}{\pi D^2 E_p} \qquad \text{for } Q_T \leq Q_s$$

$$S_e = \frac{4[Q_T L - Q_s(1-K_e)(L-L_o)]}{\pi D^2 E_p} \quad \text{for } Q_T \geq Q_s \qquad \textbf{2-24}$$

Where L_o = Pile length where negligible shaft load transfer occurs

K_e = Effective column length factor

E_p = Elastic modulus of the pile material

For the estimations of elastic shortening, the concrete modulus, E_c is assumed to be around 27 x 10^6 kN/m^2, similar to that used by Brown (2004) and that suggested by Fleming (1992). The effective column length factor, K_e is taken as an average value of 0.4 Knappett and Craig (2012). The L_o term allows the exclusion of a length along the pile where it is considered that there will be negligible shaft load transfer taking place for example where the pile is installed in made ground.

Although a number of the key parameters in equation 2-24 can be estimated for the in-situ soil conditions, the shaft and base resistance contribution to pile capacity remain unknown. Due to the variable nature of the parameters, an automated regression analysis is used to determine a solution. Utilisation of the solver tool in Microsoft Excel has allowed the CHD load test data to be analysed using the hyperbolic method. The solver function is programmed to vary the soil modulus E_B along with the percentage split produced from the shaft and base capacity whilst keeping the error value as low as possible. The error value is determined as the difference between the measured settlement of the CHD pile and the settlement determined through the hyperbolic analysis. The ultimate pile capacities are assumed to equal those determined from the prediction methods in Table 4-3, whilst the soil modulus value is limited to the ranges given in Table 4-6.

From the analysis of the CHD pile data it has been found that the selection of the soil modulus E_b can have a significant affect on the shape of the hyperbolic curve depending on the type of soil the pile has been installed in. For clay soil, the range of soil modulus E_b values suggested in Table 4-6, has little influence on the hyperbolic load-settlement curve produced as can be seen from Figure 4-13a. In sands however, a higher degree of sensitivity to the soil modulus value has been

found. As shown in the example in Figure 4-13b, the choice of base modulus tends towards the upper values suggested in Table 4-6. The selection of the lower range values tends to give an over prediction on the pile stiffness at low settlements (typically less than 0.16D). This has been found for all the CHD piles in the database which have been installed in sands.

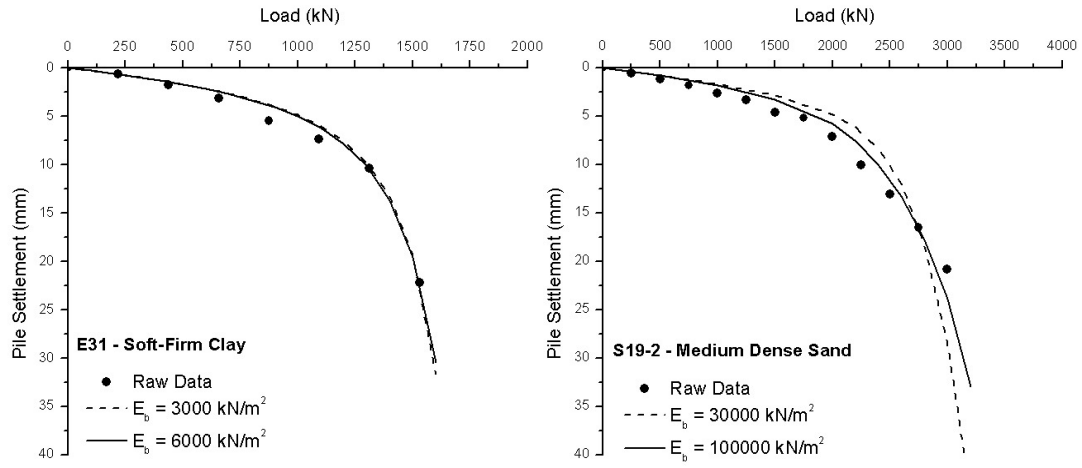

(a) **(b)**

Figure 4-13. Effect of varying the soil modulus parameter in the hyperbolic analysis of CHD piles installed in (a) clay soil and (b) medium dense sand.

Using the appropriate soil modulus E_b which produces the closest representation of the raw data, the hyperbolic method allows the determination of the shaft and base capacities. As would be expected, it is found that the shaft contribution to overall pile capacity increases with an increase in pile slenderness ratio, Figure 4-14. Since the CHD pile diameter is the same for all the test piles, the increase in shaft contribution can be correlated to an increase in pile length, similar to that witnessed by Fleming *et al* (2009). The shaft contributions suggested by the hyperbolic method are seen to be typically lower than those derived from the CPT design process carried out in section 4.4.2 as shown in Figure 4-21.

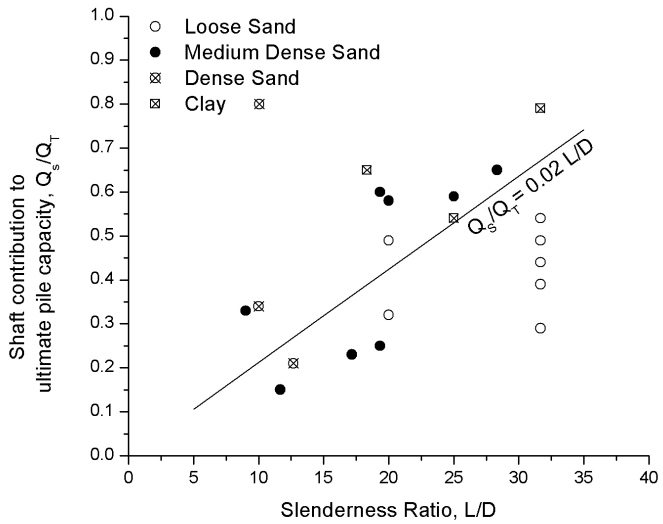

Figure 4-14. Variation of shaft contribution to total pile capacity based on hyperbolic prediction method with slenderness ratio

The hyperbolic settlement prediction method is generally a useful technique to allow the prediction of the load-settlement curve and subsequent separation of the base and shaft components to the overall capacity of a pile. The application of the method to the case of the CHD test piles in the database has been found to be problematic however. Numerous assumptions regarding soil and pile properties are required in order to conduct an accurate analysis. The selection of the soil property parameters can have a significant effect on the shape of the load-settlement curve as well as the shaft and base capacities.

These shaft-base ratios are based on the assumptions of pile and soil properties made in equation 2-23. In order to gain a more accurate understanding of the shaft-base ratio, installed CHD piles must be subjected to larger loads which cause greater settlement during the load test. Ideally, instrumentation of a pile would allow the direct determination of parameters which have currently been assumed. Direct measurement of the load distribution throughout the CHD pile would allow an accurate shaft-base capacity ratio to be established. With this, back figured parameters such as E_b which are applicable to CHD piles can be achieved. The current outputs of the hyperbolic analysis are based purely on best guess and do not give a definitive answer.

4.5.2 Load-transfer analysis

It is clear that there have been difficulties in determining the total ultimate capacity along with the base and shaft capacity of the piles from the available load test data. An alternative approach to pile analysis is to investigate the load-settlement response which can be expected based on the stiffness of the in-situ soil. Randolph and Wroth (1978) discuss a method of evaluating the load-settlement response of a pile in order to determine the individual shaft and base components of the total pile capacity, known as a load-transfer analysis. The pile capacity and settlement response is determined through the calculation of the shear stresses in the soil surrounding the installed pile in order to obtain the load-settlement behaviour.

The load-transfer analysis assumes that the pile shaft capacity is developed due to the soil shear stresses surrounding the pile. The shear modulus of the soil is used to estimate the expected settlement based on the applied shear stresses using equation 4-1. The shear stress of the soil is found to decrease in proportion to the radial distance from the pile surface. Theoretically the shear stresses will continue to infinity, however Randolph and Wroth (1978) suggest a limiting radius denoted as r_m where the shear stresses can be considered negligible.

$$w_s = \frac{\tau_0 r_0}{G}\zeta \qquad \textbf{4-1}$$

Where w_s = Shaft settlement

τ_0 = Shear stress

r_o = Pile radius

G = Shear modulus

$$\zeta = \ln\left(\frac{r_m}{r_o}\right)$$

r_m = Maximum radius

The magnitude of the maximum radius is empirically estimated to be approximately equal to the length of the pile (Fleming *et al* (2009), however the radius is defined by Randolph and Wroth (1978) in equation 4-2.

$$r_m = 2.5L\,(1-\nu) \qquad \textbf{4-2}$$

Where ν = Poisson's Ratio of the soil

The soil-pile stiffness of the shaft friction is determined by assuming the pile as a rigid body in order to obtain the expression in equation 4-3.

$$\frac{Q_s}{w_s} = \frac{2\pi L G_{avg}}{\zeta} \qquad \textbf{4-3}$$

Where G_{avg} = average shear modulus over pile length

Similar to the shaft, the base stiffness response can also be determined through the use of shear modulus values. At the pile base, the effects of the shaft are ignored and the base is treated as a rigid foundation which penetrates the soil layer (Gourvenec (2005) and Fleming *et al* (2009)) to determine the base stiffness in equation 4-4.

$$\frac{Q_b}{w_b} = \frac{2DG_{base}}{(1-\nu)} \qquad \textbf{4-4}$$

Where G_{base} = soil shear modulus below the pile tip

The overall pile stiffness can be determined by combining equations 4-3 and 4-4 to give equation 4-5. In order to create a dimensionless overall stiffness, the total pile load over total settlement, Q_T/w, has been divided by the pile diameter and the shear modulus at a depth equal to the pile length G_L. The effect of variations in soil stiffness along the pile length is taken into consideration in equation 4-5.

$$\frac{Q_T}{wDG_L} = \frac{2\eta}{(1-\nu)}\frac{G_{base}}{G_L} + \frac{2\pi}{\zeta}\frac{L}{D}\frac{G_{avg}}{G_L} \qquad \textbf{4-5}$$

Where η = Base enlargement ratio (equal to 1 for CHD piles)

In order to evaluate the load transfer behaviour of the CHD piles, a number of parameters in equation 1-5 have to be determined.

The Poisson's ratio value has not been directly measured for the ground conditions encountered on each project site however estimations can be made based suggestions made in literature such as those in Table 4-7 by Das (2000).

Table 4-7. Poisson's ratio estimates for different soil types from Das, (2000)

Soil Conditions	Poisson's Ratio
Loose Sand	0.2 – 0.4
Medium-Dense Sand	0.25 – 0.4
Dense Sand	0.3 – 0.45
Silty Sand	0.2 – 0.4
Soft Clay	0.15 – 0.25
Medium Clay	0.2 -0.5

The shear modulus throughout the soil strata can be determined from the modulus of elasticity *E* of the soil using equation 4-6.

$$G = \frac{E}{2(1+\nu)} \qquad \textbf{4-6}$$

The modulus of elasticity can be correlated to the standard penetration *N* number by using the relationship determined by Schmertmann (1970) in equation 4-7. It can also be related to the CPT cone resistance qc using equation 4-8 as discussed by Das (1997).

$$E = 766N \qquad \textbf{4-7}$$

$$E = 2.5q_c \qquad \textbf{4-8}$$

E is given in MPa (N/mm^2)

For each one metre soil layer throughout the length of the installed CHD piles discussed in Table 4-3, the SPT *N* number or the CPT cone resistance values were used to determine the in-situ soil shear modulus. The shear modulus at the depth equal to the pile length G_L and the average shear modulus along the pile length G_{avg}, can be calculated. The base shear modulus G_{base} is determined from the site investigation data which has been carried out at a depth below the location of the pile tip. The shear modulus variation with depth throughout the length of the installed CHD piles typically show an increase with depth (Figure 4-15) as assumed by Fleming *et al* (2009). Due to the varying nature of the soil strata encountered, the variation in shear modulus with depth was not always a linear increase. The shear modulus values determined from the site investigation methods can be used to calculate the shaft stiffness using equation 4-3, assuming that the pile is a rigid body. It is unclear at what strain level the shear modulus is calculated at.

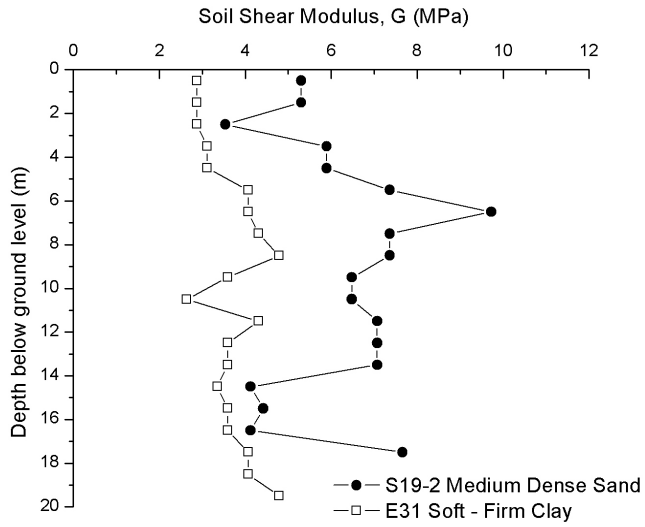

Figure 4-15. Typical variation of soil shear modulus with depth for sand and clay soils from the CHD pile database site investigation reports

The predicted load settlement plots determined from equation 4-7 can be plotted against the measured load settlement data from the pile tests. For this analysis, settlements for varying load values were determined. It can be seen in Figure 4-16 that the predicted load-settlement plots based on the load transfer analysis produce a linear relationship and do not represent a hyperbolic relationship which is the typical response in load settlement plots. The load transfer analysis prediction

represents the pre yield portion of the load settlement curve, where the soil responds elastically to the applied load.

The shear modulus is known to degrade with increased shear strain (Brown (2004)) and as such, it is to be expected that the soil-pile stiffness will degrade with increased pile settlement. In order to determine the ultimate capacity, the degradation of the soil shear modulus must be considered. The degree of shear modulus degradation within the soil structure during the pile test is unknown and therefore an accurate pile settlement determination using the load transfer analysis with the available pile test data is difficult. What can be seen however in Figure 4-16 is that the stiffness response of the CHD pile under loads is higher than the anticipated values based on the in-situ soil properties. In loose sand, the measured load at a settlement equal to $0.01D_f$ (6mm) is almost double the predicted load transfer value. The measured loads in medium dense and dense sands are also larger than those determined from the load transfer analysis, typically 20 – 40% greater. This analysis suggests that the installation of the CHD piles causes a greater stiffness response than would be anticipated from the in-situ soil conditions.

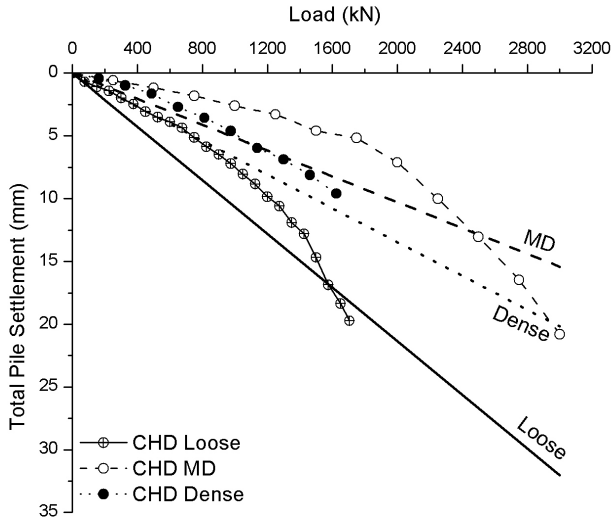

Figure 4-16. Load settlement predictions based on soil stiffness analysis compared to measured CHD test results in varying relative densities

In order to obtain a true understanding of the stiffness contributions made from the base and shaft of the pile, the CHD must be instrumented in order to measure the axial load capacity produced from the base and shaft.

The load-transfer analysis conducted using equation 4-3 also assumes the pile to be a rigid body so that the settlement experienced at the pile head will be equal over the pile length. This is however not the case as pile compressibility should be considered. This can be conducted manually through calculations discussed by Randolph and Wroth (1978) and Gourvenec (2005), however it can also be carried out using a pile analysis computer program which takes into consideration the soil and pile properties to determine an estimated pile capacity with appropriate shaft-base contributions along with an appropriate load-settlement curve.

4.5.3 Pile analysis software

A number of commercially available pile analysis programmes such as RATZ (Randolph (2003)), PILE (Oasys Ltd (2011)) or OPile (Cathie Associates (2008)), can be used to predict the load-settlement response of a pile through the use of the in-situ soil data. For the investigation of the CHD pile data, the OPile analysis software has been used. The OPile analysis programme predicts the load-settlement using analytical methods such as effective stress or CPT based design methods depending on the available site investigation data. The programme was developed primarily to model offshore driven piles and as such the available design methods are based on those suggested for use in offshore design. Some methods used in the programme have been discussed in section 2.5, such as the UWA-05, API or the ICP pile design methods.

The available soil data is entered into the programme and the analysis conducted to determine ultimate capacities. The available site investigation data dictates the analysis approach chosen. For an effective stress design approach, the API design procedures were followed in OPile. The API design procedure uses a standard effective stress design like those shown in equations 2-2 and 2-5. Although the

API (2005) guidelines stipulate design parameters for use in the equations, the OPile programme allows the manual selection of the parameters such as N_q, k or δ. For the analysis of the CHD piles, the bearing capacity factor is selected based on those suggested by Berezantzev *et al* (1961), while the interface friction angle is taken as the angle of internal friction for the in-situ soil determined from the site investigation data. The selection of the coefficient of horizontal stress can be varied until a close match between the OPile prediction load-settlement curve and the measured load-settlement curve is obtained.

For CPT data, utilisation of the Fugro-05 and the UWA-05 design procedures were followed (section 2.5.3) using equation 2-14. Although both the Fugro-05 and UWA-05 methods have subtle variations in the parameter values in each equation, when the procedures are applied to the CHD pile design, both methods gave similar prediction results for the pile shaft friction. For the overall design analysis, the Fugro-05 procedure was followed in OPile primarily due to its simplistic approach and requirement for limited parameter inputs.

In Figure 4-17 the ultimate pile capacity determined from the OPile analysis is compared to the predicted values from Table 4-3. For most piles in the database, the OPile prediction and the predicted ultimate pile capacity have a variance of ±20%, however, a number of piles show a significant difference between the OPile capacity and predicted capacity. It is seen that the apparent conservative pile capacity from the OPile analysis can be found primarily in piles which have been installed in loose to medium dense sands.

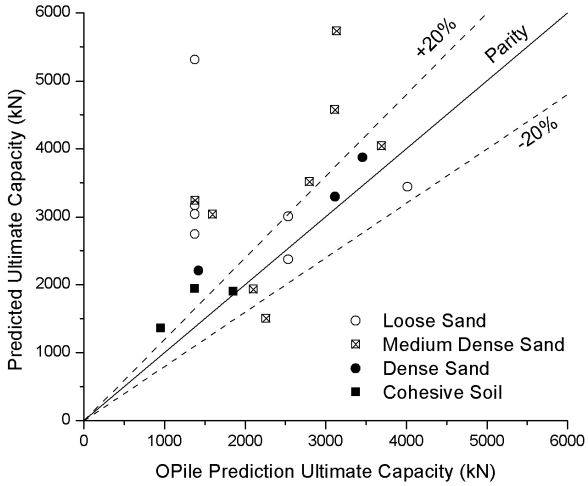

Figure 4-17. Variation of OPile analysis ultimate bearing capacity compared to those determined from prediction methods for CHD piles installed in various soil types

The capacity predictions from Table 4-3 are determined from the load-settlement data of the pile test, they account for any soil disturbance which has been caused during pile installation. The OPile analysis utilises soil information which has been determined from site investigation techniques carried out on the undisturbed in-situ soil before pile installation effects can occur. The design procedures take into account soil disturbance due to pile installation however these are tailored towards driven piles and not auger displacement piles such as CHD.

In the case of the effective stress design process using the API template, pile installation affect can be accounted for through the selection of the design parameters. The end bearing capacity factor N_q and coefficient of horizontal stress k can be manually selected in order to give a more representative load-settlement curve compared to the measured data.

As was already mentioned, for the CHD analysis, the bearing capacity factor is determined from those suggested by Berezantzev *et al* (1961) using the in-situ angle of internal friction (Figure 2-19). The in-situ friction angle can be derived from the standard penetration resistance values via the relationship developed by Peck *et al* (1974) and discussed by Tomlinson and Woodward (2008). The k values are adjusted to best fit the prediction curve to the measured data in order to see the effects it has on the curve and capacity prediction. The coefficients of horizontal stress are found to range from 0.7 to 3.

The analysis method used in the determination of the load-settlement curves is defined by the API guidelines. As such the load-settlement curve is approximated using a parabolic curve with the peak shear stress occurring at a settlement of 0.01D (Gourvenec (2005)). This approach dictates the general shape of the predicted load-settlement curve. As shown by the examples in Figure 4-18 for CHD piles installed in medium dense sand, the OPile curves show a reasonable prediction of the initial pile stiffness at a settlement of less than $0.01D_f$. The ultimate estimated pile capacity determined from the OPile analysis is similar to those estimated from the Chin and Decourt methods (Figure 4-17) at a settlement of around $0.1D_f$ so it is assumed that at increased settlements, the OPile analysis also provides a reasonable representation of the load-settlement curve. However, the OPile settlement curves predicted between a settlement of 0.01Df and 0.03Df can be seen (Figure 4-18) to give an over estimation of the measured pile stiffness. This can be attributed to the method in which the curves are determined.

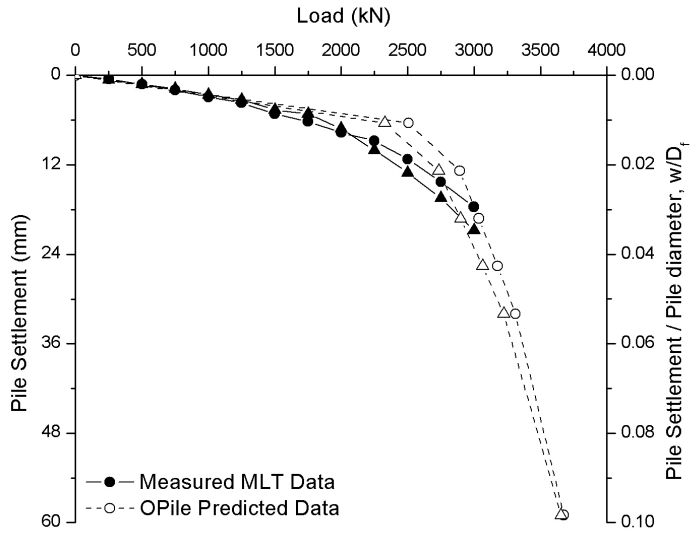

Figure 4-18. Typical OPile prediction curves compared to measured load-test data for CHD piles installed in Medium Dense sand

For the CPT design, design parameter selection is somewhat restricted since each design process has developed individual values which have been tailored to the design of driven offshore piles and are inbuilt into the OPile analysis. Although this restricts the adjustment of the parameters, it allows a comparison of the measured load-settlement response of the CHD piles to the predicted response that would be expected for a driven pile, Figure 4-19.

In Figure 4-19a, pile E16 is shown, which is typical of CHD piles installed in predominantly dense sand. The OPile prediction shows a greater stiffness response than is witnessed from measured load-displacement curve of the CHD pile. Conversely, in Figure 4-19b, where piles in project S27 have been installed in very loose to loose sand, the OPile analysis produces a conservative prediction compared to the measured load-displacement data. The variation in prediction to the measured load-settlement response between different soil types suggests that the CHD pile has greater stiffness than would be anticipated from a driven pile when installed in loose sand, however in dense sand the CHD stiffness is slightly less than that expected for a driven pile.

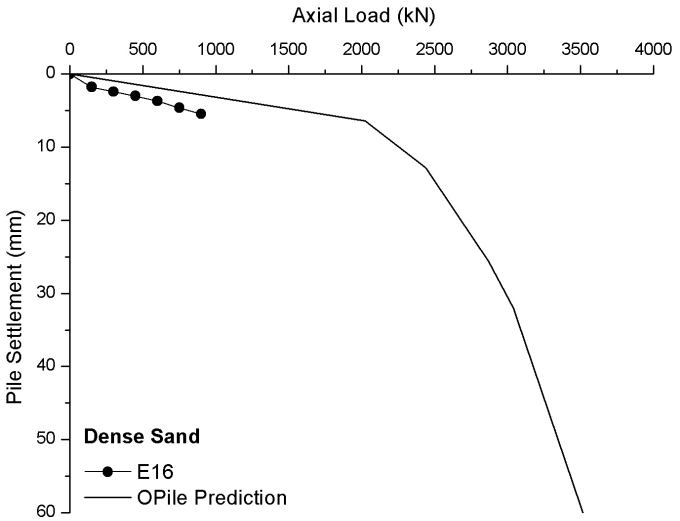

(a)

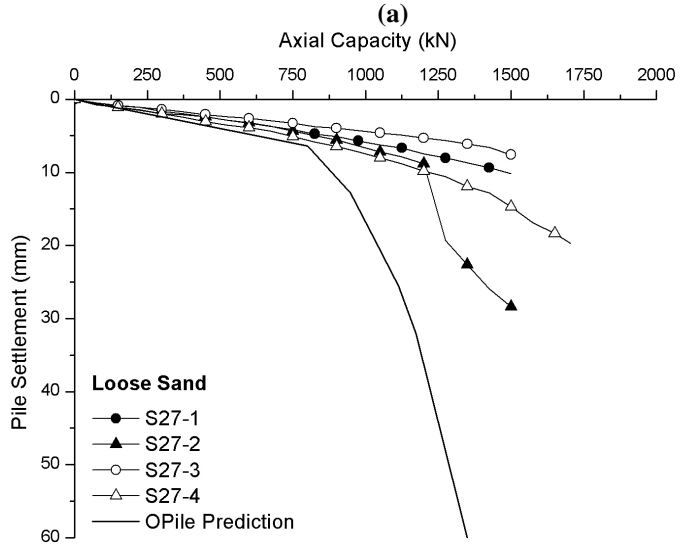

(b)

Figure 4-19. OPile load-settlement prediction using CPT cone resistances compared to measured pile data for CHD piles installed in (a) Dense sand and (b) loose sand

The OPile predictions allow the estimation of the contributions to total pile capacity from the pile base and shaft. Based on the assumed parameters which produced the closest curve match, it was found that the shaft typically contributes 20% to 50% of the overall capacity depending on the pile slenderness ratio, as shown in Figure 4-20. The average variation shown in Figure 4-20 is determined using piles installed in sands only as it is has been found that those installed in clay soils have greater shaft contributions.

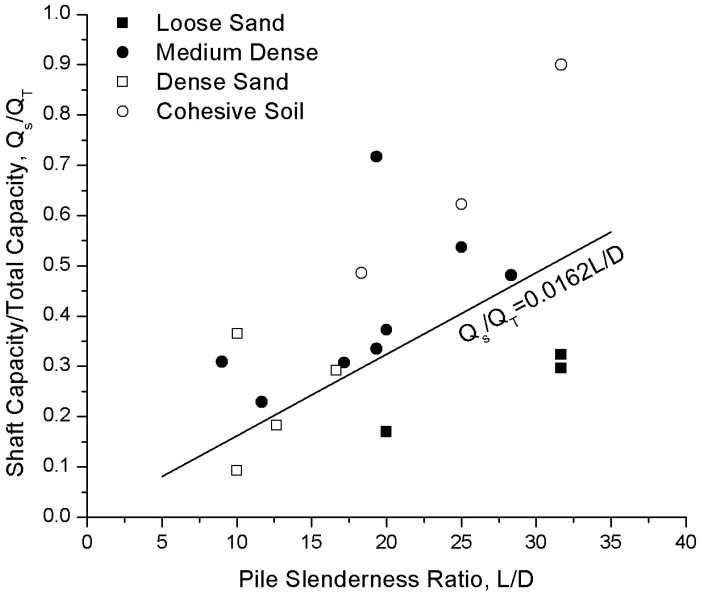

Figure 4-20. Variation in shaft contribution to total pile capacity with slenderness ratio based on the OPile analysis results

4.6 Shaft and Base contributions to pile capacity based on analysis methods

A number of pile capacity prediction methods have been utilised in order to determine the capacity of the CHD piles within the database. Some of these methods allow an estimation of the contribution made from the shaft and base resistances. The determination of the base-shaft contributions to the total pile capacity is a requirement in order to refine the pile design procedures of the CHD pile. Since they have not been measured directly during the load tests, the use of the prediction methods is required to determine the appropriate information.

The CPT design procedure, hyperbolic analysis and the OPile load-transfer analysis have all enabled shaft contributions to be estimated. They have all shown how the shaft contribution increases with the pile slenderness ratio, as would be expected. By plotting the shaft contribution estimates using all three prediction methods, a general range can be established for the shaft contribution to the overall pile capacity as shown in Figure 4-21. Although the variation in shaft contribution with relation to pile slenderness ratio is evident, it can be seen that 80% of the analysis predictions suggest the shaft contribution to the ultimate pile capacity is between 0.2 and $0.6Q_T$. By definition therefore, the base bearing pressure contributes typically between 0.4 and $0.8Q_T$. These values of shaft-base contributions to the ultimate pile capacity are similar to those derived by Gwizdala *et al* (2009) for Atlas piles installed in fine to gravelly sands. However, these values derived from Atlas piles were not measured directly through the use of instrumentation and are simply a derivation of the load test results, similar to the analysis of the CHD piles in this database.

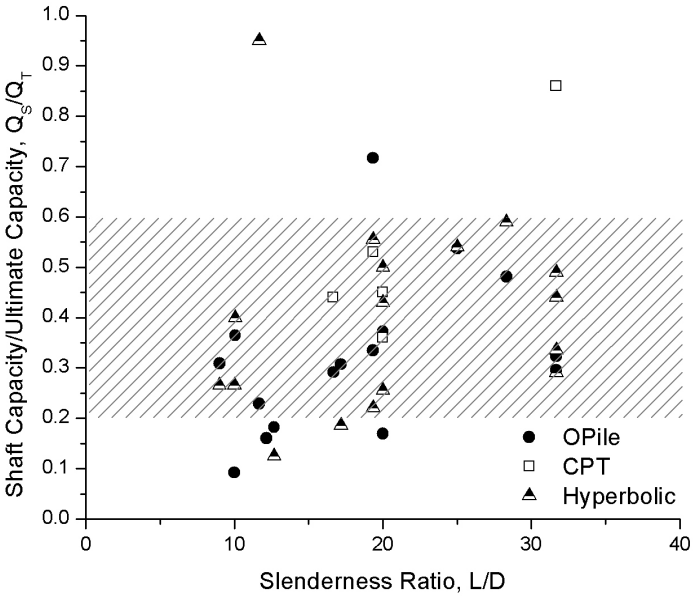

Figure 4-21. Shaft contribution estimates to ultimate pile capacity based on different prediction methods for piles installed in sand only

The determination of the shaft and base contributions to the pile capacity based on the available pile data is found to have a large range as shown in Figure 4-21. This large range makes it difficult to establish a typical ratio for the use in the CHD pile design refinement.

4.7 Field Analysis Summary

This chapter contained the analysis of the load-settlement data for a number of CHD test piles collected from field tests carried out by Roger Bullivant Ltd. Preliminary interpretation and analysis of the test data was carried out within this chapter however further analysis of the field data along with model tests results will be carried out in Chapter 6. A summary of the observations made from this chapter will be outlined as follows.

1. Upon analysis of the field data, it was found that very few piles have been subjected to large enough loads to produce settlements which allow the application of typical criteria to determine the ultimate pile capacity

2. Based on the assumption that no test pile in the database displayed ultimate capacity during the load test, an appropriate diameter selection for use in pile design calculations has been investigated. It was found that the use of a design diameter equal to 0.75D gives conservative capacity estimates. Increasing the design diameter to equal the full flight diameter, 1D, appears to still produce conservative capacity estimates. This leads to the determination that the design parameters used for CHD piles must be adjusted in order to improve the accuracy of the design capacity.

3. In order to estimate the ultimate pile capacity of the test piles, the Chin and Decourt prediction methods are applied to the load test data. The results of the prediction methods highlighted a number of issues. Firstly it was found that the application of the prediction methods required a minimum settlement of the pile in order to determine an ultimate capacity. As a general guide, a minimum settlement equal to 0.01D is required to allow the utilisation of the prediction methods.

4. The Chin method was found to over predict the CHD ultimate capacity, as had been indicated in literature for other pile types. The Decourt prediction estimated a load-settlement curve which more closely represented the

curve obtained from the load tests. The Chin prediction was determined to over-estimate the CHD ultimate capacity by a factor of 1.04.

5. With the pile capacity determined through the use of either the Decourt method or the Chin method with appropriate correction factor, it has been established that the Roger Bullivant pile design capacity determined using a design diameter equal to the full pile diameter produces conservative capacities, primarily when the piles are installed in loose to medium dense sand.

6. Where CPT cone resistance values are available, a design capacity is calculated for the project piles. It has been found that using design parameters suggested by Bustamante and Gianeselli (1993) specific for screw piles, the pile capacity is generally similar to those suggested from the pile prediction methods.

7. For piles installed in loose sand, the CPT design gives an underestimation of the ultimate pile capacity. This suggests that the design parameters for use in loose sands require refinement for use in the design of CHD piles.

8. The CPT design procedure suggests that for piles installed in sand, the shaft contribution to the total pile capacity is found to be around 45% for medium dense to dense sand and up to 81% for loose sand. In clays, the shaft contribution is found to be around 73%.

9. The Fleming (1992) hyperbolic pile settlement prediction method was utilised in the analysis of the CHD piles. It was found that in order to conduct an accurate hyperbolic analysis, a number of soil parameters around the pile shaft and base must be known. Along with the soil parameters, information regarding the pile response during the load test must also be known such as either the ultimate capacity or the shaft-base contribution ratio.

10. In the analysis of the pile data using the hyperbolic method, typical values for the soil base modulus E_b suggested by Azizi (2000) were used. It was found that the E_b values which produced the closest representation to the load-settlement tended to the upper range of suggested values. Without an accurate measurement of the base-shaft capacities of the CHD piles, exact E_b values specific for CHD piles are not possible. Again, without a more accurate estimation of the soil properties, the use of the hyperbolic method to predict CHD capacity is problematic.

11. The pile test data was investigated using a load-transfer analysis. The analysis tried to determine the individual shaft and base contributions in order to predict ultimate pile capacity based on the in-situ soil stiffness properties. The analysis was found to produce an expected load-settlement curve but only for pre-yield conditions. The basic analysis approach did not take into consideration the degradation of the soil shear modulus during pile loading. This does not allow an ultimate pile capacity to be determined.

12. The load transfer analysis did suggest that the stiffness response of the CHD pile during loading was greater than expected based on the in-situ soil properties. In loose sand, the CHD pile was twice as stiff as anticipated while in medium dense and dense the stiffness increase was typically 20-40% greater.

13. A load-transfer was conducted using a computer analysis programme called OPile. This utilises the in-situ soil and pile properties to predict the ultimate pile capacity and associated load-settlement curve using an effectives stress or CPT based design approach. The ultimate pile capacity determined from OPile was found to give conservative results for piles constructed in loose to medium dense sands compared to those determined from the Chin and Decourt prediction methods.

14. The OPile analysis demonstrates that piles installed in loose sand appear to cause an increase in soil density while those installed in dense sand appear to cause a reduction in the soil density.

15. The CPT design process, hyperbolic prediction method and the OPile analysis all allow the separation of the ultimate pile capacity into base and shaft contributions. All methods demonstrated that the shaft contribution increased with an increase in pile slenderness ratio. With the CHD pile diameter being consistent between all analysed piles, this corresponds to an increase in the installed length. From analysis of all the methods together, it is suggested that the shaft capacity of the CHD pile typically contributes to between 20-60% of the ultimate pile capacity. This range is determined to be too large to offer any real use in the refinement of the CHD design procedures.

5.0 Model Testing

5.1 Introduction

This chapter contains the results of model pile tests carried out in dry silica sand prepared at varying relative densities. The controlled laboratory conditions allow uniform and consistent test conditions to be created in order to produce model piles. Along with CHD piles, pushed-in-place and wished-in-place (WIP) piles were modelled in order to determine the effects that the pile installation technique has on the in-situ soil conditions and ultimate pile capacity.

The load-settlement behaviour of the CHD piles is compared to both pushed and WIP piles of varying diameter in order to understanding the appropriate effective diameter for use in the design of CHD piles. Instrumentation of the model piles allowed the determination of the base and shaft contributions to overall pile capacity. This information was used to investigate the accuracy of the existing design process with the aim of refining the parameters for use with CHD piles.

In order to establish how the installation process of each model pile influences the in-situ soil conditions and therefore affects the pile loading response, model cone penetration tests (CPT) were conducted at radial locations around the installed pile.

5.2 Investigation of Effective design diameter for CHD piles

The CHD may be referred to as having two different diameters, the inner core, D_c and the outer flange diameter, D_f, Figure 2-15. For design purposes, a single diameter is required in order to calculate the ultimate pile capacity. An appropriate diameter must therefore be determined, the issues regarding the selection of which have been highlighted in Chapter 2.

The load-settlement behaviour of the CHD pile is compared to that of more recognised pile installation procedures with various diameters using the first series of pile tests as described in Chapter 3. Straight shafted pushed and wished in place piles, as opposed to the helical rib nature of the CHD, were installed with two different diameters which are similar to the model CHD inner core (30mm) and outer flange diameters (60mm) and were installed to a depth of 300mm, as detailed in section 3.3. The pushed and WIP piles were installed in loose (D_r = 22%), medium dense (D_r = 48%) and dense (D_r = 78%) sand samples. The CHD piles which had a similar in-situ relative density to that of the pushed and WIP piles were selected for comparison.

The load-settlement behaviour for each pile type in the different relative densities is shown in Figure 5-1a-c. The notation outer and core associated with the descriptions of the pushed and WIP piles refer to the CHD inner core and outer flange diameter.

Changes in the initial relative density of the test bed are seen to have little influence on the relative differences to the shape of the load-settlement curves between the different types of pile installation methods. The CHD and pushed piles can be seen to out-perform the inner and outer diameter WIP piles in terms of load capacity and in stiffness at all relative densities. It is also evident that the CHD pile has a greater ultimate capacity and superior stiffness to the inner diameter pushed pile for all states of relative density.

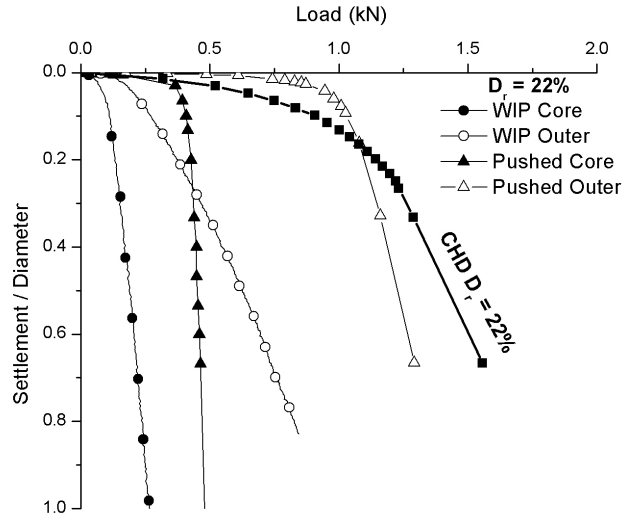

(a)

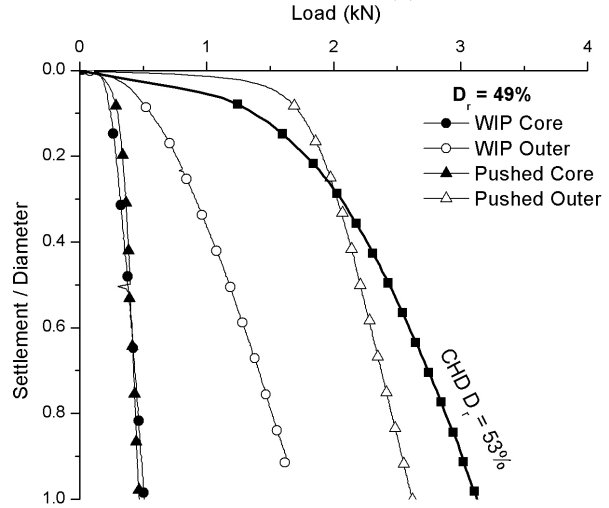

(b)

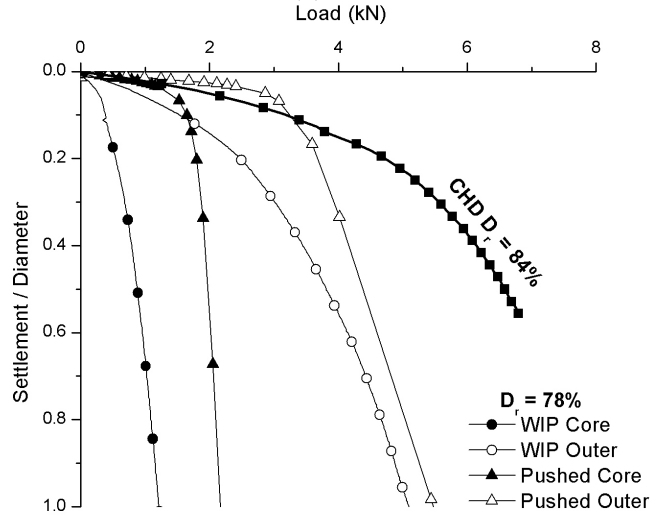

(c)

Figure 5-1. Series 1 model pile tests load-settlement behaviour variation with pile installation method and diameter selection when installed in (a) Loose, (b) Medium Dense and (c) Dense sand

The ultimate capacity of the CHD piles tends to exceed the values obtained from the outer diameter pushed piles. At all relative densities, the ultimate capacity of the CHD is greater than the large diameter pushed piles, however, this does occur at larger settlements.

The increased settlements in CHD piles compared to those found in the large pushed piles indicate that the CHD has a lower stiffness. Compared to the WIP piles and inner diameter pushed pile however, the CHD still has a superior stiffness response.

Although the helical nature of the CHD pile creates a varying diameter throughout the length of the pile, the test data shown in Figure 5-1 appears to suggest that, in terms of capacity, the full flight diameter of the CHD pile represents the pile diameter that should be used for design purposes.

Further evidence to reinforce this assumption is found by inspecting the completed CHD pile. After load tests had been carried out, the model CHD piles were exhumed from the test bed. By carefully excavating the test bed soil around the pile, it was found that the model CHD pile visually resembled a large diameter straight shafted pile than a helical screw pile as shown in Figure 5-2. Upon closer inspection of the piles once they had been removed from the test bed, it was found that the sand was tightly wedged or “trapped” in the gaps between the flanges, Figure 5-3. The pile shown in Figure 5-3 was installed in dense sand however similar behaviour was also witnessed in piles installed in loose and medium dense sand. The “trapped” sand around the flanges has the effect of creating a pile with a diameter equal to the flange diameter.

Figure 5-2. Freshly excavated CHD pile in dense sand showing resemblance to a large diameter straight sided pile

a) **(b)**

Figure 5-3. Typical exhumed CHD pile installed in dense sand showing (a) relatively smooth sides due to sand filled flange gaps (b) Partially cleaned pile highlighting flange details and rough helical pile surface

The tightly packed wedges of sand in-between the pile flanges ensures that the soil will shear at a soil-soil interface. This produces a higher angle of friction than found at a soil-pile interface shear zone, as shown from shear box testing in section 3.4. The entrapment of soil within the flanges is also witnessed in field

CHD piles as is shown in Figure 5-4. Although the field CHD pile does not have the perfectly smooth sides witnessed in Figure 5-3a, this could be due to the relatively rough nature in which the soil was excavated from around the field pile.

Figure 5-4. Field CHD pile showing similar trapping of soil between flanges as found in model piles

This phenomenon of soil becoming trapped between the flanges has been investigated in field tests using Atlas screw piles. As was discussed in section 2.4.1, it was found by Van Impe (1988) that the soil become lodged between the flanges of Atlas pile, highlighted in zones AB in Figure 2-16. Similar behaviour was also reported by Frangoulides (1999) from model CHD tests which had been carried out in clay samples. The shear surface in those model tests were determined to occur at a distance which coincided with the outer diameter of the piles.

Van Impe, (1988) found that the soil lodged within the flanges was found to have been remoulded and compacted, giving it greater shear strength than the surrounding in situ soil. Because of this finding he suggests that where the cast flanges are thick, it is acceptable to assume the full flange diameter of the pile for determining the total bearing capacity. Pile flanges which are of a greater thickness than the drilling auger flights are determined as being thick, Bustamante and Gianeselli (1998).

Based on the information gathered from the series 1 model tests and the evidence from the field test results in section 4.3, it would appear that future analysis of the CHD piles should assume a pile diameter equal to the full flight diameter.

5.3 Influence of pile installation on the in-situ soil properties

The installation of any pile into the ground will cause changes to the in-situ soil structure, primarily through soil movement which will cause either loosing or densification to take place. The changes experienced in the soil structure are dependant on the installation technique used as well as the physical properties of the pile. By the nature of the CHD pile installation, the soil structure will be disturbed by the advancing bullet and the subsequent casting of the pile. For the investigation of model CHD piles, both the surface and subsurface changes in the in-situ sand structure due to pile installation were investigated.

The use of cone penetration tests (CPTs), allows the subsurface influence along the pile installation depth to be investigated by comparing the changes in cone resistance. The CPTs were carried out post installation of the pile and pre load test so as to ensure the effects solely of installation are determined. By conducting CPTs at different radial distances from the pile centre, the extent to which the pile installation has an affect can be determined, establishing a zone of influence for the CHD pile. For comparison to the CHD, the changes around WIP and pushed piles are also established. The CPT investigation takes place on the series 2 piles which are installed to a greater depth than those in series 1, as discussed in Chapter 3.

5.3.1 Surface soil movements due to CHD installation

Each model pile test was performed in a prepared sample of levelled sand which allowed the surface deformations due to pile installation to be recorded. Particle

image velocimetry (PIV) would ideally be utilised to track the movement of soil particles in the soil bed during the pile installation. However, due to the nature of the experimental setup it was not possible to gain a continuous undisturbed view of the soil surface during the entire installation process. The PIV technique is also ideally suited for tracking soil particles in a 2 dimensional plane but the installation of the model piles cause movement of particles in a three dimensional plane, requiring both vertical and horizontal camera placements, neither of which would be possible in the available setup.

The surface movements were therefore recorded by visual observation and manual measurements once installation had taken place. The appearances of near surface radial shear surfaces, Figure 5-5, were visible around the pile and were particularly prominent in dense samples. Evidence of surface radial shear surfaces can be seen during the installation of the bullet however, it was during the extraction and casting of the CHD pile that the shear surfaces become as prominent as displayed in Figure 5-5. This replicates what is witnessed during field installation where ground heave primarily occurs during extraction of the bullet as opposed to during the installation.

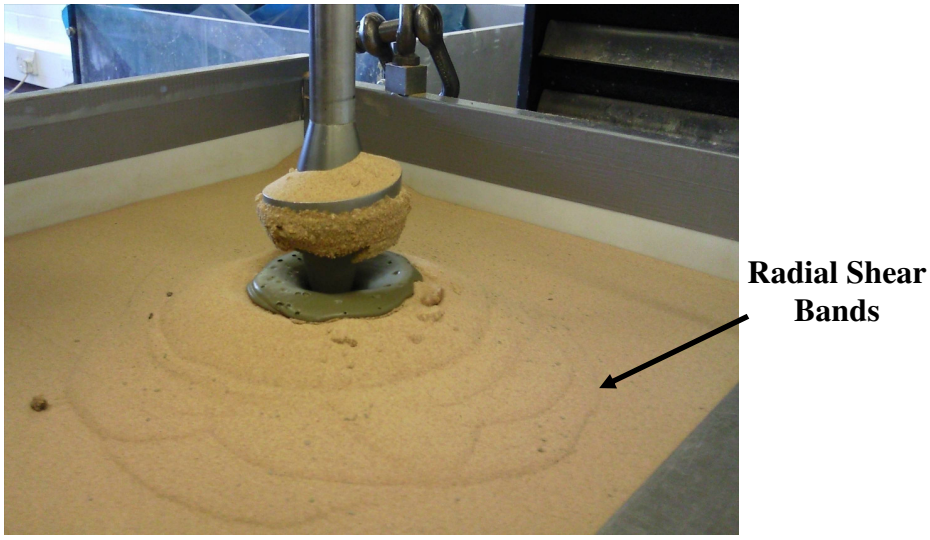

Figure 5-5. Formation of radial surface shear surfaces during CHD installation in dense sand

Both the radius of the surface shear surfaces and the vertical movement of the spoil heap were measured once the pile had been installed. Intuitively, it was found that the radial shear surfaces would expand at a much larger radial distances

in dense sands than in loose sands. As shown in Figure 5-6, the height of spoil heap produced varies with relative density, with the general trend being an increase in heap height with an increase in relative density. The height of the spoil heap is measured from the initially undisturbed sand surface within the test bed. The radial changes in surface heights are also shown to vary with relative density.

When installed in loose samples, a lateral influence of up to one and a half times the pile diameter was witnessed whilst in the dense samples this was as much as three times the pile diameter. The ratio of the box edge to pile diameter is 4.1, indicating that, for the surface influence at least, the CHD installation does not appear to be restricted by the boundary conditions of the test setup. The surface deformation due to the installation of the CHD visually reaches almost 3 pile diameters out from the centre of the pile when installed in dense sand. A minimum distance of 3 pile diameters between test piles is suggested in BS EN 1536 -2010 (2010) and is currently used as standard in the installation of CHD piles in the field.

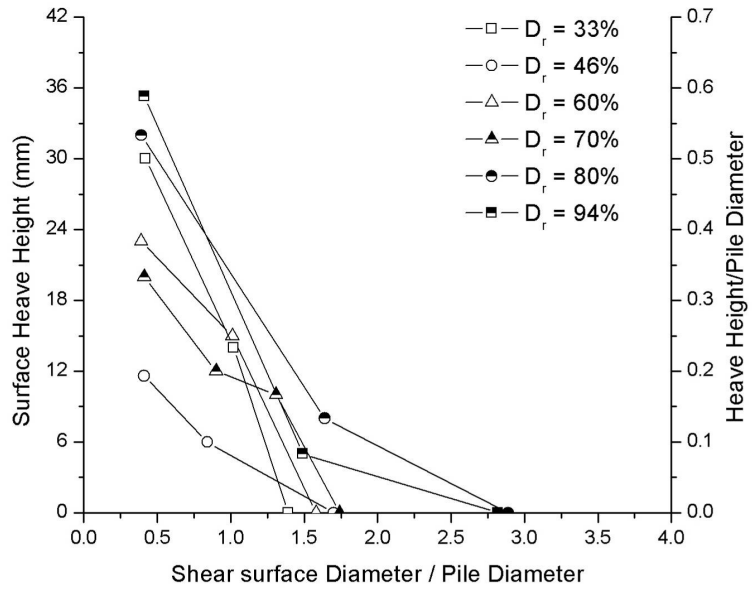

Figure 5-6. Vertical and horizontal surface heave measurements due to CHD pile installation in different relative densities

5.3.2 Use of cone penetration tests around the installed model piles

The surface deformations only give visual indications of the influence of the CHD piles during installation. In order to gain a greater understanding of the zone of influence along the installed length of the pile, a more detailed investigation took place. In order to determine the influence to the in-situ soil conditions due to pile installation, cone penetration tests (CPTs) were carried out after the installation of the pile and before a load test was carried out. Conducting cone penetration tests determines the vertical and radial variation in cone resistance which can be used to highlight changes to the sand bed density caused by the installation of a model pile. The cone resistance measured from around an installed pile is referred to as the disturbed values. The disturbed cone resistances can be compared to those obtained from sand beds which have no piles installed as detailed in section 3.3.10. Where a CPT has been conducted in a sand bed that does not have a pile installed, the values are referred to as undisturbed.

The CPT probes were penetrated at different radial locations around the installed model piles. Using the information obtained from the visual observations of influence zone in Figure 5-6 as a guide, the CPT probes were carried out at four locations equal to one, one and a half, two and just over three times the pile outer flange diameter from the centre of the pile, identified as 1D, 1.5D, 2D and 3.3D

Ideally, the cone resistance of the undisturbed in-situ sand bed would be measured before the installation of each model pile. However, carrying out a CPT probe would cause disturbance within the soil which could potentially influence the behaviour of the model pile being installed. To overcome this issue, a database of undisturbed cone resistance measurements from CPT's were accumulated for test beds of known relative density as was discussed in Chapter 3, Figure 3-25. The aim of the database is to provide a comparative cone resistance for those obtained from the pile test beds.

The disturbed cone resistances measured from the CPTs carried out around the CHD piles show consistent profiles throughout the depth of each individual test pile (Figure 5-7a-c). For clarity on Figure 5-7a-c, only the cone resistances at locations 1D and 3.3D are plotted. The shape of the cone resistance plot remained similar between different CHD piles however the magnitude of the cone resistances measured at each radial location varied. This variation is attributed to the differences in the in-situ relative density between each prepared test bed. An average cone resistance at each radial location of 1D, 1.5D, 2D and 3.3D, was determined from each of the CHD tests installed in loose, medium dense and dense sands. The averaging of the cone resistance from different the different piles gives the typical disturbed cone resistance profiles shown in Figure 5-8a-c for loose, medium dense and dense sands.

In Figure 5-7 and Figure 5-8, the disturbed cone resistance measured around the installed CHD piles are compared to the undisturbed CPT cone resistance conducted in a similar relative density to those found in the pile test bed. An increase in the disturbed cone resistance is evident in all soil densities, particularly at a distance up to 2D away from the pile. For piles installed in loose sand, there is a significant increase in cone resistance particularly within a radial distance equal to 2D from the pile. By a distance of 3.3D, the measured cone resistance tends towards the values seen for the undisturbed sand beds.

The increase in cone resistance represents a densification of the in-situ soil. It can be seen that the depth at which the densification occurs relative to the installed pile depth varies depending on the initial relative density of the test bed. In loose sand, the densification occurs almost instantly from the soil surface. As the initial soil density increases through medium dense to dense, densification does not occur until much greater depths, typically at around half the installed pile depth.

The disturbed cone resistance from the CPT carried out at a distance of 3.3D, in some cases matches the undisturbed CPT tests, such as in dense samples (Figure 5-8). Particularly in loose sand, there is a large variation between the disturbed cone resistance at 3.3D and the undisturbed CPT. The differences observed could

potentially be densification due to pile installation. It is possible however, that the slight variations are simply due to the different relative density of the sand. By using the Pushed and WIP piles, potential variations due to initial relative density differences will be investigated.

Along with the investigation of the CHD pile installation disturbance, the influence of the WIP and pushed in place piles were also investigated. Two different pile tests were carried out for each of the WIP and pushed pile types in three different relative densities (loose, medium dense and dense). For each pile type, the typical cone resistance at a radial location of 1D, 1.5D, 2D and 3.3D was determined. This was achieved by taking the average disturbed CPT cone resistances measured at each of the different relative densities (loose, medium dense and dense) in a similar manner as was carried out for the CHD piles.

The typical radial disturbed cone resistance variation with depth for the installation of pushed and WIP piles compared to the undisturbed database values are shown in Figure 5-9a-c and Figure 5-10a-c at different relative densities. The disturbed cone resistance measured around the WIP and pushed piles can be seen to differ in varying degrees from the undisturbed CPT depending on the relative soil density.

The variation in magnitude of cone resistance at each radial location for the WIP piles is seen to be lower relative to those found in the pushed pile tests, suggesting that as expected, the installation of the WIP does not significantly alter the initial relative density. Typical variation between 1D and 3.3D for WIP piles in both loose and dense sand is around 14%. The cone resistance variations in the pushed piles have a similar 14% difference between the 1D and 3.3D CPTs in loose sand but have up to a 30% difference in the dense sand. There is also a large increase in cone resistance recorded around the pushed pile installed in loose sand, likely to be due to the densification of the surrounding soil beneath the pile base during installation. The typical variation between the 1D and 3.3D disturbed cone resistances for CHD piles in loose sand are up to 50% while in dense sand it is as high as 72%.

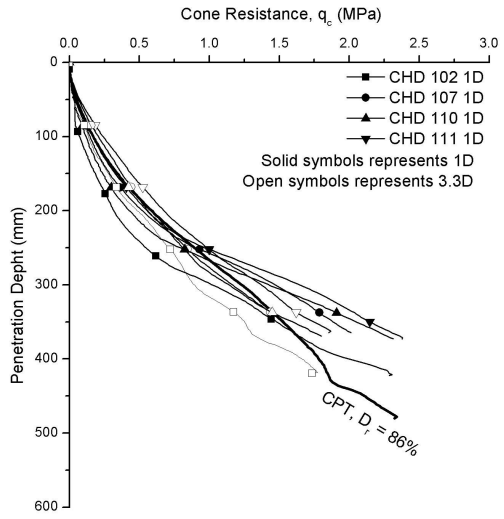

(a)

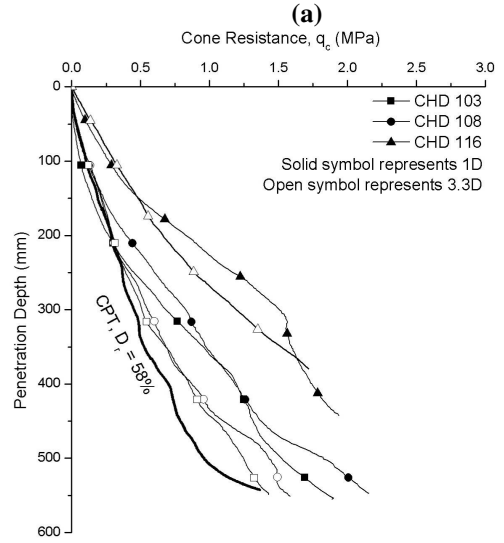

(b)

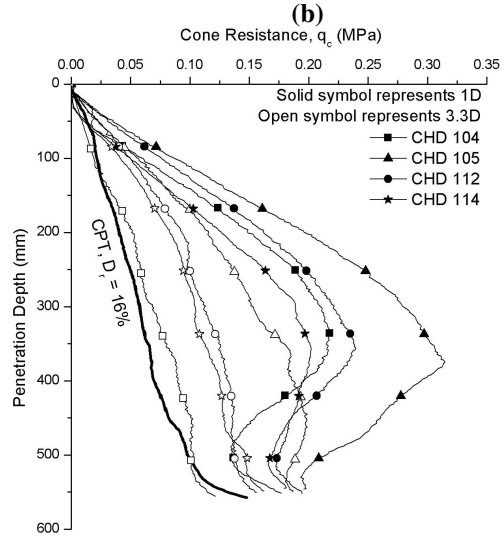

(c)

Figure 5-7. Disturbed CPT cone resistances at a radial distance of 1D and 3.3D for all CHD piles in (a) Dense (b) Medium Dense and (c) Loose sand compared to undisturbed CPT cone resistances

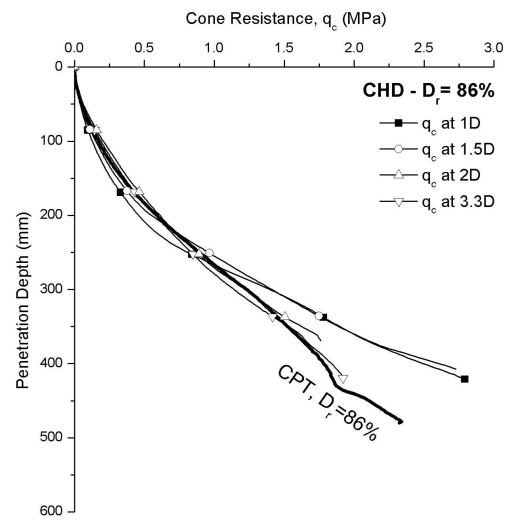

(a)

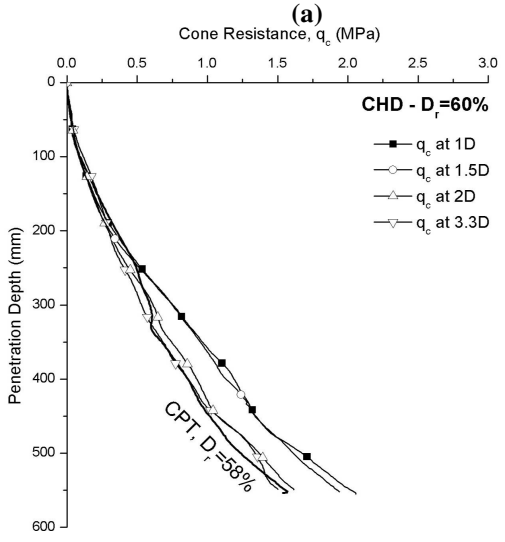

(b)

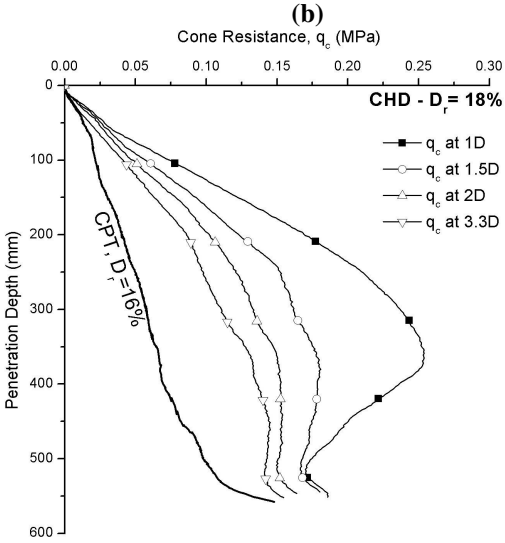

(c)

Figure 5-8. Characteristic disturbed cone resistance around CHD piles installed in (a) Dense (b) Medium Dense and (c) Loose sand beds compared to undisturbed CPT measurements

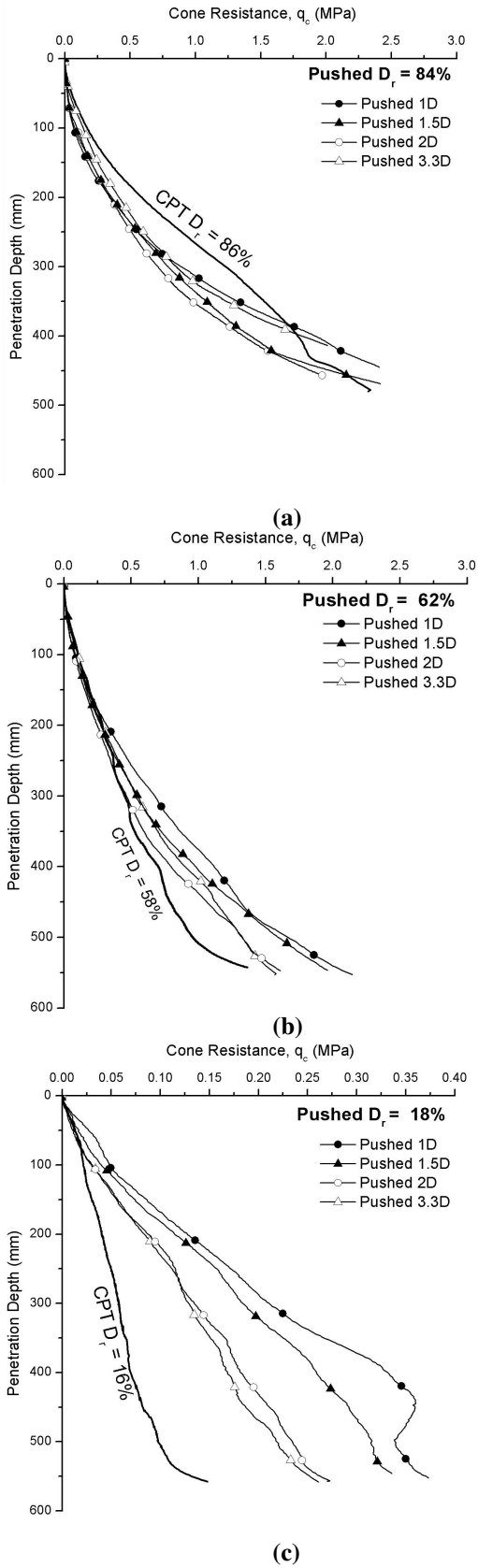

Figure 5-9. Average radial cone resistance variation with radial distance around Pushed piles installation in (a) Dense, (b) Medium Dense and (c) Loose sand

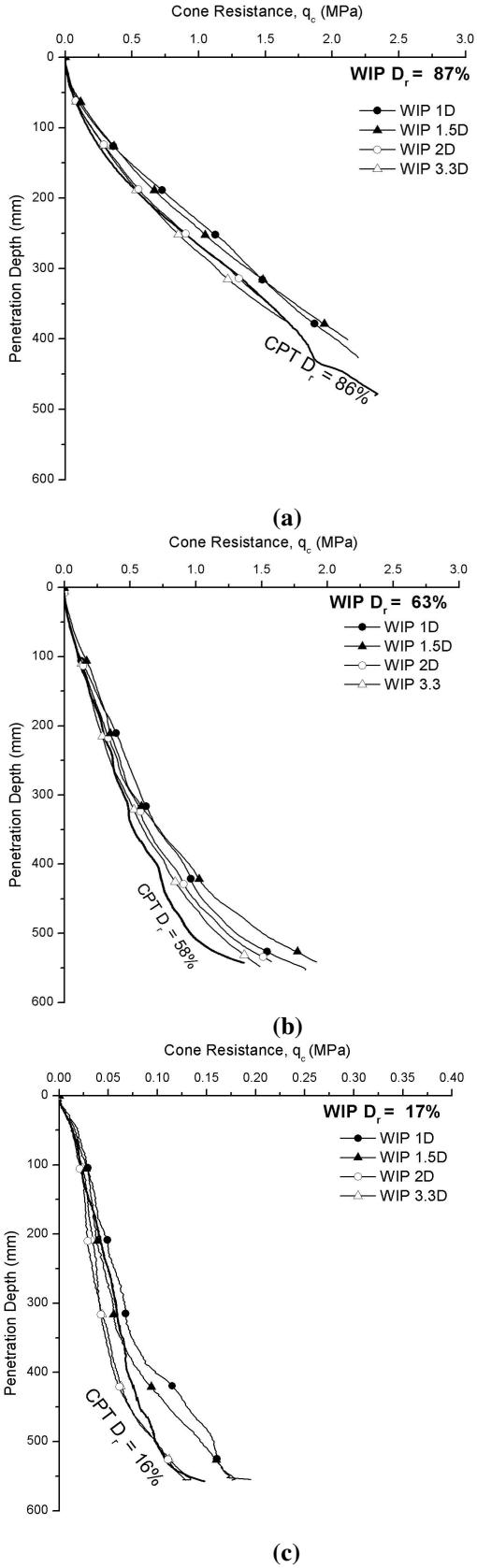

Figure 5-10. Average measured radial cone resistance around installed WIP piles in (a) Dense, (b) Medium Dense and (c) Loose sand

It is evident from Figure 5-10 that the cone resistance measured at each radial location around the WIP piles has very little relative variation. It can therefore be assumed that the cone resistances measured around the installed WIP pile are not influenced by the pile installation processes and that they reflect the initial undisturbed soil relative density, as would be expected since the piles have been cast in-situ.

Assuming that the disturbed cone resistances measured around the WIP pile represents the initial soil properties, it can be seen in Figure 5-10 that there is a difference between the disturbed cone resistances from the CPT probes carried out around the WIP pile and those recorded from the undisturbed cone resistance CPT. Variations also occur between the disturbed CPT cone resistances around the pushed piles and the undisturbed cone resistances, however this variation could potentially be due to installation effects of the pushed pile.

The variations between the disturbed cone resistances measured around the installed WIP pile and the undisturbed cone resistance values can be attributed to differences in the relative density of the sand bed the piles are installed in and the sand bed prepared for the undisturbed CPT. The in-situ relative density of the sand bed that the WIP and Pushed piles are installed in compared to that of the undisturbed CPT is shown in Figure 5-11, where it can be seen that an exact match in relative densities do not occur.

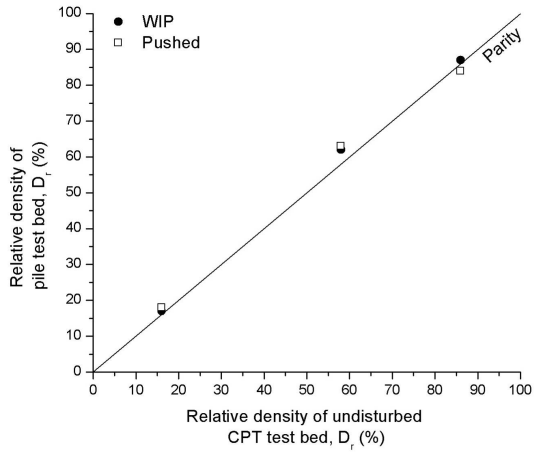

Figure 5-11. In-situ relative density variations between test beds prepared for WIP and Pushed piles and the undisturbed CPT beds

It is noted that the variations in the initial relative density of the pile test beds compared to the undisturbed CPT test beds shown in Figure 5-11 corresponds to the variation in the disturbed cone resistance carried out at a radial distance of 3.3D to the undisturbed cone resistances witnessed in Figure 5-9a-c and Figure 5-10a-c. This is particularly highlighted in medium dense sand where the relative density of the sand test beds for WIP and Pushed piles were of a slightly higher density than that used for the undisturbed CPT. As a results of this, the cone resistances measured around the installed piles (Figure 5-9b and Figure 5-10b), are greater than the undisturbed measurements.

For tests such as the WIP loose tests, there is little difference between the initial relative density of the pile test bed and the relative density of the undisturbed CPT test bed and this is reflected in almost no variation in the measured cone resistance. However, in the Pushed loose test, a difference in relative density between the Pushed pile test bed and the undisturbed CPT test bed of only 2.5% causes significant variation in measured cone resistance.

The sensitivity of the cone resistance to changes in relative density means the use of a cone resistance from an undisturbed test would have to be carried out at identical relative densities to those found in-situ for each of the model piles. Pluviation of test beds to a tolerance of a range of ±1% change in relative density would be almost impossible to achieve consistently.

In order to determine the effects of pile installation on the in-situ soil conditions, the CPT carried out at a radial distance of 3.3D is assumed to represent an undisturbed cone resistance for the test bed and will be used as a reference. For tests such as the pushed dense sample where the in-situ relative density of the pile test is within 1% (Figure 5-9a) of the relative density of the undisturbed CPT cone resistance, the correlation between the 3.3D and undisturbed cone resistance is good, giving further evidence that the use of 3.3D cone resistance can be used to represent an undisturbed test bed.

The suitability of using the in-situ CPT cone resistance carried out at 3.3D can be checked by comparing the readings with those obtained from CPTs carried out in

undisturbed soil beds, shown in Figure 5-12. For a select number of model pile tests it seems reasonable to use the undisturbed cone resistance values, however for other tests, the undisturbed values will give inaccurate representations of the in-situ soil conditions. The use of the cone resistance at 3.3D can be used as a compromise in order to maintain a consistent approach in the analysis of changes to in-situ soil conditions due to pile installation.

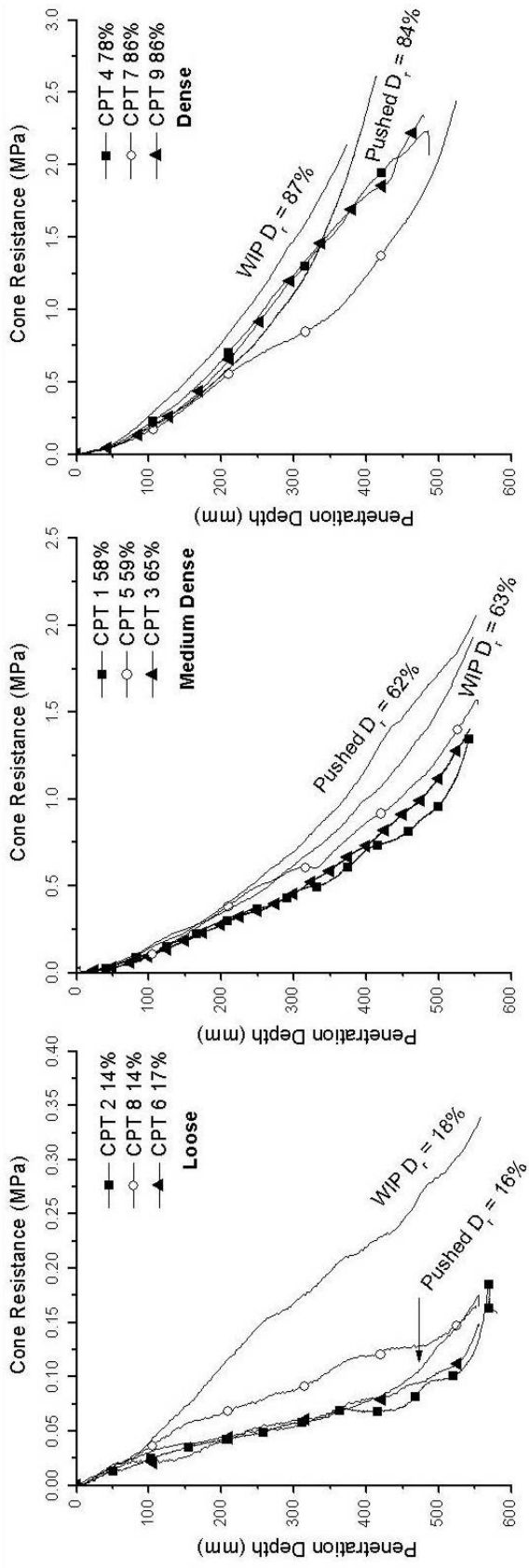

Figure 5-12. Undisturbed CPT cone resistance compared to those measured at a distance of 3.3D from Pushed and WIP pile tests

5.3.3 Sub surface soil disturbance due to pile installation using CPT

The cone resistance variations due to the installation of the piles for loose, medium dense and dense sand are shown in Figure 5-13a-c. The cone resistance at each radial location is normalised using the cone resistance from a location of 3.3D based on the assumptions made in section 5.3.2 regarding cone resistance measurements of the disturbed and undisturbed test beds. The penetration depth of the CPT probe, z_{CPT}, is normalised using the embedded length of the pile, L.

In the plots of radial influence of the model piles, a $q_c/q_{c3.3D}$ value greater than 1 indicates a densification of the sand compared to undisturbed in-situ conditions, while a value lower than 1 indicates a loosening of the in-situ soil conditions. The low effective stress causes significantly lower cone resistances at the soil surface, to a depth of around 0.04L. This low cone resistance causes some large data spikes during the normalisation of the data in Figure 5-13. This erratic looking data is simply due to the calculations during normalisation and not errors in the collected data

Cone penetration in the dense sand was not taken as deep as in the other sand densities purely due to the fact that the loads experienced on the CPT cone load cell had reached the safe working limit and as a result the penetration was stopped. In most instances, the penetration of the CPT manages to equal the installation depth of the pile.

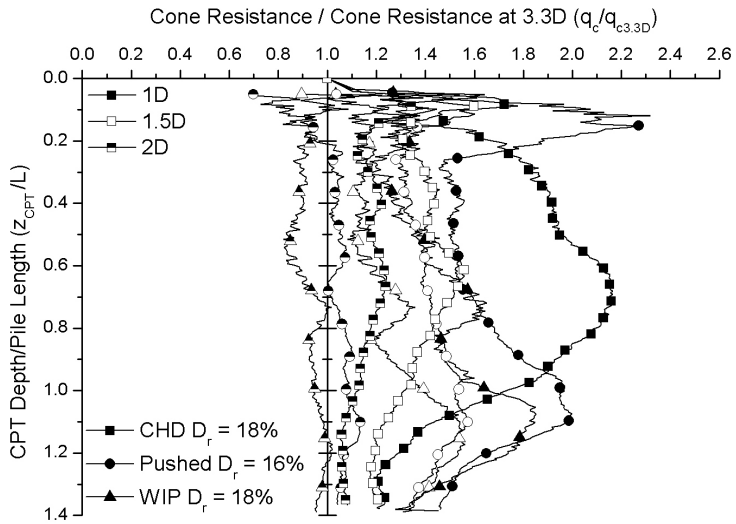

(a)

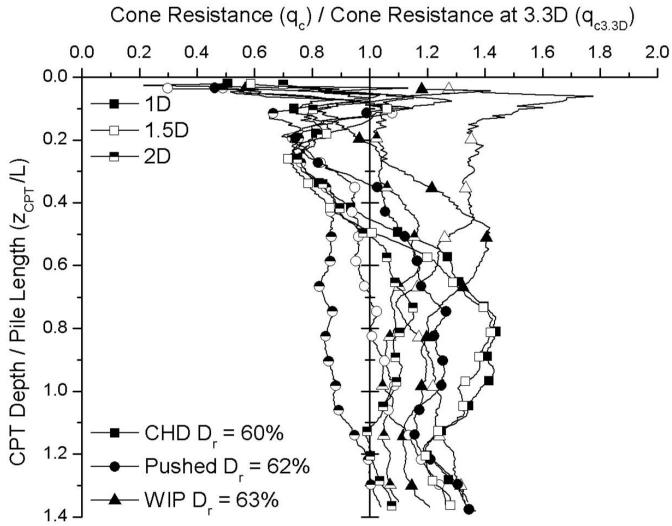

(b)

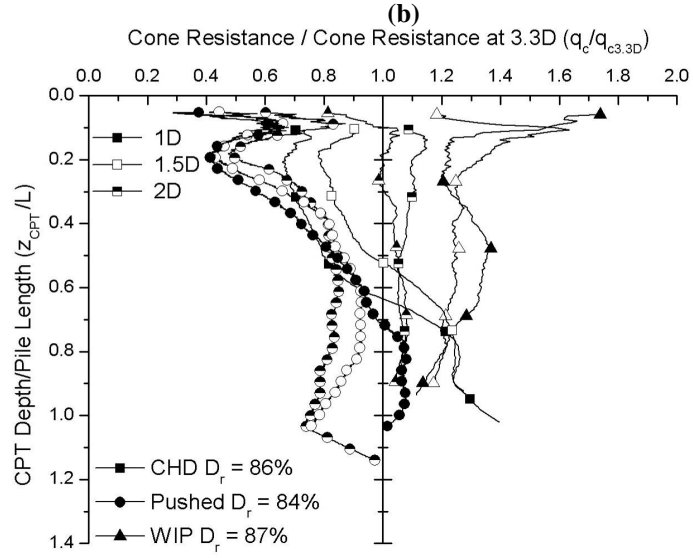

(c)

Figure 5-13. Relative change in disturbed cone resistance along pile length at different radial locations for model piles installed in (a) loose, (b) medium dense and (c) dense sand

The WIP piles generally show consistency in behaviour regardless of sand density. As would be expected very little variation occurs across the test bed due to the installation of WIP piles. It is noted that there is an apparent increase in cone resistance at a distance of 1D around the WIP piles installed in medium dense and dense sands. This 'increase' is not due to the pile installation and is most likely to a local densification during pluviation. It is known that the relative density of pluviated sands will be affected by the particle falling speed (Ueno (2000)). The presence of the WIP pile during the pluviation process will cause turbulent airflow around the vicinity of the pile surface as well as causing sand particles to bounce off the pile itself, both of which is likely to cause a denser sand layer to accumulate in the area around the in-situ pile. Because of the nature of the method of this pile installation there is very little that can be done to stop this local densification, however it is only applicable to the WIP piles, both the pushed and CHD piles were absent during the pluviation process.

Both Pushed and CHD piles show increases in cone resistance to some degree in all soil densities. The greatest cone resistance change is found closest to the installed pile. The magnitude of the change is clearly dependant on both the initial in-situ relative density and the pile installation method. It is also found that the relative location along the pile depth at which densification takes place also varies with both relative density and pile installation method.

In loose sand an average cone resistance increase of $1.5q_{c3.3D}$ is caused due to the pushed pile installation over a depth equal to $0.7z_{CPT}/L$. For CHD piles installed in loose sand, an average cone resistance increase of $2q_{c3.3D}$ occurs primarily between a z_{CPT}/L of 0.2 and 0.9. At the pile tip, both CHD and pushed piles show significant changes in cone resistance. The magnitude of cone resistance around CHD piles reduces by around a third from a peak value of 0.25MPa at the pile tip to a value of 0.18MPa depth of 1.2L, similar to undisturbed in-situ values. The pushed pile however, displays an increase in cone resistance of $0.5q_{c3.3D}$ to a depth of $1.3z_{CPT}/L$, after which the cone resistance value return to expected in-situ values. As the lateral distance from the pile increases, a similar behaviour is observed for both CHD and pushed piles however the magnitude of the average increase in cone resistance along the installed pile depth decreases. By a radial

distance of 2D, the effects of the installed pile on in-situ soil conditions have become negligible.

For the medium dense tests, both the CHD and pushed piles show a similar influence on the in-situ soil. Both piling types appear to induce loosening of the sand, particularly at shallow installation depths. For CHD piles, typical loosening equal to $0.8q_{c3.3D}$ takes place up to a depth equal to 0.45L. For pushed piles, a similar magnitude of loosening occurs but to a slightly shallower depth of 0.35L. For both CHD and pushed piles, after the initial loosening of the sand, densification occurs throughout the pile depth. CHD causes up to $1.4q_{c3.3D}$ densification whilst the pushed pile is around $1.25q_{c3.3D}$. The level of densification which occurs in medium dense sand is lower in magnitude than that found in loose sand. It also occurs at a much greater h/L value, where h is the depth along the pile length. The cone resistance increase measured around the model CHD piles installed in medium dense sand is similar to that found by Busch *et al* (2010) for cone resistance changes around an auger displacement pile. Full scale radial CPT testing around an auger displacement pile in medium dense sand also showed a loosening of the sand towards the ground surface by Busch *et al* (2010), as has been witnessed in the model testing. Similar to what occurred in loose sand, the CHD influence reduces significantly below the pile tip and by a depth of 1.2L, the effects of the CHD pile are difficult to detect. The increase in cone resistance beneath the pushed pile appears to occur by about 25% but not to the same magnitude as found in the loose sand which increased by 100%. The cone resistance appears to continue to increase at depths greater than 1.2L however, this occurs in all model pile tests and it is probable that the CPT is being influenced by the base of the test box.

Similar behaviour is displayed in dense sand. The loosening effect caused by the CHD extends to around 0.6L to a magnitude of about $0.7q_{c3.3D}$, which is both deeper and greater loosening than found in medium dense sand. The loosening of sand caused by the installation of the pushed pile extends to 0.7L, slightly greater than what was found for the CHD pile, and causes nearly twice as much of a reduction in cone resistance, particularly at depths of around 0.25L. Densification begins to occur at 0.6L for CHD and 0.7L for pushed piles at distance of 1D from

the installed pile. The CHD pile causes an increase in cone resistance of up to four times that caused by the pushed pile. Due to the capacity restraints of the CPT loadcell which have already been discussed, the CPT in dense sand is unable to penetrate deep enough to determine the effects of installation below the pile tip. The large increase in cone resistance found below the pushed pile is therefore assumed based on the tests carried out in loose and medium dense sand. The affect of the CHD pile installation is evident to around 1.2L below the pile tip and is relatively consistent between the different densities already tested. It is therefore assumed that similar results would be witnessed in the dense sand.

The increase in cone resistance around an installed CHD pile at a distance of 1D is highlighted in Figure 5-14 with the variation represented using power law curves. The parameters for the ideal curve fit can be seen to vary with relative density. The curve fit gives a representation of the variation in the cone resistance due to the CHD installation with depth and takes into account the loosening that occurs in both dense and medium dense sands. The variation to the initial cone resistance is seen to vary both with the sand density and depth in relation to the pile length. Utilisation of the suggested curves is acceptable where CHD piles are installed in a uniform sand deposit, however it becomes difficult where varying sand densities are encountered at varying depths throughout the pile. Due to this, average adjustment factors are presented for each relative density condition.

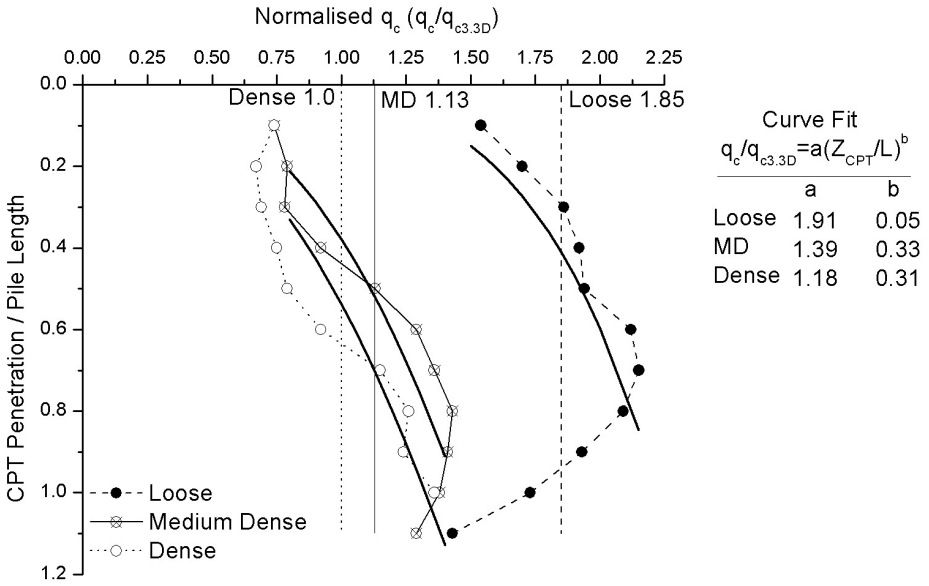

Figure 5-14. Measured changes to cone resistance at a distance of 1D around an installed CHD pile at different relative densities represented by power law curves and showing average values

The cone resistance is seen to vary throughout the installation depth of the pile as is shown in Figure 5-15a-b for loose, medium dense and dense samples. The cone resistance q_c values for each radial position around the piles are normalised by the outermost CPT probe results. The radial distance at which the probe is penetrated r_p, has been normalised by the pile radius r. Two depths have been selected for comparison, one equal to the full pile length and one at half the pile length.

It is clear that when installed in loose sand both the CHD and Pushed piles cause densification of the initial in-situ sand. The CHD is seen to produce a greater degree of densification over the entire length of the pile compared to the pushed pile which primarily causes densification at the pile base.

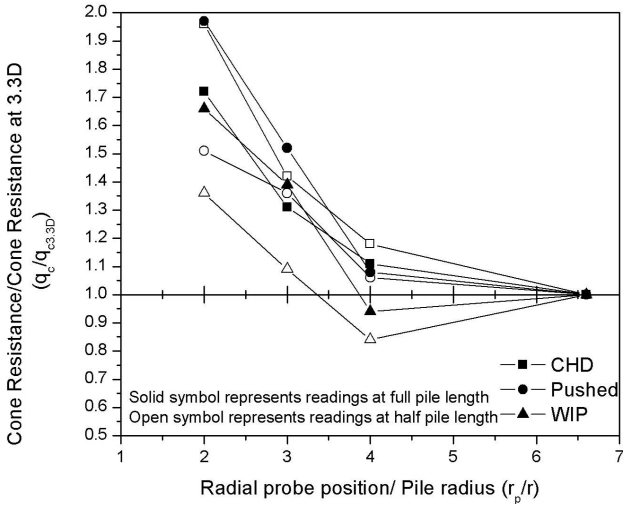

(a)

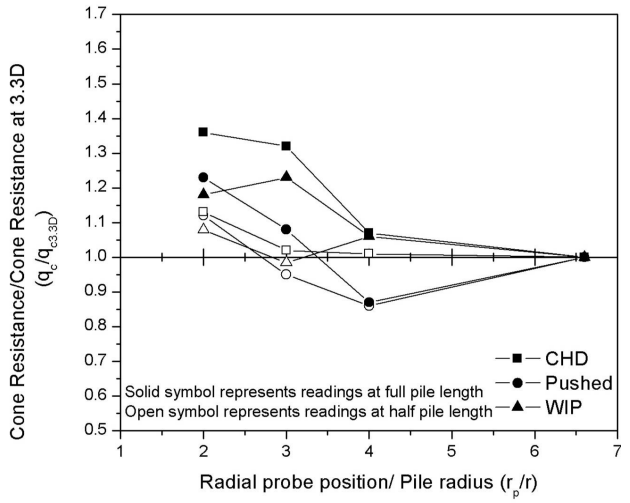

(b)

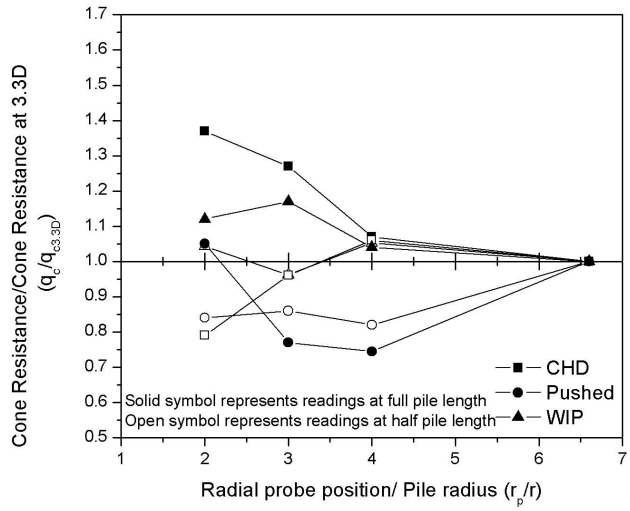

(c)

Figure 5-15. Change in cone resistance at increasing radial distance from the installed model piles for in (a) loose sand, (b) medium dense sand and (c) dense sand at a depth of 0.5L and 1L

Lateral densification is clearly caused by the CHD pile installation in all relative densities to a varying degree. Displacement piles are seen to cause less pronounced lateral densification and more vertical densification around the pile tip, as shown by Randolph and Gourvenec (2011). This is of course intuitive behaviour when the installation process is considered as shown in Figure 5-16. Auger displacement piles installed in clay by Hird *et al* (2011) have been found to cause significant lateral soil displacements during installation while vertical soil displacement is similar behaviour to that indicated from the model test piles.

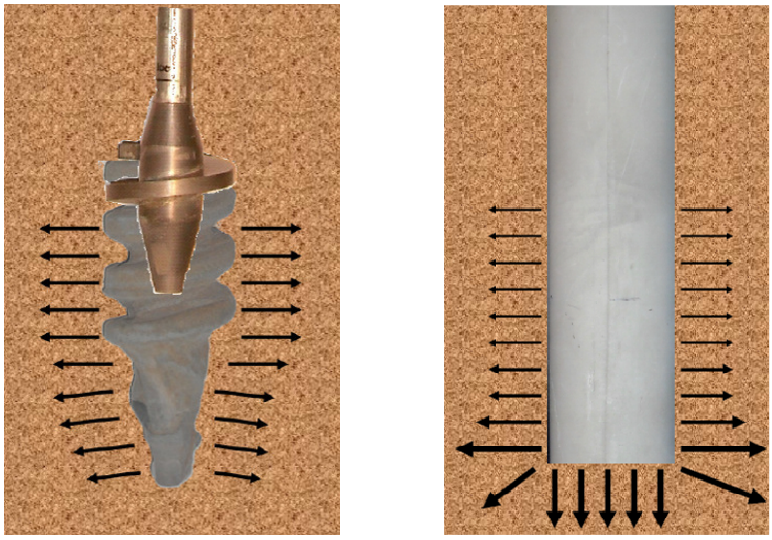

(a) **(b)**

Figure 5-16. Characteristic soil movement around installed piles for (a) CHD pile and (b) Displacement pile

5.3.4 Changes to relative density around installed piles based on CPT cone resistance

The effects of installation of the model piles on the in-situ soil bed have so far been discussed in terms of changes in cone resistance from the CPTs carried out at locations around the piles. The cone resistance changes give an indication as to the soil displacement around the pile and give an indication of the soil property changes however it would be beneficial to be able to quantify the change in cone resistance in terms of relative density.

The relationship between relative density and soil parameters such as the angle of friction can be easily correlated (Robertson and Campanella (1983)). However the direct correlation between CPT cone resistance and relative density which is applicable to all sands is difficult to determine as discussed by Bolton and Gui (1993). The cone resistance varies with both relative density and the in-situ vertical effective stress, as shown by Lunne *et al* (1997) and Bolton and Gui (1993).

A number of empirical methods have been suggested for the determination of relative density from CPT cone resistance as discussed by Lunne *et al* (1997) or Hsein Juang *et al* (2002). Some of the more common methods suggest a relationship between cone resistance and relative density are those suggested by Kulhawy and Mayne (1990) in equation 5-1 and by Baldi *et al* (1986) shown in equation 5-2. The expressions are based on a series of CPTs carried out in calibration chambers.

$$D_r^2 = \frac{q_{c1}}{305 Q_c Q_{OCR} Q_A} \qquad \textbf{5-1}$$

Where:

$$q_{c1} = \frac{(q_c / p_a)}{(\sigma_v' / p_a)^{0.5}}$$

P_a = Atmospheric pressure

Q_c = Compressibility factor (0.91-1.09)

Q_{OCR} = Overconsolidation factor =$OCR^{0.18}$

Q_A = Ageing factor

$$D_r = \frac{1}{C_2} \ln\left(\frac{q_c}{C_0 [\sigma_{VO}']^{C_1}} \right) \qquad \textbf{5-2}$$

Where: C_1, C_2 and C_0 are soil constants

The soil constants C_1, C_2 and C_0 are given as 0.55, 2.41 and 157 respectively for the normally consolidated Ticino silica sand used in the calibration chamber.

Application of equations 5-1 and 5-2 to determine the relative density of the undisturbed CPTs carried out proved to produce consistent under estimations, presumably due to the assumed constants not being applicable to the specific sand used during the model tests.

Alternative methods for determining the relative density from CPT cone resistance are suggested by Jamiolkowski *et al* (1985) and Bolton and Gui (1993). Jamiolkowski *et al*, (1985) used large calibration chambers to conduct extensive tests to determine the relationship between cone resistance and relative density of numerous test sands. Normalising the cone resistance by the square root of the effective stress and plotting it against the relative density, Figure 5-17 , a relationship shown in equation 5-3 was determined for medium compressibility sands.

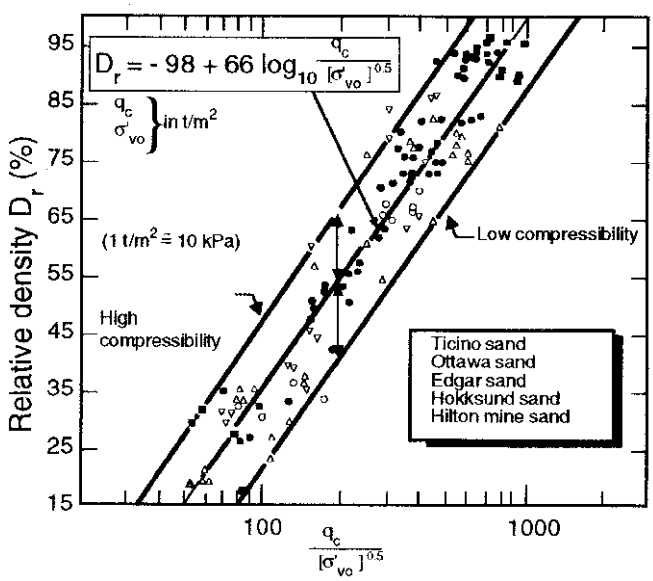

Figure 5-17. Estimation of relative density from CPT cone resistance from Jamiolkowski *et al* (1985)

$$D_r = -98 + 66 \log_{10} \frac{q_c}{\left(\sigma'_{vo}\right)^{0.5}} \qquad \textbf{5-3}$$

Bolton conducted similar experiments in a centrifuge as opposed to a calibration chamber. His tests were carried out in Fontainbleau silica sand. Using similar

normalisation and plotting techniques, a relationship was determined as shown in equation 5-4

$$D_r = 0.2831\left(\frac{q_c - \sigma_v}{\sigma_v'}\right) + 32.964 \qquad \textbf{5-4}$$

Using the cone resistance data from undisturbed model CPT, the relative density calculation methods are assessed for suitability for use at model scale. The accuracy of the prediction methods was found across the loose, medium dense and dense sand samples prepared. The typical accuracy found is highlighted using the data from the dense sand bed. As is shown in Figure 5-18, the accuracy of the relative density prediction methods investigated give varying results. Both the Baldi and Bolton proposed relationships underestimate the in-situ relative density by 41% and 32%, while the Kulhawy relationship is over estimating by 25% at the full pile length. The Jamiolkowski relationship provides the closest estimation of the in-situ relative density. Bolton et al (1993), limits the use of equation 5-4 for relative densities greater than 50%, while Lunne *et al* (1997) notes that the correlations proposed for the relative density magnitude from cone resistance can only be used as approximate for soils similar to those used in the calibration chamber and will be highly sensitive to variations to the in-situ sand type and stress history.

It can be seen that all prediction methods display a hyperbolic curve and do not give a constant result until an apparent 'critical depth' is reached. In terms of the model pile length, this critical depth equates to 0.75d. Until this point is reached, the relative density determined from using the in-situ CPT cone resistances will be significantly lower than the actual density values.

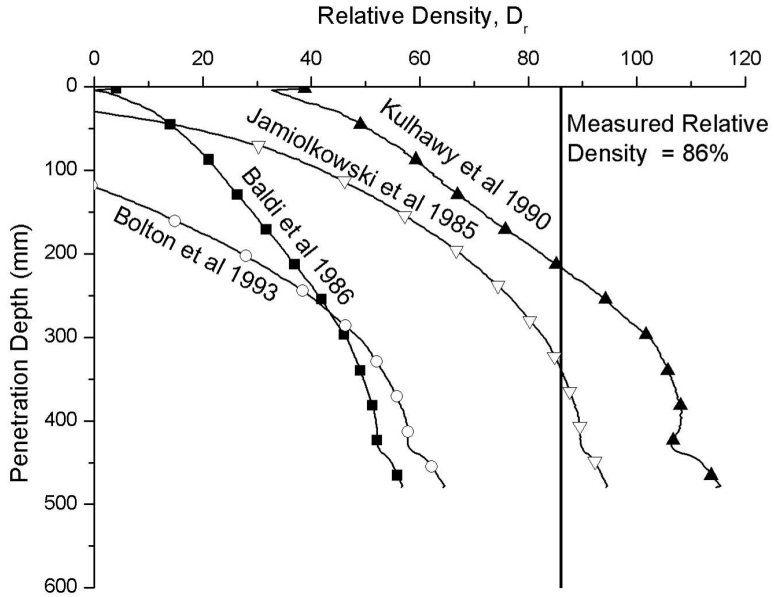

Figure 5-18. Accuracy of available prediction methods for determining relative density from model CPT cone resistance installed in dense sand.

Investigations into the use of CPT cone resistance to determine the relative density of the in-situ sand with accuracy have shown that the results are highly dependant on the individual properties of the in-situ sand. The application of a particular estimation method discussed above is found to be unsuitable, particularly in the model scale. It would therefore be beneficial to use the undisturbed CPT cone resistances, along with the relative densities determined from density pots to create correlations specific to the model tests.

The Jamiolkowski et al (1985) relationship is used as a basis for a determining a relationship for the model test bed relative densities since it produces the closest representation of the in-situ relative density. The normalised cone resistance q_c is plotted against the square root of the vertical effective stress σ'_{vo} for each of the model CPT undisturbed cone resistances, Figure 5-19. From Figure 5-18 it is known that the predicted relative density varies with embedment depth however, in reality, the relative density of the soil is the same at all depths. In order to ensure that an estimation of relative density throughout the test box, selected depths through the sand bed are used. The depths selected correspond to 0.25L, 0.5L, 0.75L, 1L and 1.23L of the installed pile depths. These depths allow a cross section of density change to be determined through the test bed. The specific

readings obtained from the model testing can be used to develop the general plot shown in Figure 5-20.

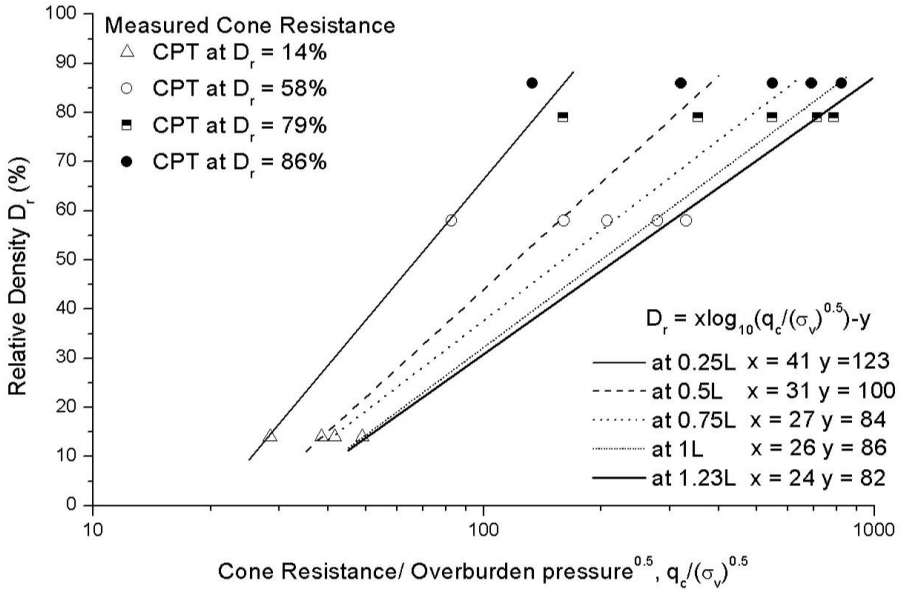

Figure 5-19. Application of the model CPT cone resistance using the Jamiolkowski *et al* (1985) for known relative densities of the test bed showing a variation with embedment depth

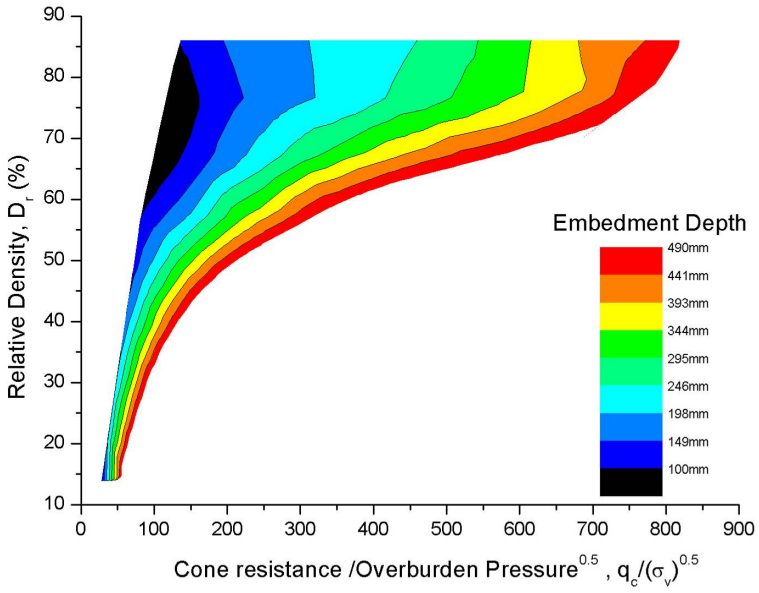

Figure 5-20. Relative density determination from model CPT cone resistance at varying embedment depths

The relative densities at the selected depths are calculated using the relationships determined in Figure 5-20 for each of the horizontal radial locations for the model piles. The relative densities for the CHD pile tests are shown in Figure 5-21. The

dashed lines labelled 18%, 60% and 83%, represent the average measured relative density for the pile tests based on the density pots buried in the sand. For the CHD piles, the variance between the measured pot density and the 3.3D cone resistance estimated relative density is typically within 10% and falls within the expected range from the recorded pot values.

As a comparison, the pushed pile influence on the in-situ relative density is shown in Figure 5-22. Similar to the CHD piles, the variation between the relative density determined from the density pots and the 3.3D CPT is typically around 10%.

The affects of the CHD installation on the in-situ sand relative density is clearly visible from Figure 5-21. Using the cone resistances recorded at the 3.3D to determine the undisturbed relative density, the effect of the CHD installation can be seen to cause on average, a doubling of the undisturbed relative density in loose sand at a radial distance of one pile diameter, (Figure 5-23). The magnitude of the increase in relative density decreases as the distance from the pile increases. The increase in the relative density remains fairly constant throughout the depth of the pile and becomes visibly less prominent below the pile tip.

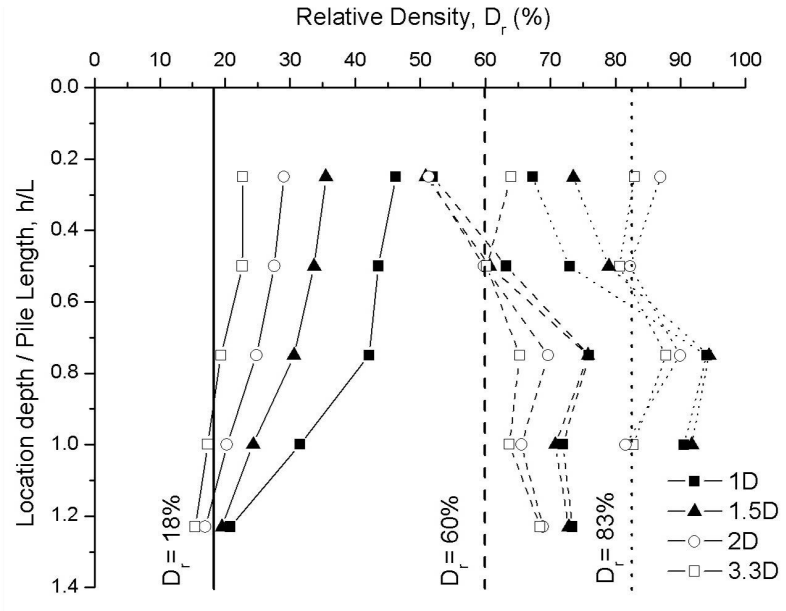

Figure 5-21. Relative density estimates along the installed pile length for CHD piles based on CPT cone resistances at different radial distances from pile

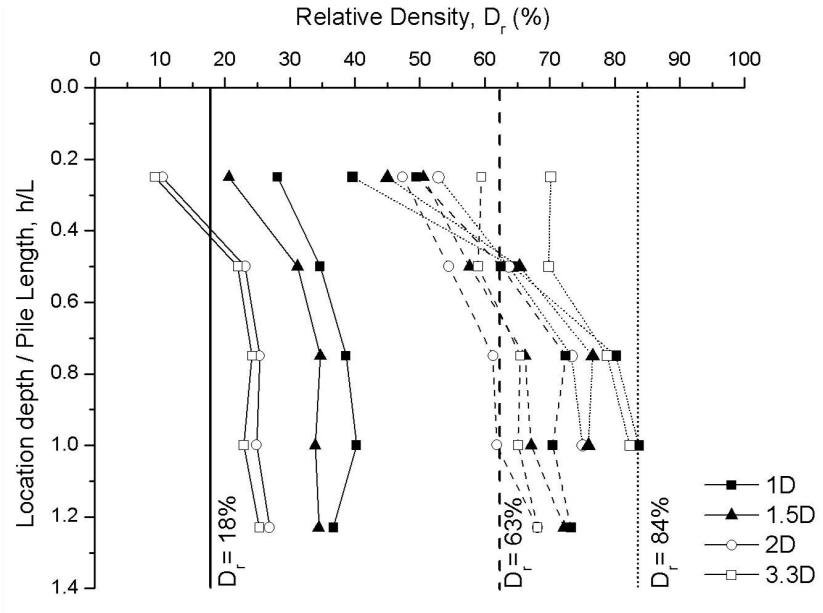

Figure 5-22. Relative density estimates along the installed pile length for Pushed piles based on CPT cone resistances at different radial distances from the pile

In medium dense sand the influence of the CHD installation on the relative density can be seen to vary with pile penetration depth. A reduction to the relative density of 25% is evident until a depth of 0.5L. Between a depth of 0.5L and 1L, the CHD is seen to increase the relative density by an average of 30%. Around the toe of the pile, an increase in the relative density is found to be around 25% down to a depth of 1.2L.

For dense sand, the CHD is again seen to cause a slight loosening of the soil by an average of 20% to a depth of 0.5L. After the initial loosening, an average densification of 10% takes place, significantly less than what was found in loose or medium dense sands.

For pushed piles installed in loose sand, an average increase of 60% in the relative density is witnessed throughout the entire length of the installed pile and even up to 1.2L below the pile tip. A reduction in relative density typically of around 16% is experienced within medium dense but in dense sand it can be as high as 57%. The loosening in medium dense to dense sand occurs to a depth of about 0.5L. Densification within medium dense to dense sand is typically in the order of 1%-10% of the soil density found at a location of 3.3D.

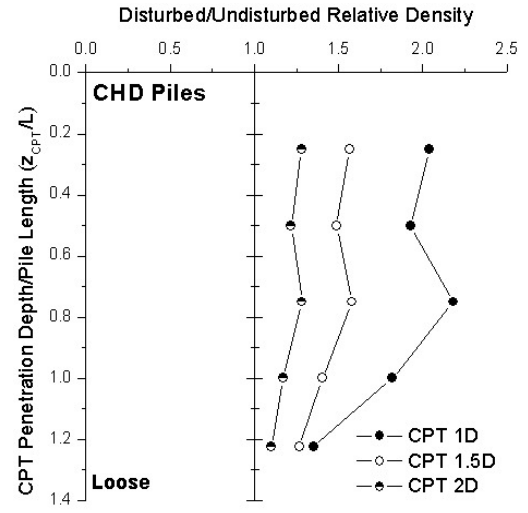

(a)

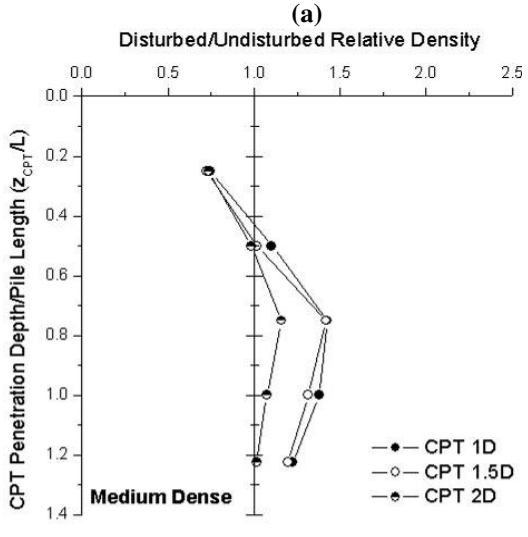

(b)

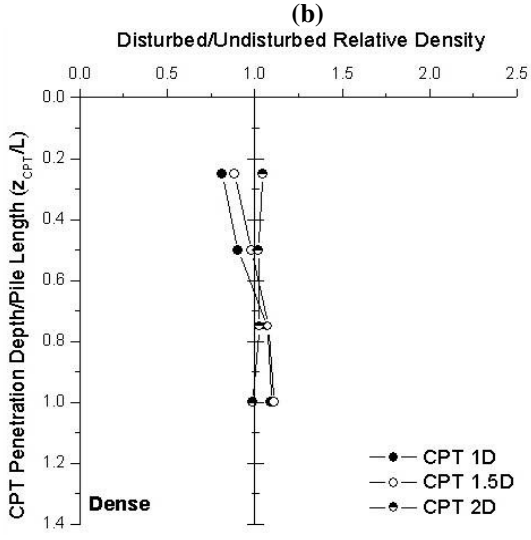

(c)

Figure 5-23. Change in the initial relative density due to CHD pile installation at different radial locations around pile.

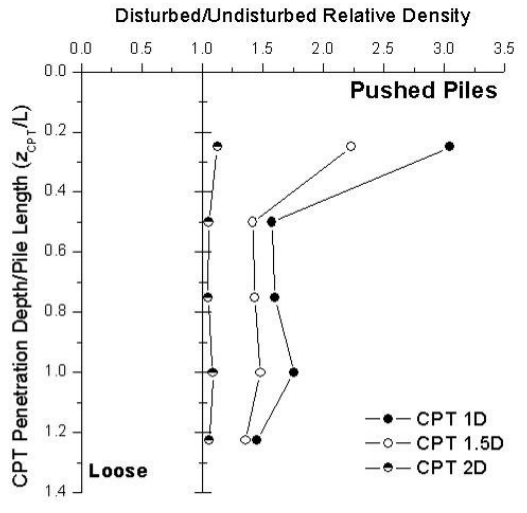

(a)

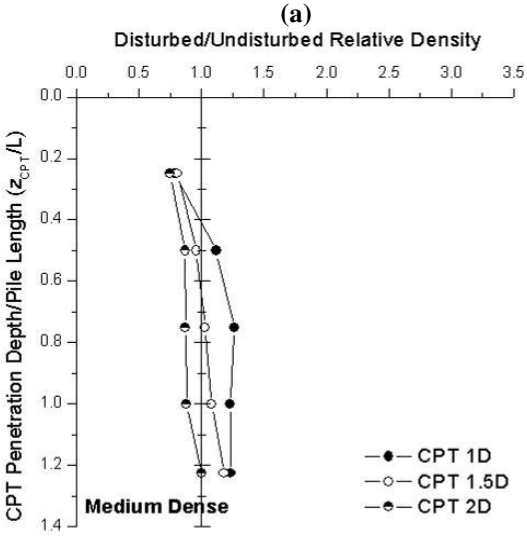

(b)

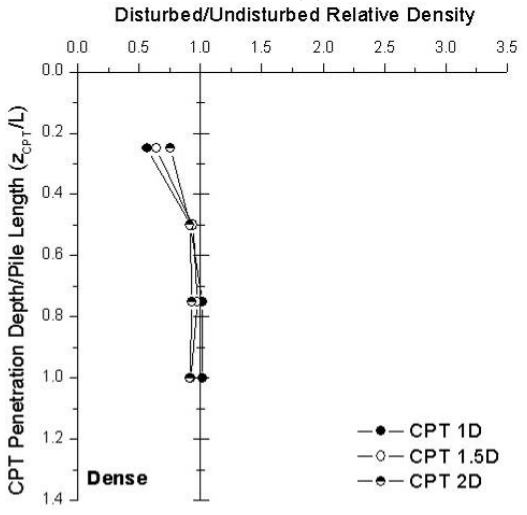

(c)

Figure 5-24. Changes in the initial relative density due to Pushed pile installation at different radial locations around pile.

The average correction factors to the initial relative density due to the installation of CHD and pushed piles are summarised in Table 5-1. It has been found that in general, the CHD piles cause the greatest improvement in loose sands however some density increase is experienced at all relative densities.

Table 5-1. Summary of average density correction factors at a distance of 1D for base and shafts due to the installation of CHD and pushed piles

		Loose Sand	Medium Dense Sand	Dense Sand
CHD	Shaft	2.0	1.25	1.0
	Base	1.5	1.25	1.1
Pushed	Shaft	1.6	1.2	1.0
	Base	1.6	1.2	1.0
WIP	Shaft	1.0	1.0	1.0
	Base	1.0	1.0	1.0

5.4 Ultimate capacity of model piles

As in all pile testing, it is necessary to determine the ultimate pile capacity. In the model testing, the ultimate load capacity of the CHD pile is compared to alternative piling techniques. As is discussed in Chapter 2, the capacity of a pile is made up of base and shaft resistances which will be investigated to determine the individual contributions.

The piles constructed in series 1 tests as discussed in section 5.2 did not allow determination of the individual base and shaft resistance components, only the total applied head load was measured. In order to measure the base and shaft components, another series of model piles were constructed that incorporated instrumentation that would allow the separation of base and shaft resistance, known as series 2 piles. The instrumented series 2 piles were constructed to a greater depth than those in previous tests in order to achieve more realistic L/D ratios for prototype scale piles. Similar to previous model tests, the instrumented CHD pile performance is compared to both pushed and WIP piles.

5.4.1 Instrumented model CHD piles load-settlement behaviour

In total, 11 series 2 model CHD piles were constructed which produced suitable load test results to allow comparisons with Pushed and WIP piles. Out of the 11 model CHD piles constructed, 4 were instrumented. Since the CHD piles are installed in-situ, there is a degree of variability in the quality of the piles produced as is discussed in Chapter 3. On rare occasions the piles did not form correctly due to failures in the grout delivery system or some unforeseen problems, see Figure 5-25. The poor quality of a pile was initially highlighted during drilling stage, by using the volume of delivered grout as a guide. When load testing took place it was instantly apparent that a pile was sub-standard based on the load capacity achieved. Piles which were substandard were excluded from further analysis.

In order to gauge the quality of the CHD pile, the pile is exhumed once load testing has been carried out and inspected. The exhumed pile dimensions are recorded and presented in Table 5-2 to be used in conjunction with Figure 5-26. All piles presented in Table 5-2 formed to an acceptable standard such that flanges were of consistent thickness and diameter and were therefore suitable for load test comparisons. It is seen that the dimensions of the constructed CHD pile are consistent regardless of the in-situ relative density of the test bed.

(a) (b)

Figure 5-25. Example of a poorly formed CHD pile (a) and a well formed acceptable CHD pile (b)

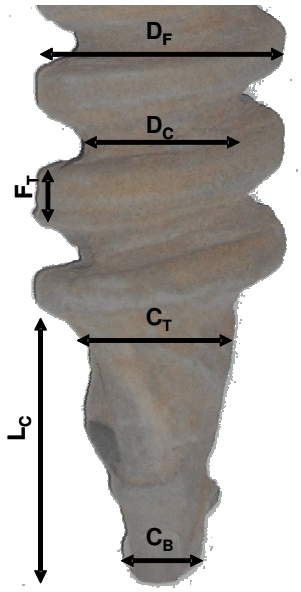

D_f = Flange Diameter
D_c = Core Diameter

F_T = Flange Thickness

C_T = Cone Diameter at Top
C_B = Cone Diameter at Base

L_C = Cone Length

Figure 5-26. CHD dimension identification for use with Table 5-2

Table 5-2. Model CHD dimensions based on Figure 5-26

CHD Pile	Relative Density (%)	Pile Length (mm)	F_T (mm)	Diameter		Cone		
				D_c (mm)	D_f (mm)	L_C (mm)	C_T (mm)	C_B (mm)
102	78	400	11	40	60	54	34	19
103	59	400	10.9	40	60	50	37	18
104	17	395	9.9	40	60	44	31.6	23
105	17	398	10	40	60	50.9	35.2	23.2
107	84	400	10	40	60	50	40	16
108	61	400	10	39	60.7	60	40	20
110*	82	400	10.5	40.4	60.8	55	34.4	20
111*	86	405	10	42	61	55	38.1	23.2
112*	20	400	10.5	49	62	45	39.2	21.6
114*	19	400	10	48	61	45	40	19
116	63	400	10.1	40	61	46	36	20

* Denotes instrumented pile

The load-settlement behaviour of the model CHD piles, Figure 5-27, shows good repeatability and consistency. Some variation occurs between individual tests which can be attributed to the different relative densities between each individually pluviated test bed. Only the total pile resistance, Q_T, has been plotted for the CHD piles at this stage.

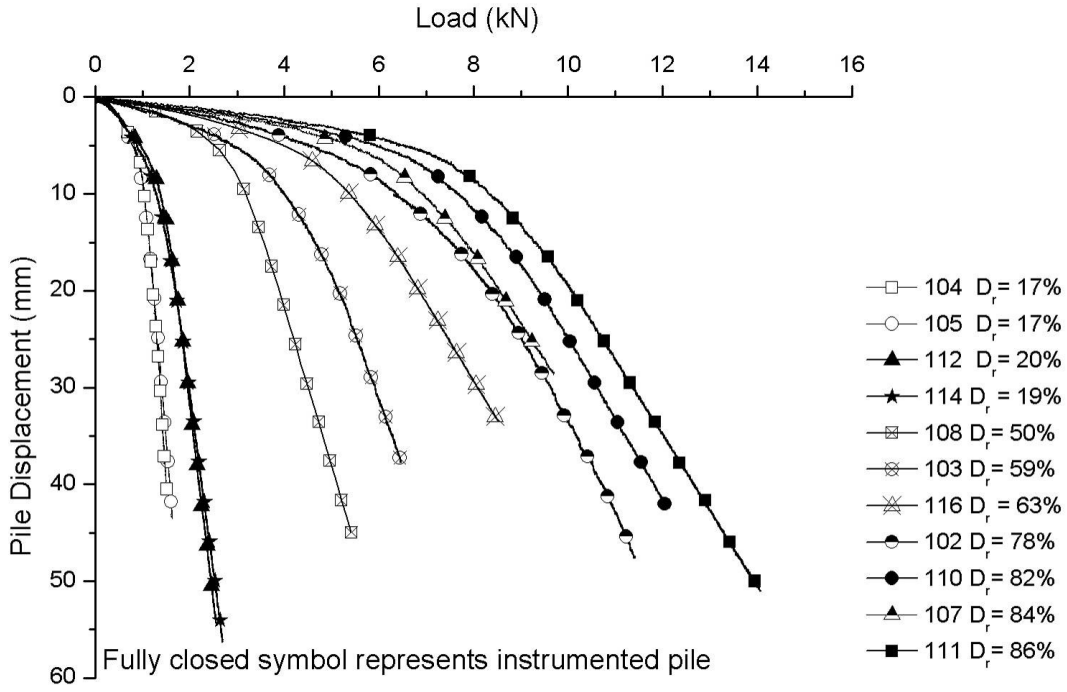

Figure 5-27. Total pile resistance for all model CHD piles installed at different relative densities

Due to the nature of the CHD pile installation, instrumentation is slightly more difficult to install at model scale compared to the pre-cast pushed and WIP piles. Instrumentation took the form of strain gauged aluminium rods inserted into the freshly cast pile as discussed in section 3.3.8. Not all CHD piles have instrumentation which allows the effects of the installation of the aluminium rod into the pile to be taken into consideration. From investigating the total pile resistances shown in Figure 5-27, the effects on load bearing capacity of the insertion of the aluminium rod appear to be minimal with the stiffness of the pile varying with relative density. It is assumed in the analysis of the model piles that the insertion of the rod can be deemed to have no effect on the pile load-settlement behaviour or ultimate capacity.

The strain gauge instrumentation system as described in Chapter 3 was installed in four CHD piles. Two CHD piles installed in dense sand and two in loose were instrumented in order to show performance in the two density extremes. The strain gauges produce an output voltage caused by applied strain in the pile. The output voltage is in milli-volts and is converted to a strain measurement using equation 5-5.

$$V = \frac{B_V G_F \varepsilon N}{4} \qquad \textbf{5-5}$$

Where V = Output voltage from strain gauge (mV)

B_V = Bridge excitation voltage (V, =10V in tests)

G_F = Gauge factor (2.1 for gauges used)

ε = Strain (microstrain)

N = Number of active arms in Wheatstone bridge (= 2 in this case)

The mechanics of engineering materials dictates that the stress, σ in a structural element is directly proportional to the strain, ε in the material along with the modulus of elasticity, *E*, shown in equation 5-6. This relationship is commonly known as Hooke's law and is described in numerous literature publications such as in Beer and Johnston (1992) and is the basis for calculating an applied load based on the strain readings.

$$\sigma = E\varepsilon \qquad \textbf{5-6}$$

Hooke's law is more generally arranged in the format of applied load as opposed to stress by introducing the cross section area of the element in question to give equation 5-7.

$$P = \varepsilon AE \qquad \textbf{5-7}$$

Where P = Applied load

A = Cross sectional area

In order to determine the load distribution within the pile, both the cross sectional area and the modulus of elasticity must be known. The application of Hooke's law to determine the load distribution through a cast in situ pile is made difficult, particularly with the CHD pile, due to the face the cross sectional area is non-uniform throughout the length of the pile. Typically, the modulus of the concrete, or grout in the model case, would be determined through laboratory testing of

cylinders following BS 1881-121 (1983). However, the model piles also have an aluminium rod in them which must be considered.

Research conducted on instrumentation of bored piles has found that the modulus of elasticity of concrete is a function of the imposed load being applied and will therefore vary during the loading of a pile, Li and Ruban (2009), Hayes and Simmonds (2002), which will influence the values used in the model piles. It is also advantageous to obtain in-situ material properties as opposed to those obtained from 'ideal' tests in order to ensure the accuracy of future parameter calculations. To overcome these issues, a number of methods are available which can allow calculation of the concrete modulus using the pile load test data.

A non linear representation of the stress-strain relationship of the pile material suggested by Delpak et al, (1998) attempts to determine the tangent modulus of both the individual materials used in the pile. This variable stiffness approach to estimate material modulus is shown in equation 5-8.

$$E_{CT} = \frac{P - E_A A_A \varepsilon_1}{\varepsilon_1 A_{CT1}} \qquad \textbf{5-8}$$

Where E_{CT} = Tangent modulus of concrete (kN/mm^2)

E_A = Modulus of elasticity of Aluminium rod (taken as 70kN/mm^2)

A_{CT1} = Area of concrete at level 1 (mm^2)

ε_1 = Strain from gauge at level 1 (microstrain)

P = Axial applied load (kN)

Level 1 is considered to be the strain measured above ground level

By ensuring that a section of the installed pile is cast above ground level and is therefore be uninfluenced by pile shaft friction, the variable stiffness method attempts to determine the concrete modulus. This approach produces reasonable results in full scale pile tests, however in model scale, back figured estimates for grout modulus proved to be widely inaccurate. The inaccuracy occurred due to the large influence the aluminium elastic modulus has in the back calculation.

An alternative method to determine the elastic modulus is proposed by Fellenius (2001) known as the tangent modulus analytical method. The method aims to account for the composite pile material alone. Similar to the variable stiffness approach, the tangent modulus approach requires strain gauge data which is uninfluenced by shaft friction. The tangent modulus of the composite material is found using a stress-strain plot using equation 5-9.

$$M_t = \left(\frac{d\sigma}{d\varepsilon} \right) = A\varepsilon + B \qquad \textbf{5-9}$$

Where M_t = tangent modulus of the composite pile material

A = slope of the tangent modulus line

B = y-intercept of the tangent modulus line (initial tangent modulus)

ε = measured strain

In the model CHD piles, both the cross section area and the measured strain is known at the strain gauges at level 6 (Figure 3-19), therefore the determination of the tangent modulus is possible. The tangent modulus of the composite grout-aluminium pile material was found to be consistent throughout the entire load test for each pile. However, the modulus is seen to vary in magnitude depending on the in-situ soil density, Figure 5-28. The higher tangent modulus in the dense sands reflects the greater loads imposed on the pile.

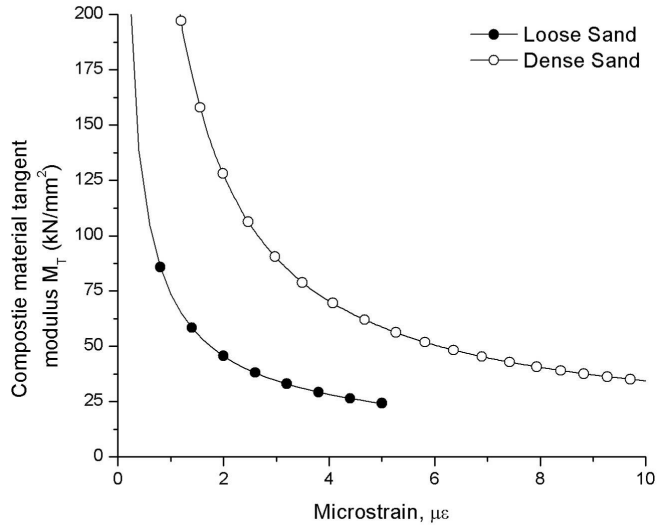

Figure 5-28. Composite pile material tangent modulus values determined for CHD piles installed in dense and loose sands

In order to determine the stress throughout the pile from each strain gauge, the composite tangent modulus is used to calculate the secant modulus. The secant modulus of the composite pile material, E_s, is found by integrating equation 5-9, and substituting $\sigma = E_s\varepsilon$ to give the relationship in equation 5-10.

$$E_s = 0.5A\varepsilon + B \qquad \textbf{5-10}$$

The secant modulus which has been calculated is used in equation 5-7 to determine the load at each gauge location throughout the pile. The area of the pile must be determined at each strain gauge location in order to establish the axial load. The varying cross section of the CHD piles still produces a problem in the determination of an appropriate diameter. In order to aid in the diameter selection, the pile was split into three sections where changes in pile geometry occurred. The sections corresponds to the pile cap which encases strain gauge 6, the main helical pile body which encases strain gauges 2 to 5 and the pile tip cone where strain gauge 1 is found, (see Figure 3-19).

The pile cap diameter is easily determined due a standard cross sectional area. The diameter of the tip cone can also be determined with reasonable accuracy, leaving only the main helical pile body as a source of variability. The physical presence of grout within the pile is what affects the stress in the pile therefore the diameter of

the main helical pile body is estimated as the average of the core and outer flange diameters. For each of the instrumented piles, Table 5-3 shows the diameters of each of the pile sections.

Table 5-3. Diameters of instrumented piles for use in calculations of load distribution

Location on pile – Strain Gauge No.	Design Diameter (mm)			
	CHD 110	CHD 111	CHD 112	CHD 114
Pile Cap SG 6	50	50	50	50
Main Pile Body SG 2-5	57.4	58.5	57.8	57.2
Tip Cone SG 1	27.2	30.7	30.4	27.6

The calculated average diameters in Table 5-3 can be evaluated by finding the volume of the CHD piles. The piles can be submerged in a container of water and the volume of the displaced water measured. From the displaced water volume, an estimated pile volume of the piles can be determined. By dividing the pile volume by the total length, including the pile cap, an average area and therefore diameter can be calculated for each pile. The diameters obtained through volume analysis (D_v) are compared to the averaged measured full flight diameter (D_f) Table 5-4. The diameter from volumetric analysis D_v show a strong comparison with those measured over the main pile body.

Table 5-4. Volumetric diameter estimation compared to measured averages

Pile	Pile Volume (m^3)	Total Pile Length (mm)	Average Diameter from Volume Analysis, D_v (mm)	Measured Design Diameter, D_f (mm)
110	1.105×10^{-3}	475	54.4	57.4
111	1.09×10^{-3}	475	54.1	58.5
112	1.15×10^{-3}	475	55.5	57.8
114	1.11×10^{-3}	475	55.2	58.2

Before the instrumented aluminium rod was inserted into the cast pile, all strain gauges were zeroed by balancing the Wheatstone bridge arrangement via the

Flyde data acquisition unit. The load required to install the rods into the cast piles was recorded via the Instron and was typically less than 0.5kN. The installation load was only evident during the penetration process and once the rod had reached is final positions and further advancement had stopped, the measured loads dropped to zero. Fluctuations in the output signals from the strain gauges were evident during the installation process of the rod and then for a period of time after installation. These fluctuations were attributed to the bedding in process of the strain gauges which were exposed to varying temperatures during hydration of the grout, along with the loads exerted during installation. Visual observations showed the shrinkage of the grout during hydration to be negligible.

It has been found by Fellenius (2002) that locked in stresses can develop within a pile during the curing process. These locked in stresses can cause what are known as residual loads within an installed pile and although they tend to be more prominent in driven piles they have also been found to occur in bored piles. Ideally, continuous data acquisition of the strain measurements during the curing process of the CHD piles would be carried out to determine any effects residual loads which may occur. However, data acquisition during the entire curing process of the CHD piles was not practical for the model tests and therefore continual measurements of any residual loads were not made. The voltage outputs from the strain gauges were measured during the installation process and then again before load testing took place in order to determine any locked in loads. It was found that there were minor differences between the voltage readings, ensuring any locked in loads in the model piles is negligible.

During the period between the strain-gauged rod installation process and carrying out the load test of the cured pile, a small number of gauges failed and stopped producing information. Despite all efforts to ensure full protection of the strain gauges on the rods, most piles experienced a failure of at least one gauge. The two piles installed in dense sand experiencing a failure of two gauges. The reason for the failures, particularly in a controlled laboratory environment is unknown. It is believed that a short circuit occurred due to loss of insulation around the wires installed in the grout. The very small diameter wire used in the electrical circuit which was necessary due to space limitations had a delicate insulation which may

have been breached once installed in the grout, causing a short circuit. The wires were covered with insulating tape in order to increase the protection upon insertion into the grout. Due to the apparent delicate nature of the wires, it is recommended that this type of wire be avoided for any future use in this application.

In the case of the single gauge failure in pile CHD 112, the axial load at the failure gauge location can be estimated by subtracting the sum of the load measured at the working gauges from the total applied load. Where two gauge sets failed at different levels for piles CHD 110 and CHD 111, it was bit more difficult to distribute the axial loads to the failed gauge locations. Luckily, in both CHD 110 and CHD 111, the gauge failures occurred at two different locations. By looking at the distribution of axial load in one pile, an estimation of the likely distribution of axial load at the failed gauge locations can be made based on the percentage split determined from the sister pile. By using the data from both piles, the axial load distribution is determined for all gauge locations.

The axial distributed load measured through the CHD piles, shown in Figure 5-29, Figure 5-30, Figure 5-31 and Figure 5-32 for selected pile settlements. The axial loads generally increase down the length of the piles. In CHD piles 110 and 111 which were installed in dense sand, the load appears to be distributed across the entire length of the pile. For the CHD installed in loose sand, the axial load was confined to the lower half of the pile length.

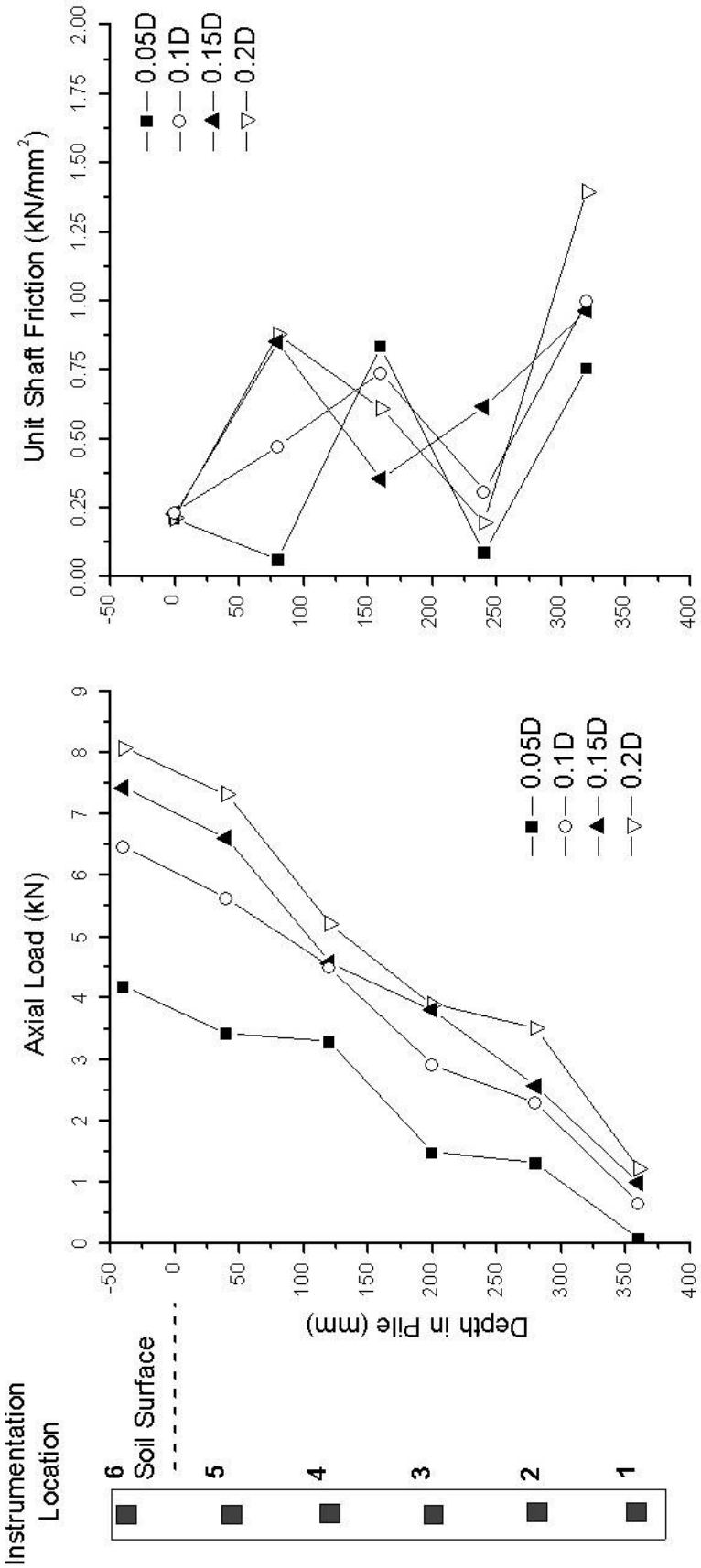

Figure 5-29. Axial load and shaft friction distribution based on instrumentation of CHD 110 (Dense sand) at selected pile settlements

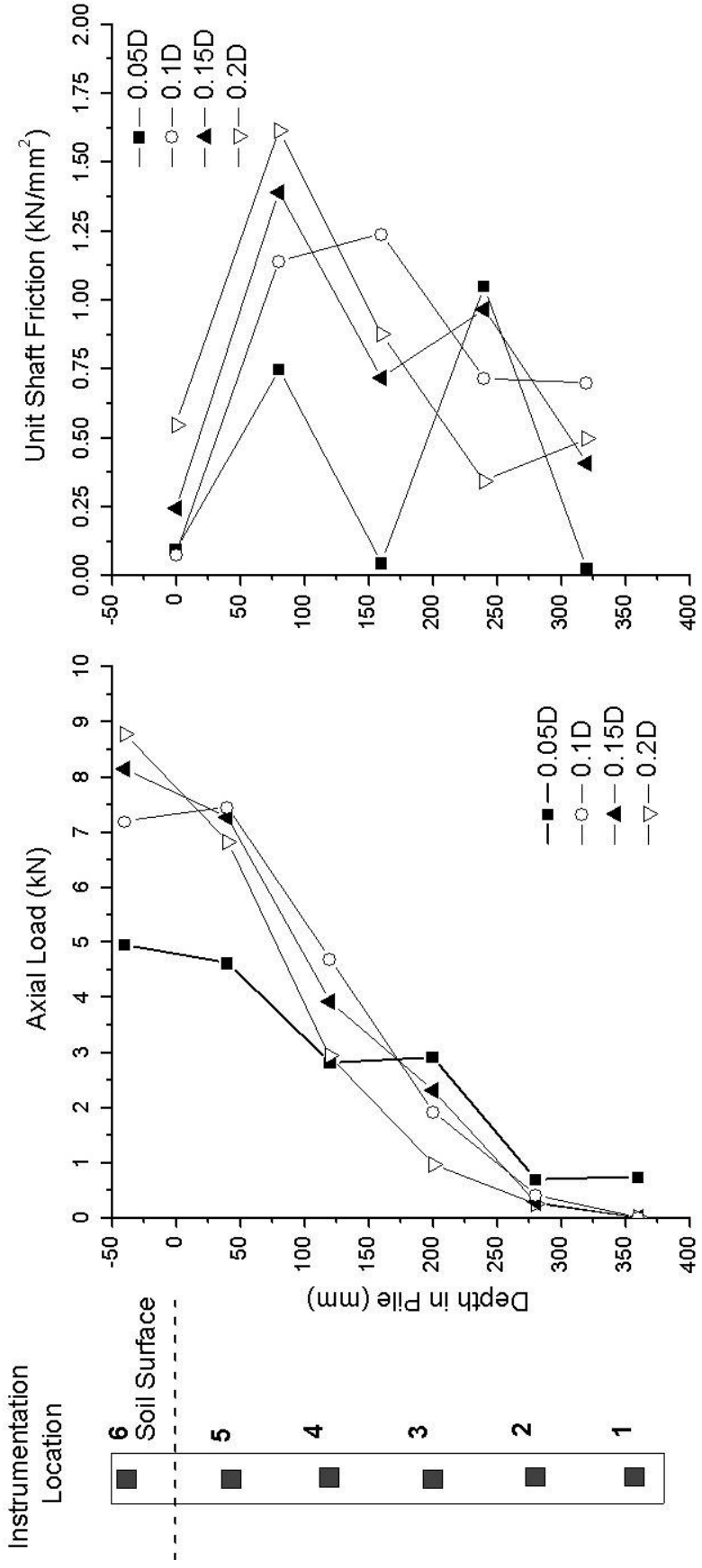

Figure 5-30. Axial load and shaft friction distribution based on instrumentation of CHD 111 (Dense sand) at selected pile settlements

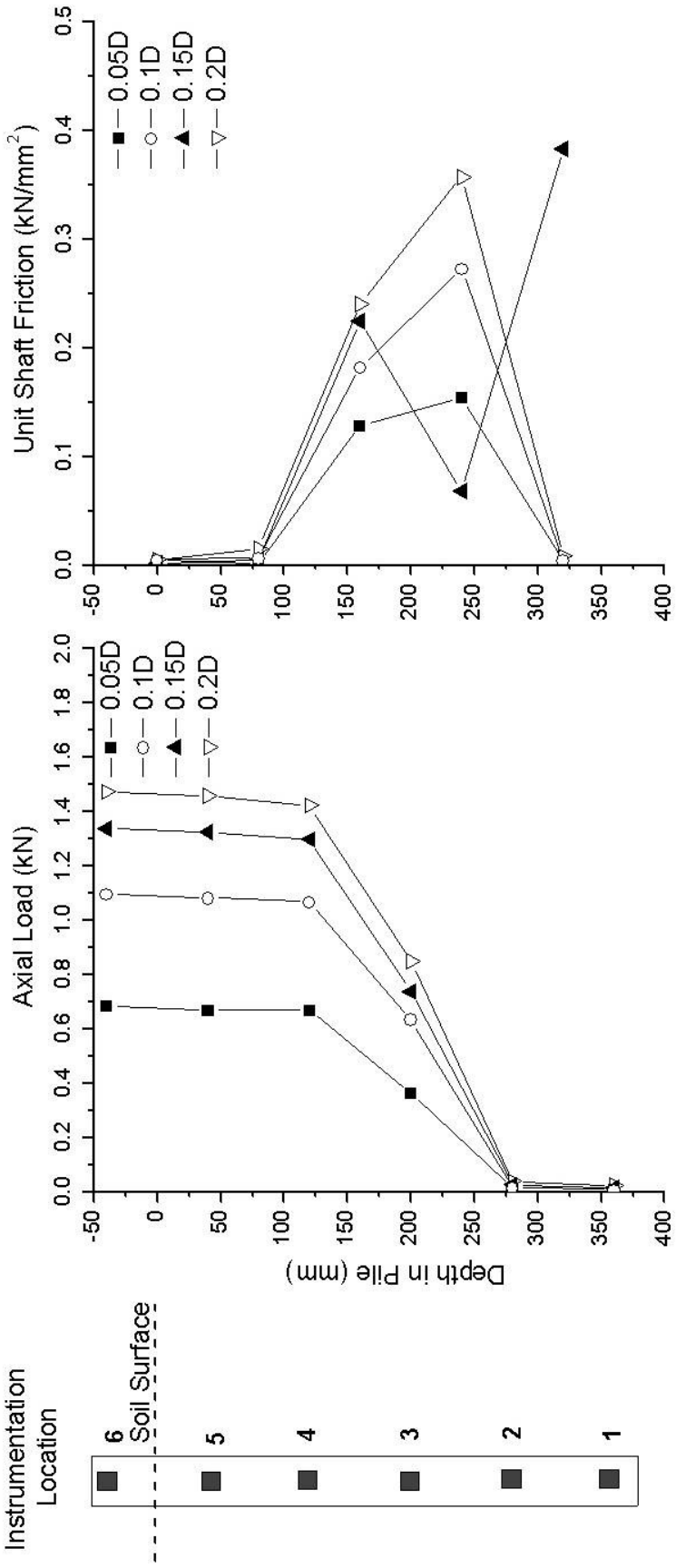

Figure 5-31. Axial load and shaft friction distribution based on instrumentation of CHD 112 (Loose sand) at selected pile settlements

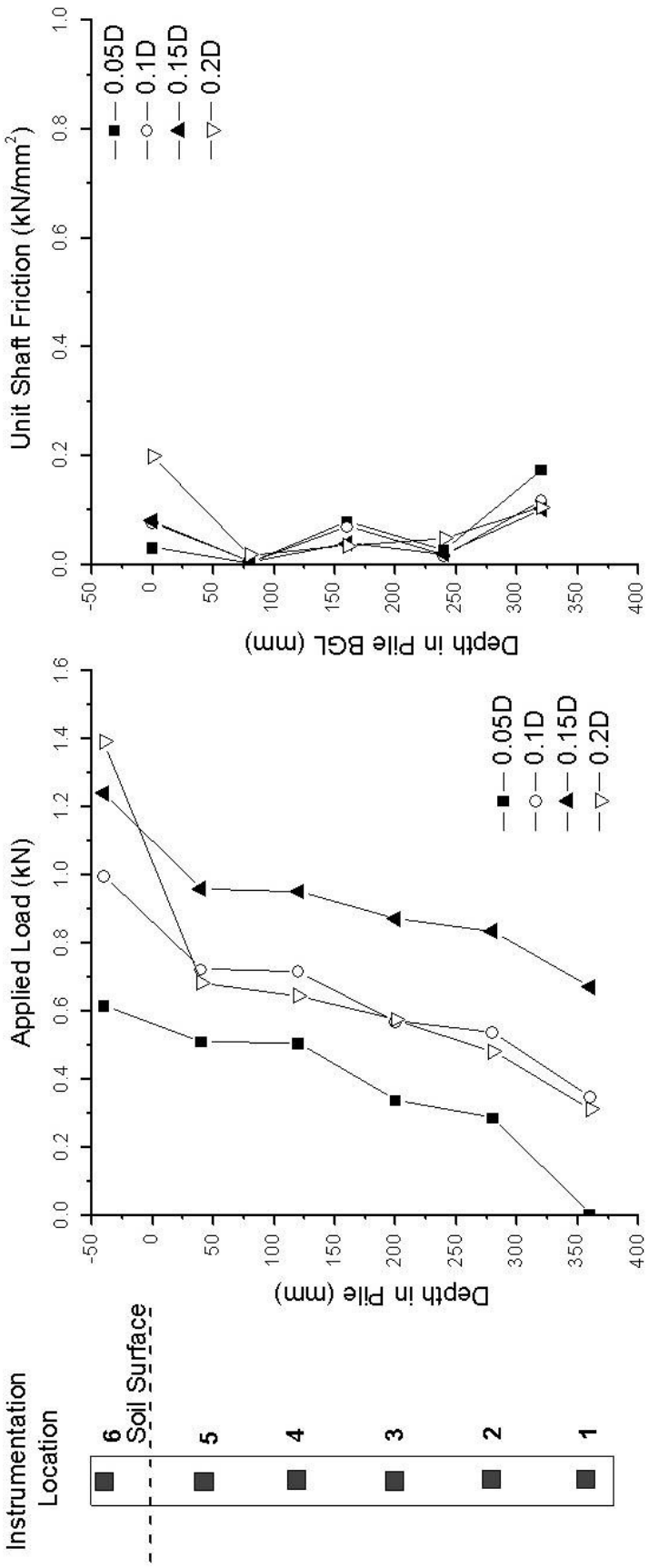

Figure 5-32. Axial load and shaft friction distribution based on instrumentation of CHD 114 (Loose sand) at selected pile settlements

The loads are used to calculate the unit shaft friction over the CHD pile the length. The change in load recorded between each gauge location is divided by the pile circumference around the strain gauge using equation 5-11 to give the unit shaft friction.

$$\tau_s = \frac{\Delta L_{AX}}{\pi D_{AVE}} \qquad \textbf{5-11}$$

Where: τ_S = Unit shaft friction

ΔL_{AX} = Change in axial load between strain gauges

D_{AVE} = Average pile diameter between strain gauges

The unit skin friction is then correlated to a shaft resistance using equation 5-12.

$$Q_S = \frac{\tau_S}{\Delta h} \qquad \textbf{5-12}$$

Where: Δh = Difference in height between strain gauges

The unit skin friction for each pile is also shown in Figure 5-29, Figure 5-30, Figure 5-31 and Figure 5-32. The magnitude of the unit shaft friction is seen to increase along the length of the pile. The piles installed in dense sand show a large contribution of skin friction to capacity over the total pile length whilst the pile installed in loose sand does not have a shaft friction input until a depth of approximately 60mm (1D). The mobilisation of the shaft friction is seen to occur at lower settlements after which load transfer occurs at the tip.

The unit shaft friction determined along the length of the pile can be used to calculate the total capacity produced from the shaft of the CHD piles. The pile diameters determined in Table 5-3 which vary at different locations along the pile length, are used to determine a pile surface area at each gauge location. The calculated surface area can then be multiplied with the unit shaft frictions determined from the strain gauge measurements in Figure 5-29 to Figure 5-33 to

establish the shaft load Q_s at different pile settlements. Using the measured total applied axial load Q_T and axial shaft load Q_S, the base Q_B resistance can be determined. The separated base-shaft is plotted in Figure 5-33 a-b for loose and dense sands.

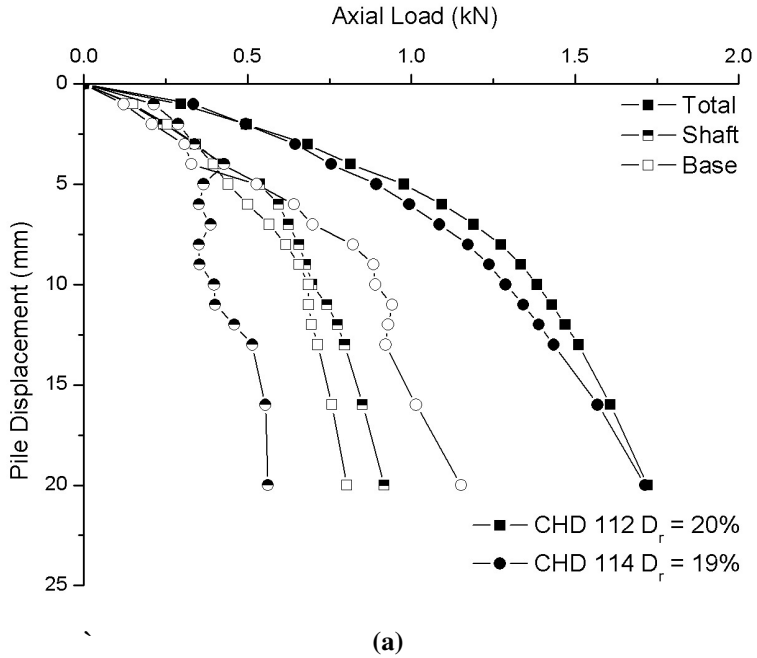

(a)

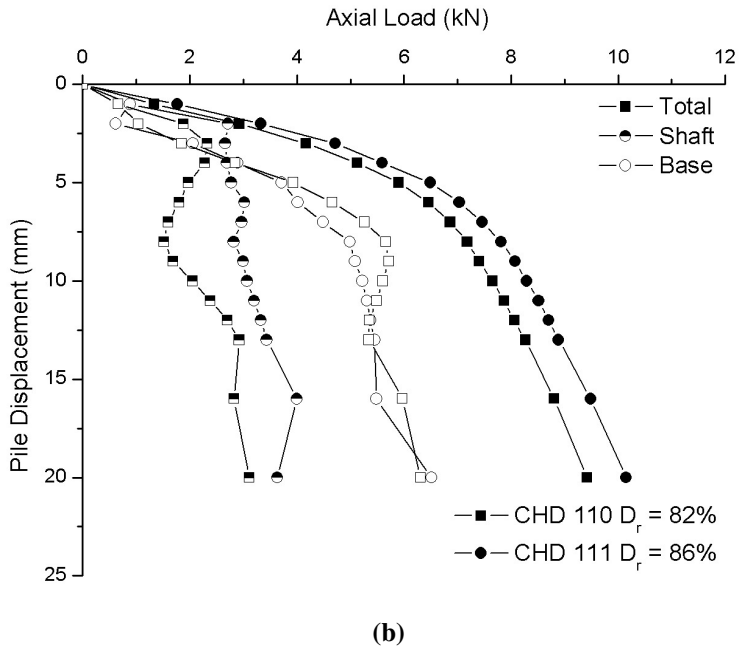

(b)

Figure 5-33. Load contribution from shaft and base for CHD piles in (a) loose and (b) dense sands based on model pile instrumentation

The shaft and base split in ultimate capacity is seen to vary depending on the in-situ soil density. In loose sand, the shaft resistance can be seen to provide 30% to

50% of the ultimate capacity at large settlements i.e. settlements greater than 10% of the pile diameter, 0.1D. For piles installed in dense sand, the shaft resistance provides much of the initial capacity, however as pile settlement increases the base contribution begins to mobilise and the shaft becomes fully mobilised. The shaft capacity for the model CHD pile in dense sand typically contributes 28% to 38% of the ultimate capacity at settlements greater than 0.1D.

The shaft resistance in dense sand accounts for 79% to 82% of the entire pile capacity at settlements less than 0.03D and 49% to 58% in loose sand. The full mobilization of the shaft capacity at a pile settlement of 0.03D is similar to that found for 800mm diameter CFA piles installed in sandy ground conditions carried out by Gavin *et al* (2009), an indication that the CHD pile has similar behaviour to large diameter bored piles.

The greater shaft resistance observed in the loose sand can be explained by looking at the CPT cone resistances recorded at radial locations around the installed CHD pile as shown in Figure 5-13a. The sand density around the pile shaft is found to be up to twice that that found around the base of pile due to the horizontal soil displacement during the installation of the CHD pile. The greater density around the pile shaft will lead to higher shaft capacities.

In the dense sands, the radial density increase due to pile installation is not as significant as in loose sands (Figure 5-13c), and this is reflected in the reduction in the shaft friction contribution to pile capacity.

5.4.2 Instrumented model Pushed and WIP piles load-settlement

The model pushed and WIP piles installed in sand beds prepared at different relative densities were also load tested. During the load testing of series 2 piles, both the total applied load and the base loads were recorded independently. The average shaft resistance was deduced from the difference between the total and base recorded loads, as described in Chapter 3. The load-settlement behaviour is

investigated and compared to that of the CHD piles. Similar to the instrumented CHD piles, both the Pushed and WIP instrumented series 2 piles were 400mm long as opposed to the 300mm used in series 1.

The load-settlement plots for pushed and WIP model piles are shown in Figure 5-34 and Figure 5-35. For the pushed and WIP piles, two piles each were installed in beds prepared at loose, medium dense and dense relative densities. As can be seen, piles installed in similar relative densities appear to have consistent load-settlement response. Slight variations can be attributed to slight different in-situ relative densities between each pile test.

The consistent data for both the pushed and WIP piles allowed average behaviour for total, base and shaft loads to be determined for loose, medium dense and dense sand conditions. Taking average values allowed a quick comparison to the CHD piles without having to handle numerous data sets. The average load-settlement plots for pushed and WIP piles are shown in Figure 5-36 a-c, for loose, medium dense and dense sand.

It can be seen that the WIP piles, particularly in loose to medium dense sands, has a lower bearing capacity and stiffness than the pushed piles. In dense sand, there is very little difference in both capacity and stiffness between pushed and WIP piles.

It is interesting to note that the shaft friction for both pushed and WIP piles are similar, showing that the installation of the pushed pile gives no improvement to the shaft friction resistance. Both pushed and WIP model piles derive up to 90% of the capacity from base resistance.

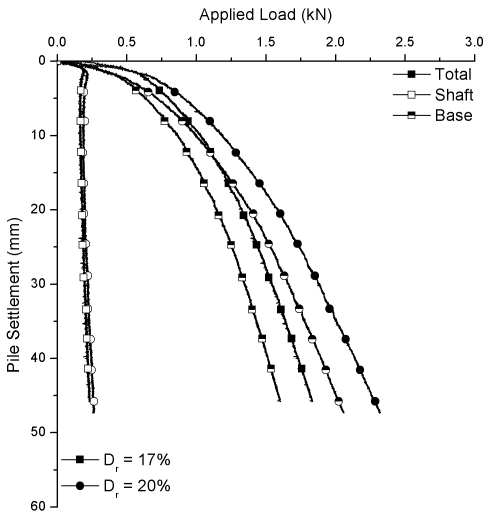

(a)

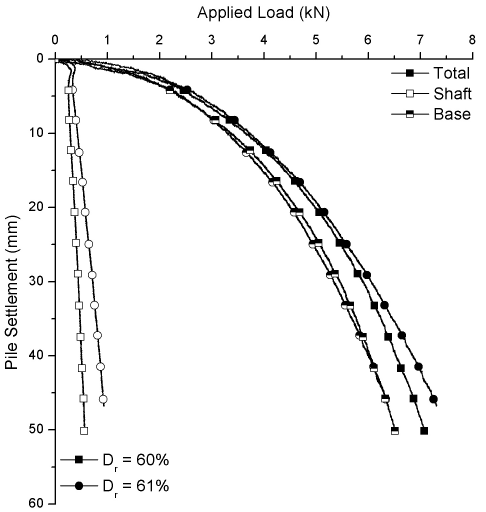

(b)

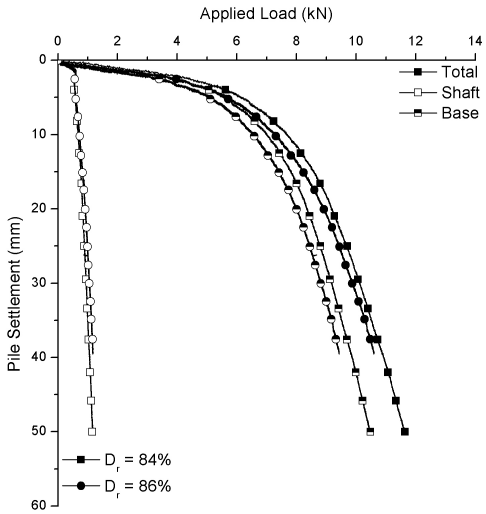

(c)

Figure 5-34. Instrumented load test data for Pushed piles installed in (a) loose, (b) medium dense and (c) dense sand

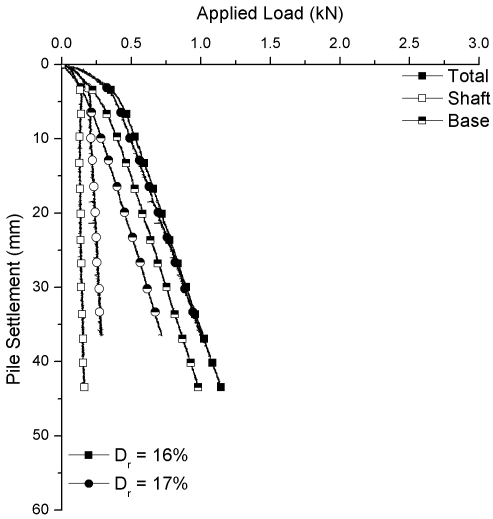

(a)

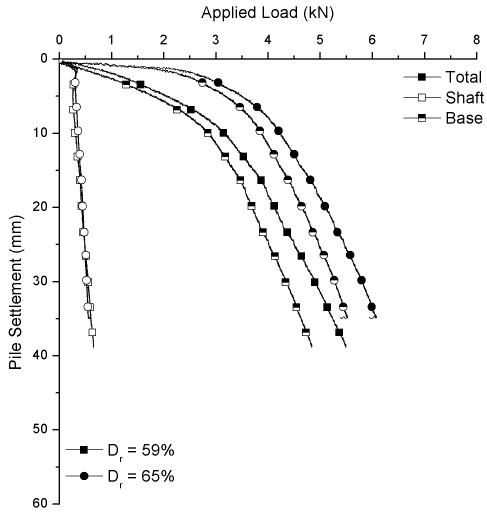

(b)

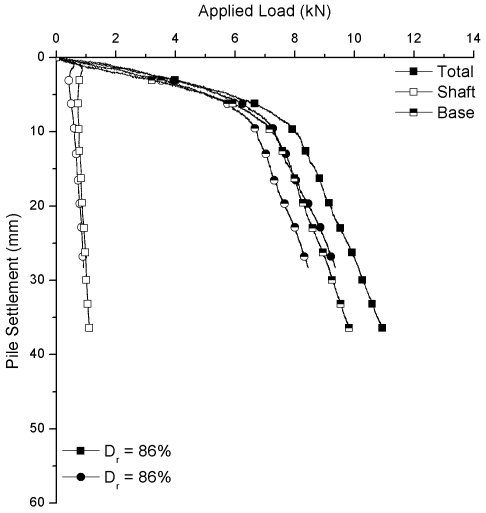

(c)

Figure 5-35. Instrumented load test data for WIP piles installed in (a) loose, (b) medium dense and (c) dense sand

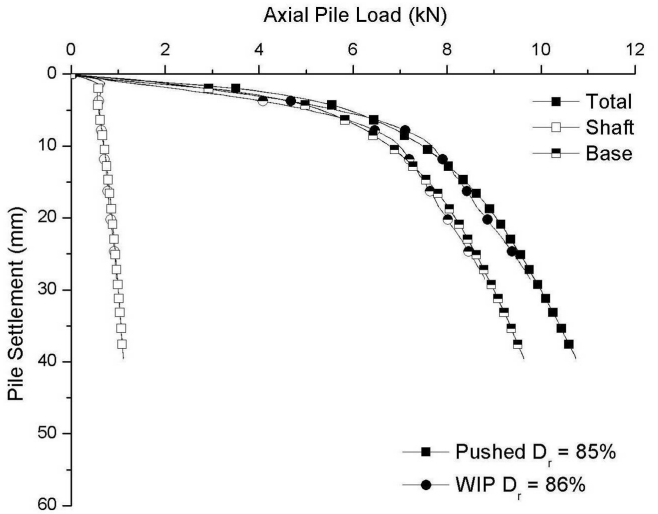

(a)

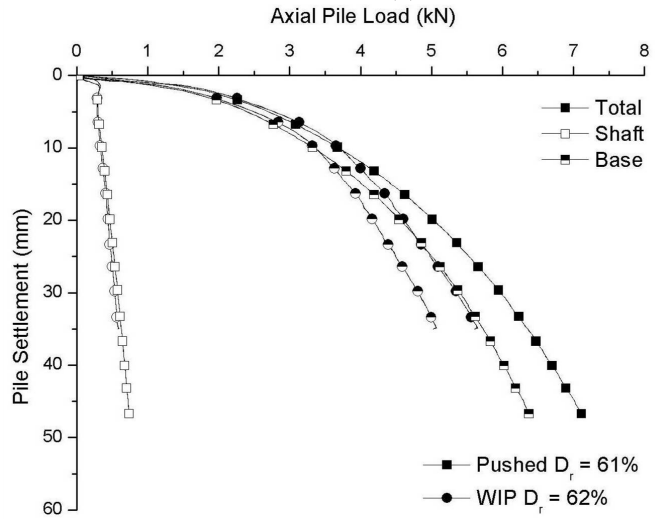

(b)

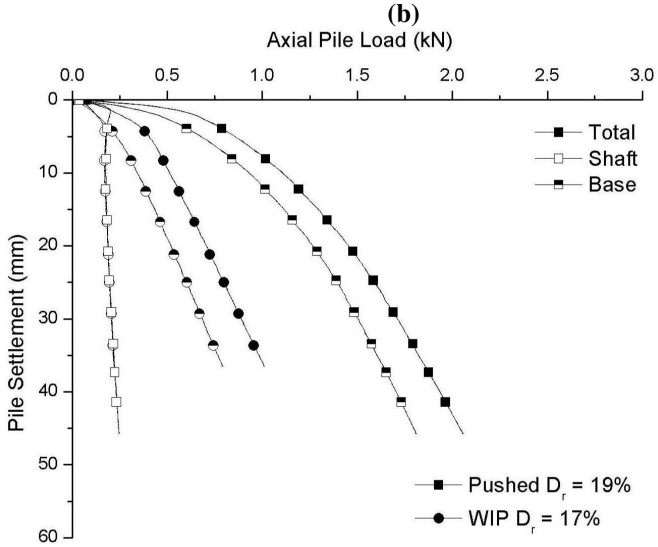

(c)

Figure 5-36. Average Pushed & WIP load-settlement curves for (a) Dense (b) Medium Dense and (c) Loose sands

5.4.3 Defining the model pile capacity

Determination of the load capacity of the pile is important in design as an accurate capacity will allow a more accurate design process to be developed. The definition of the ultimate capacity of a pile is subject to some debate, as has been discussed in Chapter 2.

As discussed in section 2.6.1 a number of definitions of pile capacity are given by Fleming et al (2009), Tomlinson (1994) or Weltman (1980) such as the point at which settlement of the pile increases with no additional applied load (post yield behaviour as shown in Figure 2-23) or when the pile reaches a settlement of 10% of the pile diameter.

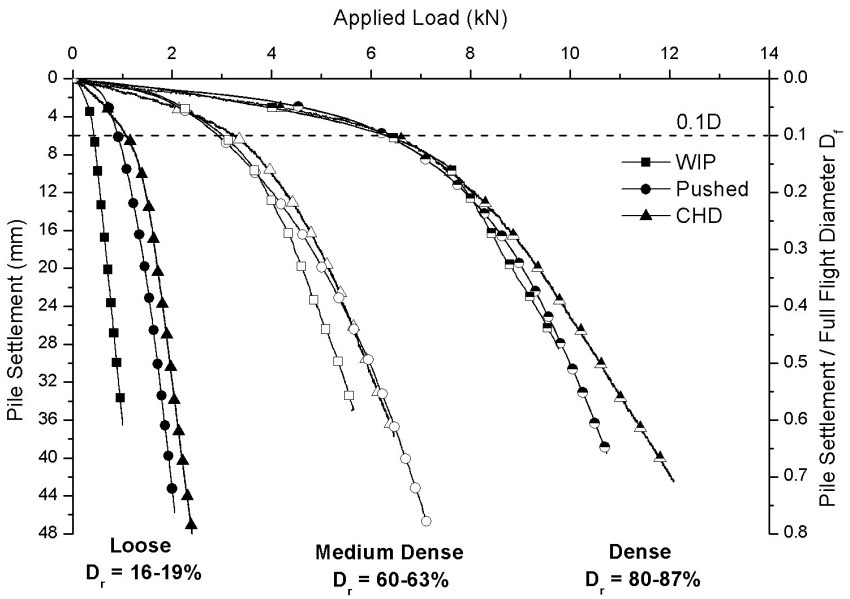

Figure 5-37.Characteristic model pile load-settlement plots for a range of relative densities showing the 0.1D settlement criteria

Implementation of the 10% diameter settlement criteria is known to give conservative estimated capacities, Fleming *et al* (2009). By inspecting the load-settlement curves for model piles, Figure 5-37, it can be seen that a blanket application of the 10% diameter settlement appears to give a pre-yield estimation of the capacity of piles.

The load-settlement curves for the CHD piles in Figure 5-37, do not appear to demonstrate a distinct display of post yield behaviour. The nature of the curves leads to an ambiguous interpretation of the ultimate pile capacity. In order to overcome the ambiguity associated with the selection of this point, utilisation of the intersection of lines method discussed by Fellenius (2006) is used to give a more regimented selection criteria. The process involves drawing two straight lines over the pre-yield and post yield zones on the load-settlement plots. The intersection of these lines dictates the ultimate capacity of the pile. The method can be sensitive to the axis scale on which the data is plotted, in order to eliminate this sensitivity for the determination of model pile ultimate bearing capacities, the axis scale for each pile type remained at constant.

The ultimate pile capacities determined using the intersection of lines for each of the model piles types are shown in Figure 5-38. Compared to the pile capacity determined based on the load at a settlement of 0.1D, the intersection of lines method gives a pile capacity which is on average 7% greater. The ultimate capacity for CHD piles are seen to be similar to those achieved by pushed piles while both are typically greater than WIP piles. The settlements at which these ultimate bearing capacities occur are presented in Figure 5-39. The average settlement at which the ultimate capacity occurs for each pile type is also highlighted on the chart. The assumption that the ultimate capacity is associated at an arbitrary settlement of 0.1D is shown not the case for the model piles, which range of 0.12D to 0.2D for the different installation methods.

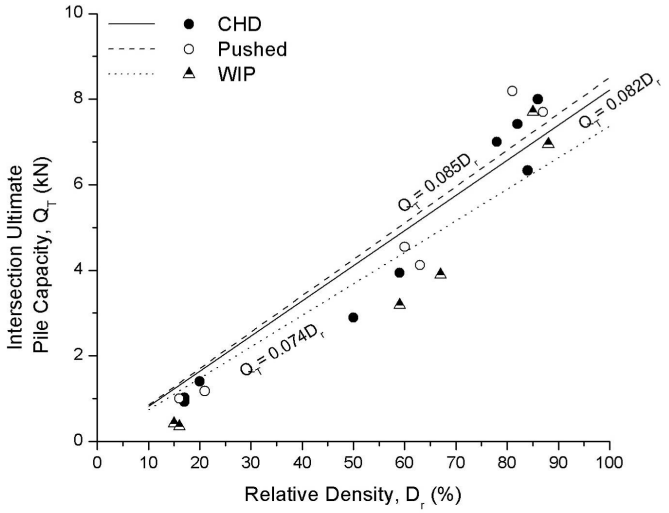

Figure 5-38. Ultimate pile capacities for model piles determined using the intersection of lines procedure from load-settlement curves in Figure 5-37 at different relative densities

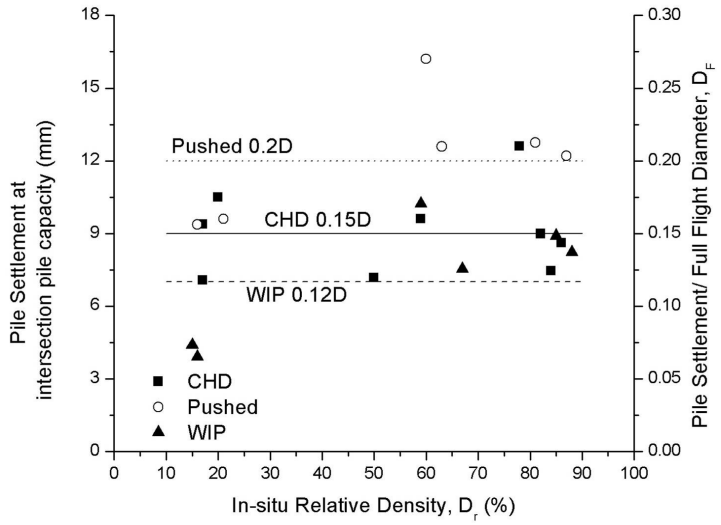

Figure 5-39. Settlements at which the ultimate pile capacity determined through the intersection of lines method occurs for each model pile type

5.5 Model pile stiffness

The load-settlement response of the model piles has been investigated so far in terms of capacity however it should also be reviewed in terms of stiffness. The relative pile-soil stiffness for each of the model piles can be determined by normalising the load settlement data by a common value. For the analysis of the model piles, the load is normalised by the measured load at a settlement equal to

0.2D (12mm). This settlement corresponds to the settlement where the ultimate capacity was found to occur for the pushed piles.

The analysis shows that the CHD piles, in most instances have comparable stiffness to that found in the WIP piles. In some instances the CHD stiffness either tends towards or exceeds the stiffness of the pushed piles however this occurs at large settlements (greater than 0.1D) particularly in loose to medium dense sands. In dense sand, the stiffness of all pile types all display similar characteristics.

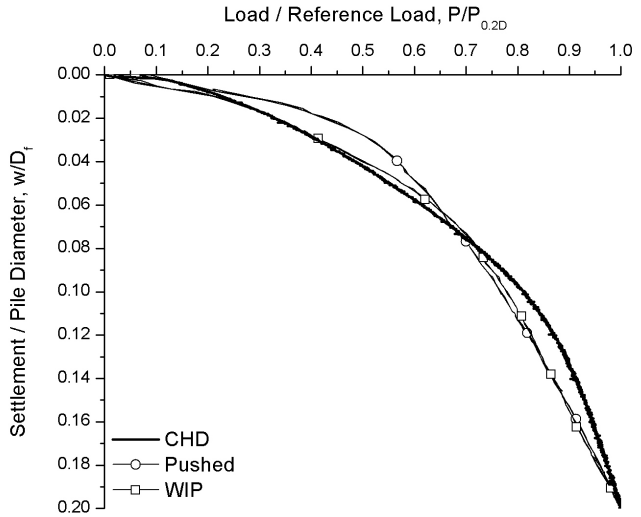

(a)

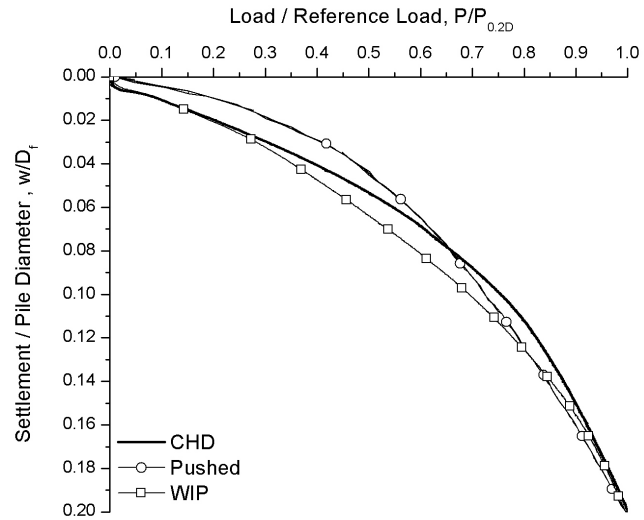

(b)

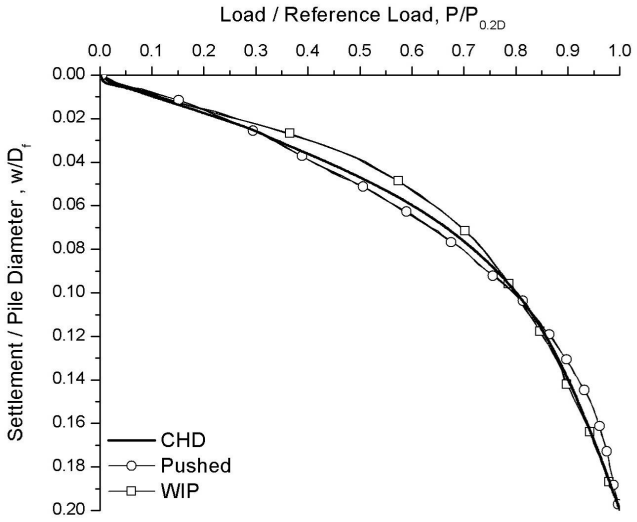

(c)

Figure 5-40. Model pile total pile-soil stiffness plots for (a) loose, (b) medium dense and (c) dense sand

The comparative stiffness of the piles in terms of base and shaft contributions is shown in Figure 5-41 and Figure 5-42. Each pile has been normalised using data readings at a pile settlement equal to 0.2D (12mm). The stiffness of the CHD base compared to both the WIP and Pushed piles is lower in both loose and dense sand beds for settlements less than 0.1D (Figure 5-41). At settlements greater than 0.1D, the stiffness of the CHD pile shows a similar trend to that displayed by the WIP and Pushed piles.

The stiffness of the shaft shown in Figure 5-42 shows that the CHD pile stiffness when installed in loose sand has similar characteristics to Pushed and WIP piles. In dense sand however, the CHD stiffness is notably lower than both Pushed and WIP piles at all piles settlements.

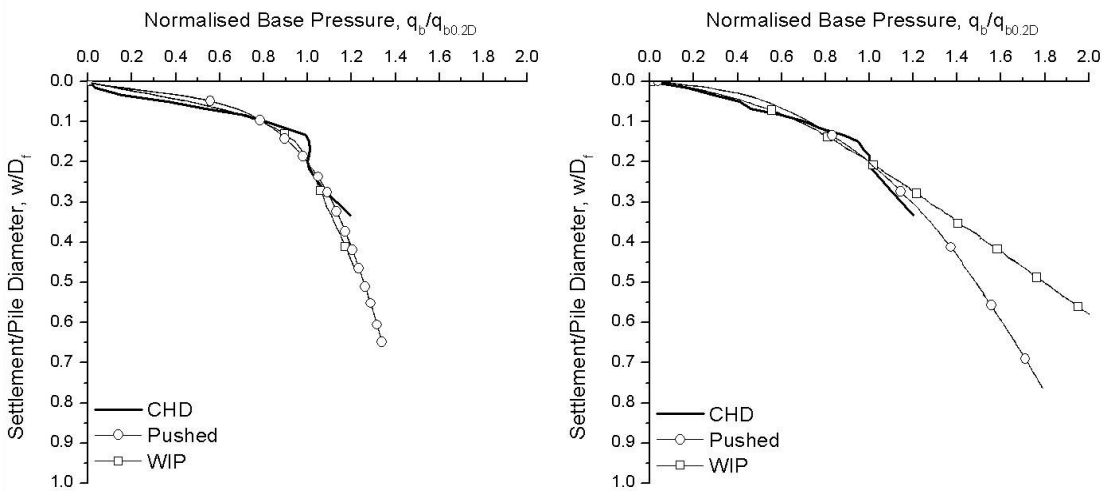

Figure 5-41. Model pile normalised base stiffness for piles installed in (a) loose and (b) dense sand

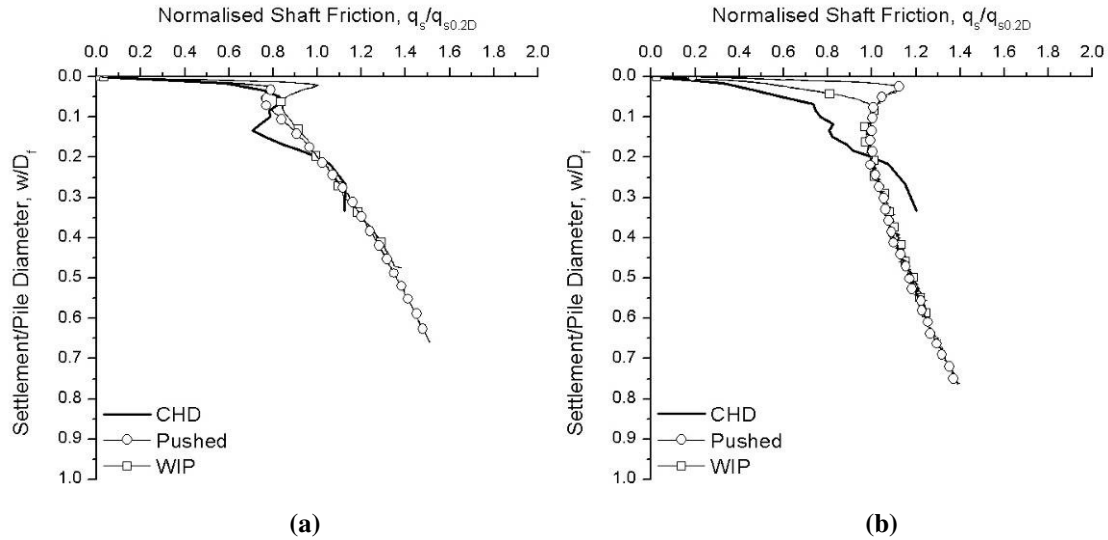

Figure 5-42. Shaft stiffness variation between model pile types installed in (a) loose and (b) dense sand

The pile-soil stiffness is utilised in settlement prediction methods such as the hyperbolic method as described in section 2.6. The soil base modulus E_b of the piles can be taken as a quarter of the ultimate base load Azizi (2000), which has already been determined in for each model pile (section 5.4). The base modulus values determined for the model piles are shown in Figure 5-43. The base modulus values determined for the CHD piles are seen to be predominantly lower than the range of values determined from Pushed and WIP piles, particularly when the soil density increases.

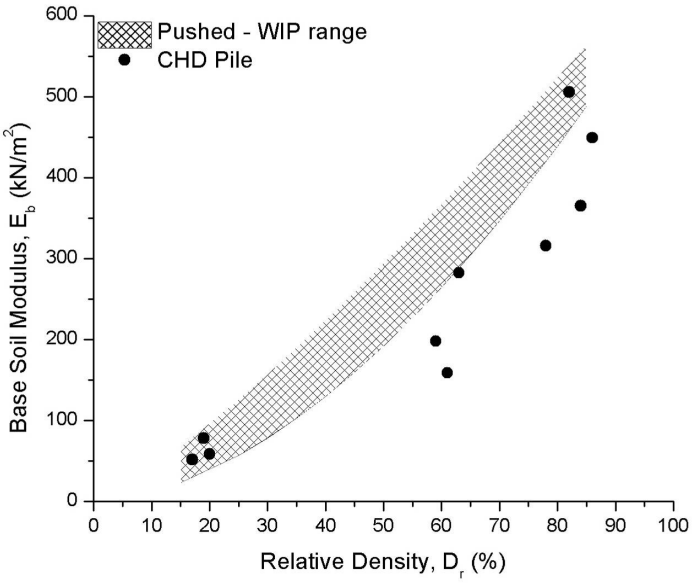

Figure 5-43. Base soil modulus value determined for CHD piles compared to the range of base soil modulus values determined for model Pushed and WIP piles

5.6 Pile design parameters based on instrumented data

The ultimate capacities for each of the model piles have been determined through load testing. With the use of pile instrumentation the base and shaft components are also known. The ultimate capacity determined from the load tests is utilised in the design approaches discussed in Chapter 2 in order to refine the design procedure, making it more accurate. The base-shaft capacity ratio determined from the instrumented model CHD piles is applied to the non-instrumented CHD piles in order to give an estimation of the typical base-shaft capacities for use in the pile design procedure analysis, as shown in Figure 5-44. The typical shaft contribution to the ultimate pile capacity is found to be 38% at a displacement equal to those determined in the previous section.

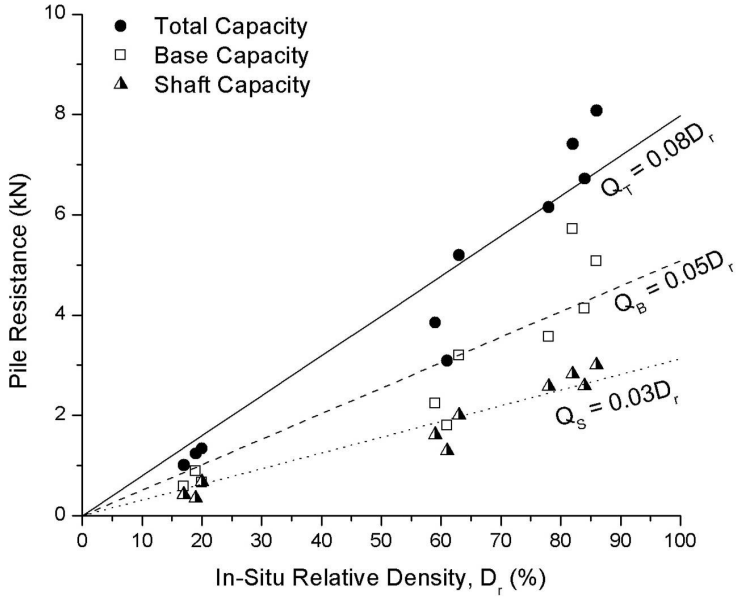

Figure 5-44. Model CHD piles shaft-base contribution to ultimate pile capacity variation with initial relative density

The procedure used in the design of piles is determined by the site investigation methods carried out as has been discussed in Chapter 2. Typically, an effective stress approach utilises soil parameters derived from the site investigation process such as an SPT investigation. Alternatively, the pile design capacity can be determined using relationships with CPT cone resistance. Both design approaches have parameters which are dependent on pile installation and the aim of this section will be to determine these parameters for use in CHD piles. For all back calculations carried out, the design diameter of the CHD pile is taken as the full flight diameter, 60mm in model scale.

5.6.1 Effective Stress design approach

The effective stress design approach is a basic model which is widely used in current design practice particularly for CHD piles (see Chapter 2). For pile design using an effective stress approach (equations 2-2 and 2-5), the unknown parameters are the bearing capacity factor, N_q and the coefficient of earth lateral earth pressure, k.

$$Q_T = Q_S + Q_B = q_s A_s + q_b A_b \qquad \textbf{2-1}$$

Where $q_b = N_q \sigma_v^{'}$ **2-5**

$q_S = k\sigma_v^{'} \tan\delta$ **2-2**

During the back figuring of design parameters from the model piles, the effects of the low overburden pressure are taken into account by using appropriate friction angles determined from shear box testing at low effective stress (section 3.4).

The end bearing load determined through the model tests is used to determine a back figured end bearing factor for each pile type. The end bearing loads are converted to stress by dividing the load by the base surface area. The base surface area for the pushed and wished-in-place piles can easily be defined due to their circular nature. The base surface area of the CHD is somewhat more complex to define due to the conical shape produced during installation. On the pre-cast model piles with a diameter equal to the outer flight diameter of the CHD, the end bearing surface area equates to 2827mm^2. Measurements of the model CHD cone shows a typical end bearing surface area of 3051mm^2, 8% greater than the pre-cast piles. Although the conical shape of the CHD pile base gives a slightly large surface area than found on a typical precast pile, the maximum base diameter equals the outer flight diameter D_f. As such the, D_f is utilised in the determination of the end bearing pressure in order to calculate the capacity factor N_q.

The end bearing values calculated for all model piles are compared to those suggested by Berezantzev *et al* (1961) in Figure 5-45. The back figured bearing capacity factors are plotted against the peak angle of friction for sand-sand shear determined from shear box tests in section 3.4.

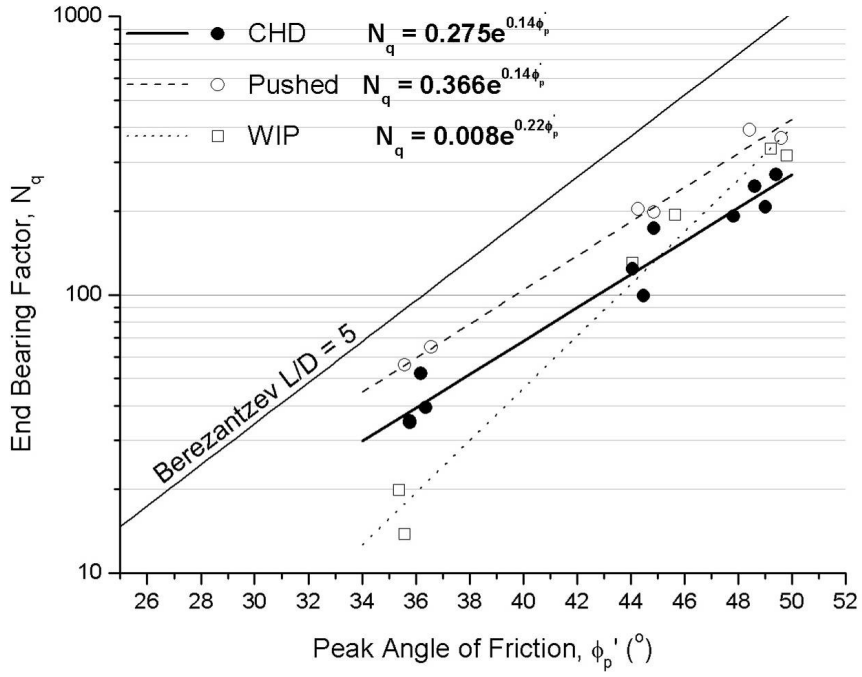

Figure 5-45. Model pile end bearing capacity factor variation with peak angle of friction for the initial test bed sand density compared to Berezantzev et al, 1961 values

The end bearing factors back-figured from model tests show that the values suggested by Berezantzev appear to give an over-estimation. The pushed piles give the closest correlation to the suggested N_q values however they are still typically half the value of those suggested by Berezantzev.

The WIP piles show there is a significant over-estimation of the Berezantzev end bearing capacity factors in loose sand. As the sand density increases, the WIP end bearing factors tend towards those derived for pushed piles. The Berezantzev capacity factors were determined through model testing of driven piles in fine, dense sand. The capacity factors utilise data from driven pile tests and states how the accumulation of compacted soil below the pile base will affect the failure conditions of the soil during pile loading. Compacted soil does not accumulate below the WIP pile and as such they are likely to have a different failure mechanism than what is beneath the pushed or driven piles, leading to different values than those suggested by Berezantzev. Knappett and Madabhushi (2008) have also found the Berezantzev base capacity factors to over estimate by as much as 2 for non-displacement piles.

The CHD pile shows bearing capacity factors which lie between the pushed and WIP piles at low relative densities. In general, the end bearing capacity factor derived for CHD piles are up to a fifth of those suggested by Berezantzev. For increased relative densities, the CHD bearing capacity factor reduced to lower than those suggested for pushed and WIP piles. The variations in the back-figured end bearing capacity factors for the CHD piles follow similar behaviour to those found in the research of shape effects on the bearing capacity of foundations. Research into shallow circular foundations for offshore structures has investigated the effects of the conical shape on the bearing capacity compared to flat plates. It has been found that the bearing capacity is affected by the cone angle and soil relative density, Cassidy and Houlsby (2002), White *et al* (2008). Although this research was carried out in shallow foundations, the similarities witnessed in the bearing capacity results of the CHD suggest that the cone shape of the pile tip likely to causes variations in the bearing capacity of the pile.

Using the pile shaft friction determined from the pile tests, the coefficient of earth pressure, k, is found using equation 2-2, using the initial soil parameters for each test bed. The $\tan\delta$ term is taken as the peak soil-soil interface friction angle for CHD piles and the peak soil-pile interface friction angle of both pushed and WIP piles, all of which were determined through shear box testing in section 3.4.

The variation of k with relative density for each pile type is plotted in Figure 5-46. The earth pressure coefficient can be seen to vary not only per pile type but also with relative density. Some current design procedures, such as those discussed by Fleming *et al* (2009), suggest a single value of k depending on the pile installation method. Typically an assumed k of 1.2 is used for driven piles while 0.7-0.9 can be used for bored piles as discussed in Chapter 2. This blanket application of earth pressure coefficient values will clearly not provide accurate pile designs since k will vary with the initial relative density of the sand test bed.

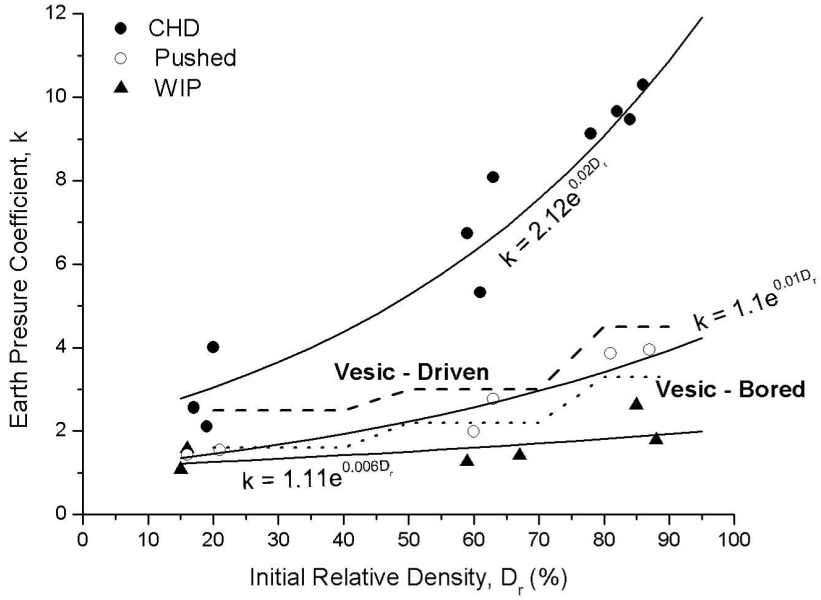

Figure 5-46. Variation of model k values with relative density for each pile installation method showing values suggested by Vesic (1964)

Previous research into the determination of earth pressure coefficient values by Vesic (1964), Meyerhof (1976) and Kulhawy (1964) have shown the relationship between k and the in-situ angle of internal friction. The suggested *k* values by Vesic (1964) are compared to the back figured model values in Figure 5-46. It can be seen that the model pushed and WIP *k* values show similar characteristics to the Vesic values, while CHD values are seen to be up to twice as much as the driven piles.

The model earth pressure coefficients variation with the peak angle of internal friction is compared to those suggested by Meyerhof (1976) for Driven and Bored piles in Figure 5-47. The back figured *k* values for the model pushed and CHD piles display similar trends to those suggested for driven piles. Both pushed and CHD *k* values show increases of up to twice as much compared to the Meyerhof relationship at lower friction angles. In dense sands where the friction angles are greater, the CHD *k* values tend towards those suggested by Meyerhof for driven piles. The WIP piles are shown to have little variation of the *k* value regardless of in-situ friction angle. What can be seen in Figure 5-47 is that the piles to tend towards those suggest by Meyerhof (1976) for driven piles in loose soils while in dense soils, the *k* values are seen to be lower the Meyerhof bored piles.

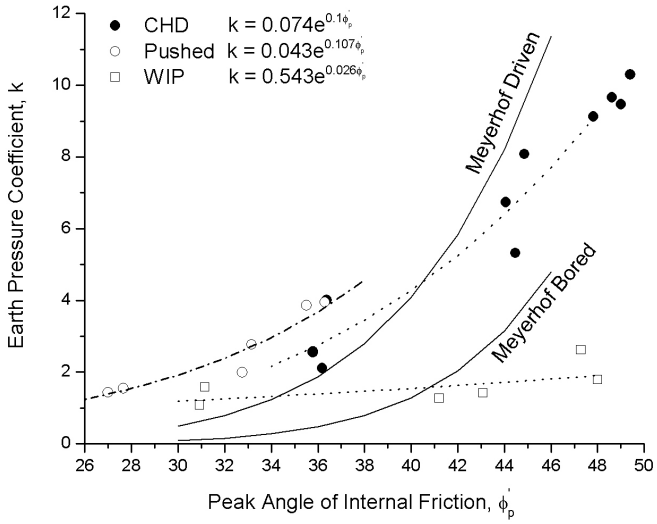

Figure 5-47. Variation of model pile k determined from initial soil properties with the peak angle of friction in relation to those determined by Meyerhof (1976)

The *k* values determined in Figure 5-47 were based on the initial soil properties measured for each test. These *k* values mask the effects of soil disturbance experienced during the pile installation. Using the information determined in Figure 5-23 regarding the relative density change around the installed CHD pile, a *k* value can be determined based on the disturbed soil properties. The *k* value determined from disturbed soil properties are compared to those determined from initial soil properties in Figure 5-48. It is clear that when the effects of pile installation disturbance to the soil conditions are taken into consideration the CHD *k* values tend to larger values suggested for driven piles at low angles of friction. When the angle of friction increases, the CHD *k* values tends more to the values suggested for bored piles.

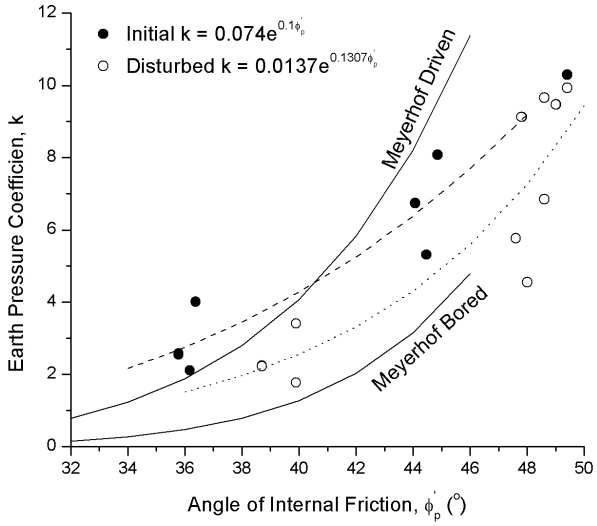

Figure 5-48. Earth pressure coefficient values for model CHD piles determined from initial and disturbed soil property variation with angle of internal friction compared to Meyerhof (1976) relationships for driven and bored piles

Determination of the earth pressure coefficient can also be related to the in-situ earth pressure coefficient K_o through the relationship proposed by Mayne and Kulhawy (1982b) shown in equations 2-3 and 2-4, although the model piles are all installed in sand which is normally consolidated. A range of typical ratios of k/K_0 for different pile installation techniques are given by (Tomlinson, 1994) based on research carried out by Kulhawy (1964). These limiting factors are compared to the range of factors determined for the model piles (Figure 5-49).

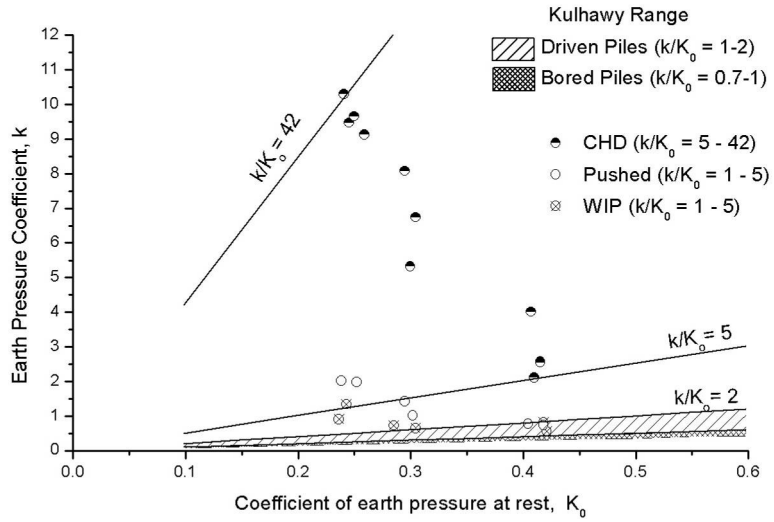

Figure 5-49. Variation of k with the sand bed K_0 values for model piles compared to those suggested by Kulhawy (1984) for Driven and Bored piles

The k/K_0 values determined for pushed and WIP piles range from 2-5. These are up to five times greater than as those suggested by Kulhawy (1984), particularly at greater soil densities. The k/K_0 ratio range for CHD piles is seen to fall between 5 and 42, significantly higher than for alternative piles.

The determination of the earth pressure coefficient from model tests show that the CHD produces up to four times the values determined for driven piles, suggesting that the CHD pile develops far greater shaft resistance compared to pushed and WIP piles. The large increase of k with relation to the in-situ earth pressure coefficient suggests that the installation of the CHD causes significant densification of the in-situ soil conditions, leading to increased developed shaft resistance. It is also seen that the selection of the k value will vary with the in-situ relative density.

5.6.2 CPT Design approach

The cone penetration design method utilises the cone resistance of the in-situ soil conditions to determine the ultimate capacity of an installed pile. A number of design methods exist which are primarily linked to the design of off-shore driven piles however, Bustamante & Gianeselli (1982) produced a design approach which is used for on-shore piles. The Bustamante & Gianeselli (1982) method can accommodate the design of wide range of pile installation methods but it is one of the few methods which specifically account for the design of screw displacement piles.

The end bearing coefficient k_c as defined in equation 2-17 is determined for each of the model piles. The equivalent average cone resistance is calculated from the in-situ CPT cone resistance, in the model scenario this equates to the CPT carried out at a distance of 3.3D, which are referred to as the undisturbed values. The model tests also have the advantage of having CPT cone resistance values which take into account the effects of pile installation. This cone resistance is taken at a distance of 1D away from the installed pile and is referred to as the disturbed

values. For calculation of the pile capacity, the undisturbed cone resistance are used.

$$q_B = k_c q_{ca} \qquad \textbf{2-17}$$

The end bearing capacity factors for the model piles are shown in Figure 5-50. Also highlighted is the range suggested by Bustamante and Gianeselli (1993) for auger displacement piles. The values for CHD piles are seen to be typically greater than those suggested, particularly in loose soils. However, at increased densities, the values tend towards the suggested range. This compliments what was found from the analysis of the field data where piles in medium dense and dense sands had a more accurate design capacity than those installed in loose.

The CHD end bearing coefficients are consistently seen to be lower than those calculated for both the pushed and WIP piles. The k_c values determined for pushed and WIP piles initially appear to be excessively large compared to suggested typical values of 0.4-0.5 Bustamante and Gianeselli (1982), however, Schneider *et al* (2010) and Xu *et al* (2008) show that the range of k_c values for driven piles can range from as little as 0.4 to as high as 1.3. The values recorded from the current model tests lie within this suggested range and therefore appear to be acceptable representations of the k_c for each pile type.

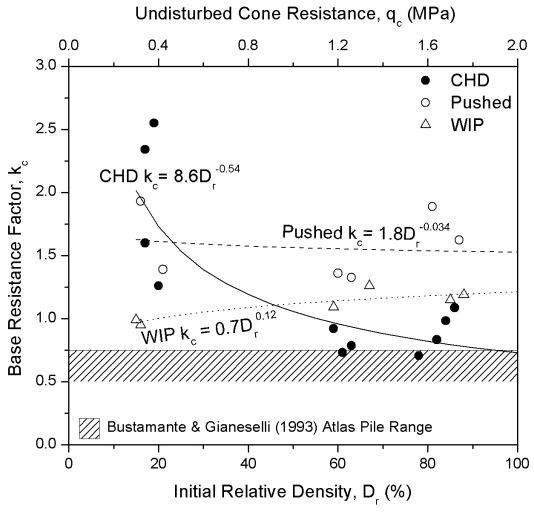

Figure 5-50. Model end bearing capacity factors determined from initial soil properties compared to suggested auger displacement range from (Bustamante and Gianeselli, 1993) for an Atlas piles

The base resistance factors in Figure 5-50 have been determined using the initial cone resistance. The base resistance can also be determined using the disturbed cone resistances measured around the installed CHD piles. The base resistance values determined from the disturbed cone resistances are compared to those determined using initial cone resistances in Figure 5-51.

The back figured k_c values determined in Figure 5-50 using the undisturbed cone resistances suggest pile end bearing pressures which are greater than the CPT cone resistances. Although this is unusual, the back figured base resistance factor using the disturbed cone resistances show a trend towards a value of 1.0, Figure 5-51. The apparent high k_c values suggested, particularly at low relative densities, therefore take into consideration the densification and therefore increase in CPT cone resistance that the CHD pile installation causes.

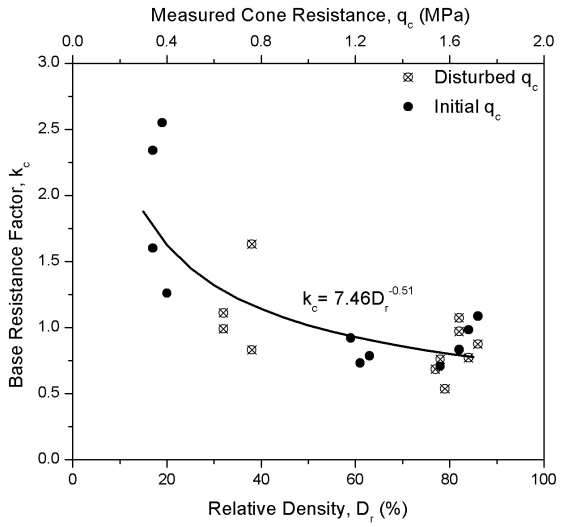

Figure 5-51. Comparison of base resistance factors determined using initial and disturbed sand properties for model CHD piles

The determination of the shaft friction developed in the pile is estimated using a friction coefficient α as defined by Bustamante and Gianesilli in equation 2-18. The friction coefficients for the model piles, Figure 5-52, are calculated using the average cone resistance q_c over the pile length. The range suggested by Bustamante and Gianesilli (1982) is based on the in-situ CPT cone resistance. Typically, a cone resistance of less than 5MPa would suggest loose soil and the application of a friction coefficient of 60 would be used. For cone resistances

greater than 5MPa, indicating medium dense sand, a friction coefficient of 100 would be applied. Since the model scale CPT cone resistances are lower than those found in the field, the range of 60-100 is used as a guide as to the actual friction coefficients that should be expected. It can be seen that for the pushed and WIP piles, the back figured coefficients increase with relative density, as per the field values, indicating that similar the model values follow a similar trend to field values.

Both the Pushed and WIP piles coefficients fall within the expected range of coefficient values, however the CHD values are consistently much lower. This can be attributed to the greater contribution that shaft friction displays in the pile method.

$$Q_s = \frac{q_c}{\alpha} \qquad \textbf{2-18}$$

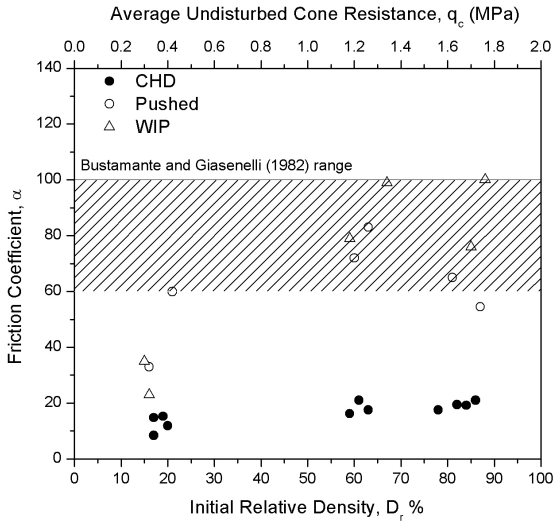

Figure 5-52. Model pile friction coefficients determined from undisturbed soil properties compared to the range of values based on those suggested by Bustamante & Gianeselli (1982)

The comparatively low friction coefficients determined for the CHD piles are investigated further by comparing the unit shaft friction q_s with unit shaft friction limits for auger displacement piles determined by Bustamante and Gianeselli (1993) in Figure 5-53. The design curves suggested by Bustamante and Gianeselli (1993) are applicable for different average cone resistance from initial

measurements but are known to be conservative in nature Bustamante and Gianeselli (1998).

It can be seen that the unit shaft friction of the model CHD piles typically tends to values greater than the suggested values for auger displacement piles by Bustamante and Gianeselli (1998). The characteristic unit shaft friction readings measured for CHD piles correspond to a greater average cone resistance.

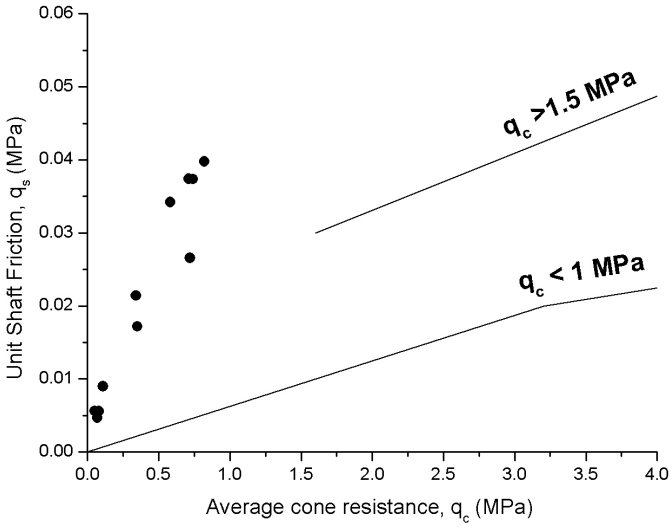

Figure 5-53. Model CHD unit shaft friction compared to correlations with those suggested for cast-in-place screw piles in sand by (Bustamante and Gianeselli, 1993) plotted against the average initial cone resistance along pile shaft

5.7 CHD pile capacity in relation to installation torque

The ability to determine the pile capacity of an installed pile during the installation process is something that could potentially provide an instant indication of the quality of the pile before any load testing has taken place. Research carried out on auger displacement piles, such as that done by Van Impe (1988), utilises the installation parameters to determine the specific energy required to install the pile. It has been discussed by Baxter *et al* (2006) that the specific energy method is not intended to determine the pile capacity and is purely used as a comparison of the efficiency between bored pile installation methods. The specific energy method requires a number of different parameters such as the vertical thrust, penetration speed, revolutions, installation torque and also the

installation bore diameter. Typically, the vertical thrust required to install a CHD pile is not recorded from drilling rig logging instrumentation. The installation bore diameter can also be debatable. As an alternative to the specific energy, the installation torque can be utilised to determine the bearing capacity of the pile, something that is suggested by Bustamante and Gianeselli (1998). Looking at the recorded installation torque from the model tests in Figure 5-54, it can be seen that there is a clear relationship between the in-situ relative density and the required installation torque.

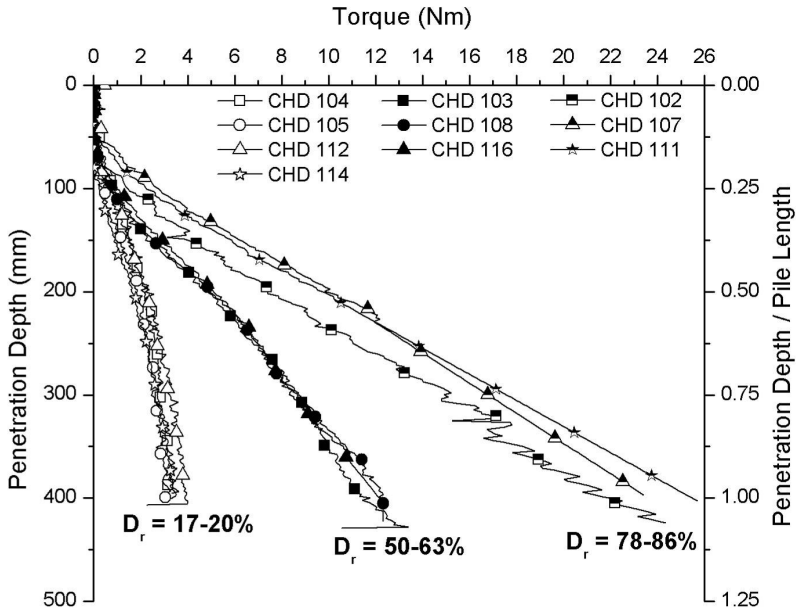

Figure 5-54. Installation torque variation with depth for model CHD piles constructed at different relative densities

For each CHD pile the torque recorded during the installation increases linearly with penetration depth and the magnitude of the required torque at a specific penetration depth increases with relative density of the sand in a similar fashion to those recorded for CFA piles found by Kenny *et al* (2003). The research by Kenny *et al* (2003) focused on optimising the installation torque to enable sound pile construction, but a relationship between installation torque and ultimate pile capacity was not discussed.

The use of torque as a method of predicting pile capacity is not commonly used in capacity design processes for bored or displacement piles, however it is used extensively for the installation of helical screw piles. Helical screw piles generally consist of a tubular shaft with a small number typically 1-3, helical plates along

the shaft length. The helical plates are typically around three times the diameter of the tubular shaft. The pile is installed in the ground using both rotation and vertical thrust in a similar manner as the CHD drilling auger. Hoyt and Clemence (1989) proposed the relationship between the installation torque and pile capacity using the relationship in equation 5-13.

$$Q_T = K_T T \qquad \textbf{5-13}$$

Where Q_T = ultimate axial pile capacity (kN)

K_T = torque correlation factor (m^{-1})

T = Applied torque (kNm)

Extensive research has been carried out in order to determine appropriate torque correlation factors based on physical pile dimensions and in-situ ground conditions by a number of authors including Perko (2009) and Tsuha and Aoki (2010). This research however, relates to helical screw pile performance, therefore the design parameters for CHD piles are expected to be different. The CHD data can be applied to equation 5-13 in order to obtain suitable torque correlation factors.

The average installation torque over the penetration depth is used in equation 5-13 along with the measured ultimate pile capacity. The total, base and shaft capacities are compared to the installation torque in Figure 5-55. The base capacity is compared to the installation torque taken at the pile base, in the case of the model CHD piles this is at a depth of 400mm. The shaft capacity is compared to the average installation torque. The average installation torque is determined from the linear portions of the plots displayed in Figure 5-54 which corresponds to a depth of between 100mm and 400mm for the model CHD piles. The installation torque is negligible until the CHD auger has penetrated the sand to a depth of typically 100mm (0.25L, 1.67D). The total pile capacity is compared to the average torque along the length of the installed pile. It can be seen that there is a linear relationship between the required installation torque and the component parts of the pile capacity.

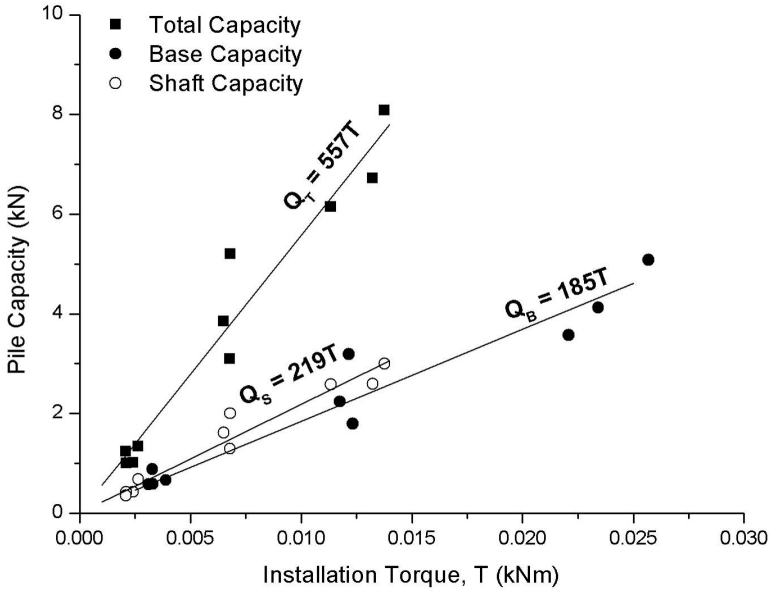

Figure 5-55. Relationship between the average installation torque and total, shaft and base capacities

The average torque varies linearly with the ultimate pile capacity giving an average torque correlation factor of 557 for Q_T, 185 for Q_B and 219 for Q_S. These compare to the range of 47-304 for model helical pile anchors for Q_T (Tsuha and Aoki (2010)). Tsuha and Aoki (2010) created a large database of torque correlation factors determined from numerous tests in both full scale field and model tests. It was found that when the number of helical plates are increased, the torque correlation factor, and therefore bearing capacity, increases but only to a limit after which an increase in the amount of helical plates provides no further increase. In relation to the helical screw pile, the CHD has up to five times more 'helical plates', therefore an increased torque correlation factor will be expected.

The lack of research in the area of installation torque to pile bearing capacity limits the comparisons of the model data to full scale tests. The application of the above correlations should be reinforced with further model and field tests before being used in full scale correlations.

5.8 Model Testing Summary

The results of the model tests carried out on CHD, pushed and WIP piles have been presented through this chapter. The application of the information learned from this chapter will be discussed in Chapter 6, however a summary of the primary observations and results are presented as follows.

1. Model testing with different pile types of varying diameters are compared to CHD piles and it has been determined that the ultimate capacity and total stiffness of the CHD piles tends towards that found in pushed pile which has a similar diameter to the CHD outer flight diameter.

2. The model CHD piles have been found to cause the trapping of the soil between the flanges. The trapped soil is found to be tightly compacted, causing an equivalent large diameter straight shafted pile.

3. Soil surface movements due to the CHD installation are found to occur up to a distance equal to three times the pile diameter when installed in dense sand. The surface heave of the soil is found to also increase with an increase in relative density.

4. The subsurface soil disturbance due to the pile installation is determined through the use of CPTs carried out at radial distances around the installed pile. Variations in cone resistances were found to primarily occur up to a distance of 2D around the pile. Variations in the disturbance magnitude are found between the pile installation types.

5. CHD piles are found to cause soil disturbances primarily in a radial horizontal direction around the installed pile, while pushed piles cause a greater soil disturbance vertically below the pile base.

6. Soil disturbance around the shaft varies depending on the relative density of the original in-situ soil. CHD piles cause densification of the loose sand

corresponding to a doubling of the in-situ relative density. In medium dense sand, the relative density is increased by a third while in dense sand negligible soil density increase was found. This compared to an increase of around a third in loose sand a fifth in medium dense sand and no increase for pushed piles.

7. Soil disturbance around the base of CHD piles is found to cause relative density increases of 50% in loose sand, 25% in medium dense and 10% in dense sand. For pushed piles the increase in relative density below the pile base is found to be 60% in loose sand, 20% in medium dense while remaining unchanged for dense sands.

8. The installation of the piles caused some loosening in dense sand at low L/D ratios, however based on the surface heave measurements, it is felt that this loosening only takes place due to the low effective stress experienced.

9. The model pile ultimate capacity was determined using the intersection of lines method. It was found that the ultimate capacity of the CHD corresponds to a settlement of 0.15D, pushed piles at 0.2D and WIP piles at 0.12D

10. Instrumentation of the model CHD piles show that at ultimate capacity, the shaft contribution is typically around 38%. In pushed piles this contribution is around 11% and for WIP piles its 19%.

11. Back figuring of design parameter calculations show that the bearing capacity factors suggested by Berezantzev *et al* 1961 are greater than those determined for CHD piles. The CHD pile N_q values are typically a factor of 0.68 lower than those determined for pushed and WIP piles, suggesting the conical base typical on the CHD piles causes a reduction in end bearing pressure compared to equivalent diameter flat base piles.

12. The earth pressure coefficient *k* for Pushed and WIP piles were found to increase with relative density within the expected range suggested by Vesic (1964). For CHD piles, the *k* was found to significantly increase for high relative densities. For loose densities, the *k* value tends to those suggested by Vesic (1964). In terms of *k* variation with the peak angle of friction, the CHD was found to be greater for lower angles of friction than those suggested by Meyerhof (1976), however as the peak friction angle increases the *k* values tend towards those suggested for bored piles. The *k* value can be represented using $k = 0.074e^{0.1\phi_p'}$.

13. CPT design procedures analysis suggest that the base resistance value k_c tends towards the values suggested by Bustamante and Gianeselli (1998) for Atlas piles in high relative densities. In loose sands the factor is found to be double the suggested Atlas values indicating an increase in the end bearing pressure compared to Atlas piles.

14. The friction coefficient determined from CPT design procedures correlate to those determined from the design curves for screw piles suggested by Bustamante and Gianeselli (1993).

15. The installation torque of the CHD pile is found to increase in relative density and linearly with penetration depth for a uniform sand deposit

16. A relationship between the ultimate capacity and the installation torque has been determined. The shaft capacity is related to the average installation torque along the entire pile length. The base capacity is related to the average installation torque around the pile base.

6.0 Application of model test findings to field data

6.1 Introduction

The analysis of the field data provided some initial observations to be made regarding the loading response and settlement behaviour of the CHD piles. Model testing was undertaken to compliment the field data in order to gain a greater understanding of the behaviour of the CHD pile with the aim of improving the design procedures.

This chapter combines what has been learnt from the model testing regarding the soil disturbance around an installed CHD pile and the selection of design parameters and applies it to the field data. Based on the model test results, ideal parameters are determined for the field piles.

6.2 Diameter selection

The selection of the CHD diameter for use in the design process was investigated in the model testing and was found to tend to behaviour similar to large diameter displacement piles. The outcome of the investigation suggests that the use of full flight diameter, D_f is suitable for CHD pile design for piles installed in sands. This compliments what has been suggested from the investigation of the full scale pile tests in section 4.3. It will therefore be assumed in all design calculations regarding the CHD pile installed in sands, that the pile diameter is equal to the full flight diameter.

6.3 Soil disturbance due to CHD installation

The model testing carried out in Chapter 5 allowed the disturbance effects to the in-situ soil properties due to the installation of the CHD piles to be quantified. The design parameters determined from model testing account for these disturbance effects caused by the CHD installation. The disturbance effects are shown in order

to highlight the effects the CHD pile has on the soil conditions during installation in order to better understand its performance.

6.3.1 CPT cone resistance

The CPT cone resistances measured around the installed model CHD piles shows that the soil properties change to varying degrees depending on the original in-situ soil conditions as shown in Figure 5-13. The average cone resistance correction factors around the pile shaft, denoted as η_{CPT}, determined from CHD model testing in Figure 5-14, are given in terms of relative density of the in-situ soil. The relative density bands can be related to typical cone resistance values based on the suggestions made by Bustamante and Gianeselli (1982) as shown in Figure 6-1.

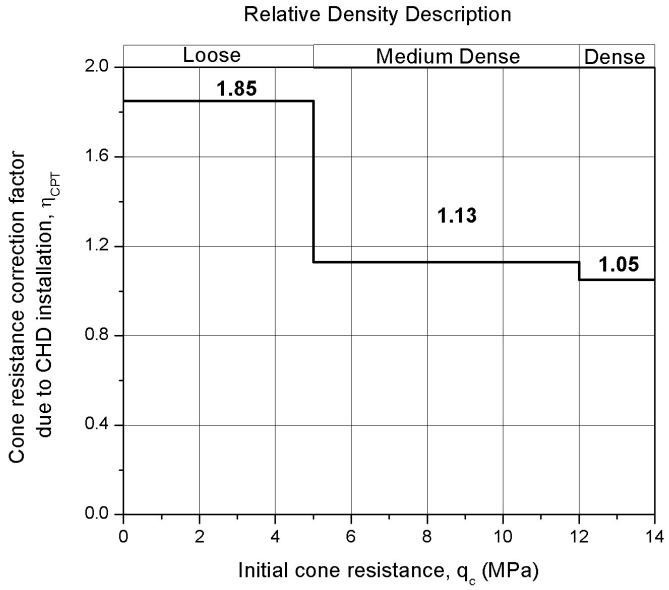

Figure 6-1. Correction factors for CPT cone resistance along the shaft an installed CHD pile

6.4 Using Model parameters for field CHD pile capacity design

During the model testing of CHD piles, design parameters have been determined for both effectives stress and CPT design procedures. The design parameters take into consideration the disturbance effects of the CHD installation process highlighted in section 6.3.

The model parameters are applied to the field CHD data and the accuracy of the design capacity is compared to the predicted capacities determined in Table 4-3 (Chapter 4).

6.4.1 CPT Design procedure

The design of piles using CPT cone resistances is carried out using equations 2-17 and 2-18 for the base and shaft capacities calculations. For the base calculations, the end bearing factor k_c from the model tests in medium dense to dense sand were found to tend towards those suggested for Atlas piles. For those installed in loose sands the factors were found to increase, as shown in Figure 5-50.

For the shaft capacity, it was determined from model testing that the unit shaft limits suggested for Atlas piles by Bustamante and Gianeselli (1998), were too conservative in nature for CHD piles. The unit shaft friction is therefore determined using the design charts suggested by Bustamante and Gianeselli (1998), however at this stage, the disturbed cone resistance is used in the calculation. Appropriate correlations to the initial cone resistance can be made at a later stage. The disturbance factors determined in Figure 6-1 are applied to the initial measured cone resistances for the field CHD piles in order to calculate the unit shaft friction.

As shown in Figure 6-2, the design capacity determined for field piles using model parameters appears to give over-predicted design capacities for piles installed in medium dense sands. For piles installed in loose sand however, a slight under prediction occurs. The apparent discrepancies in the design capacity could be due to the quality of the predicted pile capacity determined from the field load settlement data. However, with no other means of establishing the CHD ultimate capacity it is assumed that the predicted values are accurate.

The outlying project which had an estimated capacity of over 5000kN is pile S27-1. The load-settlement behaviour for this pile has been re-checked and found to produce a much greater capacity than the other piles installed in the same location. Using all available site investigation data, no cause for the under prediction in

design capacity can be determined based on the soil properties. It is known that the pile was installed in very loose to loose sand. Based on the experience gained from the model CHD piles, piles installed in loose sands can undergo significant dimension changes from subtle variations in pumping pressure. If pile S27-1 had a raised pumping pressure or increased concrete delivery rate, it could potentially cause a significantly larger pile than is assumed during the design calculations. Without exhumation of the pile, it is impossible to determine the final pile dimensions. Based on the evidence available, it is clear that pile S27-1 had substantially greater ultimate capacity than could be determined from the insitu soil properties. It is assumed that this increase in capacity is due to increased dimensions of the installed pile through a larger overall diameter, an increased base diameter or a mixture of both, and as such it will be excluded from further analysis.

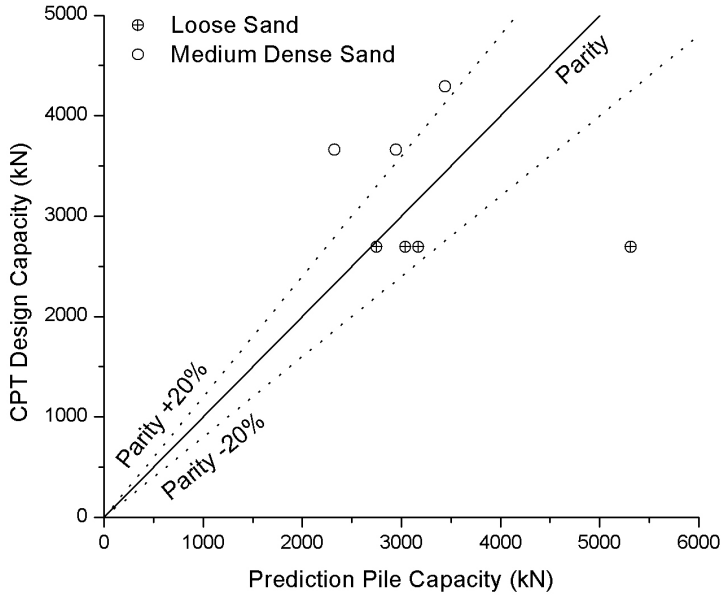

Figure 6-2. Designed capacity using parameters determined from model testing taking into account an increased cone resistance due to CHD pile installation for piles installed in sands

It is clear from Figure 6-2 that the model design parameters require refinement in order to improve the calculated design capacity. From inspection of the shaft and base contributions to the total design pile capacity, it was found that the base design typically accounted for over 60% of the capacity. From experience gained in the CHD pile, this appears to be an over estimate.

Assuming that the shaft capacity determined using the Bustamante and Gianeselli (1998) limits in conjunction with the disturbed cone resistance is accurate an appropriate base capacity can be established. The bearing capacity factor k_c can be determined. Back figured base factors are calculated and plotted compared to those suggested from model testing in Figure 6-3. The suggested upper limit is determined based on the available model test data.

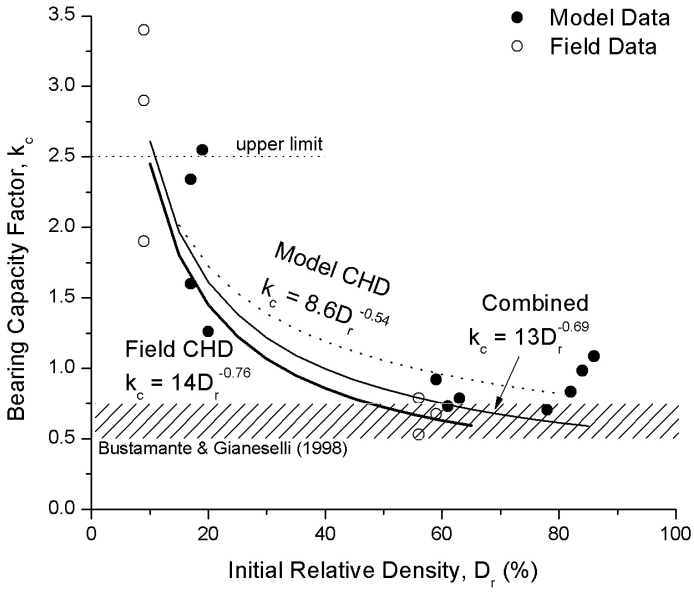

Figure 6-3. Bearing capacity factor values for CPT design determined for field data using model parameters along with model CHD values and the combined average ideal fit

The back figured field bearing capacity factors for loose sands tend to significantly higher values than those suggested by Bustamante & Gianeselli (1998). As the relative density of the sand increases the bearing capacity factors reduce to those suggested by Bustamante & Gianeselli values. The k_c value trend determined for the field CHD data can be represented by equation 6-2.

$$k_c = 14 D_r^{-0.76} \qquad \textbf{6-1}$$

for $16 \geq D_r \leq 86$

The best fit curve using both the model and field values can be represented by equation 6-3.

$$k_c = 13 D_r^{-0.69} \qquad \textbf{6-2}$$

for $16 \geq D_r \leq 86$

This combined relationship can be used to establish typical k_c values for use with CHD piles presented in a similar manner to Bustamante and Gianeselli (1982) shown in Table 6-1.

Table 6-1. Bearing capacity factors determined for CHD piles compared to those suggested for Atlas piles by Bustamante and Gianeselli (1998)

Soil Type	Typical q_c (MPa)	Current k_c Values	CHD k_c Values	
			Range	Mean
Loose Sand	≤5	0.75	2.60 - 1.21	1.9
Medium Dense	5 to 12	0.63	1.21 - 0.67	0.94
Dense	≥12	0.5	0.67 - 0.58	0.63

The unit shaft resistance has been determined from the design curves suggested by Bustamante and Gianeselli (1998). The disturbed cone resistance determined from the measured cone resistances adjusted using the correction factors in Figure 6-1 have been used For the purpose of design, it is beneficial to utilise the initial measured cone resistance without having to apply correction factors. For each of the unit shaft resistance values, the corresponding cone resistance determined by Bustamante and Gianeselli (1998) is reduced by the correction factors in Figure 6-1, giving a suitable cone resistance for use with CHD piles. The correlation curves for CHD piles are presented in Figure 6-4.

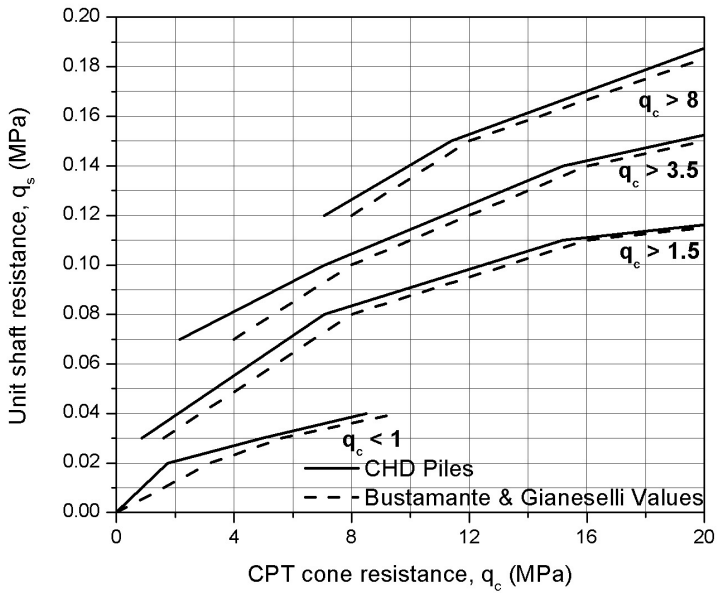

Figure 6-4. Suggested pile shaft resistance values for CHD piles compared to those suggested by Bustamante & Gianeselli (1998) using the measured in-situ CPT cone resistance

6.4.2 Effective Stress Design

The contribution to pile capacity from the base and shaft components can be determined from equations 2-5 and 2-2.

$$q_b = N_q \sigma_v^{'} \qquad \textbf{2-5}$$

$$q_s = k\sigma_v^{'} \tan\delta \qquad \textbf{2-2}$$

Where the interface friction angle δ is assumed to equal the friction angle for soil-soil shear as is typical for cast in situ piles Tomlinson and Woodward (2008).

The bearing capacity factor N_q, for CHD piles are found to be lower than the suggested values by Berezantzev *et al* (1961) based on the model tests as shown in Figure 6-5. The bearing capacity factor can be determined for CHD piles using equation 6-4

$$N_q = 0.275\exp\left(0.14\phi_p^{'}\right) \qquad \textbf{6-3}$$

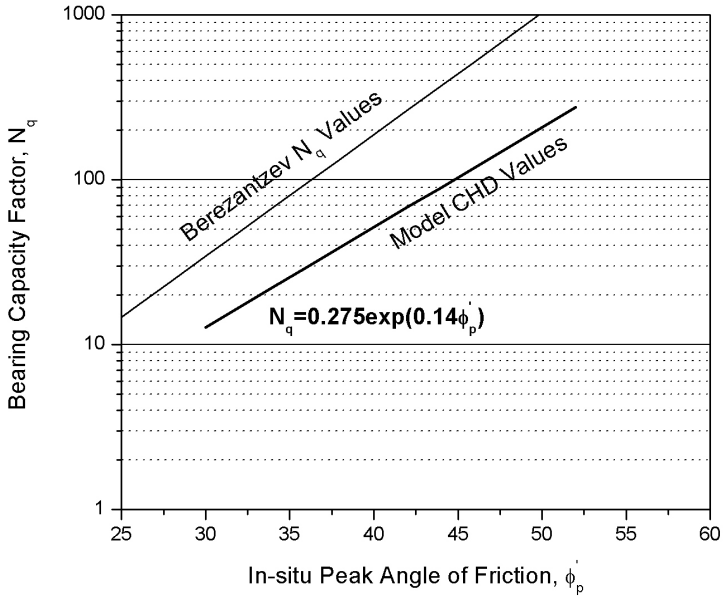

Figure 6-5. Bearing capacity factors determined for CHD piles compared to suggested Berezantzev (1961) values using the peak angle of friction of the in-situ soil

The earth pressure coefficient *k* value was previously determined from model testing of CHD piles as shown in Figure 5-48. It is determined from the initial peak friction angle of the in-situ sand. These values have then been applied to the design of field CHD piles. The capacity determined using design procedures based on the model design parameters is compared to the predicted ultimate pile capacity in Figure 6-6. The design capacity determined from the current RBL design procedures are also shown for comparison. The pile capacities determined using the model parameters can be seen to give, in some cases, a significant increase in the design capacity compared to the original RBL values.

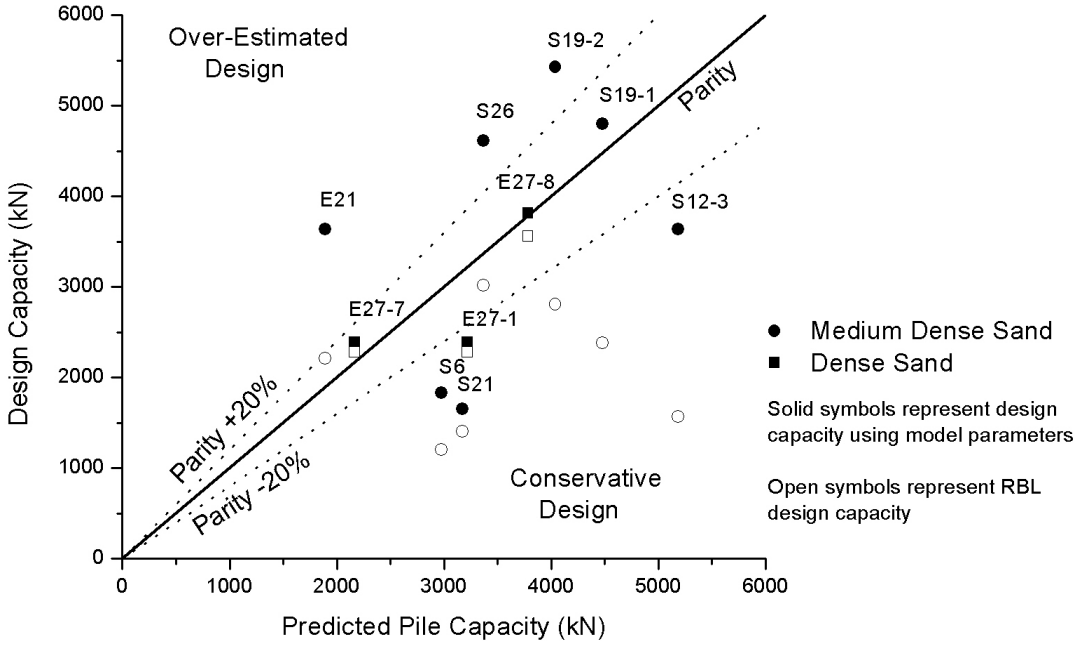

Figure 6-6. Effective stress design capacity using parameters determined from model CHD piles compared to the predicted ultimate pile capacity for field CHD piles installed in sands

It can be seen that for piles installed in dense sand, the model design parameters give a reasonable fit to the prediction capacity however a greater degree of variation occurs in medium dense sand. This variation could be due to the quality of the capacity predictions determined from the original load-settlement test data. As has been discussed previously, the accuracy of the prediction method can depend on the measured load settlement curve determined from the pile load test, with greater accuracy obtained for piles which reach high settlements. All the field piles in Figure 6-6 had relatively low settlements, typically less than 0.03D which

could affect the quality of the predication capacity. However, without any other means of determining the ultimate pile capacity of the tests piles, it must be assumed that the predicted capacities are accurate and therefore the design parameters are determined accordingly.

For three of the projects installed in medium dense sand (E21, S26 and S19-2), the model parameters give an over-estimation of the pile capacity. In the case of pile S19-2, similar ground conditions were encountered as in pile S19-1 at the same site. Applying the same design properties to pile S19-1 does not give the same over-prediction that is observed in pile S19-2. The variation in the design capacity between the two piles at the same project location highlights the variability to the CHD pile design, presumably due to subtle variations to ground conditions around the installed piles.

Assuming that the ultimate pile capacity determined from the prediction methods is accurate, the parameters which give the best fit of design capacity to predicted capacity can be determined. Since it has been indicated that the CHD piles derive the majority of the capacity from shaft resistance it is assumed the selection of the shaft resistance will have a greater influence on the total pile capacity. The total base capacity, Q_b, determined using the bearing capacity factors in Figure 6-5 are subtracted from the total pile capacity Q_T to establish an ideal total shaft capacity Q_s. Using this ideal shaft capacity, back figured earth pressure coefficients k can be determined.

The back figured ideal earth pressure coefficients for the CHD field piles are compared to those determined from model testing in Figure 6-7. For the field data, the k values are plotted against the angle of friction determined from the SPT N values. The ideal values of earth pressure coefficients determined for the field piles tend more to the values suggested by Meyerhof (1976) for driven piles than those found in the model CHD piles.

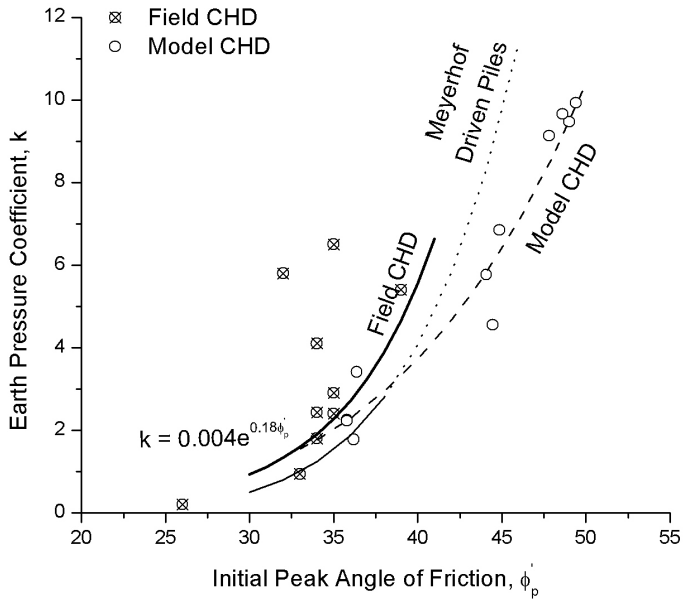

Figure 6-7. Ideal earth pressure coefficient values determined for field CHD piles compared to those determined from model CHD piles and suggested values for driven piles by (Meyerhof, 1976)

Based on the current available data, it would seem that the *k* value for CHD piles tend towards the Meyerhof (1976) driven pile earth pressure coefficient values. The Meyerhof (1976) *k* values can be represented using equation 6-5. This expression should be limited to sands with a peak angle of friction between 30° and 40°.

$$k = 0.0016e^{0.195\phi'_p} \qquad \textbf{6-4}$$

verified for sands with $30° \geq \phi'_p \leq 40°$

Using this relationship, characteristic *k* values can be determined for use in CHD pile design for different soil conditions as shown in Table 6-2. The relationship between soil density classification and peak angle of friction is based on those suggested by Peck *et al* (1974).

Table 6-2. Suggested k values for CHD piles for different soil conditions

Soil Density Classification	Peak Angle of Friction ϕ (°)	Suggested *k* values for CHD piles
Loose	< 30	< 0.9
Medium Dense	30 – 36	0.9 – 2.7
Dense	36 – 41	2.7 – 6.6
Very Dense	> 41	> 6.6

Based on the information determined from the model and field testing, equations for effective stress design procedures can be determined in terms of the initial soil properties. The base capacity Q_B is determined using equation 6-6 and the shaft capacity Q_s is determined using equation 6-7. Both design equations take into account the disturbance effects found to occur due to the installation of the CHD piles.

$$Q_B = A_B \sigma_v^{'} \left(0.275 \exp\left(0.14 \phi_p^{'}\right)\right) \quad \textbf{6-5}$$

$$Q_s = A_s \left(0.004 e^{0.18 \phi_p^{'}}\right) \sigma_v^{'} \tan \phi_p^{'} \quad \textbf{6-6}$$

6.5 Estimated shaft and base contributions to ultimate capacity

The contributions to the total pile capacity from shaft and base resistance are investigated for the field piles designed using the parameters determined in section 6.4. The shaft contribution variation to the ultimate pile capacity with the slenderness ratio of the CHD pile is shown in Figure 6-8. Along with the CHD projects, comparisons are also made to CFA piles installed in dense to loose sand by Gavin *et al* (2009) and to an auger displacement pile installed in a medium dense sand to firm clay by Bell (2010)

The shaft contribution is seen to increase with the pile slenderness ratio. For high ratios, the shaft capacity accounts for up to 80% of the ultimate capacity, similar to what is witnessed in CFA and alternative auger displacement piles.

The shaft contribution at the ultimate capacity shows that under working loads, the CHD pile is likely to develop the most of its resistance from the shaft with little base resistance being mobilised.

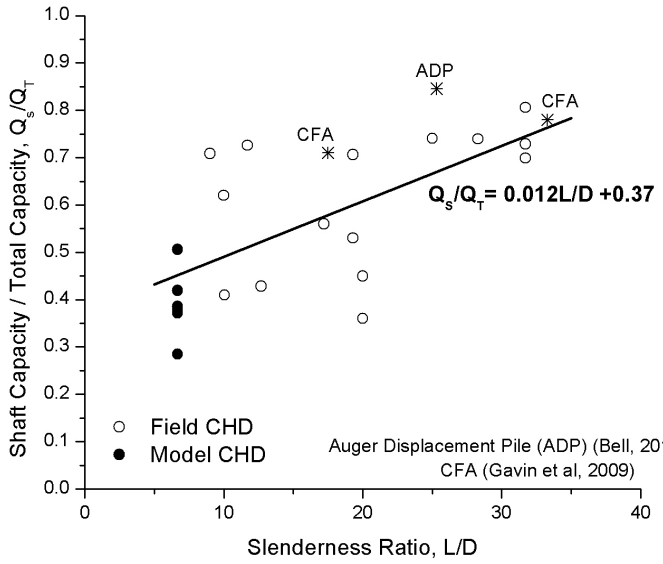

Figure 6-8. Variation of shaft contribution with slenderness ratio for model and CHD piles also showing examples of CFA and Auger Displacement piles

6.6 Summary

The information determined from model testing regarding the CHD pile has been collated and applied to CHD piles installed in the field. Model testing showed how the CHD pile installation causes a densification of the in-situ soil as shown by an increase in the CPT cone resistance. The degree of densification that occurs depends on the original in-situ density, with a greater increase found in loose sands. Correction factors which can be applied to the measured CPT cone resistance in order to account for the installation of the CHD pile have been proposed. Due to the increased effective stresses involved in field piles, the soil disturbance caused by the CHD installation on model scale are likely to be exaggerated compared to those in field piles. However, the design parameters determined from the model tests are applied to the field piles as an initial step on determining ideal values.

Model testing produced design parameters which took into consideration the disturbance of the soil around an installed CHD pile. The parameters determined from the model tests were used in the design of full scale field piles. For effective stress design, the reduced Berezantzev *et al* (1961) N_q values suggested from model tests are applied and a suitable earth pressure coefficient k is back figured. A relationship between peak angle of friction and the selection of k is proposed which is similar in nature to that suggested by Meyerhof (1976) for driven piles. Due to the similarity, it is suggested that the Meyerhof (1976) k values are used in the design of CHD piles.

For CPT design, the shaft fiction limits suggested by Bustamante and Gianeselli (1998) were found to give conservative estimates for CHD piles. To determine the shaft friction for CHD piles, the initial cone resistance was adjusted to account for the disturbance due to the pile installation using the appropriate correction factor. Correlations have then been made to allow the determination of the unit shaft friction based on initial cone resistance for the use in CHD design. With the shaft friction determined, the base resistance factor k_c is back figured. Proposed base resistance factor values for use in CHD design are found to be greater than those suggested by Bustamante and Gianeselli (1998) for Atlas piles.

Based on the design parameters determined from the analysis of model and field data, design procedures can be established for CHD piles. The design procedures using these parameters are described in Figure 6-9.

The suggested modifications to the design practice outlined in Figure 6-9 are based upon laboratory scale model pile tests with comparisons to prediction estimates of field performance. Based upon the limitation of the field study dataset it is recommended that any modifications to design parameters are verified against fully instrumented field tests. Piles must be adequately mobilised to display ultimate shaft and base behaviour.

Figure 6-9. Suggested design process for CHD piles

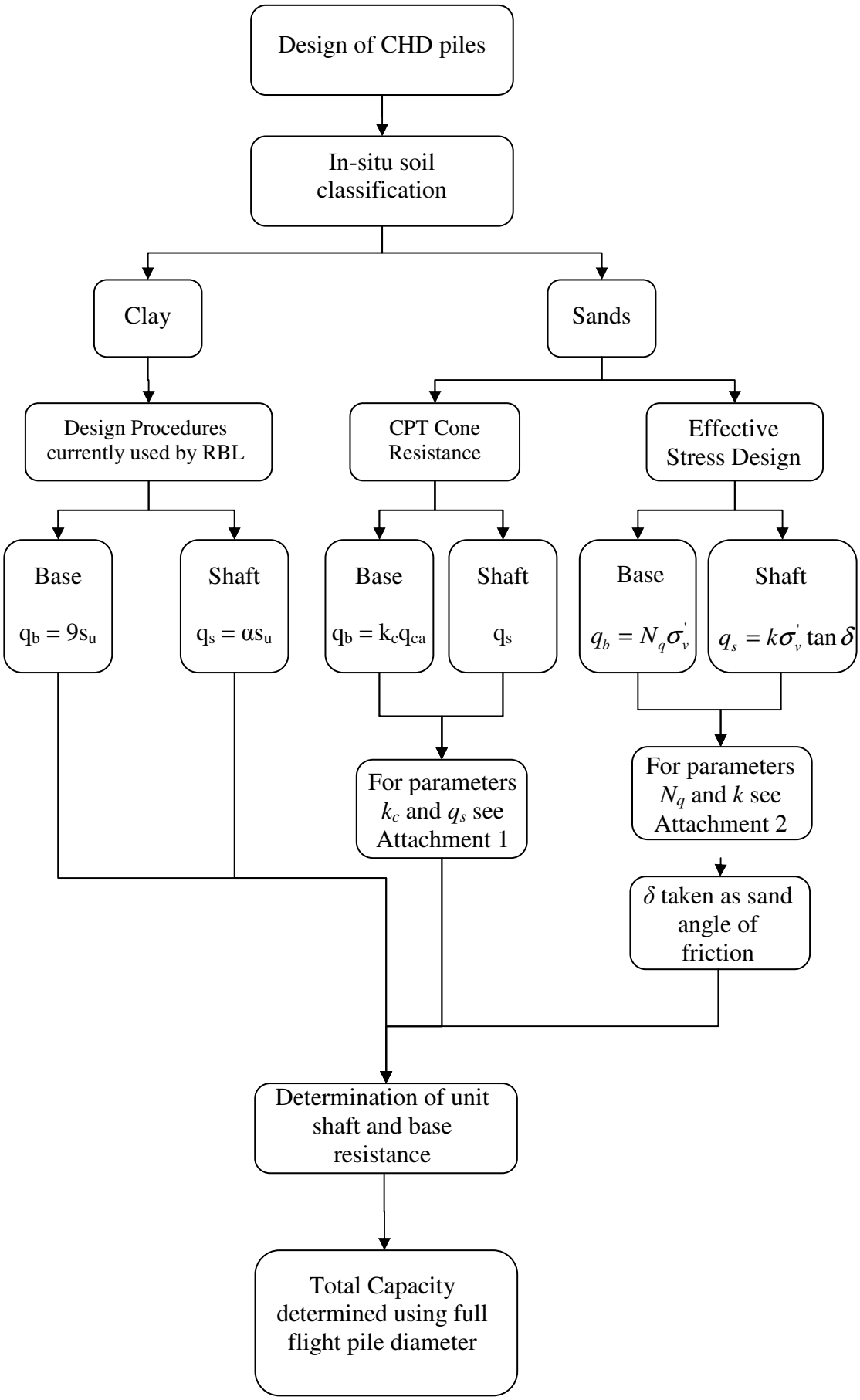

Attachment 1

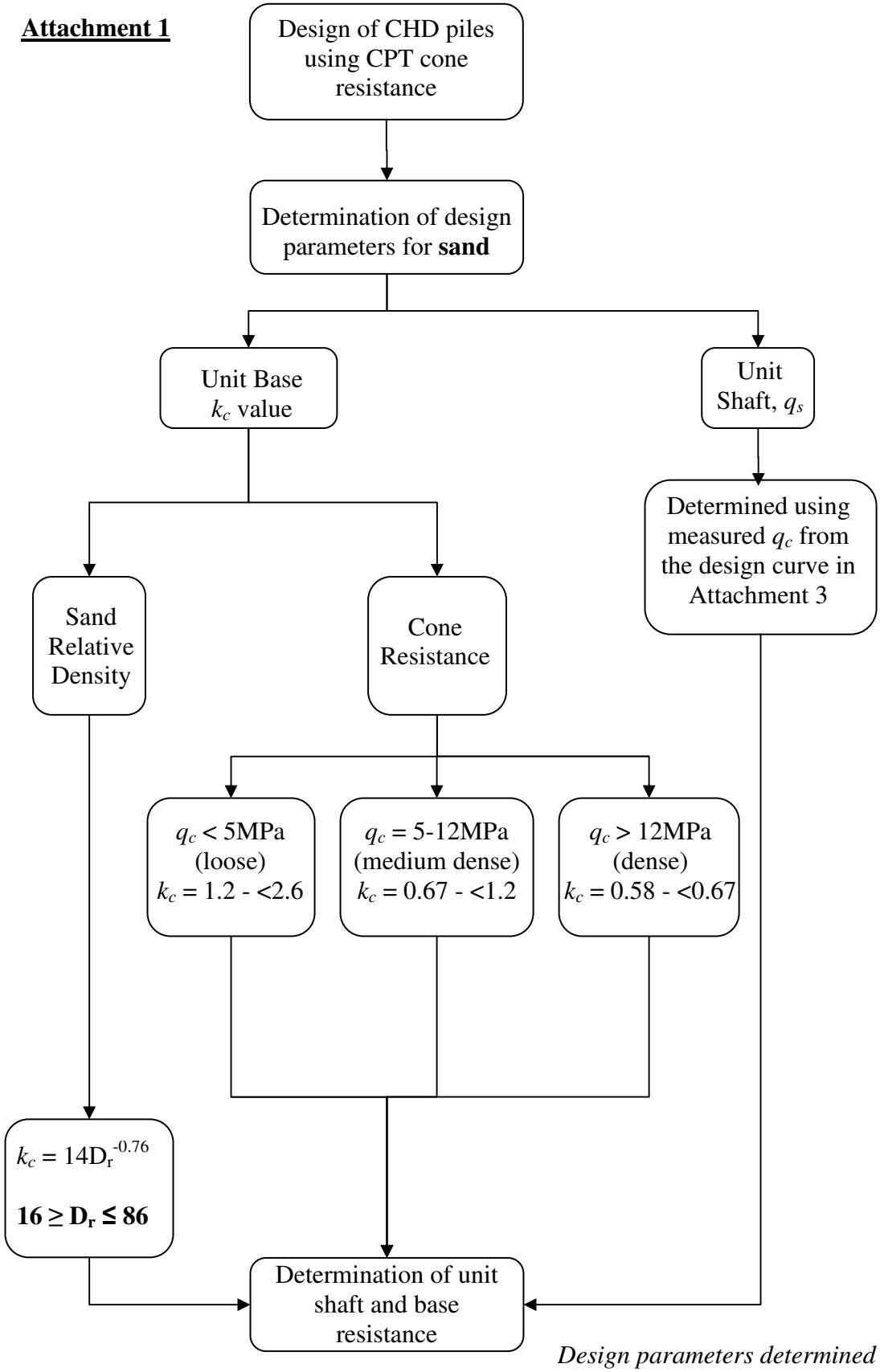

Design parameters determined for sands based on model tests

Full details regarding parameters are found in section 6.3

Attachment 2

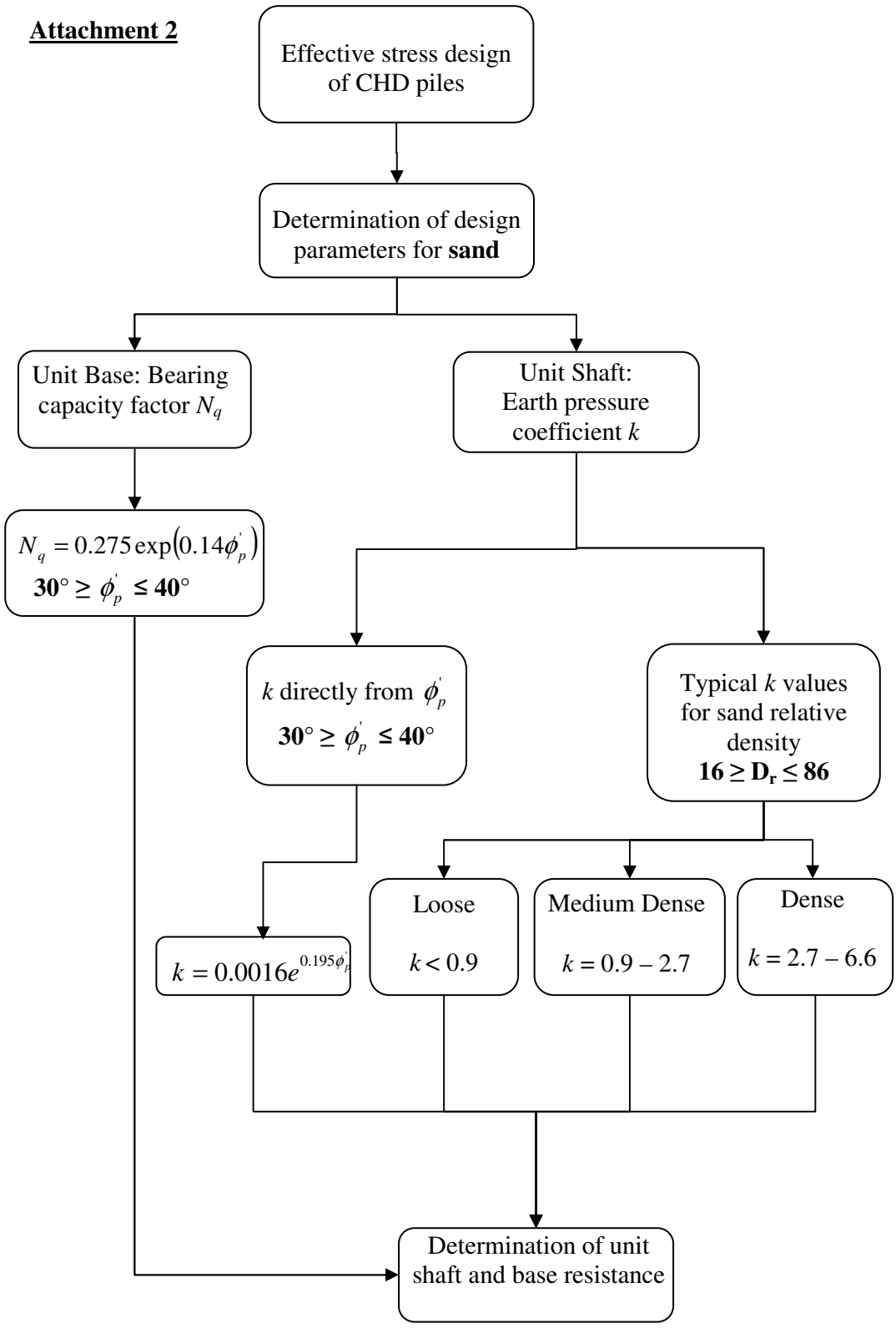

Design parameters determined for sands based on model tests

Full details regarding parameters are found in section 6.3

Attachment 3

For CHD piles installed in sand

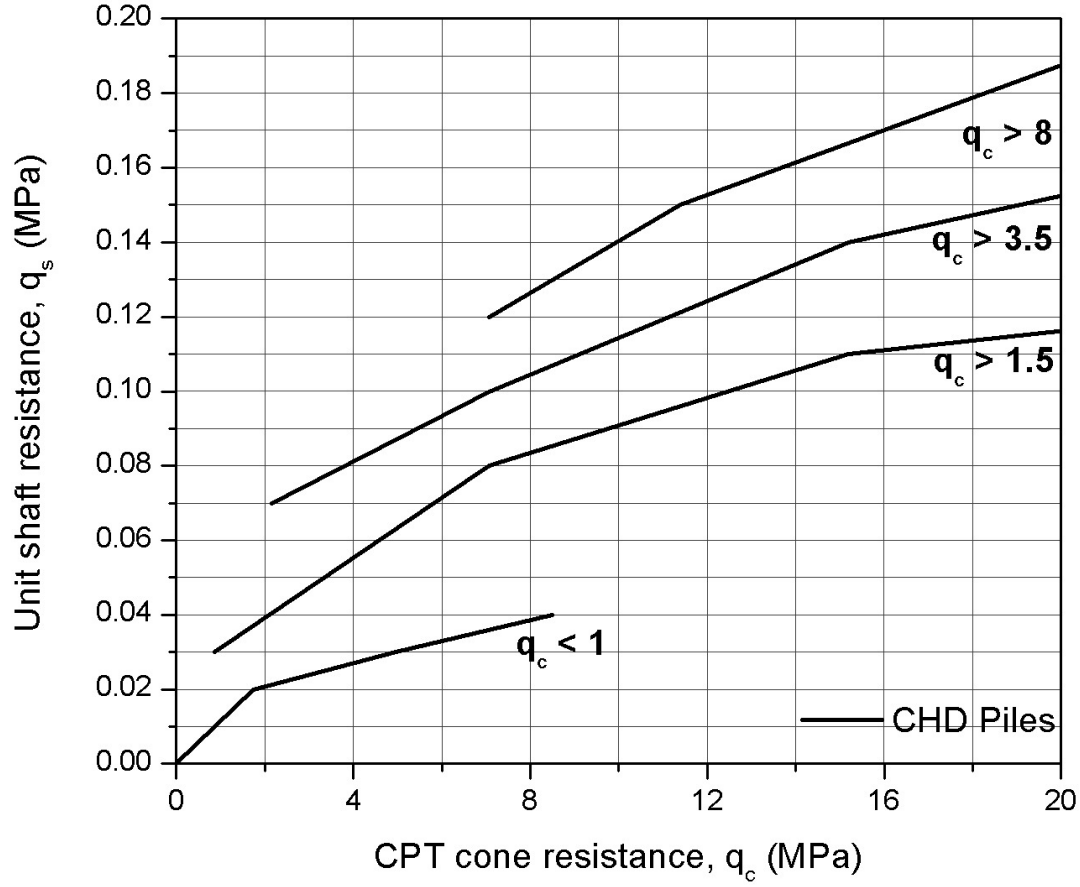

7.0 Summary and Conclusions

The continuous helical displacement pile (CHD) is an auger displacement pile developed by Roger Bullivant Ltd in the UK. Based on field experience, it has been found that the load capacity performance of the CHD pile significantly exceeds the current design predictions in a variety of soil conditions, particularly in sands.

In order to determine the reasons for the improved performance of the CHD piles, a body of research was undertaken at the University of Dundee. This study has investigated the CHD pile through the analysis of field data and by conducting model tests in an effort to improve the current understanding of the piling technique. Results established from the model testing have been applied to the field data to determine appropriate parameters suitable for improved CHD design. Conclusions from the study are presented in this chapter.

7.1 Field data

The following is a summary of the conclusion made from the investigation of the CHD field data.

1. The current use of a design diameter equal to 0.75D, where D is the full flight diameter gives conservative capacity estimates for the CHD piles installed in both sands and fine grained soils. When the existing RBL design procedures are followed, the use of the full flight diameter, 1D would appear to provide improved accuracy of the pile design capacity. For CHD piles installed in sands, the increased design diameter still provides conservative capacities.

2. The load tests which have been carried out on field CHD piles, in most instances did not reached an appropriate magnitude to cause enough pile

settlement to allow an accurate determination of the ultimate pile capacity directly.

3. Prediction techniques such as the Decourt (1999) and Chin (1972) methods allow an estimation of the ultimate pile capacity from pile tests which have not reached the ultimate capacity. It has been found that the Chin method appears to give an over-estimation of the ultimate capacity. For the CHD pile, a reduction factor of 0.96 is found to give Chin predictions similar to those determined from the Decourt method which was found to produce a closer prediction of ultimate capacity.

4. The ultimate pile capacity determined from the Decourt and Chin prediction methods is dependent on a minimum pile settlement being reached during the load test. An appropriate settlement which allowed predictions to take place varied between test piles. In general, it was found that a minimum pile settlement equal to 0.01D should be attained before the prediction methods should be applied.

7.2 Model pile tests

A number of conclusions were obtained from the CHD model testing, a summary of which are presented here.

1. Comparisons of the load-settlement behaviour of the CHD pile to displacement and non-displacement piles show that the CHD pile shows greater similarities to displacement piles of an equal diameter to the CHD full flight diameter, both in terms of ultimate capacity and stiffness. Ultimate capacity of the CHD pile is found to be 10% greater than found for displacement piles and typically 20% greater than non-displacement piles. It was also determined that the sand becomes compacted between the pile flanges, producing a pile equivalent to a cast in place pile with a diameter that matches the full flight of the CHD bullet. Based on the

evidence of the model testing, it would appear that the CHD piles can utilise the full flight diameter with respect to design.

2. Cone penetration tests carried out around the installed model CHD piles demonstrates the changes in soil properties. It was found that densification occurs to the in-situ soil due to the CHD installation. Densification of the in-situ soil is seen to occur up to a distance equal to twice the pile diameter, 2D, around the pile. This influence and densification appears to decrease beyond a distance of 2D and by 3.3D, there is little influence of the pile installation.

3. Densification of the in-situ sand due to the installation of the CHD pile is evident at all densities however it is more prominent in loose sand. The degree of densification varies with depth and initial soil density. For loose sands, densification occurs along the entire installed pile length. In medium dense and dense sands, a loosening of the in-situ soil occurs up at to a depth equal to half the installed pile length, after which densification occurs. The average increase to the initial in-situ CPT cone resistance q_c along the shaft of the pile length is found to be $1.85q_c$ in loose (D_r = 19%), $1.13q_c$ in medium dense (D_r = 61%) and $1.0q_c$ in dense sand (D_r = 83%). The increase in cone resistance directly below the base of the CHD pile is found to be $1.85q_c$ in loose, $1.38q_c$ in medium dense and $1.25q_c$ in dense.

4. Assessment of the model CHD load tests showed that the percentage of the ultimate pile capacity derived from shaft friction was twice that found in a typical non-displacement pile and over three times what from a displacement pile. At an L/D ratio of 6.6, the model CHD piles suggest that the shaft contribution accounts for around 38% of the ultimate pile capacity.

5. Back figuring the design parameters for the CHD piles shows that for effective stress design methods, the end bearing factors N_q suggested by Berezantzev (1961) give an over-estimation. An overestimation is also found for the model displacement and non displacement piles however the

CHD piles have the greatest variation. The model tests suggest an empirical relationship for the bearing capacity factor with the peak angle of friction using $N_q = 0.275e^{0.14\theta_p'}$.

6. The earth pressure coefficient *k* has been found in most case, to be greater than the 1.2 value currently used in the RBL design process. The earth pressure coefficient *k* has also been found to vary with the peak angle of friction in a similar manner to the suggestions by Meyerhof (1976) for driven piles.

7. For CPT design, the shaft friction values suggested by Bustamante and Gianeselli (1998) for Atlas piles were found to give conservative estimates for CHD piles. The end bearing factor was found to tend to those values suggested by Bustamante and Gianesilli (1998) for medium dense to dense sands. However, in loose sands, the end bearing factor should be increased.

8. Recording of the installation torque of the model CHD bullet shows a correlation with the in-situ relative density and required installation torque. A correlation between the torque and the ultimate pile capacity has been developed based on the model piles. Correlation of the installation torque to the ultimate pile capacity can be used to establish an estimated pile capacity during the installation of the CHD pile. The CHD bullet effectively becomes a ground investigation technique which provides information on the in-situ ground conditions.

7.3 Application of model results to field data

The design parameters determined from the model tests are applied to the collected CHD field data in order to allow design capacity estimates to take place. The following conclusions are made from the application of the model test parameters to the field data.

1. The reduced Berezantzev *et al* (1961) end bearing factor found from model testing are applied to field CHD piles installed in sand, allowing a back figured earth pressure coefficient to be calculated. The back figured k values can be represented by $k = 0.004e^{0.18\theta_p^{'}}$ .Average k values determined for CHD piles are found to be 0.9 in loose, 1.8 in medium dense and 4.65 when installed in dense sand. These values are almost 50%greater than those suggested by Meyerhof (1976) for displacement piles in loose sands, while in medium dense to dense sands the values are typically 30% greater than those for displacement piles suggested by Meyerhof (1976).

2. Determination of the unit skin friction using the initial measured cone resistance with the Bustamante and Gianeselli (1998) gives conservative results. Application of correction factors to the measured cone resistance which takes account of the CHD installation gives improved unit skin friction values. Correlations have been developed for use with the CHD pile to allow the determination of unit skin friction based directly from the initial cone resistances measured for the in-situ sand. These correlations are presented in Chapter 6, Figure 6-4.

3. The end bearing capacity coefficient k_c that have been back figured for CHD piles can be represented by the expression $k_c = 14D_r^{-0.76}$. Average coefficient values for different bands of cone resistance for field CHD piles are given as 1.9 for loose sand (q_c less than 5 MPa), 0.9 for medium dense sand (q_c between 5 and 12 MPa) and 0.63 for dense sand (q_c greater than 12 MPa). These are larger than the current Bustamante and Gianeselli (1998) suggestions of 0.75, 0.63 and 0.5 for loose, medium dense and dense sands

4. Based on the design capacities determined for field CHD piles, estimated shaft and base contributions are determined. These estimations highlight that for CHD piles installed in the field, the low settlements experienced during the load tests, very little base resistance is mobilised and that the majority of the pile capacity can be attributed to shaft friction.

7.4 Implications for industrial practice

The research conducted in this project has been focused on providing a greater understanding of the CHD pile with the intent on being able to improve the efficiency of the piling method.

It has been shown that the CHD pile can be designed using a pile diameter equal to the full flight diameter. It is also shown that the design capacity of the CHD pile assuming the current design procedure, as discussed in Chapter 2, produces an under estimate of the true pile capacity. By taking into consideration the disturbance to the local soil conditions that is caused by the CHD pile and the design parameters suggested from this research, an improved design capacity can be determined.

An improved accuracy of the design capacity will allow potential reductions in the required pile installation depths. This will correspond to financial savings due to reduced concrete volumes and also improved efficiency with less time spent installing unnecessary pile lengths.

The suggested design procedures with suitable parameters for CHD piles are presented in Figure 6-11.

8.0 Recommendations for future work

This chapter details recommendations which have been determined throughout the course of the research carried out in this project. Recommendations have been established for implementation to field CHD piles and also suggestions for further model testing.

8.1 Field Data

Based on the collected data from CHD test piles, a number of recommendations are determined in order to gain further in depth knowledge on the piling method.

1. In order to obtain the measured ultimate pile capacity of the CHD, load tests need to be carried out to greater magnitudes to induce greater settlements of the CHD pile. The piles which have been investigated as part of this study have shown that significant loads should be applied in order to determine the ultimate pile capacity. Large loads can cause problems, particularly when using maintained load tests, such as safety issues or failure of reaction piles. In order to ensure that an ultimate capacity of a CHD test pile is established at a manageable load, it would be advisable to install a test pile to a length which is shorter than the estimated design length.

2. Further to determining the ultimate capacity of the CHD pile, instrumentation of the pile would be of significant benefit. With instrumentation, an understanding of the load distribution throughout the pile would be obtained. Having the load distribution, will allow a greater understanding of the shaft to base capacity split, allowing the design parameters to be assessed in full scale piles.

3. To establish the degree of disturbance by CHD pile installation on the in-situ ground conditions, it would be beneficial to carry out cone penetration

tests prior to and then following the CHD installation, in a similar manner to those conducted in the model tests. Cone resistances at increasing distances around an installed CHD pile should be compared to those determined in the original undisturbed soil conditions. With the change in cone resistances measured around an installed pile, correlations can be made to the design charts for selection of the skin friction factors. It can also give greater detail on the horizontal influence of the CHD pile on the in-situ ground conditions and how this will affect the behaviour of pile groups within a project site.

4. The exhumation of an installed CHD pile would allow a greater understanding of the true formation of the flanges along the installed length. Coupled with a detailed record of concrete flow rates, an accurate correlation between concrete flow rate and finished pile dimensions can be established which would give a real time indication on the soundness of the pile. It would also be beneficial to establish the shape of the CHD base when formed in the field in order to assist in the capacity design calculations.

5. As was established from model testing of CHD piles, a relationship between installation torque of the CHD pile and the ultimate capacity can be determined. To conduct an improved investigation regarding this relationship, the installation torque on full scale CHD piles should be recorded in more detail. The current torque measurements are based on hydraulic pressures applied to the bullet rig, however the direct measurement of the applied torque exerted on the bullet should be established. Correlations with installation torque and pile capacity can allow real time feed back on expected pile performance during the installation process.

8.2 Model Testing

Some modifications to the existing model testing equipment are suggested to improve future testing.

1. The biggest problem with conducting model tests, as was discussed in Chapter 2, is scaling issues. In order to reduce the effects of scaling issues, centrifuge tests could be conducted. Centrifuge testing would allow the removal of the low effective stress issues experienced in the current testing programme. Although the centrifuge would remove the problems of effective stress, a number of issues would be caused due to the requirement to automate the entire installation process without the ability of human interaction. Significant investment would be required to create a fully automate the current stages of construction of the model testing procedure.

2. Further use of the 1g model setup would benefit from development to allow the use of a larger test box which will reduce or remove any boundary effects which have been experienced in the current testing programme. Increasing the test box dimensions would not allow the use of the Instron, testing machine therefore an alternative would be required. This could be provided through a larger Instron style unit or through the design of a system which produced controllable vertical movement.

3. Improvements to the pluviation system would also be advisable for future research. A semi automatic hopper system similar to that developed by Lauder (2010) would allow sand beds to be prepared whilst removing the potential of variation due to human input. Although consistent sand densities were achieved within each prepared test box, it was difficult to ensure that identical densities were prepared between each test. In some instances, sand beds prepared were anticipated to be medium dense samples, however the final density was found to tend towards dense. A more automated pluviation system could potentially reduce this variation.

4. As was determined from the investigation of the CHD field data, a large percentage of full scale piles are installed in varying soil strata throughout the pile length. Model testing which introduces different soil layers would improve the understanding of the CHD interaction with the in situ soil and how capacity is derived in different soil layers.

5. The instrumentation of the CHD piles during this study consisted of strain gauged rods as discussed in Chapter 3. A number of problems occurred during the implementation of this instrumentation and as such, a number of recommendations are made to improve this for future research. The primary source of error appears to stem from the wiring of the strain gauges. By using a hollow aluminium tube as opposed to a solid rod, the wires could be run through the central core thus avoiding contact with the model grout. Inspection of the rods which had been installed in the grout appeared to show that the applied protection was adequate in ensuring that no grout penetrated through to the strain gauges themselves therefore the use of this protection technique could be repeated. Application of heat shrink wrap along the exposed wires would also significantly reduce the possibility of wire damage during the installation into the CHD pile.

6. The model testing showed that the CHD base was formed as a cone and not a flat surface. The effects of the different shapes on the pile base on the end bearing pressure could be investigated in order to better understand the relationship between suggested end bearing factors and the ideal values.

7. The soil displacement around the installed CHD pile was initially investigated as described in Chapter 3. Further development of this testing procedure would allow the radial influence of the CHD pile to be measured. It would also allow further investigation of the pile base shape influence on soil movement.

References

Abdelrahman, G. E. (2002). Prediction of ultimate pile load from axial load tests and penetration tests. *The Egyptian Geotechnical Journal of Soil Mechanics and Foundation Engineering* Vol. 10.

API (2005). Recommended Practice for Planning, Designing and Constructing Fixed Offshore Platforms - Working Stress Design. *2A-WSD*, Washington DC: American Petroleum Institute

Azizi, F. (2000). *Applied Analysis in Geotechnics.* London: E & FN Spon.

Baldi, G., Bellotti, R., Ghionna, V. Jamiolkowski, M. (1986). 'Interpretation of CPTs and CPTUs; 2nd Part: Drained penetration of sands.' *Proceedings of the 4th International Geotechnical Seminar*. Singapore 1986. pp143-156

Basu, P. and Prezzi, M (2009). *Design and application of drilled displacement (Screw) piles*. FHWA/IN/JTRP-2009/28, Purdue University, Indiana Department of Transportation & US DoTFHA.

Baxter, D. J., Dixon, N., Fleming, P.R., Hadley, S.P. (2006). 'The design and formation of bored displacement piles - A United Kingdom perspective'. *10th International Conference on Piling and Deep Foundations*, Amsterdam 31st May – 2nd June 2006

Beer, F. and Johnston, E.R. (1992). *Mechanics of Materials.* 2nd Edition in SI units. McGraw-Hill.

Bell, A. (2010). Foundation solutions for the urban regeneration of Glasgow city centre. *The DFI and EFFC 11th International conference: Geotechnical Challenges in Urban Regeneration*. 26th – 28th May 2010, ExCel London, UK. Peterborough: Emap Networks

Bell, A. and Robinson, C (2012). 'Single Piles,' in Burland, J., Chapman. T., Skinner, H., Brown, M. (ed.) *ICE Manual of Geotechnical engineering*. London 2012: ICE Publishing.

Berezantzev, V. G., Khristoforov, V.S., Golubkov, V.N. (1961). Load Bearing Capacity and Deformation of Piled Foundations. *Proc. 5th International Conference on Soil Mechanics and Foundations Engineering*, Paris.

Bolton, M. D. (1986). The strength and dilatancy of sands. *Geotechnique* 36, No. 1, pp 65-78.

Bolton, M. D. and Gui, M.W. (1993). The study of relative density and boundary effects for cone penetration tests in centrifuge. *CUED/D-Soils/TR256*. University of Cambridge.

Bottiau, M., Meyus, I.A., Van Impe, P.D., Russo, G. (1998). 'Load testing at Feluy test site: Introducing the Omega B+ pile.' *Deep Foundations on Bored and Auger Piles BAP III: Proceedings of the 3rd International Geotechnical Seminar*. Ghent, Belgium, 19th – 21st October 1998. Balkema. pp 187-199

Brinch Hansen, J. (1961). A general formula for bearing capacity. *The Danish Geotechnical Institute* Bulletin No. 11. Copenhagen 1961. pp 38-46

British Standards Institution (1986). '*Code of practice for foundations*', BS 8004:1986. London BSI, Superseded/Withdrawn

British Standards Institution (2000). '*Testing Hardened Concrete - Part 1: Shape, dimensions and other requirements for specimens and moulds*'. BS EN 12390-1: 2000. London BSI

British Standards Institution (1990). '*Methods of test for soils for Civil Engineering purposes Part 7: Shear strength tests (total stress)*', BS EN 1377-7:1990. London BSI

British Standards Institution (2010). '*Execution of special geotechnical works - Bored Piles*' BS EN 1536-2010. London BSI

Brouwer, J. J. M. (2007). *In-Situ Soil Testing*. 2nd Edition. Bracknell: IHS BRE Press.

Brown, M. J. (2004). *The rapid load testing of piles in fine grained soils*. PhD Thesis. University of Sheffield.

Brown, M. J. (2012). 'Pile Capacity Testing' in Burland, J., Chapman. T., Skinner, H., Brown, M. (ed.) *ICE Manual of Geotechnical engineering*. London 2012: ICE Publishing

Busch, P., Grabe, J., Gerressen. F., Ulrich, G. (2010). Use of displacement piles for reinforcement of existing pile foundations. *The DFI and EFFC 11th International conference: Geotechnical Challenges in Urban Regeneration*. 26th – 28th May 2010, ExCel London, UK. London, Emap Networks

Bustamante, M. and Gianeselli, L (1982). Pile bearing capacity prediction by means of static penetrometer CPT. *Proceedings of the 2nd European Symposium on Penetration Testing*. Amsterdam, 24th-27th May 1982.

Bustamante, M. and Gianeselli, L. (1993). Design of auger displacement piles from in situ tests. *Deep Foundations on Bored and Auger Piles, BAP II, Proceedings of the 2nd international geotechnical seminar*. Belgium, Ghent, 1st-4th June 1993. Balkema.

Bustamante, M. and Gianeselli, L. (1998). Installation parameters and capacity of screwed piles. *Deep Foundations On Bored And Auger Piles, BAP V, Proceedings of the 5th international geotechnical seminar*. Belgium, Ghent, 8th-10th September 2008. Balkema.

Canadian Geotechnical Society (2006). *Canadian Foundation Engineering Manual*. 4th Edition. Richmond, British Columbia: Canadian Geotechnical Society.

Cassidy, M. J. and Houlsby, G.T. (2002). Vertical bearing capacity factors for conical footings on sand. *Geotechnique.* Vol. 52, No. 9, pp687-692.

Cathie Associates (2008). *OPile - Single Pile Axial and Lateral Analysis Instruction Manual*. Cathie Associates SA/NV [Online]. Available at http://www.cathie-associates.com/uploads/imagegallery/opile/opile%20downloads/OPILE%20Help%20File.pdf. (Accessed 19th June 2012)

Chin, F. K. (1970). 'Estimation of the ultimate load of piles not carried to failure'. *Proceedings of the 2nd South East Asia Conference on Soil Engineering*. Singapore, 11th-15th June 1970.

Chin, F. K. (1972). 'The inverse slope as a prediction of ultimate bearing capacity of piles'. *The 3rd Southeast Asian Conference on Soil Engineering*. Hong Kong, 6th-10th November 1972. The Southeast Asian Society of Soil Engineering. pp 83-91

Das, B. M. (1997). *Advanced Soil Mechanics.* 2nd Edition. Taylor & Francis.

Das, B. M. (2000). *Fundamentals of geotechnical engineering*. California: Brooks/Cole.

Davisson, M. T. (1973). 'High Capacity Piles'. *Proceedings, Lecture Series, Innovations in Foundation Construction*. January to May 1973. Illinois Institute of Technology: American Society of Civil Engineers.

De Cock, F. and Lhoest, C (1993). The vibration free realisation of soil retaining walls, using Atlas screw piles. *Deep Foundations on Bored and Auger Piles, BAP*

II, Proceedings of the 2nd international geotechnical seminar. Belgium, Ghent, 1st-4th June 1993. Balkema.

Decourt, L. (1999). Behaviour of foundations under working load conditions. *Proceedings of the 11th Pan-American Conference on Soil Mechanics and Geotechnical Engineering*. Foz Dolguassu, Brazil, August 1999. pp 453-488

Ellis, H.R., Williams, A.F. (1972) 'The Capacity of Bored Piles in Dense Sand'. *Proceedings of the 3rd South East Asian Conference on Soil Engineering.* Hong Kong. The SEASSE.

Emmett, K. (2007). *Movement of soil and groundwater around piles in layered ground*. PhD. University of Sheffield.

Fellenius, B. H. (2001). 'From strain measurements to load in an instrumented pile'. *Geotechnical News Magazine*. Vol. 19. pp 35 - 38.

Fellenius, B. H. (2001). 'What capacity value to choose from the results of a static loading test'. *The Newsletter of the Deep Foundations Institute*. Winter 2001. (Winter 2001). DFI. pp19 -22.

Fellenius, B. H. (2002). 'Determining the true distributions of load in instrumented piles'. *International Deep Foundation Congress 'Down to Earth Technology*'. Orlando, Florida, 14th – 16th February. American Society of Civil Engineers.

Fellenius, B. H. (2011). Basics of Foundation Design: Electronic Edition. December 2011 [Online] www.fellenius.net. Accessed 18th June 2012.

Fleming, K., Weltman, A., Randolph, M.F., Elson. K. (2009). *Piling Engineering.* 3rd Edition. London: Taylor & Francis.

Fleming, W. G. K. (1992). A new method for single pile settlement prediction and analysis. *Geotechnique,* 42(3). pp 411-425.

Fleming, W. G. K. (1995). 'The Understanding of continuous flight auger piling, its monitoring and control'. *Proceedings of the Institution of Civil Engineers: Geotechnical Engineering*. 113(3): 157-165. London, Thomas Telford.

Frangoulides, A. C. (1999). *Research into the behaviour of Continuous Helical Displacement piles*. Master of Engineering. Cambridge University.

Gavin, K. G., Cadogan, D., Casey, P. (2009). 'Shaft Capacity of Continuous Flight Auger Piles in Sand'. *Journal of Geotechnical and Geoenvironmental Engineering*. ASCE, June 2009. Vol. 135, Issue 6, pp 790 - 798.

Gavin, K. G. and Lehane, B.M. (2007). 'Base Load-Displacement response of piles in sand'. *Canadian Geotechnical Journal.* Vol. 44, No. 9, September 2007 pp 1053-1063.

Geotechnical Consulting Group (1998). *CHD Pile Design Review*. Roger Bullivant Ltd. August 2008. London, Geotechnical Consulting Group.

Gourvenec, S. (2005). 'Offshore Geomechanics Handbook'. *CIVL4122 Offshore Geomechanics 610.452*. University of Western Australia.

Gwizdala, K., Krasinski, A., Brzozowski, T. (2008). 'The assessment of load-settlement curve for Atlas piles correlated with CPT tests'. *Deep Foundations On Bored And Auger Piles, BAP V, Proceedings of the 5th international geotechnical seminar*. Belgium, Ghent, 8th-10th September 2008. Balkema.

Hayes, J. and Simmonds, T. (2002). 'Interpreting strain measurements from load tests in bored piles'. *DFI 9th International conference on Piling and Deep Foundations*. Nice, France, 3rd-5th June 2002. Paris: Presses de l'ecole nationale des Ponts et chaussees .

Hird, C. C., Ni, Q., Guymer, I. (2008). 'Physical modelling of displacements around Continuous Flight Augers in clay'. *BGA International Conference on Foundations.* Dundee, Scotland, 24th-27th June 2008. London: IHS BRE Press.

Hird, C. C., Ni, Q., Guymer, I. (2011). Physical modelling of deformations around piling augers in clay. *Geotechnique* Vol. 61, No. 11, pp 993-999.

Hird, C. C. and Stanier, S.A. (2010). 'Modelling helical screw piles in clay using transparent soil'. *7th International Conference on Physical Modelling in Geotechnics*, Zurich, June 28th - July 1st 2010. London: Taylor and Francis.

Holeyman, A. and Charue, N (2003). 'International pile capacity prediction event at Limelette'. *Belgian Screw Pile Technology: Design and Recent Developments : Proceedings of the Second Symposium on Screw Piles*: Brussels, 7th May 2003. London: Taylor and Francis. pp 215-234.

Hollingsworth, J. R. and Imbo-Burg, R.M. (1992). 'The Atlas screw pile - construction, design and performance'. *Piling, European Practice and Worldwide Trends: Proceedings of a Conference Organised by the Institution of Civil Engineers*. London, 7th-9th April 1992. London: Thomas Telford.

Hoyt, R. M. and Clemence, S.P. (1989). 'Uplift capacity of helical anchors in soil'. *12th International Conference on Soil Mechanics and Foundation Engineering*. Rio de Janeiro, Brazil, 13th-18th August 1989. London: Taylor and Francis Group. pp 1019-1022.

Hsein Juang, C., Lu, P.C., Chen, C.J. (2002). 'Predicting geotechnical parameters of sands from CPT measurements using neural networks'. *Computer-Aided Civil and Infrastructure Engineering*. Vol. 17, No. 1, pp. 31-42. January 2002. Wiley-Blackwell.

Huybrechts, N. and V. Whenham (2003). 'Pile Testing campaign on the Limelette test site & Installation techniques of screw piles'. *Belgian Screw Pile Technology:*

Design and Recent Developments : Proceedings of the Second Symposium on Screw Piles: Brussels, 7th May 2003. London: Taylor and Francis. pp 71-130.

Institution of Civil Engineers (2007). ICE Specification for Piling and Embedded Retaining Walls, SPEWR. Institution of Civil Engineers. London: Thomas Telford.

Jamiolkowski, M., Ladd, C.C., Germaine, J.T., Lancellotta, R. (1985). 'New developments in field and laboratory testing of soils'. *Proceedings of the 11th International conference on soil mechanics and foundation engineering*. San Francisco, 12th-16th August 1985. London: Taylor and Francis Group. Pp57-153

Jardine, R., Chow, F., Overy, R., Standing, J. (2005). *ICP design methods for driven piles in sands and clays*. London: Thomas Telford.

Jeffrey, J. R., Schwamb, T., Brown. M.J., Ball. (2010). 'Understanding CHD pile performance in granular soils'. *The DFI and EFFC 11th International conference: Geotechnical Challenges in Urban Regeneration*. 26th – 28th May 2010, ExCel London, UK. Peterborough, Emap Networks.

Kenny, M. J., Guasti, S., Zsak, P. (2003). 'Continuous flight auger boring in sandy soils'. *BGA International Conference on Foundations: Innovations, Observations, Design and Practice : Proceedings of the International Conference Organised by British Geotechnical Association*. Dundee, 2nd-5th September 2003. London: Thomas Telford.

Kishida, H. and Uesugi, M (1987). 'Tests of interface between sand and steel in the simple shear apparatus'. *Geotechnique* Vol. 37, Issue 1, pp. 46-52.

Klotz, E. U. and Taylor, R.N. (2001). 'Development of a new pile driving actuator and a fully instrumented model pile for use in the centrifuge'. *International Journal of Physical Modelling in Geotechnics.* Vol.1, No 3, pp 1 - 16.

Knappett, J. A. and Craig, R.F. (2012). *Craig's Soil Mechanics*. 8th Edition. CRC Press.

Knappett, J. A. and Madabhushi, S.P.G. (2008). 'Liquefaction-Induced settlement of pile groups in liquefiable and laterally spreading soils'. *Journal of Geotechnical and Geoenvironmental Engineering.* Vol. 34, Issue 11, pp 1569-1690.

Kulhawy, F. H. (1984). 'Limiting tip and side resistances, fact or fallacy'. *Symposium on Analysis and Design of Pile Foundations*, San Francisco, 1984. American Society of Civil Engineers.

Kulhawy, F. H. and Mayne, P.W. (1990). 'Manual on estimating soil properties for foundation design'. *Electric Power Research Institute, Cornell University. Geotechnical Engineering Group*. Electric Power Research Institute.

Lauder, K. (2010). *The performance of pipeline ploughs*. PhD. University of Dundee.

Lehane, B. M., Schneider, J.A., Xu, X. (2005). 'The UWA-05 method for prediction of axial capacity of driven piles in sand'. *Frontiers in Offshore Geotechnics ISFOG 2005: Proceedings of the First International Symposium on Frontiers in Offshore Geotechnics*. University of Western Australia, Perth, 19-21 September 2005. Taylor & Francis.

Li, B. and Ruban, T. (2009). 'Static axial load test on strain gauge instrumented piles'. *GeoHalifax - 62nd Canadian Geotechnical Conference & 10th Joint CGS/IAH-CNC Groundwater conference*. Halifax, Canada, 20th-24th September.

Lunne, T., Robertson, P.K., Powell, J. (1997). *Cone penetration testing in geotechnical practice.*2nd Edition. Spon Press.

Mayne, P. W. and Kulhawy, F.H. (1982). 'K_0-OCR Relationships in Soil'. *Journal of the Geotechnical Engineering Division*. Vol. 108, No 6 June 1982: pp. 851-872.

McNeilly, L. (2010). *Comparison of Continuous Helical Displacement Piles*. Honours year project. University of Dundee.

Meigh, A. C. (1987). *Cone penetration testing: methods and interpretation*. CIRIA. Butterworths.

Meyerhof, G. G. (1976). 'Bearing Capacity and Settlement of Pile Foundations'. *Journal of the Geotechnical Engineering Division*. Vol. 102(No. GT3): pp. 197-228.

Nesmith, W.M. (2002) 'Design and installation of pressure-grouted, drilled displacement piles'. *DFI 9th International conference on Piling and Deep Foundations*. Nice, France, 3rd-5th June 2002. Paris: Presses de l'ecole nationale des Ponts et chaussees .

O'Neill, M. W. and Reese, L.C. (1999). *Drilled Shafts: Construction, procedures and Design Methods.* FHWA-IF-99-025, Federal Highways Administration.

Oasys Ltd (2011). *Oasys Pile V19.2 Operation Manual*. Newcastle Upon Tyne, Oasys-Arup. [Online] Available at http://www.oasys-software.com/media/Manuals/Latest_Manuals/Pile19.2_manual.pdf. (Accessed: 18th June 2012).

Peck, R. B., Hanson, W.E., Thornburn, T.H. (1974). *Foundation Engineering*. 2nd Edition. New York, John Wiley.

Perko, H. A. (2009). *Helical Piles - A practical guide to design and installation.* John Wiley & Sons.

Phillips, R. and Valsangkar, A.J. (1987). 'An Experimental Investigation of Factors Affecting Penetration Resistance in Granular Soils in Centrifuge Modelling'. Cambridge University Engineering Department.

Randolph, M. F. (2003). 'RATZ Manual Version 4-2 - Load Transfer Analysis of Axially Loaded Piles', University of Western Australia.

Randolph, M.F. (2003). 'Science and empiricism in pile foundation design'. *Geotechnique* Vol., 53. No. 10 pp 847-875.

Randolph, M. F. and Gourvenec, S. (2011). *Offshore Geotechnical Engineering*. Perth, Western Australia. CRC Press.

Randolph, M. F. and Wroth, C.P. (1978). 'Analysis of Deformation of Vertically Loaded Piles'. ASCE *Journal of the Geotechnical Engineering Division*, 104(GT12): pp 1465 - 1488.

Robertson, P. K. and Campanella, R.G. (1983). 'Interpretation of cone penetration tests. Part I: Sands'. *Canadian Geotechnical Journal*. Vol. 20, pp 718-733.

Roger Bullivant Ltd (2007). 'Roger Bullivant saves the client the expense of cart-away'. *GeoDrilling International*.

Schawmb, T. (2009). *The Continuous Helical Displacement pile in comparison to conventional piling techniques*. Masters of Science. University of Dundee.

Schmertmann, J. H. (1970). 'Static cone to compute static settlement over sand'. ASCE *Journal of the Soil Mechanics and Foundations Division*. Vol. 96, No. SM3 pp1011-1043.

Schneider, J. A., Xu, X., Lehane, B.M. (2010). 'End bearing formulation for CPT based driven pile design methods in siliceous sands'. *CPT '10 - 2nd International Symposium on Cone Penetration Testing*. Huntington Beach California, 9th-11th

May 2010. Technical Committee TC-16 of the International Society for Soil Mechanics and Geotechnical Engineering.

Subba Rao, K. S., Allam, M.M., Robinson, R.G. (1998). 'Interface friction between sands and solid surfaces'. *Proceedings Of The Institution Of Civil Engineers-Geotechnical Engineering.* Vol. 131, Issue 2, pp 75-82.

Thorburn, S., Greenwood, D. A, Fleming. W.G.K. (1993). 'The response of sands to the construction of Continuous Flight Auger Piles'. *Deep Foundations on Bored and Auger Piles, BAP II, Proceedings of the 2nd international geotechnical seminar*. Belgium, Ghent, 1st-4th June 1993. Balkema.

Tomlinson, M. J. (1994). *Pile design and construction practice*. 4th Edition. Spon Press.

Tomlinson, M. J. and Woodward, J. (2008). *Pile design and construction practice* Fifth Edition. Taylor & Francis.

Troughton, V. and Hislam, J. (2012). 'Piling Problems' in Burland, J., Chapman. T., Skinner, H., Brown, M. (ed.) *ICE Manual of Geotechnical engineering*. London 2012: ICE Publishing

Tsuha, C. d. H. C. and Aoki, N. (2010). 'Relationship between installation torque and uplift capacity of deep helical piles in sand'. *Canadian Geotechnical Journal*. Vol. 47, No. 6, pp 635-647.

Ueno, K. (2000). 'Methods for preparation of sand samples'. *Centrifuge 98: Proceedings of the International Conference Centrifuge 98*. Tokyo, Japan, 23-25 September 1998. Taylor and Francis.

Van Impe, W. F. (1988). Considerations on the auger pile design. *Deep Foundations on Bored and Auger Piles, BAP I, Proceedings of the 1st international geotechnical seminar*. Belgium, Ghent, 7th-10th June 1988. Balkema

Van Impe, W. F. (2004). *The overview of almost two decades of full scale research on screw piles*. International Society of Soil Mechanics and Geotechnical Engineering. April 2004.

Van Impe, W. F., Van den Broeck, M., Thooft, K. (1988). 'End shaft bearing capacity of piles evaluated separately out of static pile loading test results'. *Deep Foundations on Bored and Auger Piles, BAP I, Proceedings of the 1st international geotechnical seminar*. Belgium, Ghent, 7th-10th June 1988. Balkema

Van Weele, A.F. (1988) 'Cast-in-situ piles - Installation methods, soil disturbance and resulting pile behaviour'. *Deep Foundations on Bored and Auger Piles, BAP I, Proceedings of the 1st international geotechnical seminar*. Belgium, Ghent, 7th-10th June 1988. Balkema

Vesic, A. S. (1964). 'Investigations of Bearing Capacity of Piles in Sand'. *North American Conference on Deep Foundations*. Mexico City 1964.

Wade, S., Handley, B., Martin, J. (2012). 'Types of bearing piles' in Burland, J., Chapman. T., Skinner, H., Brown, M. (ed.) *ICE Manual of Geotechnical engineering*. London 2012: ICE Publishing.

Weltman, A. and Healy, P.R. (1978). *Piling in 'boulder clay' and other glacial tills*. CIRIA Report PG5: London, Construction Industry Research and Information Association.

Weltman, A. J. (1980). *Pile Load Testing Procedures. DOE and CIRIA Piling*. Development Group report PG7 PSA Civil Engineering Technical Guide 25.

White, D. J. (2002). *An Investigation into the behaviour of pressed-in piles*. PhD. University of Cambridge.

White, D. J. and Bolton, M.D (2004). 'Displacement and strain paths during plane-strain model pile installations in sand'. *Geotechnique* Vol., 54. No. 6 pp 375-397.

White, D. J., Deeks, A.J., Ishihara, Y. (2010). 'Novel Piling: Axial and rotary jacking' *The DFI and EFFC 11th International conference: Geotechnical Challenges in Urban Regeneration*. 26th – 28th May 2010, ExCel London, UK. Peterborough, Emap Networks.

White, D. J., Teh, K.L., Leung, C.F., Chow, Y.K. (2008). 'A comparison of the bearing capacity of flat and conical circular foundations on sand'. *Geotechnique*. Vol. 58, No. 10, pp 781-792.

Wood, D. M. (2004). *Geotechnical Modelling*. Spon Press.

Xu, X., Schneider, J.A., Lehane, B.M. (2008). 'Cone penetration test (CPT) methods for end-bearing assessment of open and closed ended driven piles in siliceous sands'. *Canadian Geotechnical Journal*. Vol. 45, Issue 8, pp. 1130-1141.

Young, H. D. and Freedman, R.A. (2000). *University Physics*. Tenth Edition. San Francisco: Addison Wesley Longman.